THE UNIVERSITY
of EDINBURGH

Intensification of Industrial Processes: Auto-Tandem and Molecular Weight Enlarged Catalysis

Lewis M. Fenton

University of Edinburgh

Submitted for the degree of Doctor of Philosophy

August 2017

Declaration

The work described in this thesis is entirely my own, except where I have either acknowledged help from a named person or given reference to a published source. Text taken from another source will be enclosed in quotation marks and a reference given. This thesis has not been submitted, in whole or in part, for any other degree.

Signature:

Date:

Acknowledgements

I am grateful to Prof. Dieter Vogt who provided me with the opportunity to return to work and study in the city and department that I love. I wish you all the best in Dortmund.

I am indebted to Prof. Jason Love for his assistance, guidance and support during the writing of this thesis.

I am incredibly grateful to Dr Jenni Garden. You are a star. Your pep-talks, intelligence, determination, optimism and kindness are inspiring. In the final days of writing it was you who saved the day.

My many thanks to the Vogt group as it was when I joined: Dr. Dennis Pingen, Dr Coen Hendriksen, Alberto Cavalieri, and Evert Boymans. Then when we grew: Dr Maria Segarra Masset, Dr Daniel 'Dani 1' Peral, Dr Anna Falk, and George Murray. Finally when we parted: Eszter Fazekas, Veronica Forcina, Laura Puig-Urrea, and Viktor Söderholm. I must also include the visiting students: Nicola Piens, Bachir Bibouch, Judith Schwaderer and Dani 'Dani 2' Herrera. It has been a pleasure working with such a great team of people. The Travelling Peas.

I also thank my two MChem students Alice Doyle and Sami Gesslbauer for all their hard work, interesting questions and putting up with my supervision.

My gratitude to Dr John Iggo for kindly running the high pressure NMR experiments presented in chapter 3.

My fellow students especially Amy Challinor and Emily MacDonald. Emily, your friendship and encouragement got me through the toughest times and enriched my life in Edinburgh in ways I could never have imagined. My gratitude also to Rūta Karolytė for always reminding me to have a sense of humour in difficult times.

My multitude of friends in Edinburgh and beyond. I am extremely fortunate to have such a diverse and rich collection of wonderful people to guide, inspire and influence my life. My deepest gratitude to the staff and alumni of Roche Continents 2016 for an unforgettable experience. I will always hold you in my heart and strive for the magic that united us.

My family: you were what pushed me through no matter what.

Abstract

The chemical industry is an essential part of modern society and therefore has a responsibility to develop solutions for the problems facing it. A major problem is continuing to match the material demands of a growing global population whilst simultaneously decreasing the consumption of finite natural resources and limiting the emissions of greenhouse gasses. An optimised catalytic system that shortens, or intensifies, the process chain for the production of chemicals can be an effective solution to this challenge.

Auto-tandem catalysis is where a single metal-ligand complex facilitates two or more sequential transformations. For example: alkenes are hydroformylated into aldehydes which are then hydrogenated into alcohols. The alcohols have use as plasticisers or surfactants for metal extraction.

A previously reported auto-tandem catalysis system was shown to be capable of sequential hydroformylation-hydrogenation of 1-octene to nonanol. It consisted of the neutral rhodium precursor [Rh(acac)$(CO)_2$] and the bidentate ligand xantphos in 10% ^{i}PrOH/H_2O co-solvent at temperatures of 160°C. Investigations, reported in this thesis, revealed that xantphos type ligands, with their large bite-angle, and high temperatures are required to generate the hydrogenation activity. However, in contrast to the previous system, water is not necessary; with the same results produced in toluene:^{i}PrOH solutions and water:^{i}PrOH solutions.

It is proposed that the ^{i}PrOH or H_2O has a direct influence in the catalytic cycle, either as a hydrogen-shuttle or generates a cationic rhodium species, known to be active in hydrogenation. High temperature NMR studies show the standard resting state of the hydroformylation catalyst is still predominant at high temperatures therefore the proposed catalytic cycle starts from this step.

A recurring problem in the industrial process chain is the separation of the catalyst from the final products. Combing a TiO_2 ceramic membrane with a POSS (polyhedral oligomeric silsesquioxane) modified tin catalyst and phosphonium iodide co-catalyst, for the coupling of epoxides and CO_2 to make cyclic carbonates, was investigated. The catalyst system showed good substrate compatibility for a range of epoxides. In a prototype membrane set-up the system demonstrated a long catalyst life time, however significant leaching was also observed.

List of Abbreviations

MALDI-TOF	Matrix assisted laser desorption/ionisation-time of flight mass spectrometry
GC-MS	Gas Chromatography Mass Spectrometry
GC-FID	Gas Chromatography Flame Ionisation Detection
NMR	Nuclear Magnetic Resonance Spectroscopy
HSQC	Heteronuclear Single Quantum Coherence Spectroscopy
DOSY	Diffusion Ordered Spectroscopy
POSS	Polyoligomericsilsesquioxane
DEPT	Distortionless enhancement by polarization transfer spectra
COSY	Correlation Spectroscopy
Me	methyl
^{n}Bu	n-butyl
^{t}Bu	tert-butyl
^{i}Pr	Iso-propyl
MWE	Molecular Weight Enlargement
TON	Turn Over Number
TOF	Turn Over Frequency (h^{-1})
syn-gas	Synthesis Gas (a mixture of carbon monoxide and hydrogen)
BISBI	2,2'-bis(diphenylphosphinomethyl)-1,1'-biphenyl
PPh_3	Triphenylphosphine
PBu_3	Tributylphosphine
TBAI	Tertbutylammonium iodide
diop	2,3-O-isopropylidene-2,3-dihydroxy-1,4-bis(diphenylphosphino)butane
t-bdcb	trans-1,2-bis(diphenylphosphinomethyl)cyclobutane

dppe	diphenylphosphino ethane
t-dbch	trans-1,2-bis(diphenylphosphinomethyl)cyclohexane
dppp	diphenylphosphinopropane
cat.	Catalyst
NMP	N-methyl-2-pyrrolidone
l/b ratio	linear isomer/branched isomer
MeOH	methanol
^{i}PrOH	isopropanol
cod	cyclooctadiene
dppe	diphenylphosphinoethane
BINAP	2,2’-bis(diphenylphosphino)-1,1'-binaphthyl
DPEPhos	Bis((2-diphenylphosphino)phenyl ether
Triphos	bis(diphenylphosphinoethyl)phenylphosphine
T	temperature
equiv	equivalents
KOAc	Potassium acetate
KO^{t}Bu	Potassium tertbutoxide
mL	millilitre

"We are chemists, that is, hunters: ours are 'the two experiences of adult life' of which Pavese spoke, success and failure, to kill the white whale or wreck the ship; one should not surrender to incomprehensible matter, one must not just sit down. We are here for this – to make mistakes and to correct ourselves, to stand the blows and hand them out. We must never feel disarmed: nature is immense and complex, but it is not impermeable to the intelligence; we must circle around it, pierce and probe it, look for the opening or make it."

– Primo Levi, *The Periodic Table*

"CALL ME ISHMAEL."

– Herman Melville, *Moby Dick*

Table of Contents

Declaration i
Acknowledgements ii
Abstract iii
List of Abbreviations iv
Table of Contents vii

Chapter 1: Industrial Hydroformylation and Auto-Tandem Catalysis 1
1.1 Introduction 1
1.2 Hydroformylation 3
1.2.1 Discovery of Hydroformylation 3
1.2.2 The Early Days of Hydroformylation 5
1.2.3 The Change to Rhodium-catalysed Hydroformylation 7
1.2.4 Phosphorus based ligands and their influence 9
1.2.5 Phosphites as ligands in hydroformylation 10
1.2.6 Diphosphines in hydroformylation 12
1.2.7 Mechanism of hydroformylation 16
1.3 Tandem Catalysis 17
1.4 Vogt Group Auto-Tandem Catalysis Systems 24
1.5 Aims and Objectives 26
1.6 References 27

Chapter 2: 'On-Water' Hydroformylation-Hydrogenation 31
2.1 Introduction 31
2.2 On-water hydroformylation/hydrogenation reaction screenings 31
2.2.1 Effect of temperature on hydroformylation-hydrogenation 32
2.2.2 Equivalents of xantphos 46
2.2.3 Influence of gas ratio on hydroformylation-hydrogenation 47
2.2.4 Changing gas ratio 49
2.2.5 Solvent effect on the hydroformylation/hydrogenation reaction 50
2.2.6 Effect of catalyst precursor on hydroformylation-hydrogenation 53
2.2.7 Influence of the ligand on the hydroformylation-hydrogenation reaction: 56

2.2.8 Mixed ligand systems 68
2.2.9 Monodentate ligands: PPh_3 and P^nBu_3 69
2.2.10 Influence of the equivalents of water co-solvent 72
2.2.11 Summary of the screenings and reaction profiles 74
2.3 Proposed catalytic cycles 79
2.3.1 Hydrogen activation in the hydroformylation mechanism 79
2.3.2 Possible hydrogenation of aldehydes mechanism 80
2.3.3 Hemi-labile L(P,O,P) Hydrogenation Mechanism 81
2.3.4 ^{i}PrOH Assisted Proton Transfer Hydrogenation Mechanism 84
2.3.5 Inner-sphere hydrogenation Mechanism 86
2.3.6 Alternative Hydroformylation-Hydrogenation Mechanisms 89
2.3.7 Alternative roles for water in hydroformylation-hydrogenaiton mechanism 92
2.4 Conclusions and Future Work 93
2.5 Materials and Methods 95
2.5.1 Synthesis of phenoxaphos 95
2.5.2 Catalysis Procedure 96
2.5.3 Calculations for GC-FID analysis 97
2.6 References 99

Chapter 3: Molecular Weight Enlarged Catalysis 102
3.1 Introduction 102
3.1.1 Production of Carbonates 102
3.1.2 Tin catalysis 104
4.1.3 Molecular Weight-Enlarged Catalysis 105
3.2 Results and Discussion 108
3.2.1 Synthesis of POSS catalysts 108
3.2.1 ^{i}Bu$_7$-POSS NMR spectroscopic analysis 109
3.2.2 $SnMe_2$-(^{i}Bu)$_7$-POSS synthesis and spectroscopic analysis 113
3.2.3 Spectroscopic analysis of Sn(^{n}Bu)$_2$-(^{i}Bu)$_7$-POSS catalyst 118
3.2.4 Synthesis of Br$(CH_2)_3$-(^{i}Bu)$_7$POSS 123
3.2.5 Synthesis of I$(CH_2)_3$-(^{i}Bu)$_7$POSS 125
3.2.6 Synthesis of [PPh_3][I]-$(CH_2)_3$-(^{i}Bu$_7$)POSS 127
3.2.5 Epoxide/CO_2 coupling catalysis 130

3.2.6 Membrane Retention Studies 136
3.3 Conclusion and Future Work 139
3.4 Materials and Methods 140
3.4.1 Synthesis of POSS catalysts 140
3.4.2 Catalysis 142
3.4.3 NMR of substrates: 143
3.4.4 MALDI method 143
3.4.5 Calibration of membrane experiments 144
3.5 References 145

Chapter 1: Industrial Hydroformylation and Auto-Tandem Catalysis

1.1 Introduction

The global chemical industry is responsible for the production of over 70,000 different products.[1] Consequently it is central to the world's economy and is an essential part of modern society: from 2014 to 2015 world chemical sales grew by 14% and were worth a total of €3,534 billion.[1] Yet modern society is increasingly defined by an awareness of the challenges it faces, including; diminishing natural resources, an increasing human population and the existential threat of climate change. Any solution to these challenges must involve the chemical industry as a key component.[2]

When considering solutions to these challenges there is also a contradiction: an increasing population demands more goods and energy, however diminishing resources and the need to limit emissions in an effort to combat climate change, run inherently counter to this. As a result, the chemical industry must increase its production capacity whilst decreasing its energy and material consumption. In the last two decades, the European chemical industry simultaneously decreased its energy consumption by 30% and its CO_2 emissions by 50%, whilst increasing its production by 60% (figure 1.1).[2]

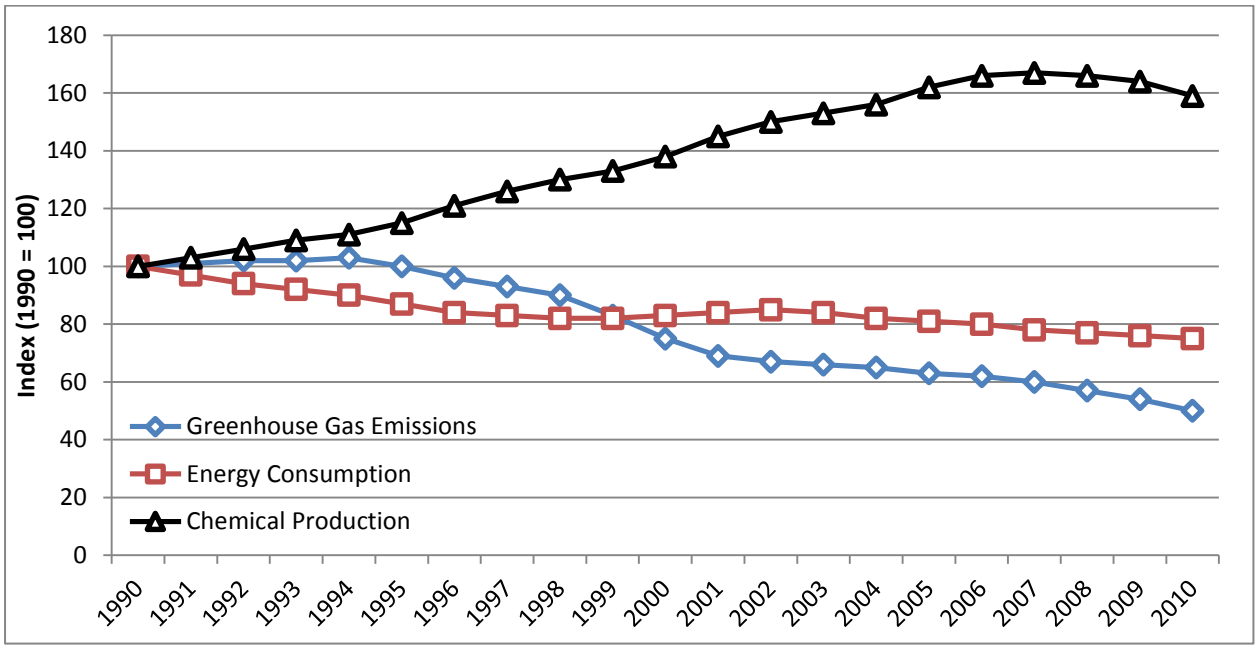

Figure 1.1 Chemical production decoupled from energy and greenhouse gas emissions (reproduced from ref. [2])

To continue to accomplish this goal the chemical industry must increase its efficiency. The production of a chemical involves a chain of reactions with accompanying purification and transportation between each reaction (figure 1.2). Each step in this chain has its own amount of energy and material consumption, carried out to different degrees of efficiency. To improve the efficiency of the entire process the individual steps can be made more efficient and/or the number of steps can be reduced.

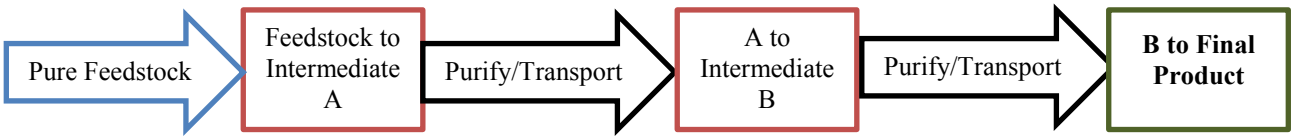

Figure 1.2 Standard process chain for the production of a bulk chemical

Catalysis is fundamental to accomplishing these ambitions. The presence of an optimised catalyst system can drastically cut the energy and material waste of an individual step. It accomplishes this by reducing the activation barrier for a thermodynamically favourable process to require less energy input to proceed.[3] By reducing the activation barrier for the most desired steps, or increasing the activation barrier for the least desired steps, the selectivity can be improved and the atom economy is improved.

Homogeneous catalysts are highly tuneable, active and selective compared to their heterogeneous counter-parts, but often heterogeneous catalysts are still preferred because of the ease of separation and their compatibility with bulk chemistry.[4] However, it is increasingly apparent that to fully optimise industrial process more radical approaches are needed to improve the applicability of homogeneous catalysts and make full use of their advantages.

To shorten the overall process chain, that is perform ‘process intensification’, the tune-ability and reactivity of homogeneous catalysis can allow the combination of multiple steps into one step: a process called tandem catalysis.[5] This eliminates purification, transportation and individual reaction steps to make a shorter more efficient process. To increase the efficiency of an individual step the lifetime of the catalyst can be improved and the purification can be simplified by making a continuous process through molecular weight enlargement of the catalyst and membrane filtration to separate this from the products to enable enhanced

recyclability (figure 1.3).[6] Thus allowing homogenous catalysis to compete with heterogeneous catalysis for use in a continuous process.

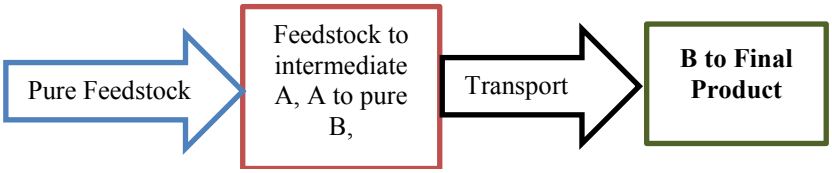

Figure 1.3 Intensified chemical process with tandem production of intermediate A and B and in-situ purification/separation of intermediate B

This thesis discusses both approaches through two different systems: an auto-tandem catalysis process for the conversion of alkenes into alcohols through hydroformylation and hydrogenation, and a molecular-weight-enlarged catalyst for the production of carbonates by coupling CO_2 and epoxides. The first three chapters concern auto-tandem catalysis and the fourth chapter discusses molecular-weight enlargement and membrane-filtration catalysis.

1.2 Hydroformylation

Auto-tandem catalysis is one of the latest technological developments in catalysis relevant to the chemical industry. However, industry has always tried to increase the efficiency and productivity of its processes. Historically this was accomplished by simply improving the performance of the catalyst. An example of the development and refinement of catalysis for a key reaction, hydroformylation, will be first discussed as tandem catalysis related to hydroformylation builds upon the knowledge of metal, ligand design and mechanistic studies developed over the years.

1.2.1 Discovery of Hydroformylation

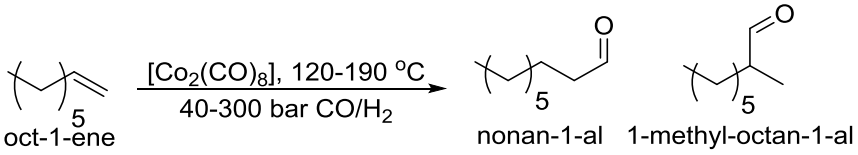

Scheme 1.1 Cobalt-catalysed hydroformylation of 1-octene to produce linear and branched aldehydes

From its discovery in 1937 by Otto Roelen at Ruhrchemie, hydroformylation (scheme 1.1), or the "oxo" process, has been inherently linked to industry. While the first German patent appeared in 1938, it was only in 1952 that the first international patent outlining the cobalt-mediated "preparation of oxygen-containing compounds from olefinic hydrocarbons at elevated temperatures and pressures" was granted.[7] In 1941, Ruhrchemie, BASF and Henkel, with investment from I G Farbenindustrie constructed a facility in Oberhausen-Holten that would, under Roelen's supervision, be responsible for the conversion of C_5-C_{17} olefins into

fatty alcohols and acids for the use of detergents, palatinol-type plasticisers and, for the smaller alkenes, to perfumes.[8]

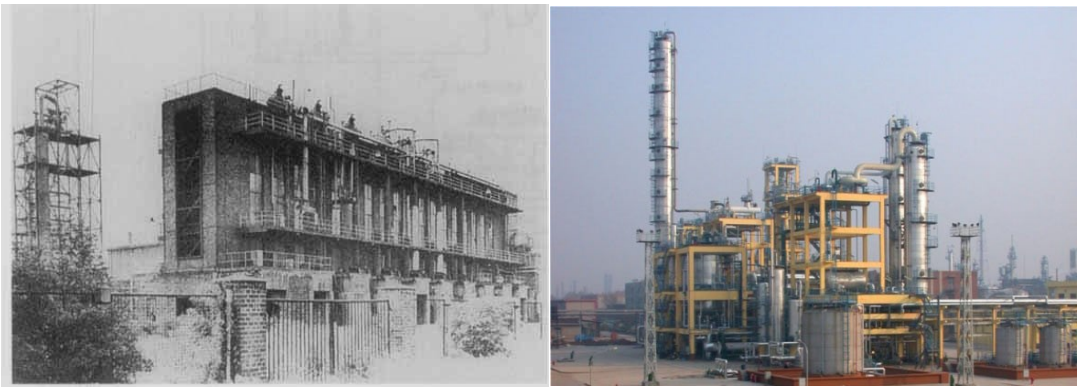

Figure 1.4 Ruhrchemie hydroformylation facility (1943) (left)[8] and the new generation of Oxo^{SM} plants (Sinopec Qilu Petrochemical Co. Ltd, China (right).[9]

The facility (figure 1.4) consisted of a pre-fractionator, a hydroformylation reactor, a hydrogenation reactor, filtration system, and distillation towers. It had an operating capacity of 10,000 t/a.[8]

By 1994, hydroformylation processes had spread globally and accounted for the production of 6 million t/a of products worldwide.[8] Only the Ziegler process for the production of polyethylene and polypropylene had a higher output for a catalytic organometallic process. By 2008, this figure had increased to 10.4 million t/a.[10]

While production has significantly increased since the 1940s, the fate of the hydroformylation products has not changed. The synthetic versatility of the aldehyde functionality facilitates conversion into a wide range of other functional groups such as alcohols, carboxylic acids, esters, amides and amines.[11] However, with each step in the industrial synthesis towards the end product comes an additional reactor, with necessary purification, and with the added construction and running costs.

A more desirable system would be capable of converting alkenes into their desired products with high selectivity in a single reactor. Additional considerations include substrate compatibility, reaction conditions and precious metal losses. Ideally, a hydroformylation catalyst should be capable of transforming a mixture of alkene isomers, which are cheaper and more abundant as feedstock than a source of pure terminal alkene. These ideals have been with hydroformylation since its inception; however, it is only within the last decades that progress has been made towards achieving these goals.

1.2.2 The Early Days of Hydroformylation

In a biographical article on Roelen; Cornils, Herrmann and Rasch provide a brief overview of the early days of hydroformylation catalysts and especially emphasize the slow acceptance of the notion of homogeneous catalysts over the established and studied heterogeneous catalysts.[8] All industrial processes at the time, including the Fisher-Tropsch synthesis (scheme 1.2) that Roelen began his career studying and that would ultimately lead him to hydroformylation, used solid metal, that is heterogeneous, catalysts.[12] It was assumed hydroformylation would follow suit despite the peculiarly high amount of cobalt dissolved in the resulting product solutions, therefore the true identity of the catalyst remained unknown until later. Cobalt separation is still of interest in current research.[13]

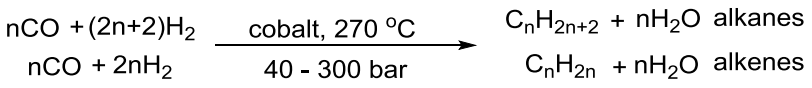

Scheme 1.2 Fischer-Tropsch process for the synthesis of alkanes and alkenes from synthesis gas

It is lamentable that there was a lack of collaboration between Roelen and his contemporary Walter Hieber. Hieber had reported the synthesis of homogeneous complexes of $[HCo(CO)_4]$ and $[Co_2(CO)_8]$ from cobalt powder in synthesis gas in 1938.[14] It is these species that are the active catalysts in hydroformylation. Unfortunately, a major collaboration between industry and academia was missed that could have provided an early insight into the mechanism of hydroformylation, and thus how to improve it. However, hydroformylation has since benefited enormously from such collaborations including the development of the Ruhrchemie-Rhone Poulenc process, again operating in Oberhausen.[15]

In the 1950s the realization, and eventual acceptance, that hydroformylation was performed by discrete cobalt complexes was successfully established by the groups of several chemists including: Storch, Natta, Berty and Marko.[16] This cumulated in mechanistic considerations by Heck and Breslow, published in 1961, for the addition of olefins to $[HCo(CO)_4]$.[17] Earlier work by Karapinka and Orchin showed that the initial alkene insertion into the cobalt complex is suppressed by high CO pressure, but not by high N_2 pressure.[18] Heck and Breslow used this as evidence for the necessity of CO dissociation to occur before alkene coordination. Thus, the active catalytic species was proposed to be a $[HCo(CO)_3]$ species. This basic premise forms the foundations for the rhodium-catalysed mechanism and also for the reasoning behind ligand effects discussed later.

In addition to investigations into the opening of the catalytic cycle, Heck and Breslow also investigated the closing of the cycle, comparing hydrogen and [$HCo(CO)_3$] as reducing agents, and also considered the mechanism of olefin isomerization (scheme 1.3).

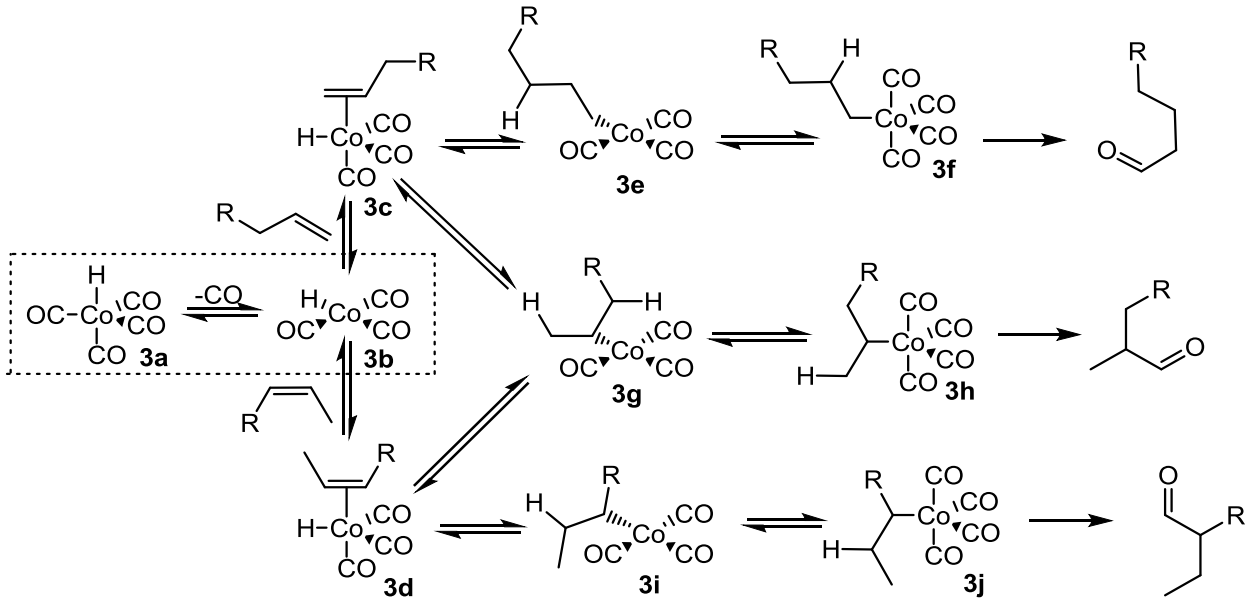

Scheme 1.3 Heck and Breslow's isomerization and hydroformylation mechanism showing the activate state [$HCoCO_3$] and the alkyl intermediates [17]

The mechanism begins by dissociation of a CO from the resting state [$HCo(CO)_4$] (**3a**) to form the active [$HCo(CO)_3$] species (**3b**). This can coordinate an olefin (**3c**, **3d**) which undergoes insertion into the Co-H bond to form alkyl Co species (**3e**, **3g**, **3i**). Depending on the type of olefin, linear or branched, and where the insertion takes place the alkyl complex, and thus the final hydroformylation product, can be linear or branched. It also determines the number of β-H available for β-H elimination to take place, reversing the process and causing isomerisation of the alkene. Once the Co-alkyl intermediates are formed another CO adds to the Co (**3f**, **3h**, **3j**) and several more steps occur before the aldehyde is released: oxidative addition of H_2 and reductive elimination of the aldehyde, regenerating the catalyst, however these will be discussed in more detail in section 1.2.7 with regards to Rh-catalysed hydroformylation mechanism.

Studies of the isomerisation mechanism are of relevance to the overall aim of process intensification by tandem catalysis, because one system of interest is isomerisation-hydroformylation, enabling the conversion of internal olefins to linear aldehydes. Therefore the rates and mechanism of the two reactions must be considered together.

Heck and Breslow noted that although 1-pentene is hydroformylated faster than 2-pentene, the isomerisation equilibrium heavily favours 2-pentene. As a consequence the linear/branched ratio of hydroformylation products starting from 2-pentene will always be limited. However this is something that can be improved upon by different catalyst systems. These discussions also reveal the necessary concepts for more selective systems *via* tandem catalysis were already under consideration in the initial days of hydroformylation research.

These academic studies began to influence industry and in 1965 Shell patented a cobalt phosphine-modified process, which had increased linear/branched ratio over the unmodified cobalt used by Ruhrchemie, with the trade-off of more side products being formed including alcohols.[19] These early patents anticipate the later work undertaken by Piet van Leeuwen both during and after working at Shell.

1.2.3 The Change to Rhodium-catalysed Hydroformylation

The first patents for rhodium-catalysed carbonylations appeared in the late 1950s.[20] One 1956 patent established that the unmodified rhodium catalyst is capable of being dissolved in the reaction mixture under conditions, which range from 60-240 °C and 70-670 bar of $CO:H_2$. Of interest to the work discussed later in this thesis, the recovery method for rhodium is reported to be by treatment of the reaction solution with water at elevated temperatures between 80–200 °C.

During the 1960s, while industry was refining cobalt-catalysed hydroformylation, in academia, (although with support from Johnson Matthey[9]) rhodium was attracting attention as a hydrogenation catalyst principally in the groups of Wilkinson[21] and Vaska.[22] Both groups modified the rhodium with phosphine ligands and the hydroformylation performance of Wilkinson's catalyst, $[RhCl(PPh_3)_3]$, was contrasted to equivalent cobalt catalysts.[23]

Wilkinson's complex $[RhCl(CO)(PPh_3)_3]$ showed a significantly higher hydroformylation activity than the cobalt complexes reported previously. It was capable of performing hydroformylation at minimum conditions of 55 °C and 10 bar of syn-gas, although as standard conditions Wilkinson used 80 °C and 100 bar of syn-gas. Reported conversions were excellent with full conversion of linear alkenes observed within 16 hours. Linear to branched ratios for the aldehyde products are typically 2.8.

However, one disadvantage of rhodium based catalysts from a tandem catalysis perspective is that using 2-pentene as a substrate produced exclusively branched isomers. This demonstrates

poor isomerization rates for Rh catalysts when compared to cobalt catalysts. Isomerization was also impaired by excess triphenylphosphine. The mechanism of isomerization for rhodium catalysts is the same for cobalt (scheme 3). In order for β-hydride elimination to occur a vacant site in the coordination sphere must be present. Excess triphenylphosphine occupies this site and inhibits the elimination. Where Breslow noted that with a cobalt catalyst 1-alkene is hydroformylated 3.5 times faster than 2-alkene, Wilkinson noted that a rhodium catalyst hydroformylates the 1-alkene 20 times faster than the 2-alkene. This is encouraging in the aim of generating linear aldehydes from internal alkenes, once the problem of low isomerization rates of rhodium can be overcome.

Wilkinson opened the way for investigations into rhodium-catalysed hydroformylation, but progress emerged mainly from the development of new ligands. Much of the mechanistic aspects remained under-investigated until John M. Brown in 1987 identified several Rh species including $HRh(CO)_y(PPh_3)_x$ where y = 1 or 2 and x = 2 or 3. Brown also used low temperature NMR spectroscopic studies to identify acyl species.[24]

Another chemist interested in the poorly understood hydroformylation mechanism, in particular the activation of hydrogen, was Piero Pino.[25] Using deuterium gas with high-pressure IR Pino showed that the pressure of H_2 and the loading of the catalyst have a profound influence on the mechanism of hydrogenation in hydroformylation (scheme 1.4).

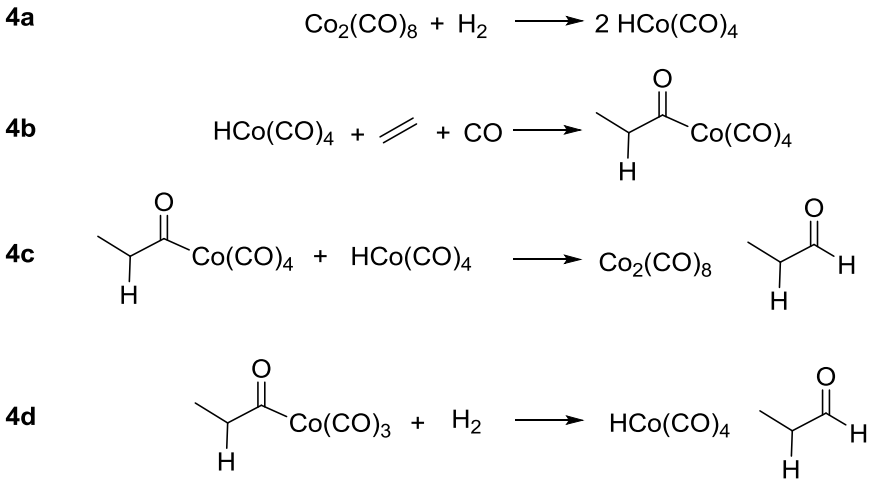

Scheme 1.4 Mechanism of hydrogen activation as investigated by Pino

In the absence of excess CO (although a small amount can be generated by decarbonylaiton of the species in **4a**), ultimately two $HCo(CO)_4$ complexes, generated by the reaction of $[Co_2(CO)_8]$ and H_2 (**4a**). The first coordinates the olefin, a molecule of CO and does migratory insertion (**4b**) and the second provides the hydride to eliminate the aldehyde and regenerate the

bimetallic [$Co_2(CO)_8$] species (**4c**). In the presence of CO, the $HCo(CO)_4$ complexes are stable enough that this does not occur and it is down to a proposed unsaturated acyl species to activate the hydrogen (**4d**). The using a mixture of H_2 and D_2 if a single Co species activates the D_2 then both atoms of D are incorporated in the final aldehyde. In the bimolecular Co pathway then there is a mixture of H and D in the final aldehyde.

In 1974, a year after Wilkinson shared the Nobel Prize with Ernst Otto Fischer, a student of Walter Hieber, the first rhodium-triphenylphosphine based plant began operations.[26] In 1976 and 1978 two more plants began to operate run by Union Carbide Corporation and Mitsubishi respectively.[27]

1.2.4 Phosphorus based ligands and their influence

One of the biggest influences in the successful development of homogeneous catalysis is the versatility of phosphorus-based ligands. These ligands, with a fundamental structure of PR_3, present chemists with a series of complexes which can have their electronic and steric properties altered in a systematic and predictable way.[28] Thus, their influence in catalysis can be studied in a controlled and quantitative manner.

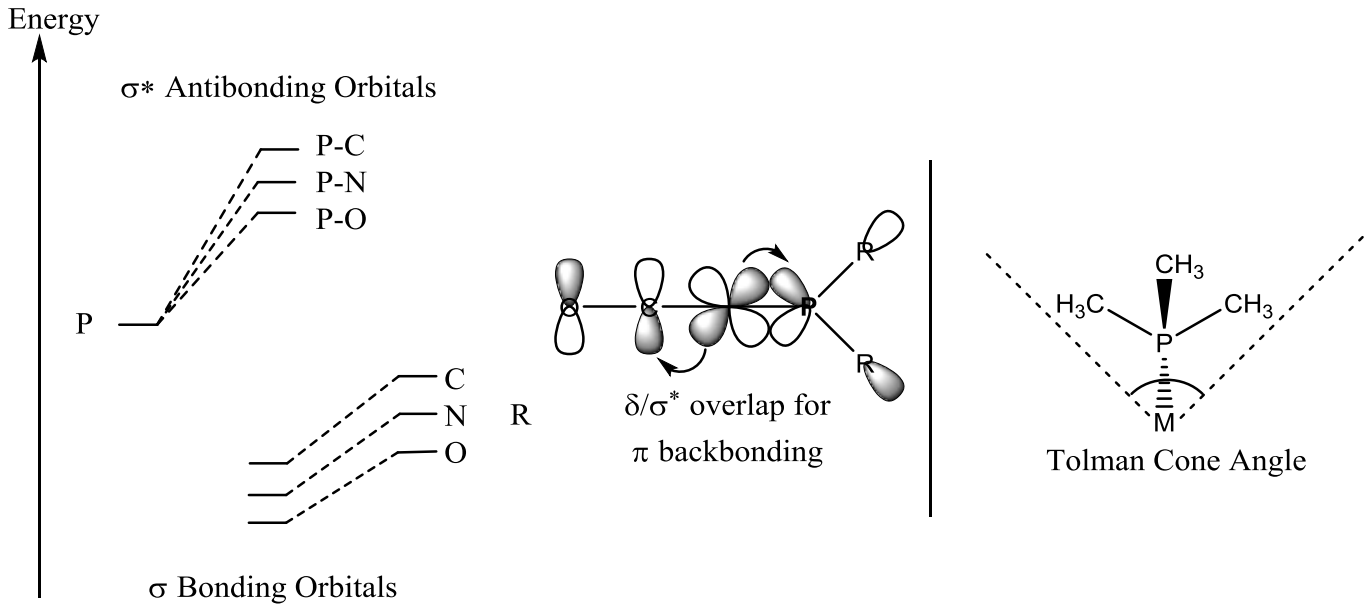

Figure 1.5 (left) *Partial orbital energy diagram of the PR bond showing stabilization of the σ*orbitals with increasing electronegativity of the R atom. Also the overlap between the σ and the σ* orbitals. [3] (right) An example of the Tolman Cone Angle (θ)*

Like the nitrogen-based ligands used by early organometallic chemists,[29] P-based ligands bind to the metal through the lone pair situated on the phosphorus, acting as σ-donors, or Lewis bases. However due to the σ* anti-bonding orbital of the PR bond, π-backbonding, or Lewis acidity, is also present. In phosphorus alkyls this σ* orbital is small, not very polarized and as a result is high in energy and π-backbonding is weak (figure 1.5). However, in more electronegative and electron withdrawing R groups the polarization of the bond stabilizes the σ* orbital, it becomes lower in energy, and it becomes more effective at accepting electrons from the metal d-orbitals. This in turn removes electron density from the M/CO bond.[3]

In 1977, Chadwick Tolman devised a systematic way of quantifying the electronic and steric properties of phosphine ligands.[30] By comparing the ν(CO) frequencies of different $LNi(CO)_3$ complexes, the extent of π-accepting character of the ligand could be quantified. The stronger σ-donors increase the electron density on the metal, which in turn has a stronger π-back donation effect into the CO ligands, which strengthens the M-CO bond at the expense of the CO bond itself, weakening it and shifting it to a lower wavenumber. For example the complex $[Ni(PEt_3)(CO)_3]$ has a ν(CO) of 2060 cm^{-1} while $[Ni(P(OEt)_3)(CO)_3]$ has a wavenumber of 2077 cm^{-1}.

The steric considerations of the ligand are expressed in the Tolman cone angle (figure 5). The angle reflects the space filling of the ligand and was originally calculated through physical models, but is now calculable by computational means.[3]

The cone angle and electronic parameters allow comparisons to be made between monodentate ligands but in terms of bidentate ligands it is often the bite angle of the P-M-P bond that is used as a main comparison, although in many cases flexible ligands can have a range of bite angles. Much of the later progress in hydroformylation would arise from the rigid bidentate ligands with fixed bite angles synthesized by Paul Kamer and Piet van Leeuwen.[31]

1.2.5 Phosphites as ligands in hydroformylation

The Union Carbide Corporation is especially notable for its fundamental research into the use of phosphites as ligands in hydroformylation. In 1969, Pruett and Smith reported the use of triphenylphosphite as a ligand.[32]

Applying Tolman's parameters retrospectively to complexes of these ligands shows that the increase in π-accepting character of the phosphites, compared to phosphines, weakens the M-CO bond by removing electron density from the metal centre. The consequence on reactivity is that the energy of CO dissociation is lower, therefore formation of Breslow's 4-coordinate

hydride should occur more often (figure 1.5). The Tolman angle for the phosphite is 20° less than the phosphine equivalent and therefore, with less steric hindrance, the alkene should bind easier. An overall increase in reactivity is expected and is observed; with benign reaction conditions of a pressure of 6 bar 1:1 H_2:CO used compared to the standard 36 bar used in phosphine-modified hydroformylation. Pressure studies showed that the lower pressure improved the yield of n-aldehyde. Changing the partial pressure ratio towards hydrogen also resulted in an increase in the linear/branched ratio of the aldehyde.

Such drastic reductions in hydroformylation conditions were extremely promising from an industrial stand-point. However, the susceptibility of the ligands to hydrolysis severely limits their applications on an industrial scale (scheme 1.4). Further decomposition pathways occur through the Arbuzov rearrangement and a variety of reactions with aldehydes, especially unfortunate in hydroformylation.

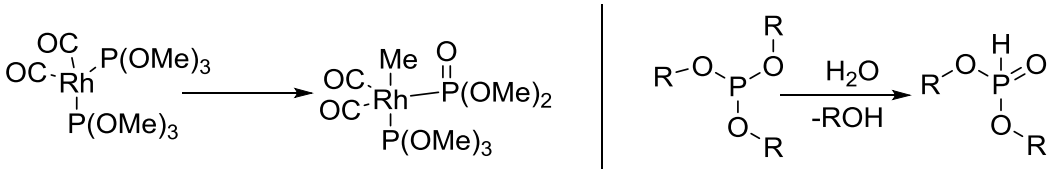

Scheme 1.5 Decomposition pathways of phosphites: Arbuzov rearrangement (left) and hydrolysis (right).[10]

To try counteract the application-limiting effects of hydrolysis and the Arbuzov reaction, the Union Carbide Corporation (USA) produced bulky diphosphites in the late 1980's (figure 1.7).[33] Other chemical companies followed suit and into the 90s BASF [34], DSM/DuPont [35] and Mitsubishi [36] were all claiming patents on bulky diphosphites.

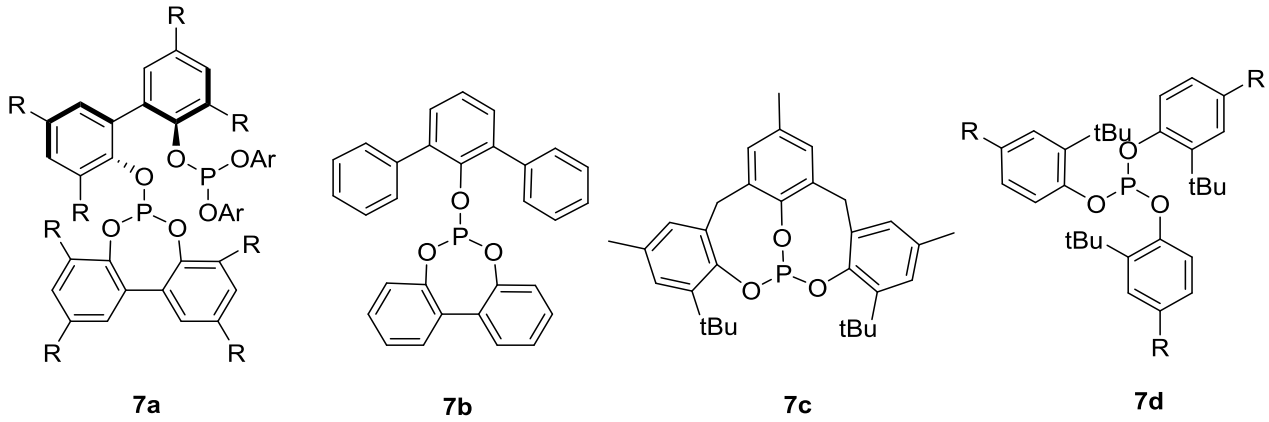

Figure 1.7 Bulky bidentate phosphites of the type synthesized by the Union Carbide Coporation (7a) and three investigated by Piet van Leeuwen (7b, 7c, 7d)

But it was Piet van Leeuwen, at Shell, who demonstrated that phosphites produced unparalleled hydroformylation activity of vinylidenic alkenes such as limonene (scheme 1.6).[37]

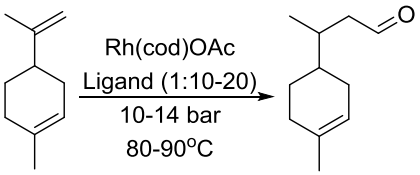

Scheme 1.6 Limonene hydroformylation when ligand is PPh3 (χ = 13, θ = 145 °) rate is 100 mol mol^{-1} h^{-1} and with P(OPh-o-^{t}Bu)$_3$ (χ = 51, θ = 175 °) the rate was determined to be 4000 mol mol^{-1} h^{-1}

Also of interest from a tandem catalysis perspective is the observation that the addition of strongly electron withdrawing ligands induced isomerization in the vinylidenic substrate. In their report, van Leeuwen and Roobeek use Tolman's parameters to rationalize their results; increased steric bulk in monophosphites results in improved regioselectivity. Bulky phosphites improved reaction rates and in the diphosphite case induced good enantioselectivity in chiral systems.[38] These rationalizations were followed by an in-depth spectroscopic investigation.[39] In a more recent study, van Leeuwen returned to the bulky phosphites, this time in the hydroformylation of ethene.[40] Other activity to emerge from the van Leeuwen group has focused on a variation of the phosphites, the phosphoramidites (figure 1.8).[41]

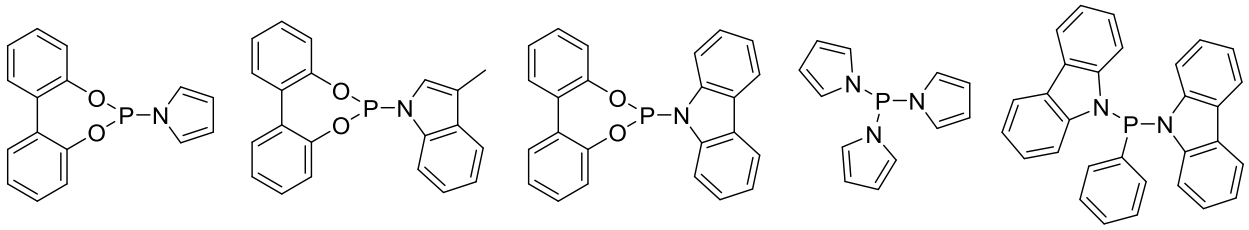

Figure 1.8 Examples of phosphoramidites [41]

As ligands, phosphites significantly increase the activity of the rhodium hydroformylation catalyst system. As a result the Rh-phosphite complexes can react with internal olefins and even traditionally unreactive substrates like limonene. However, they suffer from a weakness to several decomposition pathways and their phenomenal reactivity does not guarantee a good linear/branched ratio.

1.2.6 Diphosphines in hydroformylation

Following the success of Wilkinson's catalyst and noting that the best linear/branched ratios occur when the ratio of ligand to catalyst is extremely high, in addition to taking advantage of an improved method for the synthesis of diphosphines reported in 1962,[42] Piero Pino reported

asymmetric hydroformylation by rhodium complexes of chiral disphosphine ligands in 1973.[43] Hughes and Unruh published a 1983 investigation into the application of diphosphines in rhodium-catalysed hydroformylation.[44] Cornely and Fell published a report on diphosphines in cobalt-catalysed hydroformylation, a year after Hughes and Unruh's study.[45]

When discussing the coordination of diphosphines it became important to distinguish between the different coordination modes: *axial-equatorial (ae)*, and *equatorial-equatorial (ee)* (figure 1.9). The hydride in the ee-isomer is detectable in the ^{1}HNMR spectrum as a triplet of doublets at -9.5 ppm and should display two IR bands at approximately 2036 cm^{-1} and 1969 cm^{-1}. The presence of the ae isomer is detectable by two more IR bands at approximately 1991 cm^{-1} and 1941 cm^{-1}.[41]

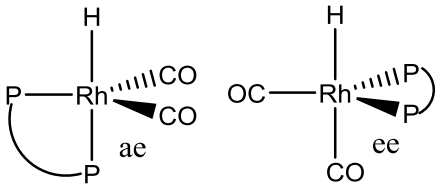

Figure 1.9 ae and ee coordination modes of the rhodium diphosphine complexes

Through NMR spectroscopic studies a link between the ratio of the ae and ee-isomers and the aldehyde l:b ratio was discovered with an increase in the proportion of ee-isomer leading to an increase in the l:b ratio.[27]

Hughes and Unruh noted that there were two different classes of diphosphines: those that increase the l/b ratio and those that do not induce higher l/b selectivity (figure 1.10). Rigid ligands like 2,3-O-isopropylidene-2,3-dihydroxy-1,4-bis(diphenylphosphino)butane (diop) and trans-1,2-bis(diphenylphosphinomethyl)cyclobutane (t-bdcb) supressed isomerisation and increase l/b ratio of the aldehyde. However, diphenylphosphino ethane (dppe), trans-1,2-bis(diphenylphosphinomethyl)cyclohexane (t-dbch) and diphenylphosphinopropane (dppp) lower the l/b ratio of the aldehyde, although they still suppress the isomerisation of the alkene.

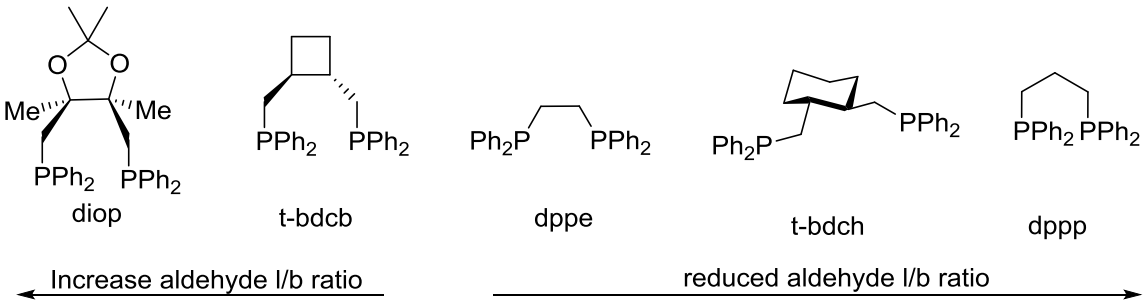

Figure 1.10 Ligands investigated by Hughes and Unruh

The authors use [HRh(CO)(PPh_3)$_3$] as a precursor and the equilibria investigated are a mix of mono- and bi-dentate phosphorus complexes. Through ^{31}P NMR investigations the authors identified that the main species that contributes to high l/b ratios is [HRh(CO)(PPh_3)(2P)] with three phosphorus atoms coordinating to the rhodium centre; two from the bidentate ligand and one from the PPh_3. [46]

A cooperative ligand effect is also observed, with the excess monodentate ligands improving the l/b ratio and supressing alkene isomerisation. This was proposed to be a consequence of coordinating three phosphorus ligands at rhodium so the vacant-site required for β-hydride elimination is not available, preventing isomerisation; the increased steric bulk favours the migration of the alkene into the Rh-H bond which is the selectivity determining step.

After the publications in the 1980s several new phosphine ligands were designed and utilised. In 1995 Piet van Leeuwen, then at the University of Amsterdam, produced xantphos and its derivatives (figure 1.11).[31]

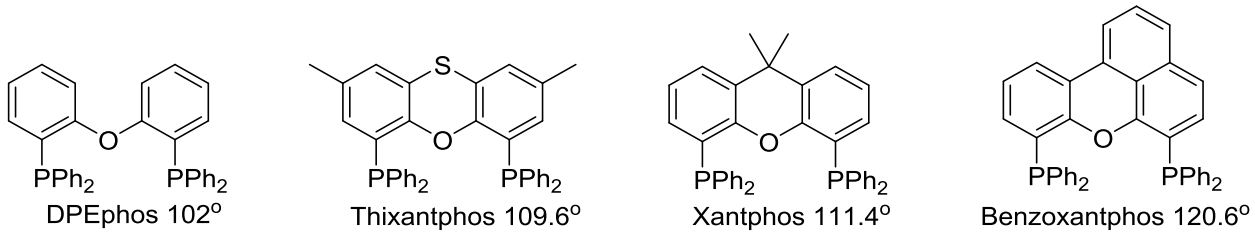

Figure 1.11 Xantphos, some derivatives, and their bite angles calculated for Rh complexes

Xantphos itself continues to enjoy enormous success as its wide bite angle of 111.4 ° is similar to the 120° required in the ee-isomer of the rhodium catalyst with trigonal bipyramidal geometry (figure 1.9). This ee coordination mode results in extremely high l/b ratios. By changing certain elements in the backbone, the size of the bite angle can also be changed in a predictable fashion. It has been found that a larger bite angle leads to a higher l:b ratio. The higher ee:ae ratio has been determined by spectroscopic studies.[47] Xantphos as a backbone has been applied to a water-soluble sulfonated version, sulfoxantphos,[48] and a phosphite and phosphoramidite derivative which are still core to the catalytic systems published in Van Leeuwen's latest work mentioned earlier.[49]

The current state-of-the-art ligands for hydroformylation are tetraphosphine ligands developed by Xumu Zhang in 2010 (figure 1.12).[50]

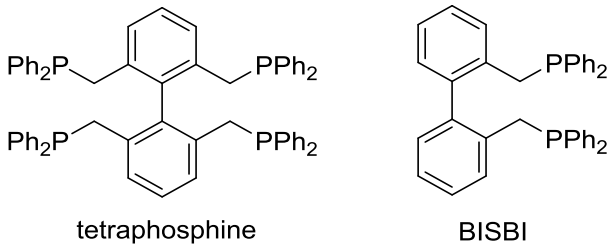

Figure 1.12 Zhang's tetraphosphane ligand and bidentate ligand BISBI

The increased phosphorus concentration around the metal is due to the presence of four phosphines in close proximity and the possibility of forming a complex with a very large bite angle. Although there are four phosphorus atoms present on the ligand the authors propose that only two coordinate at a time in several possible bidentate coordination modes, with a maximum bite angle of 180° possible if the opposite phosphines on the ligand coordinate at the same time. [51]

As a result the l/b ratios in octene hydroformylation are 53.7 at 100 °C and 45.2 at 140 °C with 5% isomerisation products, compared to the 2.4 and 24% that BISBI (2,2'-bis(diphenylphosphinomethyl)-1,1'-biphenyl), a standard bidentate phosphorus ligand (figure 9), induces. [Rh(acac)$(CO)_2$] was used as precursor and the authors do not report any hydrogenation products. The success of this ligand lends credit to Unruh and Hughes' reasoning that increased phosphorus concentration around the rhodium, but with room for association and dissociation of CO, leads to a better catalyst.

1.2.7 Mechanism of hydroformylation

The currently accepted mechanism for hydroformylation is shown in scheme 1.5.

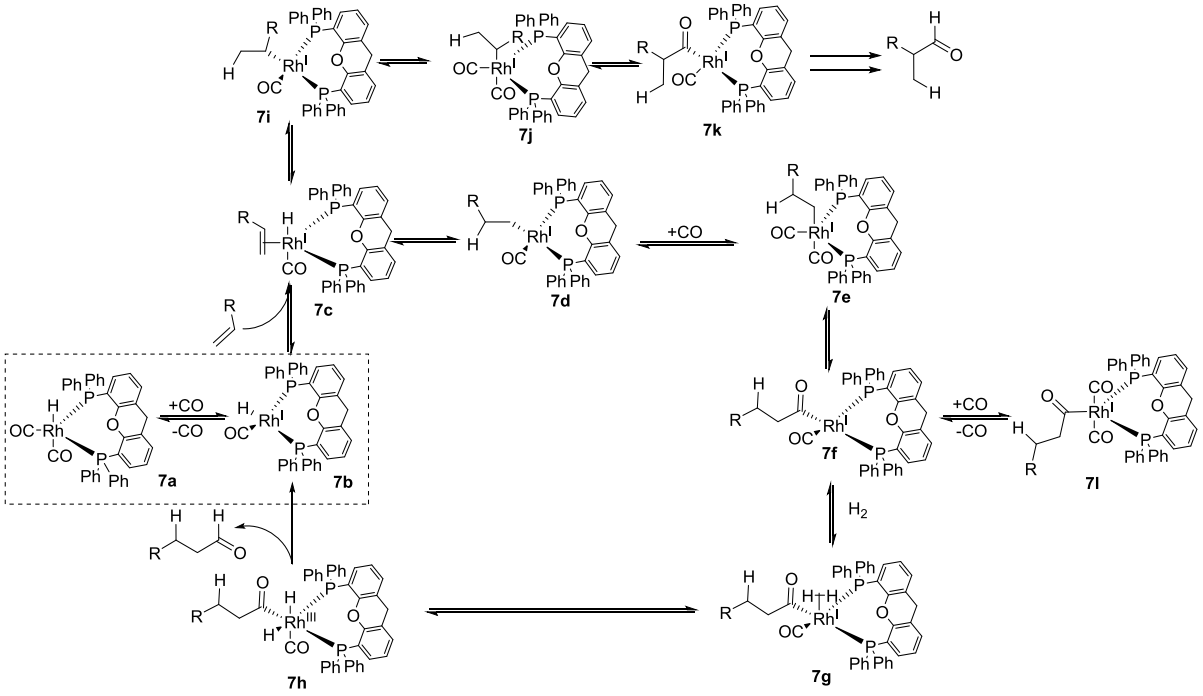

Scheme 1.7 Mechanism of hydroformylation starting from the resting state $[HRh(CO)_2(xantphos)]$ (**7a**).[27]

Starting from the 5-coordinate dicarbonyl monohydride **7a** the complex must first lose a carbonyl ligand, forming **7b**, before it can coordinate an alkene. **7a** is the species observed by in-situ NMR and IR spectroscopies under hydroformylation conditions.[52] With the electron-withdrawing phosphites the Rh-CO π* back bonding is weaker, therefore the dissociation to form the active state **7b** occurs faster than in phosphines, improving the reactivity. A similar effect is seen in the equilibria between the acyl species **7f** and the inactive complex **7l**. [53]

From the 4-coordinate **7b**, the alkene coordinates to give **7c** which undergoes migratory insertion into the Rh-H bond to form two possible complexes: the linear alkyl **7d** or the branched alkyl **7i.** This is the step that will determine the selectivity for the linear or the branched aldehyde. An insertion to form the linear alkyl **7d** is more favoured when the ligand displays a large bite angle, as linear insertion minimises the steric crowding around the metal. There are also less targets available for the β-H elimination: 2H in the linear alkyl vs 5H in the branched alkyl, so the reverse reaction is less likely to occur and the linear alkyl will hydroformylate faster.

Following this step, another CO binds to the metal to form 5-coordinate species **7e** or **7j**. CO inserts into the M-alkyl bond to form the acyl species **7f** or **7k**. In some cases the formation of

7k is reversible when the formation of **7f** is not, which can lead to an increase in the l/b ratio.[54] Another CO ligand can bind, forming the inactive 5-coordinate complex **7l**, identified by Poliakoff.[53] Alternatively **7f** can activate a molecule of H_2 to form the dihydride Rh^{III} complex **7h** via **7g**. **7h** can lose an aldehyde by reductive elimination to form **7b,** which will promptly coordinate CO and return to the resting state **7a**.

1.3 Tandem Catalysis

Under Otto Roelen, hydroformylation began as a crude cobalt-based industrial process operated at high temperatures and pressures. After realising that the active systems were discrete metal complexes in solution the next stage was to combine the academic fields of coordination chemistry with the output-focused research done in industry. Heck and Breslow led the way in building a working model of a catalytic system which would be built upon by Piero Pino, John Brown and Piet van Leeuwen. Meanwhile rhodium complexes were discovered to be a more active catalyst system especially when phosphorus-based ligands augmented its catalytic properties.

Much of the current research within industry is focussed on catalyst recovery. The Ruhrchemie-Rhone Poulenc process uses a water soluble phosphorus based ligand to perform hydroformylation under biphasic conditions with the hydrophobic organic products and reactants easily separable from the catalyst system. This presents an easy way to separate the products from the catalyst with minimal catalyst loss.[15] It is limited to smaller chain alkenes, however, relying upon an increased miscibility at high temperatures. Research continues into separation by other multi-phase methods including emulsions and ionic liquids.[55]

An orthogonal direction for hydroformylation process improvement is that of tandem catalysis. Rather than continue to refine a single step in a catalytic process in isolation from what occurs before and after, the catalyst system should have an expanded scope capable of catalysing the reactions either side of hydroformylation in the process. A simple example returns to the original intention of hydroformylation: the production of alcohols from a mixture of alkenes (scheme 1.6).

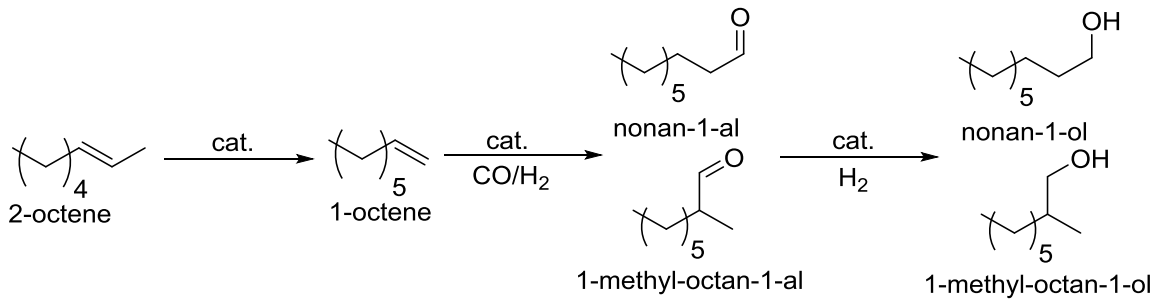

Scheme 1.8 Tandem Isomerization-Hydroformylation-Hydrogenation

Here internal olefin can undergo isomerization to the terminal alkene from which hydroformylation occurs to favour the linear aldehyde. The aldehyde is then reduced to form the linear alcohol. Often olefins come as a mixture of isomers, and over time the terminal olefin will naturally isomerise, therefore having a system capable of converting internal olefins is of great interest from a process intensification perspective.

As mentioned above, much of the progress in hydroformylation came through suppression of side-reactions, such as hydrogenation and isomerisation. Tandem catalysis returns to these reactions, but tries to control them rather than suppress them. Eilbracht wrote a comprehensive review of a majority of transformations available from hydroformylation from a synthetic organic perspective.[11]

In addition to conversion into alcohols, aldehydes are also converted into amines. An efficient process for this manipulation is the hydroaminomethylation reaction (scheme 1.7).[56] Hydroformylation and the hydrogenation of the intermediate imine/enamine are both stages that are performed by a catalyst while the condensation of the aldehyde with ammonia or primary or secondary amine is not necessarily mediated by a catalyst and occurs stoichiometricaly.

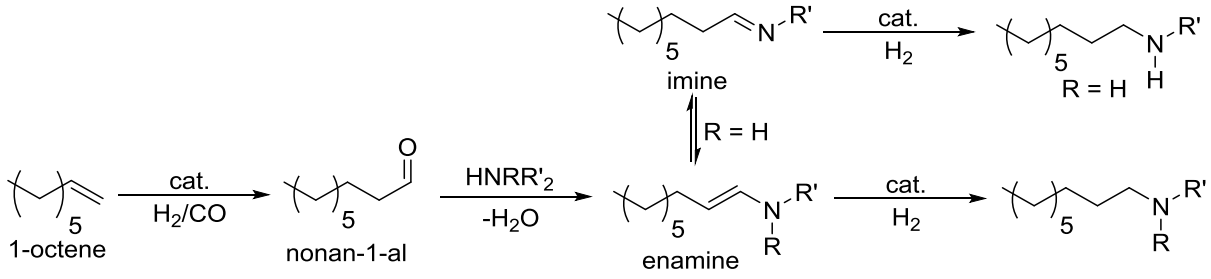

Scheme 1.9 Hydroaminomethylation cascade reaction showing hydroformylation, condensation and hydrogenation.

As Fogg and Santos note, several terms are often used interchangeably when referring to multistep processes: cascade, tandem, multifunctional and multicomponent.[5] Tandem catalysis falls into two classifications: orthogonal- and auto-. Orthogonal-tandem catalysis refers to two different catalyst systems operating in the same reaction vessel, whereas auto-tandem catalysis refers to a single catalyst system performing multiple different reactions in the same reaction vessel. Hydroaminomethylation cannot be referred to as tandem catalysis as the condensation of the amine and the aldehyde is not mediated by a catalyst and is instead referred to as a domino or cascade reaction. However, without the condensation stage the reaction resembles a tandem process and is related to the hydroformylation-hydrogenation system discussed in this thesis.

A good example of the transition from exclusively hydroformylation-orientated research to tandem catalysis emerged from the group of Piet van Leeuwen in 1999.[57] In ligand design xantphos was used as a starting point as its rigid structure and large bite angle was already shown to induce good selectivity towards linear aldehydes from terminal alkenes. Dibenzophospholyl and phenoxaphosphanyl substituents on the xantphos (figure 1.13) were proven to be effective in hydroformylation of 1-octene with turnover frequencies of up to 1100 being achieved.

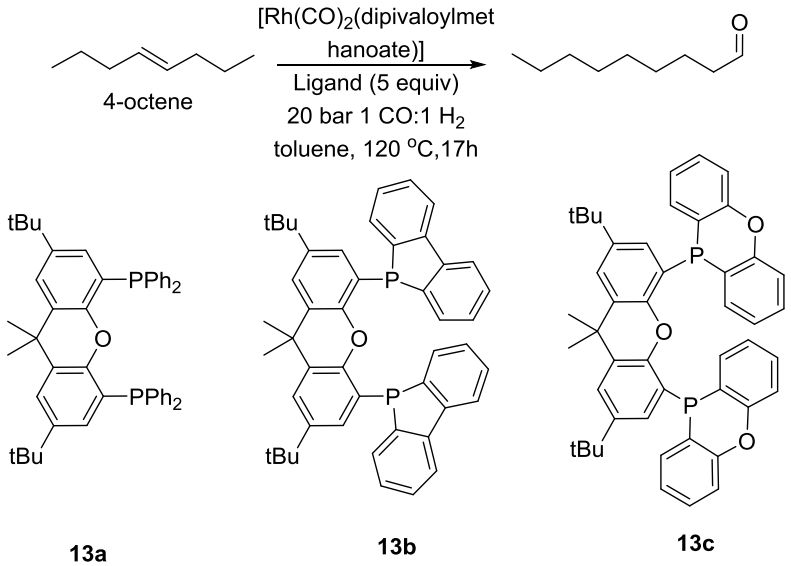

Figure 1.13 Xantphos derivatives effective in isomerization/hydroformylation auto-tandem catalysis [58]

Ligand **13c** was found to be especially effective when applied to 2-octene and 4-octene isomerisation/hydroformylation. In 4-octene hydroformylation at 120°C and 2 bar of 1:1 $CO:H_2$ 67% of 4-octene was converted after 17 hours; the l:b ratio was 4.4 and the yield of 1-

nonanal was 81% but with poor turnover frequencies of 20 h^{-1}. No hydrogenation products were reported.

David Cole-Hamilton at St Andrews has also been active in the area of auto-tandem catalysis. In 1996, he discovered that when a highly σ-donating alkyl phosphine ligand is used to perform hydroformylation in an alcohol solvent, the reduced product is formed (scheme 1.8).[59] Interestingly, when starting from the alkene there is no observation of aldehyde intermediates only the final alcohols. Yet starting from the aldehyde does also result in the reduced product. Deuterium labelling experiments revealed the mechanism for the reduction of aldehydes to be different to that of the alkene.[60]

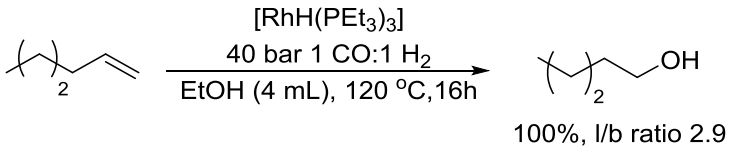

Scheme 1.10 Cole-Hamilton's hydroformylation-hydrogenation of 1-hexene[59]

The highly σ-donating alkyl ligands increase the electron density on the metal. In turn, this results in stronger π-back bonding to the carbonyl and acyl ligands. The metal acyl species is formed by insertion of the coordinated alkene into the carbonyl bond. The increased electron density in the carbonyl bond results in its protonation by the alcohol solvent. The use of trialkylphosphines alone did not produce very selective results. However, a system that mixed xantphos and the trialkylphosphine ligands resulted in improved l:b ratios 5.2 and 78% selectivity for the diol in the hydroformylation/hydrogenation of allyl alcohol.[61]

The D-labelling studies rely on the observation that the yields of $C_4H_9CHDCH_2CD_2OH/D$ and $C_4H_9CHDCH_2CHDOH/D$ under hydroformylation conditions in $EtOH/D_2$ produced 90% of the first and 10% of the second. $C_6H_{13}CHDOH/D$ and $C_6H_{13}CH_2OH/D$ were produced from the hydrogenation of heptanal in yields of 39% and 61% under the same conditions as the hydroformylation. The different ratios indicate that the alcohol is produced as a direct product in the hydroformylation-hydrogenation and does not go through an intermediate aldehyde. If the aldehyde was an intermediate then the ratio would be similar to the run in heptanal.[59]

Zhang applied the tetraphosphine ligand that was extremely successful at hydroformylation (figure 12) to hydroaminomethylation to produce excellent amine selectivity from internal olefins (figure 1.14).[62]

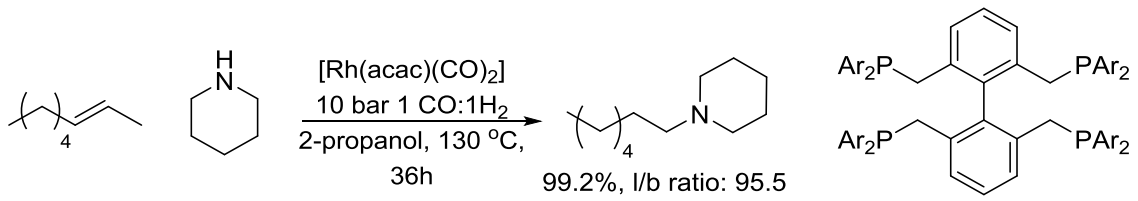

Figure 1.14 Tetraphos-catalysed HAM of internal olefins.[62]

Interestingly, a crucial difference between the hydroformylation reactions and the hydroaminomethylation reactions is a change in solvent system. Zhang's hydroformylation reactions are run in toluene and the hydroaminomethylation reactions run in pure isopropanol, which was selected after screening for methanol and ethanol. This shows that developing an auto-tandem catalysis system often requires an intensive screening of the parameters outside of the catalyst.

Another prolific chemist operating in this area is Matthias Beller at the University of Rostock. In 2002, Beller investigated the hydroaminomethylation of internal olefins using a NAPHOS ligand with different electron withdrawing substituents on the aromatic rings (figure 1.15).[63]

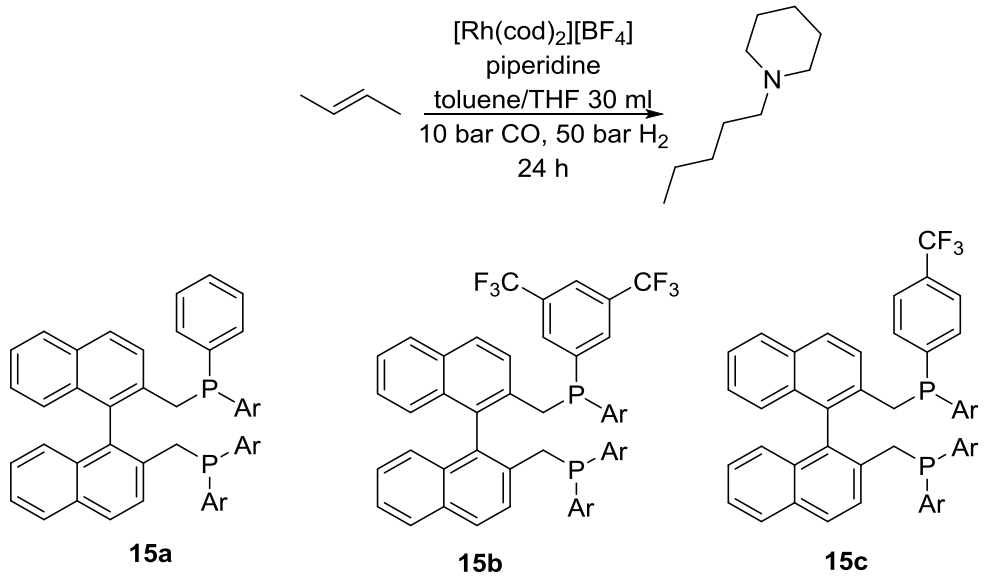

Figure 1.15 HAM catalysed by NAPHOS ligands. [63]

With the meta-substituted ligand, **15b**, 100% of the 2-butene was converted into 97% amine when piperidine was used as a substrate.[63] In comparison to standard hydroformylation, the $CO:H_2$ is heavily skewed towards H_2. Higher temperatures were found to favour higher amine selectivity but l/b ratio peaked at 9 at 120 °C. When applied to 3-hexene 88% was converted with a linear selectivity of 68%. Turnover numbers were reported as 563. Beller has also

investigated ruthenium-catalysed, domino hydroformylation/reduction reactions using nitrogen/phosphorus ligands (figure 1.16). [64]

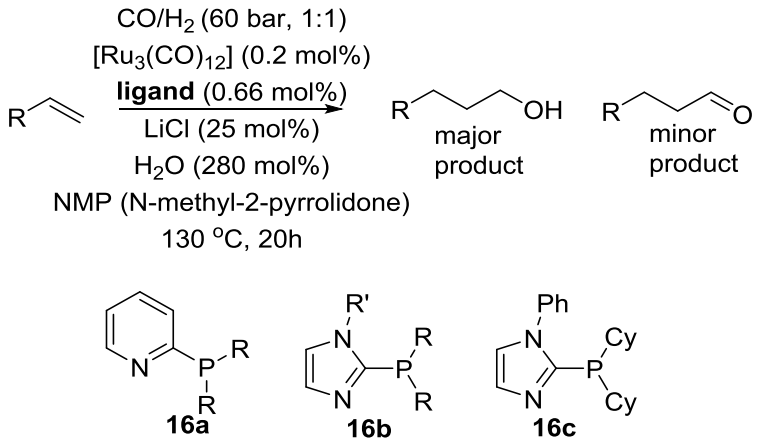

Figure 1.16 Mixed valence phosphorus/nitrogen compounds for hydroformylation-hydrogenation

The reaction conditions are shown in figure 9. For the majority of aliphatic alkenes yields of the alcohol exceeded 80% with a l/b ratio of 8. A small amount of the aldehyde remained, 3-4%, and 6% of hydrogenated starting material was detected. Applying the system to 2-octene, a 59% yield of alcohol was reported with a l:b ratio of 1.9. This is an improvement on the l:b ratio of the intermediate aldehyde detected which is 1.3. Addition of H_2O was based on the research of Philippe Kalck [65] and lithium chloride based on Haukka's work. [66] Nozaki, with support from the Mitsubishi Chemical Company, used a bulky diphosphite and a mix of ruthenium and rhodium complexes to perform isomerization/hydroformylation and hydrogenation.[67]

In addition to the rhodium and ruthenium systems, Beller also performed tandem isomerization and hydroformylation with a palladium system.[68] In hydroformylation of 1-octene, xantphos was found to be ineffective, in this case favouring hydrogenation over hydroformylation. Better results were obtained with the phosphorus and nitrogen mixed-donor ligands used in the ruthenium system. The system was shown to be effective in hydroformylation of internal alkenes. Lenero at Shell also investigated palladium catalysed isomerization/ hydroformylation.[69]

Bernhard Breit used a supramolecular ligand cage constructed around a rhodium metal center to perform tandem hydroformylation/hydrogenation of alkenes (figure 1.17). [70] [71]

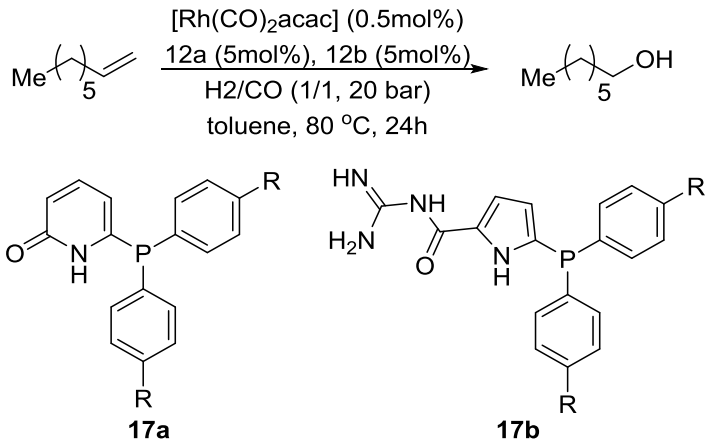

Figure 1.17 Bernhard Breit's ligands for supramolecular catalysis

As can be seen in figure 12 Breit's conditions are standard hydroformylation conditions, but a combination of **17a** and **17b** produces 99% alcohol in a >95% yield. Linear to branched ratios of the alcohol are > 9. Much like David-Cole Hamilton's xantphos/ triethylphosphine joint ligand system Breit's system is effective due to cooperative ligand effects. **17a** is effective at hydroformylation while **17b** is effective at hydrogenation. The many H-bond donor sites on the guanidine unit of ligand **17b** are capable of coordinating and reducing the aldehyde. The system was proven to be effective at performing the hydroformylation of different substrates with many different functional groups and chain lengths.

Armin Börner has also reported work in the area of isomerization/hydroformylation tandem reactions and has recently published a review of the area.[72] In 2001, Börner and Selent investigated isomerisation/hydroformylation using ligands that resemble the successful phosphites first used by UCC (figure 1.18).[73]

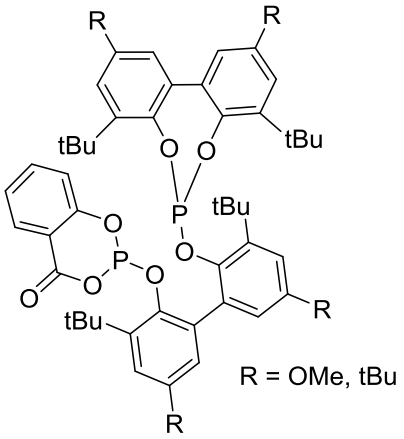

Figure 1.18 Armin Börner's ligand design

While the tandem catalysis systems discussed are good examples of new developments, there is a lack of mechanistic investigations into tandem catalysis. However, Kalck and co-workers have carried out some studies through spectroscopic means. Of particular interest to the field of tandem catalysis are two reports published in 2012. These concern rhodium-catalysed hydroaminomethylation and seek to understand the origin of the multiple catalysis activity. [74] [75]

As discussed, hydroaminomethylation consists of a metal-catalysed hydroformylation and hydrogenation either side of a condensation. The hydroformylation is catalysed by mainly neutral species, and so in hydroformylation usually neutral precursors are used eg. $[Rh(CO)_2(acac)]$. Hydrogenation is catalysed by a cationic species so an appropriate precursor is $[Rh(CO)_2(cod)][BF_4]$. With a simple diphosphine ligand, Kalck studied the transformation between the cationic and the neutral species (figure 1.19).

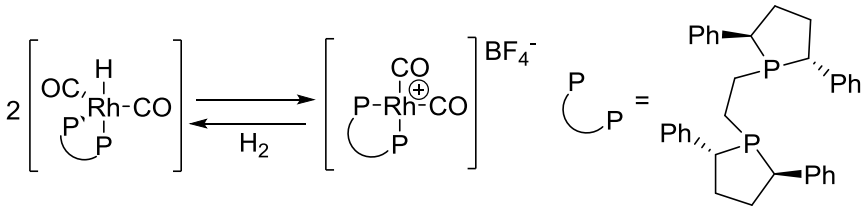

Figure 1.19 Kalck's investigations in the interconversion of cationic and neutral species.[74]

Going from the cationic species to the neutral species requires the addition of a hydride from H_2. This can be through oxidative addition or heterolysis mediated by a ligand, the counter-ion or an external Lewis base to accept the H^+. In the absence of base, no neutral monohydride species is observed. The most conclusive result was gained from DFT calculations, which revealed the energy barrier for amine acting as base is lowered and becomes feasible when a polar solvent is used.

The reverse mechanism is proposed to involve protonation of the transition metal hydride centre followed by a reductive elimination of the hydrogen. Addition of a Lewis acid generated the neutral species but the presence of the protonated amine did not. Of interest is that the cationic species was observed from $[Rh(acac)(CO)_2]$ with acac acting as a counter-ion.

1.4 Vogt Group Auto-Tandem Catalysis Systems

Tandem catalysis processes have also been investigated by the Vogt group for several years. In 2008 an investigation into hydroaminomethylation using an ionic liquid as a solvent and a rhodium complexed with a water-soluble xantphos ligand was carried out.[76] Following this

result hydroaminomethylation using a xantphos phosphoramidite ligand (figure 1.20) was investigated.[77]

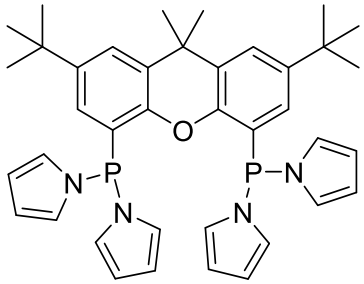

Figure 1.20 Dipyrrolylxantphos ligand (DPX) for use in hydroaminomethylation

Several ancillary studies into different aspects of hydroaminomethylation were carried out by Olivier Diebolt in the Vogt group. The result was that several new tandem catalytic pathways were discovered. Standard hydroaminomethylation conditions with a cationic rhodium source uncovered that the best selectivities and activities were obtained in alcoholic solvents (Scheme 1.9). Excluding the amine resulted in the formation of acetals with selectivities of >90%. Also observed was a significant amount of hydrogenation activity, especially in the case of DPX at 22.6% octane. The l/b ratio when xantphos is used was 42.3.[78]

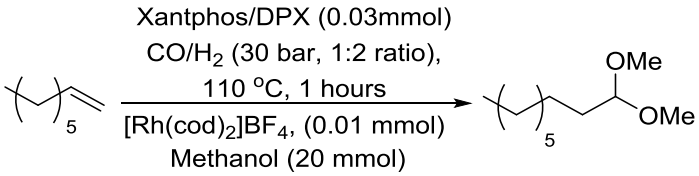

Scheme 1.11 Selective formation of acetals under hydroformylation conditions [78]

Other parameters were investigated. Of relevance to Kalck's work is the observation that [Rh(acac)$(CO)_2$] as a precursor produces only 44.5% acetal. HBF_4 itself was found to show good acetalisation activity. Lower pressures led to a higher l/b ratio of the acetals. Lower temperatures led to a lower conversion of the alkenes. Both of these results are observed for hydroformylation systems. When no ligand is present the reaction produces 15% octane and although conversion is low (49.7%) selectivity remains high, 95.6%.

The second system is related to the first. This time the neutral precursor [Rh(acac)$(CO)_2$] in the presence of a 10% water:alcohol solution and xantphos at elevated temperatures produced alcohols (scheme 1.10). [79]

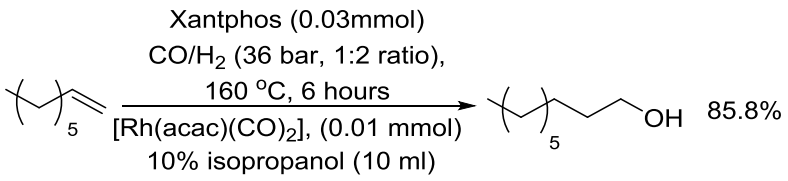

Scheme 1.12 On-water production of alcohols from olefins

The highest l/b ratio for the alcohol is 15 under optimized conditions, which features a low temperature (110 °C) hydroformylation with no hydrogenation activity observed. Hydrogenation activity only occurs at elevated temperatures of 160 °C. The use of PBu_3 as a ligand, instead of xantphos, does still produce alcohols as products but the l:b ratio dramatically falls and the amount of hydrogenated starting material also increases from 2.8% to 9.9%. When PBu_3 was used as a ligand in the acetal studies, acetal formation was suppressed and 20% alcohols and 75% aldehydes were observed. The mechanism of this system is unknown and syn-gas normally poisons hydrogenation systems. Uncovering and expanding the scope of the hydroformylation-hydrogenation reaction is the focus of this thesis.

1.5 Aims and Objectives

To meet the twin challenges of increased demand and decreased emissions the chemical industry has significantly improved the efficiency of hydroformylation systems. However to continue to meet these ambitions the efficiency of the overall process must be improved by auto-tandem catalysis: ideally isomerisation-hydroformylation-hydrogenation. A system that is capable of doing hydroformylation-hydrogenation has been reported however it requires further investigation to determine the mechanism by which the hydrogenation occurs.

The aim of the first half of this thesis is to investigate the 'on-water' hydroformylation-hydrogenation system previously published by the Vogt group. Studying any homogeneous catalytic reaction *in situ* is challenging so the first approach will be to study the influence of changing reaction parameters such as; solvent; temperature; ligands; catalyst precursor on the aldehyde selectivity, the alcohol selectivity, the l/b ratio of the aldehyde and the l/b ratio of the alcohol.

Following this reaction screening, reaction profiles will be constructed by sampling during the hydroformylation-hydrogenation reaction. High-temperature ^{1}H NMR and ^{31}P NMR spectroscopic studies will be presented to explore if the identity of the active hydrogenation catalyst can be determined. Finally the entirety of the results will be considered together and several possible catalytic cycles for the hydroformylation-hydrogenation reaction will be

presented. The screenings, the high pressure NMR experiments and the proposed cycles will form chapter 2.

The second part of this thesis, chapter 3, will concern a molecular-weight-enlarged Sn catalyst and phosphonium iodide co-catalyst for membrane filtration catalysis. The target reaction is the coupling of epoxides and CO_2 to form cyclic carbonates. A short discussion of the relevant literature will be followed by a discussion of the molecules themselves. Investigations on the coupling of CO_2 with several epoxides and then a test cat-in-a-cup experiment will be performed.

1.6 References

[1] M. Hadhri, in *Chemical Industry Profile Chapter*, Avenue E Van Nieuwenhuyse 4, B - 1160 Brussels, Belgium, **2016**.

[2] R. Cayuela Valencia, in *The Future of the Chemical Industry by 2050*, Wiley-VCH Verlag GmbH & Co. KGaA, **2013**, pp. 163-200.

[3] R. H. Crabtree, *The Organometallic Chemistry of the Transition Metals*, 4th ed., John Wiley & Sons, Inc., Hoboken, New Jersey, **2005**.

[4] W. Grünert, *Angew. Chem. Int. Ed.* **2012**, *51*, 5289-5289.

[5] D. E. Fogg, E. N. dos Santos, *Coord. Chem. Rev.* **2004**, *248*, 2365-2379.

[6] M. Janssen, C. Muller, D. Vogt, *Green Chemistry* **2011**, *13*, 2247-2257.

[7] O. Roelen, (Ed.: C. V. mbH), Germany **1938/1952**.

[8] B. Cornils, W. A. Herrmann, M. Rasch, *Angew. Chem. Int. Ed.* **1994**, *33*, 2144-2163.

[9] R. Tudor, *Platinum Met. Rev.* **2007**, *51*.

[10] R. Franke, D. Selent, A. Börner, *Chem. Rev.* **2012**, *112*, 5675-5732.

[11] P. Eilbracht, L. Bärfacker, C. Buss, C. Hollmann, B. E. Kitsos-Rzychon, C. L. Kranemann, T. Rische, R. Roggenbuck, A. Schmidt, *Chem. Rev.* **1999**, *99*, 3329-3366.

[12] F. Fischer, H. Tropsch, Google Patents, **1930**.

[13] E. T. A. van Driessche, R. D. Garton, R. F. Caers, in *ExxonMobil Chemical Patents*, **2011**.

[14] aH. Hieber, Z. Schulten, *Z. Anorg. Allg. Chem* **1937**, *232*, 29; bH. Hieber, Z. Schulten, *Z. Allg. Anorg. Chem.* **1937**, *232*, 17.

[15] H. Bahrmann, C. D. Frohning, P. Heymanns, H. Kalbfell, P. Lappe, D. Peters, E. Wiebus, *J. Mol. Catal. A: Chem.* **1997**, *116*, 35-37.

[16] aJ. Berty, L. Marko, *Acta Chim. Acad. Sci. Hung* **1953**, *3*, 177; bG. Natta, *Brennst. Chem.* **1955**, *36*, 176.

[17] R. F. Heck, D. S. Breslow, *J. Am. Chem. Soc.* **1961**, *83*, 4023-4027.

[18] L. Kirch, M. Orchin, *J. Am. Chem. Soc.* **1958**, *80*, 4428-4429.

[19] L. G. Canell, L. H. Slaugh, R. D. Mullineaux, (Ed.: G. P. DE), Shell Internationale Research **1965**.

[20] E. R. E. CO, **1958**.

[21] J. A. Osborn, F. H. Jardine, J. F. Young, G. Wilkinson, *Journal of the Chemical Society A: Inorganic, Physical, Theoretical* **1966**, 1711-1732.

[22] L. Vaska, R. E. Rhodes, *J. Am. Chem. Soc.* **1965**, *87*, 4970-4971.

[23] D. Evans, J. A. Osborn, G. Wilkinson, *Journal of the Chemical Society A: Inorganic, Physical, Theoretical* **1968**, 3133-3142.

[24] J. M. Brown, A. G. Kent, *Journal of the Chemical Society, Perkin Transactions 2* **1987**, 1597-1607.

[25] aP. Pino, A. Major, F. Spindler, R. Tannenbaum, G. Bor, Istaván, T. Horváth, *J. Organomet. Chem.* **1991**, *417*, 65-76; bP. Pino, *Ann. N.Y. Acad. Sci.* **1983**, *415*, 111-128.

[26] Nobelprize.org, **1973**.

[27] P. W. N. Van Leeuwen, *Rhodium Catalyzed Hydroformylation, Vol. 22*, Kluwer Academic Publishers, 3300 AA Dordrecht, The Netherlands, **2000**.

[28] R. H. Crabtree, *The Organometallic Chemistry of the Transition Metals*, John Wiley & Sons, Canada, **2001**.

[29] M. Calvin, M. Polanyi, *Transactions of the Faraday Society* **1938**, *34*, 1181-1191.

[30] C. A. Tolman, *Chem. Rev.* **1977**, *77*, 313-348.

[31] M. Kranenburg, Y. E. M. van der Burgt, P. C. J. Kamer, P. W. N. M. van Leeuwen, K. Goubitz, J. Fraanje, *Organometallics* **1995**, *14*, 3081-3089.

[32] R. L. Pruett, J. A. Smith, *The Journal of Organic Chemistry* **1969**, *34*, 327-330.

[33] E. Billig, A. G. Abatjoglou, D. R. Bryant, (Ed.: U. C. Corporation), **1987**.

[34] M. Roper, P. M. Lorz, D. Koeffer, in *Chem. Abstr, Vol. Ger. Offen DE 4,204,808* (Ed.: BASF), **1994**.

[35] P. M. Burke, J. M. Garner, W. Tam, K. A. Kreutzer, A. J. J. Teunissen, (Ed.: DSM/DuPont), **1997**.

[36] K. Sato, Y. Kawaragi, M. Takai, T. Ookoshi, (Ed.: Mitsubishi), **1993**.

[37] P. W. N. M. van Leeuwen, C. F. Roobeek, *J. Organomet. Chem.* **1983**, *258*, 343-350.

[38] G. J. H. Buisman, P. C. J. Kamer, P. W. N. M. van Leeuwen, *Tetrahedron: Asymmetry* **1993**, *4*, 1625-1634.

[39] T. Jongsma, G. Challa, P. W. N. M. van Leeuwen, *J. Organomet. Chem.* **1991**, *421*, 121-128.

[40] H. Tricas, O. Diebolt, P. W. N. M. van Leeuwen, *J. Catal.* **2013**, *298*, 198-205.

[41] O. Diebolt, H. Tricas, Z. Freixa, P. W. N. M. van Leeuwen, *ACS Catalysis* **2012**, *3*, 128-137.

[42] W. Hewertson, H. R. Watson, *Journal of the Chemical Society (Resumed)* **1962**, 1490-1494.

[43] G. Consiglio, C. Botteghi, C. Salomon, P. Pino, *Angewandte Chemie International Edition in English* **1973**, *12*, 669-670.

[44] O. R. Hughes, J. D. Unruh, *J. Mol. Catal.* **1981**, *12*, 71-83.

[45] W. Cornely, B. Fell, *J. Mol. Catal.* **1982**, *16*, 89-94.

[46] O. R. Hughes, D. A. Young, *J. Am. Chem. Soc.* **1981**, *103*, 6636-6642.

[47] Z. Freixa, P. W. N. M. van Leeuwen, *Dalton Transactions* **2003**, 1890-1901.

[48] M. Schreuder Goedheijt, P. C. J. Kamer, P. W. N. M. van Leeuwen, *J. Mol. Catal. A: Chem.* **1998**, *134*, 243-249.

[49] S. C. van der Slot, J. Duran, J. Luten, P. C. J. Kamer, P. W. N. M. van Leeuwen, *Organometallics* **2002**, *21*, 3873-3883.

[50] S. Yu, X. Zhang, Y. Yan, C. Cai, L. Dai, X. Zhang, *Chemistry – A European Journal* **2010**, *16*, 4938-4943.

[51] C. Cai, S. Yu, G. Liu, X. Zhang, X. Zhang, *Adv. Synth. Catal.* **2011**, *353*, 2665-2670.

[52] O. Diebolt, P. W. N. M. van Leeuwen, P. C. J. Kamer, *ACS Catalysis* **2012**, *2*, 2357-2370.

[53] J. Zhang, M. Poliakoff, M. W. George, *Organometallics* **2003**, *22*, 1612-1618.

[54] C. P. Casey, L. M. Petrovich, *J. Am. Chem. Soc.* **1995**, *117*, 6007-6014.

[55] S. M. Mercer, T. Robert, D. V. Dixon, P. G. Jessop, *Catalysis Science & Technology* **2012**, *2*, 1315-1318.

[56] W. Reppe, H. Vetter, *Justus Liebigs Annalen der Chemie* **1953**, *582*, 133-161.

[57] L. A. van der Veen, P. C. J. Kamer, P. W. N. M. van Leeuwen, *Angew. Chem. Int. Ed.* **1999**, *38*, 336-338.

[58] E. Zuidema, P. E. Goudriaan, B. H. G. Swennenhuis, P. C. J. Kamer, P. W. N. M. van Leeuwen, M. Lutz, A. L. Spek, *Organometallics* **2010**, *29*, 1210-1221.

[59] J. K. MacDougall, M. C. Simpson, M. J. Green, D. J. Cole-Hamilton, *J. Chem. Soc., Dalton Trans.* **1996**, 1161-1172.

[60] P. Cheliatsidou, D. F. S. White, D. J. Cole-Hamilton, *Dalton Transactions* **2004**, 3425-3427.

[61] I. I. F. Boogaerts, D. F. S. White, D. J. Cole-Hamilton, *Chem. Commun.* **2010**, *46*, 2194-2196.

[62] G. Liu, K. Huang, B. Cao, M. Chang, S. Li, S. Yu, L. Zhou, W. Wu, X. Zhang, *Org. Lett.* **2012**, *14*, 102-105.

[63] A. Seayad, M. Ahmed, H. Klein, R. Jackstell, T. Gross, M. Beller, *Science* **2002**, *297*, 1676-1678.

[64] I. Fleischer, K. M. Dyballa, R. Jennerjahn, R. Jackstell, R. Franke, A. Spannenberg, M. Beller, *Angew. Chem. Int. Ed.* **2013**, *52*, 2949-2953.

[65] P. Kalck, M. Siani, J. Jenck, B. Peyrille, Y. Peres, *J. Mol. Catal.* **1991**, *67*, 19-27.

[66] M.-L. Kontkanen, L. Oresmaa, M. A. Moreno, J. Jänis, E. Laurila, M. Haukka, *Applied Catalysis A: General* **2009**, *365*, 130-134.

[67] Y. Yuki, K. Takahashi, Y. Tanaka, K. Nozaki, *J. Am. Chem. Soc.* **2013**, *135*, 17393-17400.

[68] R. Jennerjahn, I. Piras, R. Jackstell, R. Franke, K.-D. Wiese, M. Beller, *Chemistry – A European Journal* **2009**, *15*, 6383-6388.

[69] D. Konya, K. Q. Almeida Leñero, E. Drent, *Organometallics* **2006**, *25*, 3166-3174.

[70] L. Diab, T. Šmejkal, J. Geier, B. Breit, *Angew. Chem. Int. Ed.* **2009**, *48*, 8022-8026.

[71] D. Fuchs, G. Rousseau, L. Diab, U. Gellrich, B. Breit, *Angew. Chem. Int. Ed.* **2012**, *51*, 2178-2182.

[72] M. Vilches-Herrera, L. Domke, A. Börner, *ACS Catalysis* **2014**, *4*, 1706-1724.

[73] D. Selent, D. Hess, K.-D. Wiese, D. Röttger, C. Kunze, A. Börner, *Angew. Chem. Int. Ed.* **2001**, *40*, 1696-1698.

[74] D. Crozet, D. McKay, C. Bijani, A. Gual, C. Godard, C. Claver, L. Maron, M. Urrutigoity, P. Kalck, *Dalton Transactions* **2012**, *41*, 3369-3373.

[75] D. Crozet, A. Gual, D. McKay, C. Dinoi, C. Godard, M. Urrutigoïty, J.-C. Daran, L. Maron, C. Claver, P. Kalck, *Chemistry – A European Journal* **2012**, *18*, 7128-7140.

[76] B. Hamers, P. S. Bäuerlein, C. Müller, D. Vogt, *Adv. Synth. Catal.* **2008**, *350*, 332-342.

[77] B. Hamers, E. Kosciusko-Morizet, C. Müller, D. Vogt, *ChemCatChem* **2009**, *1*, 103-106.

[78] O. Diebolt, C. Cruzeuil, C. Müller, D. Vogt, *Adv. Synth. Catal.* **2012**, *354*, 670-677.

[79] O. Diebolt, C. Muller, D. Vogt, *Catalysis Science & Technology* **2012**, *2*, 773-777.

Chapter 2: 'On-Water' Hydroformylation-Hydrogenation

2.1 Introduction

As discussed in chapter 1 auto-tandem catalysis presents a way for the chemical industry to increase productivity whilst decreasing waste. Building on an extensive amount of hydroformylation research new rhodium-based systems have been developed: isomerisation-hydroformylation can be catalysed by phenoxaphosphanyl xantphos like ligands [1] and hydroformylation-hydrogenation can be catalysed by supramolecular assemblies.[2] Hydroaminomethylation produces amines by a pathway involving rhodium catalysed hydroformylation and hydrogenation.[3]

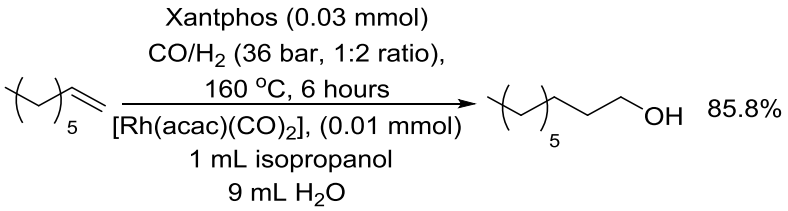

Scheme 2.1 'On-water' hydroformylation-hydrogenation

Investigations into hydroaminomethylation by the Vogt group resulted in the discovery of a system that performs hydroformylation and hydrogenation under syn-gas conditions with good selectivity (scheme 2.1).[4] The following investigations seek to uncover the mechanism by which this occurs. In addition, the investigations will establish if there is a beneficial effect to the addition of water. The investigations take the form of catalytic screenings, reaction profiles and high pressure and temperature NMR experiments. The chapter ends with several possible catalytic cycles being proposed from the data gathered and based on results from literature.

2.2 On-water hydroformylation/hydrogenation reaction screenings

The investigations began by establishing a successful hydroformylation system, then developing the extra catalyst steps and 'on-water' effects from there. One of the most successful ligands in hydroformylation and hydroaminomethylation is xantphos so this was selected as the primary ligand for the initial studies. 1-octene was selected as the standard substrate for comparison to literature and previous substrate studies by Diebolt had shown this to be most compatible with the 'on-water' hydroformylation/hydrogenation system.

The potential products include hydrogenation of the alkene (scheme 2.2), isomerization of the alkene (scheme 2.3), and the formation of a linear and a branched aldehyde as a consequence of hydroformylation (scheme 2.4).

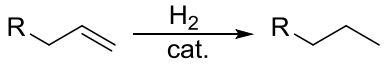

Scheme 2.2 Alkene hydrogenation

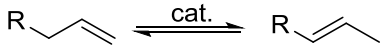

Scheme 2.3 Alkene isomerization

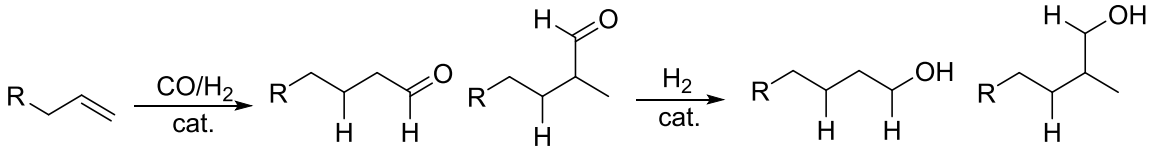

Scheme 2.4 Potential products in hydroformylation-hydrogenation

The parameters that were investigated include: temperature; the presence and volume of the water co-solvent; the number of equivalents of ligand; the gas ratio; the addition of alcohols; the catalyst precursor; the ligands used (monodentate and bidentate); the addition of extra ligands; and the amount of water added.

The results are presented in graphical format and are comprised of an average of duplicate runs. The conversions and selectivities were calculated by comparison to an internal standard of decane by methods outlined in the materials and methods section.

2.2.1 Effect of temperature on hydroformylation-hydrogenation

The success of xantphos as a ligand for hydroformylation is due to its high regio-selectivity for the linear aldehyde. In the first study of hydroformylation with xantphos, van Leeuwen demonstrated a l/b ratio (linear aldehydes/branched aldehydes) of 35 (figure 2.1).[5] Also provided are results from Hughes and Unruh with dppe (diphenylphosphinoethane) as a ligand (figure 2.1).[6]

Figure 2.1 Literature examples of hydroformylation

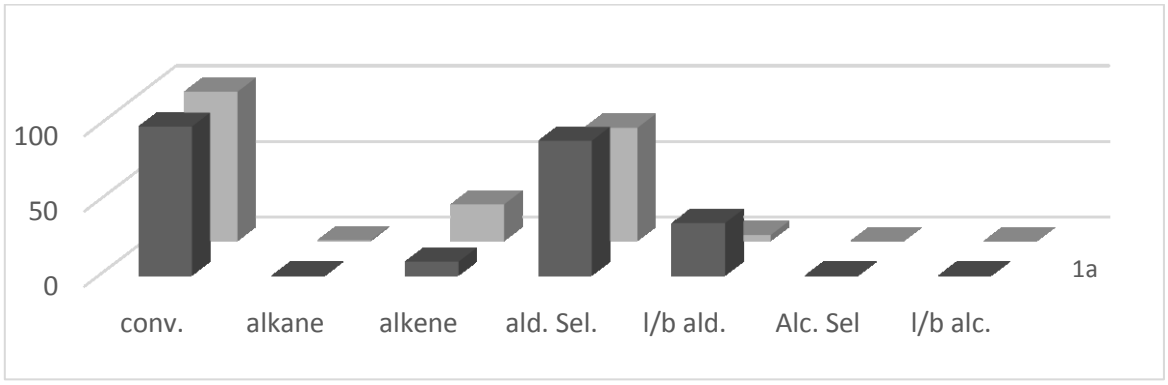

Conditions: 1[a] $[Rh(acac)(CO)_2]$ (0.15 mol%), xantphos (0.3 mol%), Rh/P (1:4.4), 1-octene (0.56 mL, 3.6 mmol), n-decane (std),) toluene (3 mL), T (80 °C), P (10 bar), $CO:H_2$ 1:1. [b] $[HRh(CO)(PPh_3)_3]$ (0.13 mol%), dppe (0.6 mol%), Rh/P (1:5.0), 1-hexene (9.0 mL, 159 mmol), benzene (std), toluene (75 mL), T (105°C), P (8 bar), $CO:H_2$ 1:1

As discussed in chapter 1, and demonstrated in figure 2.1, complete conversion of 1-octene is readily accomplished, however selectivity for the desired product, nonanal, is never guaranteed, as there are always some residual b-aldehydes formed. Toluene as a solvent, temperatures of 80-110 °C and pressures of 8-10 bar result in aldehyde l/b (l/b ald) ratios of 35 for xantphos and 4 for dppe. Dppe also shows a higher amount of isomerised alkene, 24, than xantphos with accompanying lower aldehyde selectivity. Neither ligand shows alcohol formation under these conditions.

The hydroformylation reaction run in toluene was established as a benchmark for the following series of reactions. A stock solution of dicarbonyl rhodium acetoacetate precursor ($[Rh(acac)(CO)_2]$) and ligand in either toluene or toluene/isopropanol, was prepared under argon and placed in the autoclave body. The remaining solvent was then added under argon. The degassed and dried substrate and standard were placed into the addition funnel, allowing the autoclave to be pressurized without mixing the substrate and the catalyst, and added after the pre-catalyst mixture had been stirred at temperature for an hour. Allowing time for catalyst preformation results in a higher linear/branched ratio (figure 2.2) than the original xantphos experiments (figure 2.1), a procedure established by van Leeuwen in later papers.[7] After 6 hours of reaction time the autoclave was cooled and an aliquot of the organic layer was collected, dissolved in DCM and analysed by GC-FID. The water layer was not analysed as the solubility of the long chain alkane, alkene, aldehydes and alcohols was expected to be minimal at room temperature.

The first parameter investigated was the effect of temperature in a system consisting of toluene (figure 2.2).

Figure 2.2 Hydroformylation/Hydrogenation in toluene

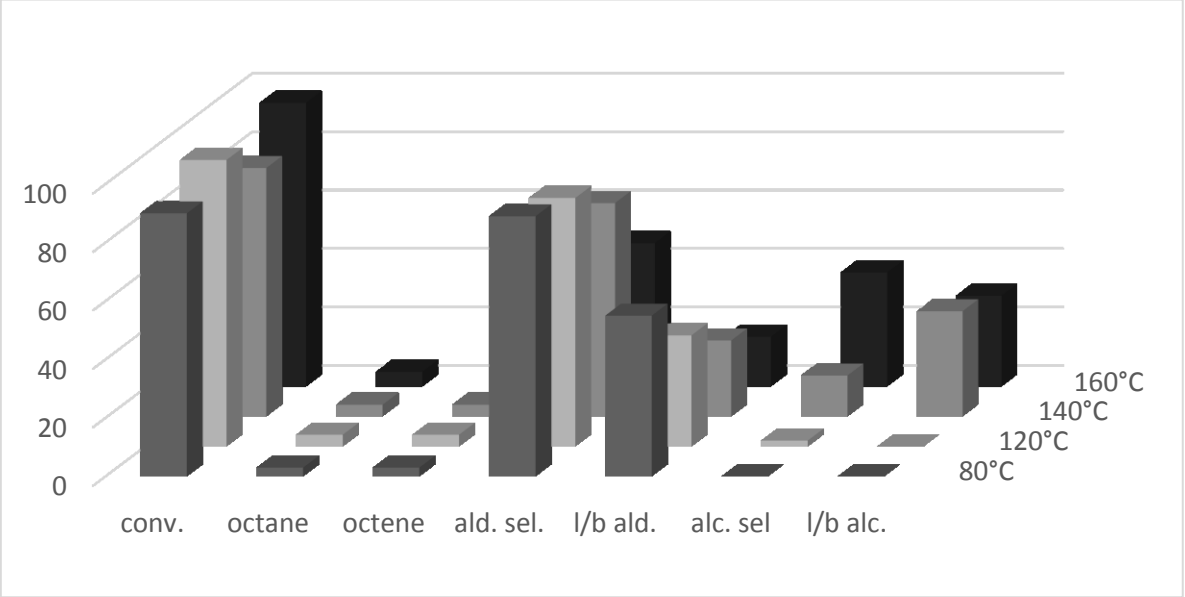

Conditions: [Rh(acac)$(CO)_2$] (2.1 mg, 0.1 mol%), xantphos (14.1 mg, 0.3 mol%), Rh/P (1:6), 1-octene (1.28 mL, 8 mmol), n-decane (0.18 mL, 1 mmol), toluene (10 mL (2 mL cat. stock + 8 mL solvent)), P (24 bar (cold)), CO:H_2 1:1 (from syn-gas bottle) , 700 rpm, t (6 hours with 1 hour preformation)

It is immediately apparent that the hydrogenation of aldehydes does not require the presence of water or alcohol solution: at 140 °C the amount of hydrogenated aldehydes becomes significant, 14%, and at 160 °C alcohol selectivity is at 39%. This disproves the initial assumption, based on the work of Diebolt, that the water is necessary for hydrogenation activity.

Previous hydroformylation research has shown that the temperature influences several competing rhodium-catalysed reactions, including hydrogenation and isomerization reactions.[8] As temperature increases, the linear to branched ratio of the aldehyde falls due to the increased rate of isomerization of the alkene, resulting in more branched aldehydes. The rate of hydrogenation of the aldehyde increases with temperature, favouring the hydrogenation of the linear aldehyde as observed in the decreased l/b ratio of the aldehyde, 38 falls to 17, and not of the alcohol, remaining above 30. The rate of hydroformylation of alkene is so much greater than the rate of hydrogenation of alkene that minimal octane is observed at all temperatures.

To supplement the reaction screenings reaction profiles of the hydroformylation-hydrogenation system in toluene at 120 ^oC and 160 ^oC were created. Creating reaction profiles is an effective way at collecting information about the system without having to resort to *in-situ* spectroscopy. The reaction profiles of Cole-Hamilton's tandem hydroformylation-hydrogenation with rhodium trialkylphosphine complexes revealed that the alcohols are formed directly from

octenes, without an aldehyde intermediate.[9] This is a different observation to the 'on-water' system which definitely showed aldehyde intermediates.[4]

2.2.1.2 Reaction profile of toluene at 120°C

From the results in figure 2.2 these are the conditions that should produce the highest amount of aldehyde products without hydrogenation products.

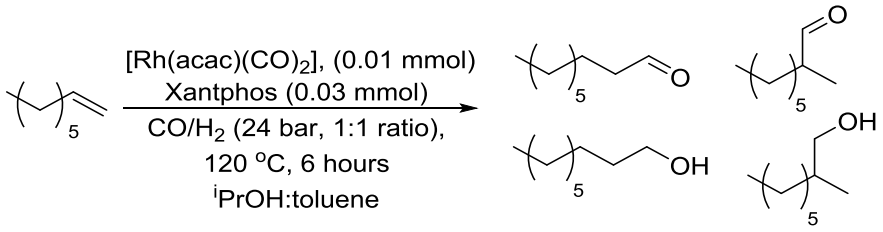

Scheme 2.5 Conditions for toluene at 120°C

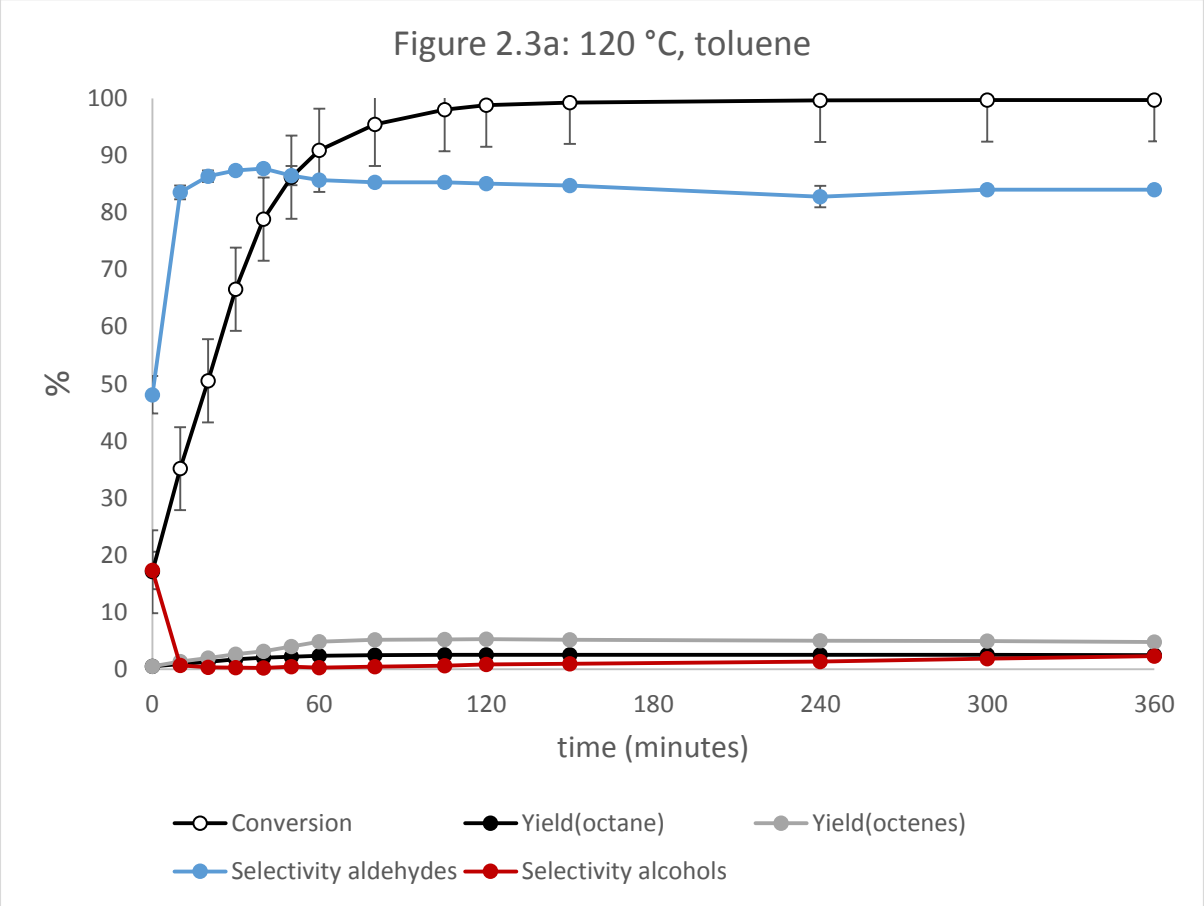

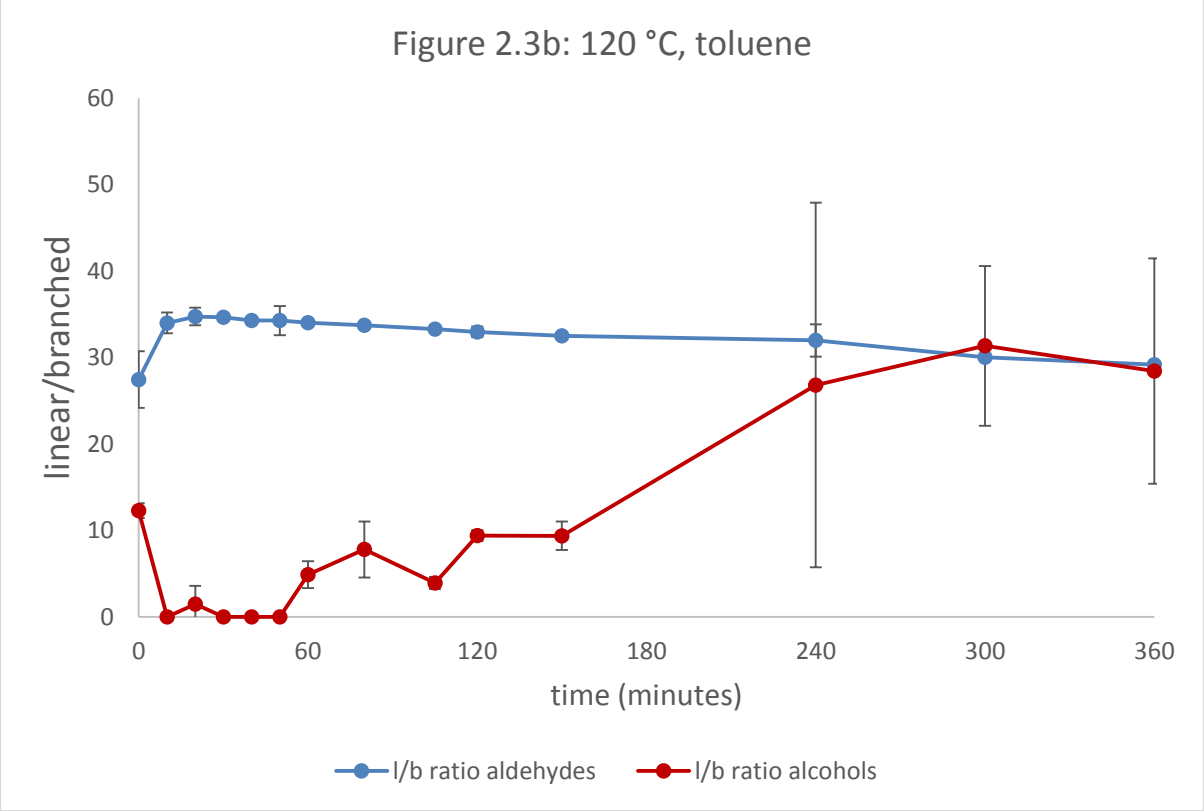

Figure 2.3a and 2.3b Conditions: [Rh(acac)$(CO)_2$] (2.1 mg, 0.1 mol%), Xantphos (14.1 mg, 0.3 mol%), Rh/P (1:6), 1-octene (1.28 mL, 8 mmol), n-decane (0.18 mL, 1 mmol), 2mL cat. stock (1mL toluene: 1mL ^{i}PrOH), toluene (8 mL), T (120 °C), P (24 bar (cold)), CO:H_2 1:1 (from syn-gas bottle) , 700 rpm, t (6 hours with 1 hour preformation)

Running the reaction in toluene at 120 °C results in a fairly fast rate of hydroformylation with complete conversion observed within 120 minutes. The selectivity for the aldehyde is immediately apparent. There is a slight increase in alcohol produced towards the end of the reaction and the sharp increase in the l/b ratio (figure 3.1b) shows that it is formation of the linear alcohol that is favoured in hydrogenation. Due to the small amount of alcohol produced the graphed l/b ratio is less neatly plotted than the aldehydes. There is a low yield of alkanes and alkenes that remains unchanged after an initial period of isomerization. The data points are the average of duplicate runs and the associated errors in the graphs are calculated by the standard deviation of this. There is a large error with the alcohol l/b ratio due to the small amount of alcohol present in the sample.

2.2.1.3 Reaction profile of toluene at 160 °C

A reaction profile was also constructed for the hydroformylation-hydrogenation in toluene at 160 °C.

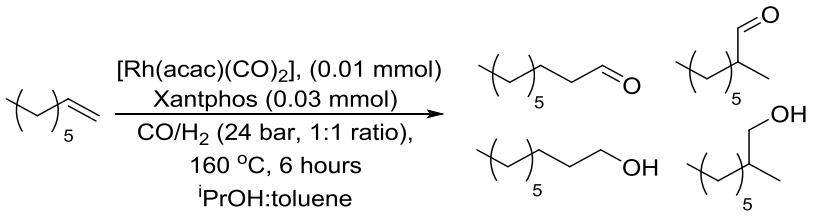

Scheme 2.6 Conditions for toluene at 160°C

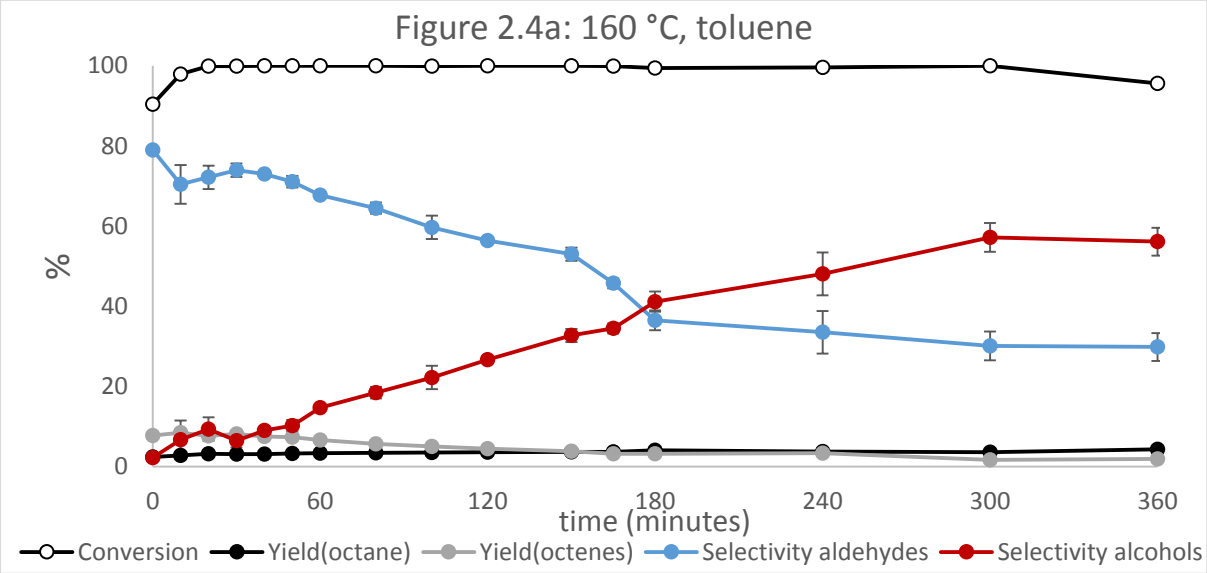

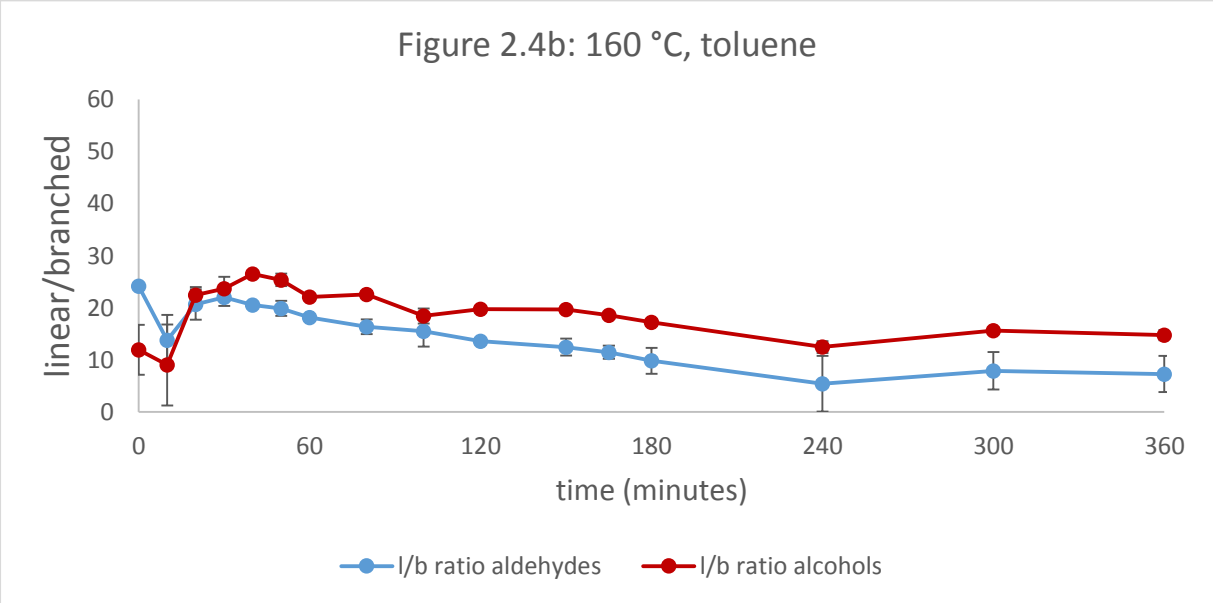

Figures 2.4a and 2.4b: Conditions: [Rh(acac)(CO)$_2$] (2.1 mg, 0.1 mol%), Xantphos (14.1 mg, 0.3 mol%), Rh/P (1:6), 1-octene (1.28 mL, 8 mmol), n-decane (0.18 mL, 1 mmol), 2 mL cat. stock (1mL toluene: 1mL ^{i}PrOH), toluene (8 mL), T (160 °C), P (24 bar (cold)), CO:H$_2$ 1:1 (from syn-gas bottle) , 700 rpm, t (6 hours with 1 hour preformation)

At higher temperatures the conversion of alkene is extremely rapid. This time by the end of the reaction there is more alcohol than aldehyde. Initially, there is a higher amount of isomerized octene than at 120 °C, as expected with the higher temperature, but this drops over time, presumably as a direct result of hydroformylation of the internal alkene, which is why the l/b ratio of the aldehyde also drops over time. The l/b ratio of the alcohol is higher than the l/b ratio of the aldehyde as it is the linear aldehyde that is preferentially hydrogenated. The l/b ratios remain in parallel and descend at the same rate. The errors with the alcohol l/b ratio are lower in figure 2.4b than in 2.3b due to a higher amount of alcohol produced although there is a larger error in the aldehyde l/b ratio due to the lower amount of this in the later stages of the reaction.

Replacing 8 mL of the toluene with 8 mL of water results in the figure 2.5.

Figure 2.5 Hydroformylation/hydrogenation in water

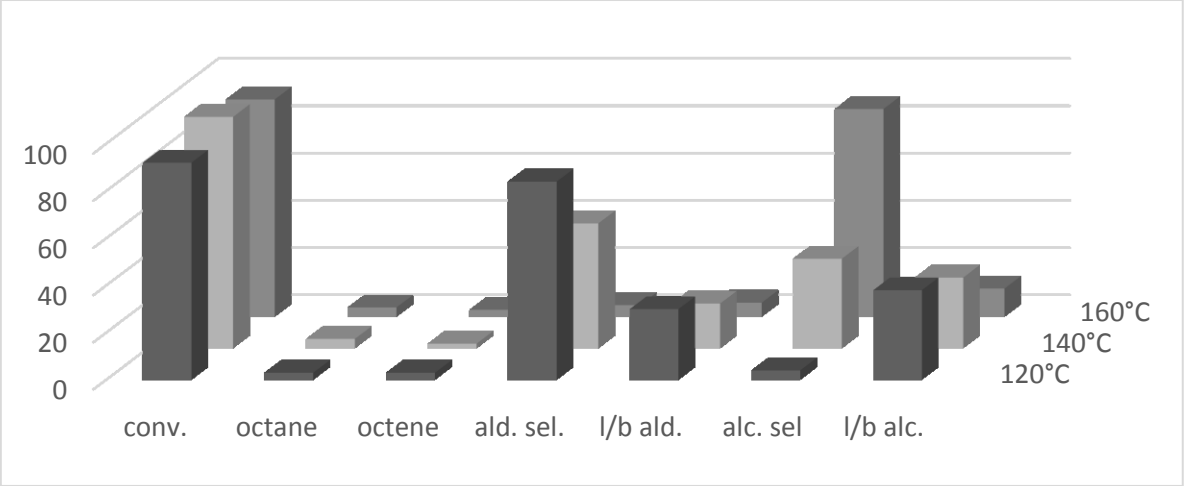

Conditions: [Rh(acac)$(CO)_2$] (2.1 mg, 0.1 mol%), xantphos (14.1 mg, 0.3 mol%), Rh/P (1:6), 1-octene (1.28 mL, 8 mmol), n-decane (0.18 mL, 1 mmol), toluene (2 mL, cat. stock), water (8 mL), T (varies), P (24 bar (cold)), CO:H_2 1:1 (from syn-gas bottle) , 700 rpm, t (6 hours with 1 hour preformation)

While the toluene only screenings (figure 2.2) demonstrated that hydrogenation activity is not exclusive to the on-water system, the results in figure 2.3 demonstrate that the addition of water increases the selectivity towards the alcohol. The reaction at 120 ˚C in water has a lower l/b ratio for the aldehyde than that in toluene. The reaction is still temperature dependent, there being no difference between 120 ˚C in toluene (figure 2.2) and in water (figure 2.3) however at 140 ºC and 160 ºC there is comparatively higher alcohol selectivity between the systems. This selectivity is much higher than the 44% in pure water reported previously by Diebolt.[4]

The l/b ratio of the aldehyde drops significantly when more of the aldehyde is hydrogenated. This may be due to a higher amount of isomerization of alkene leading to more internal alkenes being hydroformylated, building up more branched aldehydes, and more of the linear aldehyde being hydrogenated, lowering the amount of linear aldehydes. At higher temperatures, the hydroformylation of the internal alkene is driven towards completion with less opportunity for the reversal of the formation of branched acyl intermediate, which consequently forms the branched aldehyde, which is a way the l/b ratio can increase in rhodium catalysed hydroformylation, as discussed in chapter 1. [10]

2.2.1.4 Reaction profile of hydroformylation-hydrogenation in water at 120°C

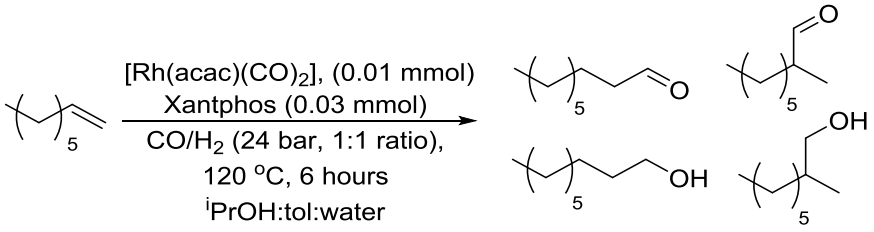

Scheme 2.7 Conditions for water at 120 °C

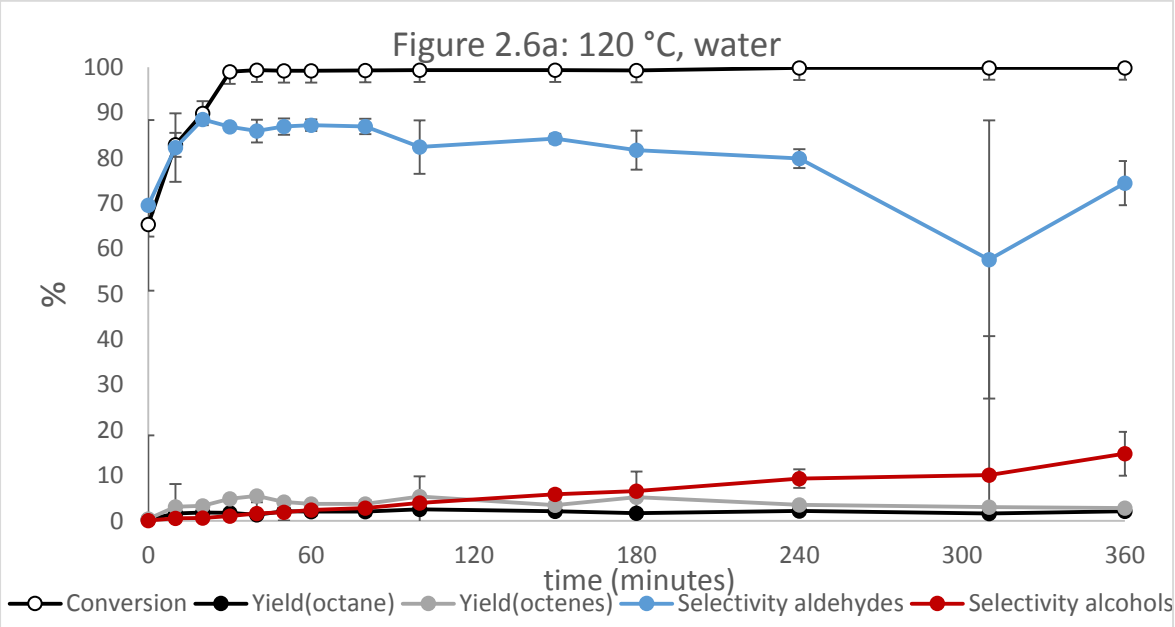

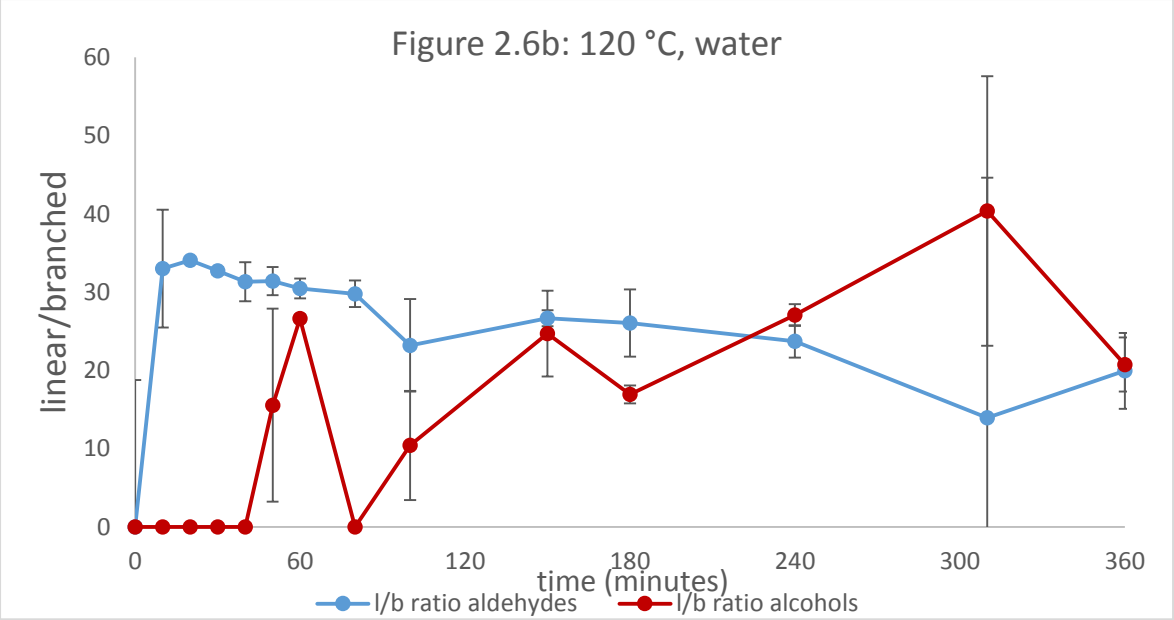

Figures 2.6a and 2.6b: Conditions: $[Rh(acac)(CO)_2]$ (2.1 mg, 0.1 mol%), Xantphos (14.1 mg, 0.3 mol%), Rh/P (1:6), 1-octene (1.28 mL, 8 mmol), n-decane (0.18 mL, 1 mmol), 2mL cat. stock (1mL toluene: 1mL ^{i}PrOH), water (8 mL), T (120 °C), P (24 bar (cold)), $CO:H_2$ 1:1 (from syn-gas bottle) , 700 rpm, t (6 hours with 1 hour preformation)

The addition of water at 120 °C shows an increase in the rate of hydroformylation, complete conversion being obtained at 50 minutes, compared to the 120 minutes in toluene. There is an increase in the rate of aldehyde hydrogenation so there is a more noticeable change in the reaction component graph. As a consequence of the hydrogenation of the aldehyde, the final l/b ratio is lower than in toluene at 120 °C. As above, at lower alcohol concentrations the data are more scattered therefore the plot of the l/b ratio is poorer than for the aldehyde, due to less products being observed. There is a small increase in the amount of isomerized octenes, compared to the toluene system: 6% vs 3%, but this falls over time as these are hydroformylated.

2.2.1.5 Reaction profile of hydroformylation-hydrogenation in water at 160°C

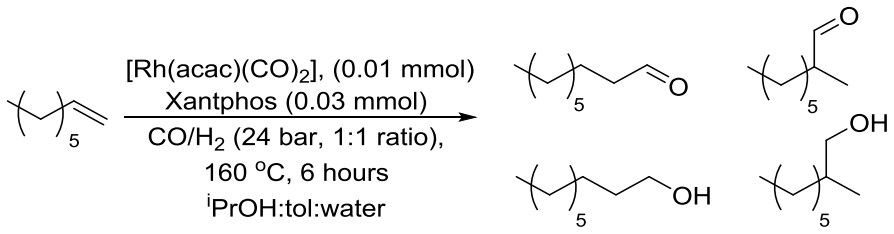

Scheme 2.8 Conditions for water at 160 °C

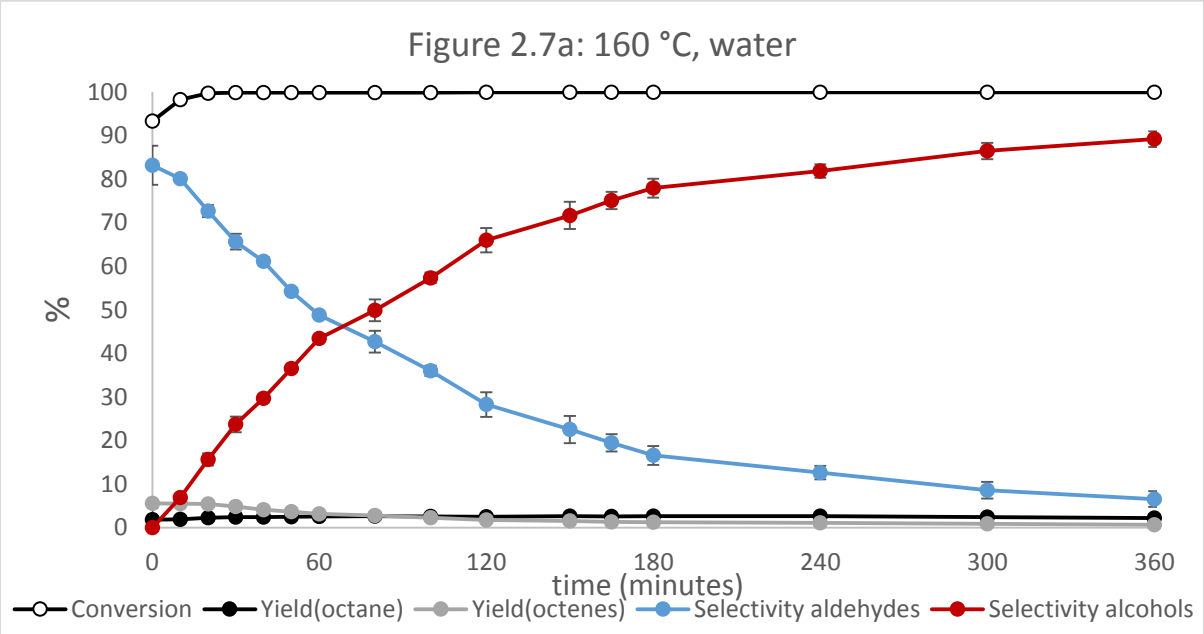

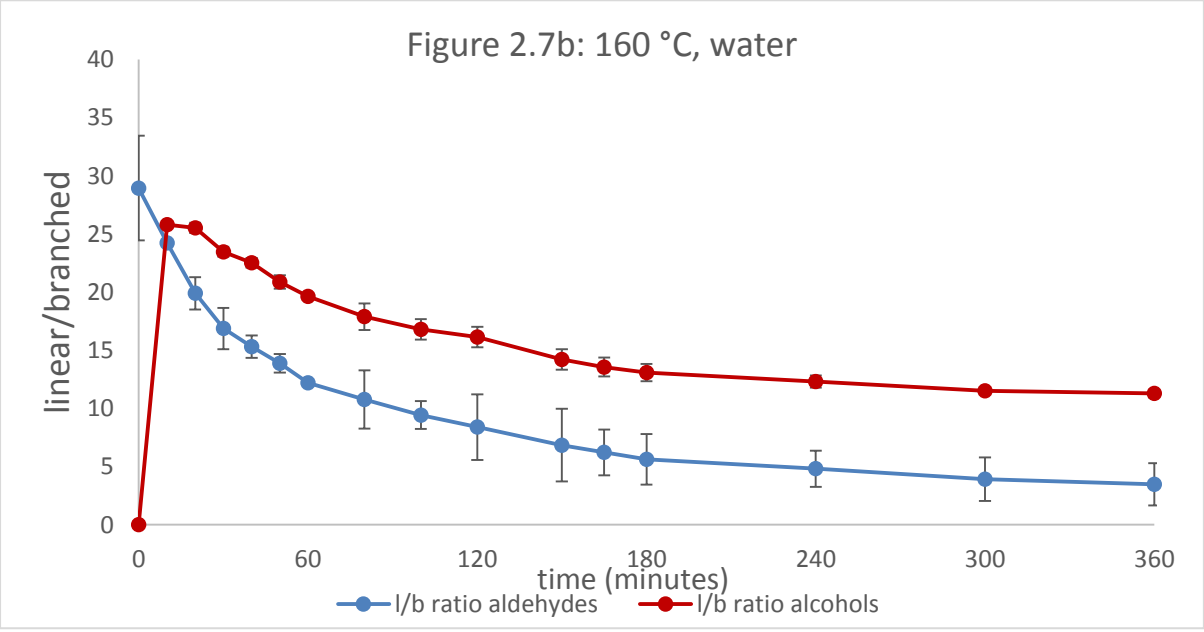

Figures 2.7a and 2.7b Conditions: [Rh(acac)(CO)2] (2.1 mg, 0.1 mol%), Xantphos (14.1 mg, 0.3 mol%), Rh/P (1:6), 1-octene (1.28 mL, 8 mmol), n-decane (0.18 mL, 1 mmol), 2mL cat. stock (1mL toluene: 1mL iPrOH), water (8 mL), T (160 °C), P (24 bar (cold)), CO:H2 1:1 (from syn-gas bottle) , 700 rpm, t (6 hours with 1 hour preformation)

In the ‘on-water’ system at 160 °C the conversion is extremely rapid reaching 100% within 20 minutes. By the end of the reaction the alcohol selectivity is 90% and the amount of aldehyde is very low. Again the l/b ratio of the alcohols is higher than the aldehydes and the two fall in parallel for most of the reaction but there is a rapid decrease in the initial aldehyde l/b ratio as the linear aldehyde is preferentially hydrogenated.

The yield of isomerised octene is much lower than in the toluene system: 5% vs 10%. This is a consequence of a rapid hydroformylation-hydrogenation reaction, rather than a suppression of octene isomerisation, as the 120 °C temperature water system showed an increase in isomerised octenes.

2.2.1.6 Reaction profile of hydroformylation-hydrogenation with excess octene

The reaction profile in figure 2.6a shows that hydroformylation rapidly reaches completion and then the hydrogenation reaction starts. There may be a possibility that the hydrogenation catalyst is formed by decomposition of the hydroformylation catalyst. To investigate this a catalytic run that had a second portion of octene added half-way through was set-up. If the hydrogenation is at the expense of the hydroformylation then the hydroformylation of the second batch of 1-octene would be slower than that present from the start.

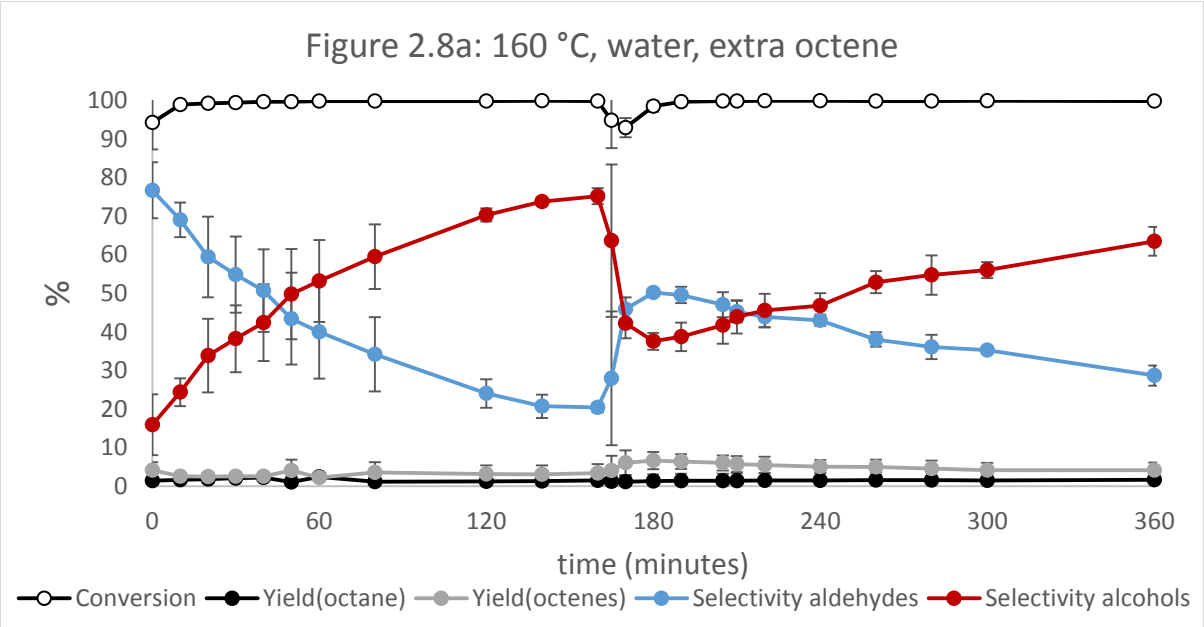

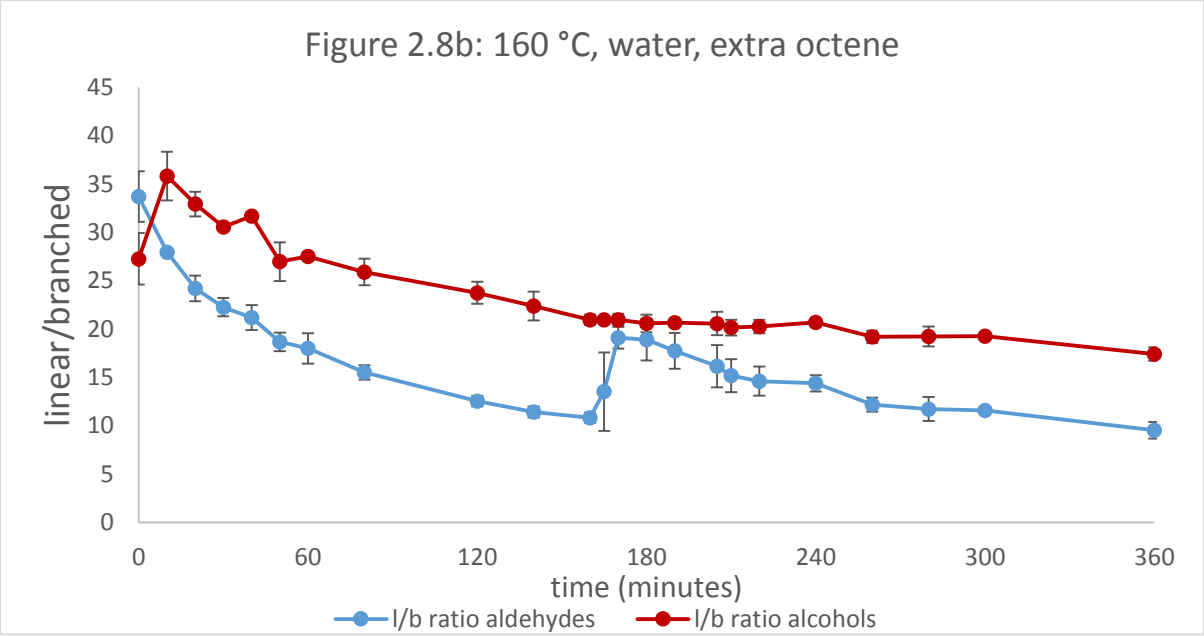

Figures 2.8a and 2.8b: Conditions: [Rh(acac)(CO)2] (2.1 mg, 0.1 mol%), Xantphos (14.1 mg, 0.3 mol%), Rh/P (1:6), 1-octene (1.28 mL, 8 mmol), n-decane (0.18 mL, 1 mmol), 2mL cat. stock (1mL toluene: 1mL iPrOH), water (8 mL), T (160 °C), P (24 bar (cold)), CO:H2 1:1 (from syn-gas bottle) , 700 rpm, t (6 hours with 1 hour preformation). Extra 1-octene (1.28 mL, 8 mmol), n-decane (0.18 mL, 1 mmol) added at t = 165 minutes

In this run the reaction was started with octene already present in the autoclave and then at 180 minutes more 1-octene/n-decane was added through the addition funnel. Adding the standard as well as the substrate ensures the GC-FID calculations are consistent. Rapid conversion was observed with all of the octene being hydroformylated during the heating-up period. The l/b ratio was higher for this reaction than previously reported due to the majority of the hydroformylation occurring at lower temperatures when the isomerization activity is less pronounced.

One hypothesis this experiment aimed to investigate was the possibility that the hydrogenation activity is gained at the expense of the hydroformylation activity through catalyst decomposition; be it ligand oxidation or nanoparticle formation. However, these results show that this is not the case as there is equally rapid hydroformylation activity after 180 minutes as there is at the start of the reaction. However, the presence of the 1-octene does seem to interfere with the hydrogenation reaction as the l/b ratio of the alcohol remains steady from 165 to 240 minutes in figure 2.7b. Following hydroformylation of most of the 1-octene, the l/b ratio of the alcohol begins to drop again.

2.2.1.7 Reaction profile of hydroformylation-hydrogenation with four equivalents of 1-octene

To investigate the observation above, that hydrogenation is only induced after hydroformylation is complete, a reaction was set-up with 4 times the normal amount of substrate as this should take longer to hydroformylate and therefore there should be a delay in hydrogenation.

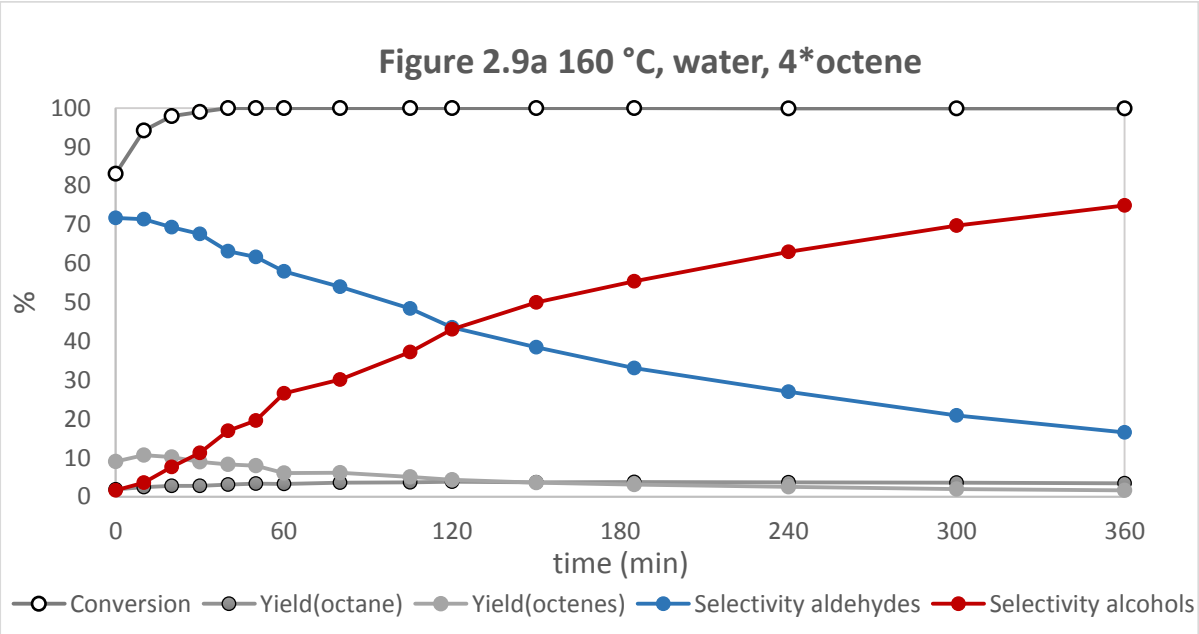

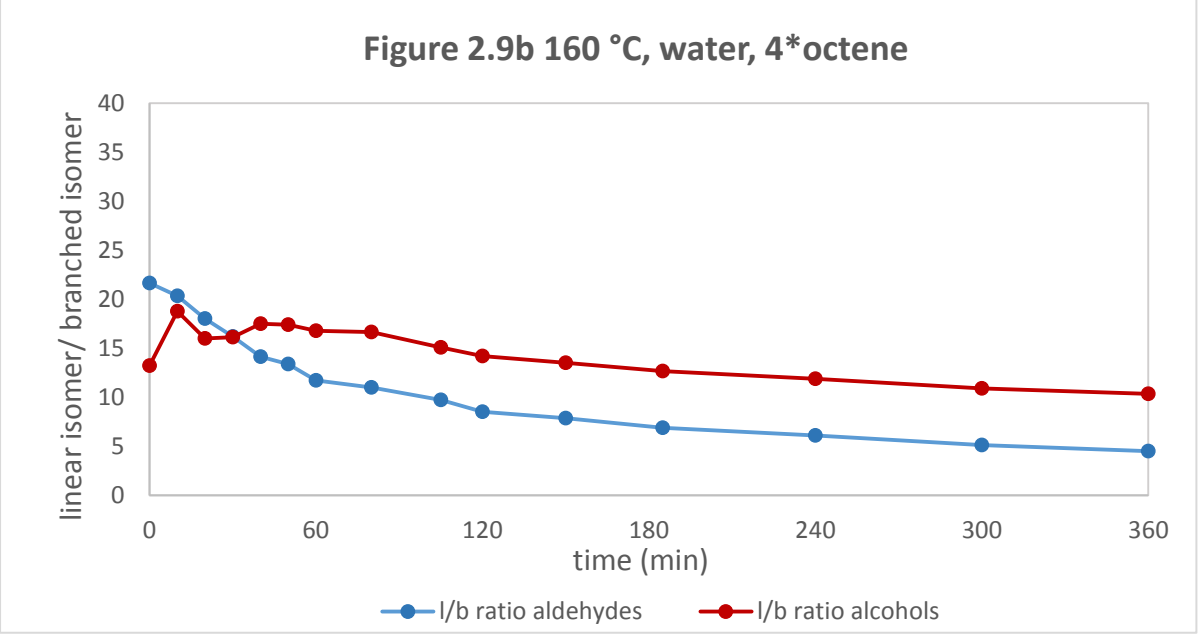

Figures 2.9a and 2.9b Conditions: [Rh(acac)(CO)2] (2.1 mg, 0.025 mol%), Xantphos (14.1 mg, 0.075 mol%), Rh/P (1:6), 1-octene (5.12 mL, 32 mmol), n-decane (0.72 mL, 4 mmol), 2mL cat. stock (1mL toluene: 1mL iPrOH), water (8 mL), T (160 °C), P (24 bar (cold)), CO:H2 1:1 (from syn-gas bottle) , 700 rpm, t (6 hours with 1 hour preformation).

The results do indicate there is a slower rate of alcohol hydrogenation when there is octene still present: a selectivity of 20% is reached after 50 minutes in figure 2.6a compared to a selectivity of 23% is reached after 30 minutes in figure 2.4a. However there is still a rapid rate of hydroformylation so the hydrogenation activity is still induced rapidly. There are more isomerization products detected and the final l/b ratio is much smaller than normally expected for these runs. It is also the aldehyde that is preferentially hydrogenated as there is not a drastic rise in octane despite there being a much greater amount of 1-octene and its isomers.

The overall conclusion from this series of experiments is: water increases the performance of the hydroformylation at 120 ^{o}C showing lower amounts of isomerised alkene and alkane. The reaction profiles show that it increases the rate of hydroformylation. At elevated temperatures hydrogenation occurs in both toluene and in the presence of water but the water greatly increases the rate of hydrogenation. The reaction profiles also show that hydroformylation is preferential to hydrogenation and excess octene can inhibit hydrogenation. Therefore the hydroformylation catalyst and the hydrogenation catalyst are linked, otherwise hydrogenation would continue at the same rate regardless of the other components in the reaction.

2.2.2 Equivalents of xantphos

The equivalents of the ligand is an important parameter in many reactions. At low ligand concentrations metal aggregation and multi-metallic clusters can form, whereas at higher ligand concentrations catalysis may be impeded by competition between reactants and ligands to coordinate to the metal.

As a bulky bidentate ligand, xantphos should be resilient to dissociation, and its unique bite angle and large size could also make the metal resistant to coordinating multiple ligands. Screenings were performed to determine if there is an influence from the equivalents of xantphos in the hydroformylation-hydrogenation system which has previously been reported as an influence in hydroformylation.[6]

Figure 2.10 Equivalents of Xantphos

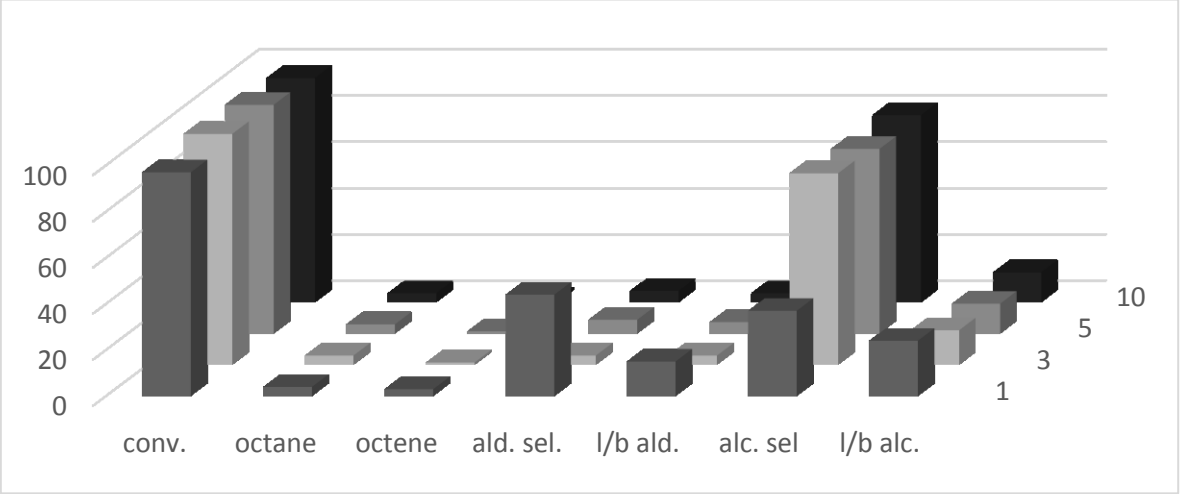

Conditions: [Rh(acac)$(CO)_2$] (2.1 mg, 0.1 mol%), xantphos (varies), Rh/P (1:6), 1-octene (1.28 mL, 8 mmol), n-decane (0.18 mL, 1 mmol), toluene (2 mL, cat. stock), 10% ^{i}PrOH/water (8 mL), T (160 ^{o}C), P (24 bar (cold)), CO:H_2 1:1 (from syn-gas bottle) , 700 rpm, t (6 hours with 1 hour preformation)

When greater than 3 equivalents of xantphos (table 2.4, entries 2,3,4) are used there is not a drastic influence on the system, a high alcohol selectivity is accompanied by a reasonable l/b ratio on increasing the equivalents of xantphos. With 1 equivalent of xantphos the alcohol selectivity drops, due to less hydrogenation of the aldehyde, but there is not a significant increase in octane or octene. The conversion drops marginally at higher equivalents and this may be due to the xantphos interfering with the binding of the octene.

In previous work on xantphos a L/Rh equivalency of 1.1 leads to a l/b ratio of 5.7, while any L/Rh equivalency higher than 2.0 leads to a l/b ratio between 40.5 and 47.6, although the conditions in that case were 40 °C and 10 bar which has a much lower isomerization activity.[5]

In a 2005 hydroaminomethylation investigation, Whitiker showed that there was an influence of the ligand:precursor ratio on the final yield of amine.[11] In this case the ligand is a diphosphite and a L/Rh ratio of less than 1.0 is required to obtain full hydrogenation of the imine intermediates, although there is a drop in the l/b ratio from 40 to 6.4. The conditions were 90 °C and 27 bar of CO:2H_2. The opposite is the case for the presented xantphos system, where lower equivalents of the xantphos results in lower hydrogenation of the aldehyde, so the ligand is an essential part of the hydrogenation activity of the system.

2.2.3 Influence of gas ratio on hydroformylation-hydrogenation

The stoichiometry for the overall tandem reaction is 1 mole of CO and 2 moles of H_2. It is common to run hydroaminomethylation with this syn-gas ratio.[12] However, standard hydroformylation reaction conditions use a 1:1 CO:H_2 mixture. A gas mixing reservoir was

therefore installed and some reactions were run under a pre-mixed 1:2 ratio, as previous reactions prepared by sequential filling of pure CO then H_2 into the autoclave had produced irreproducible results. The outcome of these reactions are presented below in table 2.1.

Figure 2.11 Gas Ratio

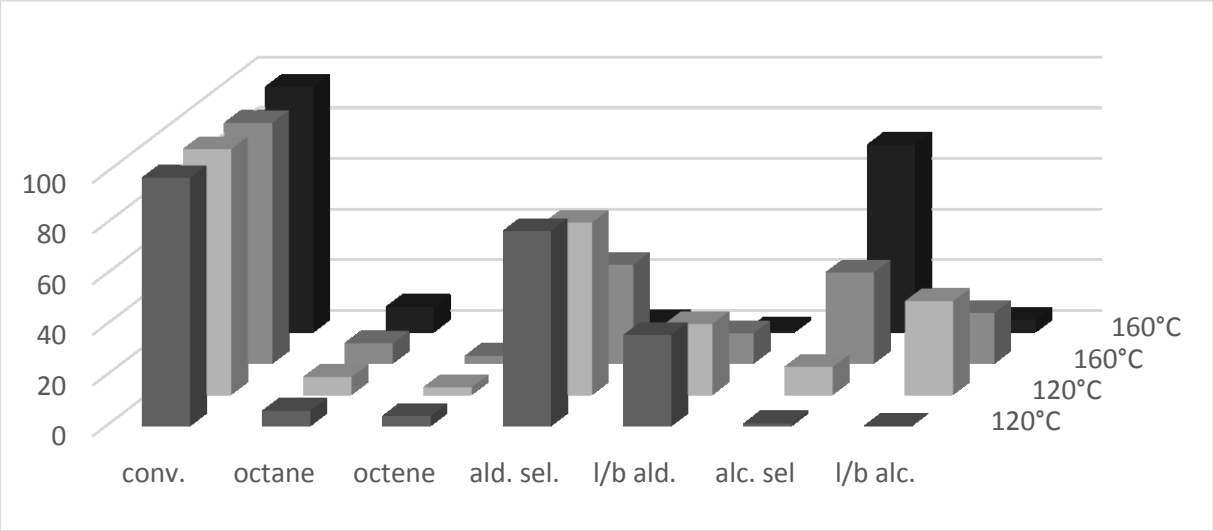

Conditions: [Rh(acac)$(CO)_2$] (2.1 mg, 0.1 mol%), xantphos (14.1 mg, 0.3 mol%), Rh/P (1:6), 1-octene (1.28 mL, 8 mmol), n-decane (0.18 mL, 1 mmol), toluene (2 mL, cat. stock), toluene (8 mL), T (160 °C), P (36 bar (cold)), CO:H_2 1:2, 700 rpm, t (6 hours with 1 hour preformation).[b]water (8 mL) solvent

Figure 2.10 shows a mixture of results for the toluene (entries 1 and 3) and water (entries 2 and 4). As for a standard 1:1 syn-gas mixture, the presence of the water dramatically increases the alcohol selectivity and appears to result in a reduction in isomerized octene.

In comparison to the results in figures 2.2 and 2.3, a higher ratio of H_2:CO leads to an increase in the amount of hydrogenated alkene. The highest amount of hydrogenated octene is 5% in syn-gas and toluene at 160 °C but it is 8% in these conditions (table 2.5, entry 3). In $2H_2$:1CO in toluene, alcohol selectivity is marginally lower, as is the l/b ratio when compared to the standard conditions.

In the on-water system, the alcohol selectivity is increased at low temperatures compared to the standard conditions (table 2.: 4% to 11%. However, there is a lower l/b ratio and alcohol selectivity at 160 °C (table 2.3, entry 3 and table 2.5, entry 2): 88% to 74% and 12 to 5, respectively.

It was expected that a syn-gas ratio equivalent to the stoichiometry of the reaction would be more beneficial to the alcohol selectivity; however, it was discovered to be detrimental to the

results with a higher amount of alkane and a lower l/b ratio. The lower l/b ratio for the alcohol is possibly due to the increased amount of hydrogenation of both isomers of the aldehyde.

2.2.4 Changing gas ratio

A reaction profile was generated for the conditions with a different gas ratio.

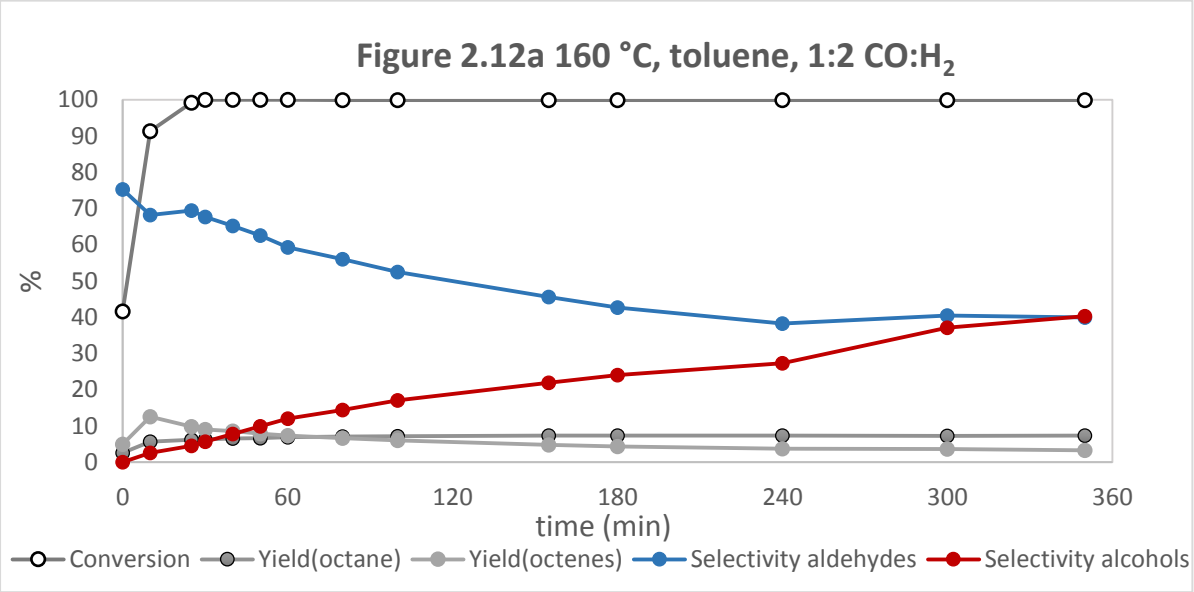

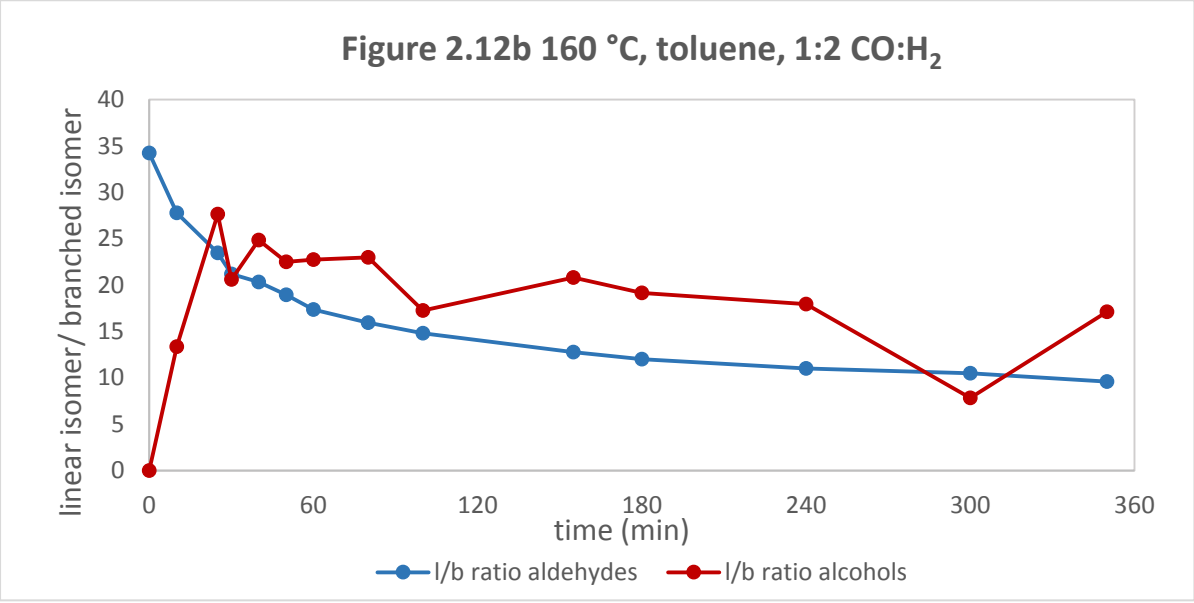

Figures 2.12a and 2.12b Conditions: [Rh(acac)(CO)2] (2.1 mg, 0.1 mol%), Xantphos (14.1 mg, 0.3 mol%), Rh/P (1:6), 1-octene (1.28 mL, 8 mmol), n-decane (0.18 mL, 1 mmol), 2mL cat. stock (1mL toluene: 1mL iPrOH), water (8 mL), T (160 °C), P (36 bar (cold)), CO:H2 1:2 (from syn-gas bottle) , 700 rpm, t (6 hours with 1 hour preformation)

In this run the gas ratio is changed from 1:1 CO:H_2 to 1:2 CO:H_2. The solvent is toluene. The conversion is slower when compared to the 1:1 CO:H_2 ratio and there is an increase in the amount of octane present. There is a peak in the isomerised octene at 10 minutes which then

descends over time as these are hydroformylated. The aldehyde selectivity is lower than in the 1:1 CO:H_2 ratio and there is no point at which the alcohol selectivity overtakes the aldehyde selectivity.

2.2.5 Solvent effect on the hydroformylation/hydrogenation reaction

Diebolt demonstrated that adding alcohol to the system had a positive effect on alcohol selectivity[4] and is an effect investigated in the group's previous hydroaminomethylation paper.[3] Experiments were set up to determine the extent of the influence of different alcohols under the different conditions as it could have an influence in hydroformylation and hydrogenation, or just one of the catalytic reactions.

Figure 2.13 Co-solvent effect in toluene at 120°C

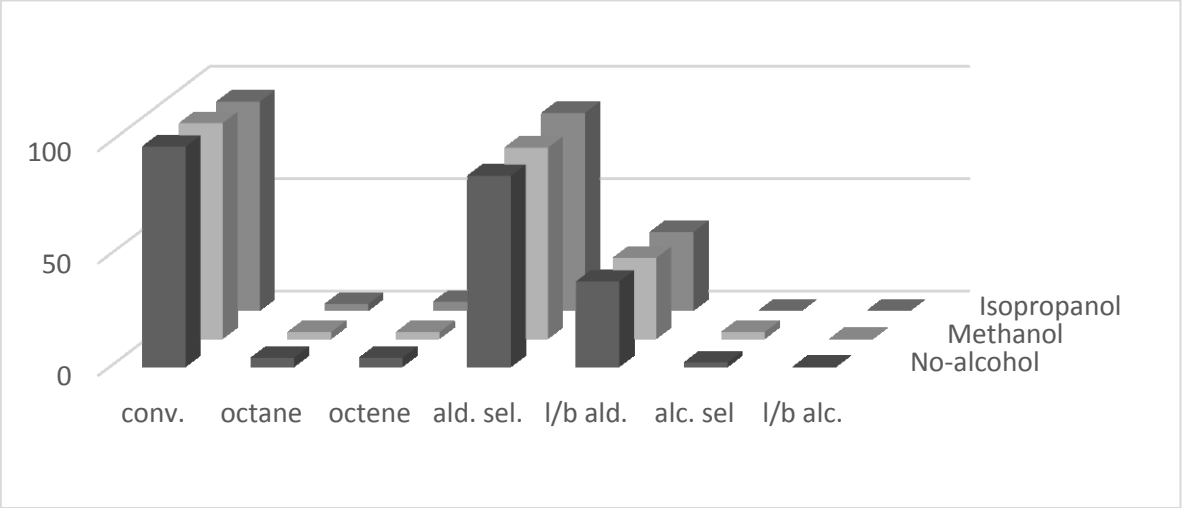

Conditions: [Rh(acac)$(CO)_2$] (2.1 mg, 0.1 mol%), Xantphos (14.1 mg, 0.3 mol%), Rh/P (1:6), 1-octene (1.28 mL, 8 mmol), n-decane (0.18 mL, 1 mmol), 2 mL cat. stock (1 mL toluene: 1 mL toluene/MeOH/^{i}PrOH), toluene (8 mL), T (120 ^{o}C), P (24 bar (cold)), CO:H_2 1:1 (from syn-gas bottle) , 700 rpm, t (6 hours with 1 hour preformation)

In toluene at 120^{o}C there is very little difference between the reactions with alcohol and those without it. There was no acetals and hemi-acetals detected by GC-MS. Therefore, there is no influence on the outcome of hydroformylation in toluene from the addition of co-solvent.

Figure 2.14 Co-solvent effect in water at 120°C

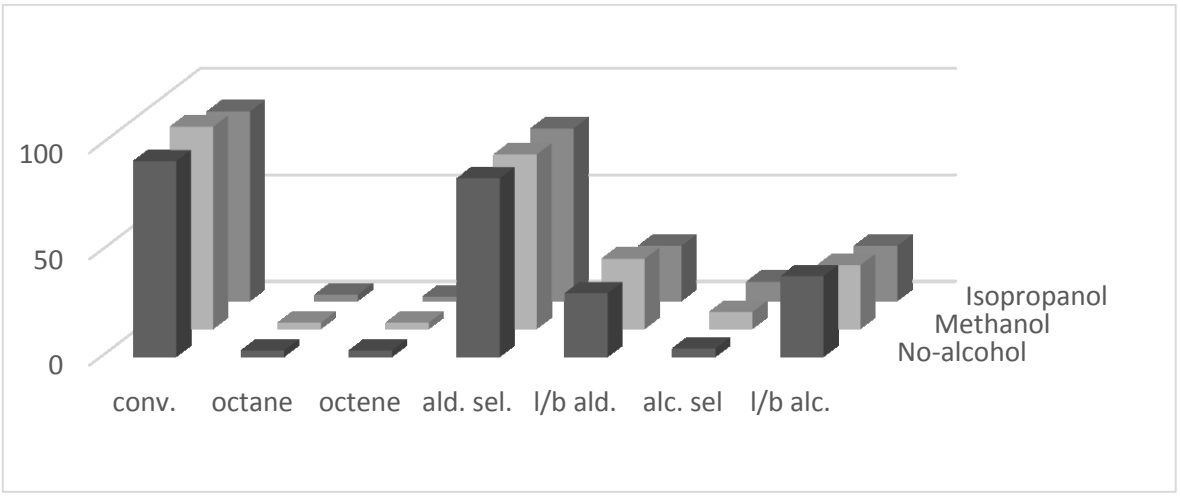

Conditions: [Rh(acac)$(CO)_2$] (2.1 mg, 0.1 mol%), Xantphos (14.1 mg, 0.3 mol%), Rh/P (1:6), 1-octene (1.28 mL, 8 mmol), n-decane (0.18 mL, 1 mmol), 2 mL cat. stock (1mL toluene: 1mL toluene/MeOH/^{i}PrOH), toluene (8 mL), T (120 ^{o}C), P (24 bar (cold)), CO:H_2 1:1 (from syn-gas bottle) , 700 rpm, t (6 hours with 1 hour preformation)

At 120^{o}C, the 'on-water' system shows a small increase in the alcohol selectivity and lower alkene conversions than the toluene counterpart. The formation of the nonanol contributes to the lower aldehyde l/b ratio. Therefore it would seem that it is the hydrogenation step that the alcohol influences.

Figure 2.15 Co-solvent effect in toluene at 160°C

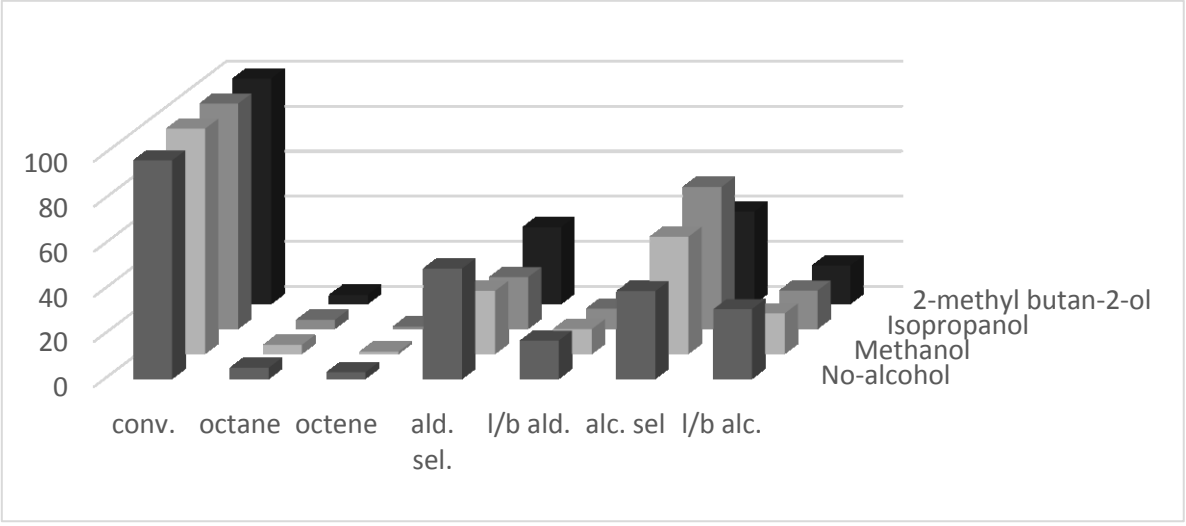

Conditions: [Rh(acac)$(CO)_2$] (2.1 mg, 0.1 mol%), Xantphos (14.1 mg, 0.3 mol%), Rh/P (1:6), 1-octene (1.28 mL, 8 mmol), n-decane (0.18 mL, 1 mmol), 2 mL cat. stock (1mL toluene: 1mL toluene/MeOH/^{i}PrOH), toluene (8 mL), T (160 ^{o}C), P (24 bar (cold)), CO:H_2 1:1 (from syn-gas bottle) , 700 rpm, t (6 hours with 1 hour preformation)

For each co-solvent, higher temperature results in more hydrogenated starting material, and there is a drop in the linear to branched ratios. The drop in l/b ratios and the increase in

isomerized alkenes is a consequence of the increased rate of isomerization. Isopropanol gives the best balance of selectivity and l/b ratio. The difference between the alcohols is more pronounced under these conditions with very definite increase in the alcohol selectivity although there is no influence on the hydrogenation of alkane.

Figure 2.16 Co-solvent effect in water at 160°C

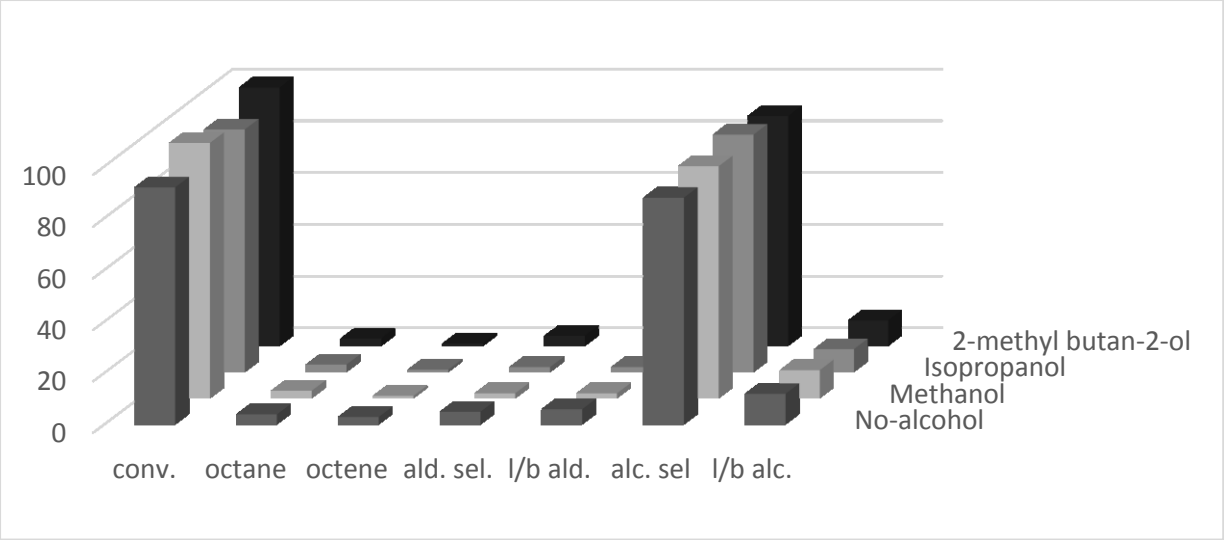

Conditions: [Rh(acac)$(CO)_2$] (2.1 mg, 0.1 mol%), Xantphos (14.1 mg, 0.3 mol%), Rh/P (1:6), 1-octene (1.28 mL, 8 mmol), n-decane (0.18 mL, 1 mmol), 2mL cat. stock (1mL toluene: 1mL toluene/MeOH/^{i}PrOH), toluene (8 mL), T (160 ^{o}C), P (24 bar (cold)), CO:H_2 1:1 (from syn-gas bottle) , 700 rpm, t (6 hours with 1 hour preformation)

In the high temperature on-water system there is minimal difference between the alcohol systems, all resulting in high alcohol selectivity, although isopropanol produces the highest selectivity again. The similar l/b ratios reveal that there is minimal effect of alcohol on the isomerization mechanism.

The observation that all the alcohols have a positive influence on hydrogenation in toluene is interesting. The alcohols could influence the phase behavior of the system or in the catalyst mechanism itself. While the best result is obtained with isopropanol, the effect does not correlate with pKa. pK_a: water (15.7), methanol (15.8), isopropanol (17.3), 2-methylbutan-2-ol (18.5).

At elevated temperatures the state of the system may change from the biphasic water/organic emulsion to a more homogenous mixture. However, a homogenous mixture would be expected to give similar results to toluene, but the conversion of the on-water system is much higher. At lower temperatures the system is definitely biphasic, which should have an influence on the

outcome of the reaction possibly by increasing the local substrate concentration. Such effects are reported by Sharpless to be beneficial in several organic reactions.[13]

Wilkinson reported that alcohol as a co-solvent improves the rate of hydrogenation in the Wilkinson's catalyst.[14] In that case, Wilkinson reported that the polar solvent may stabilize an active species with a greater dipole moment than the reacting species.

Another possibility is transfer hydrogenation to hydrogenate the nonanal by oxidizing the isopropanol. Such a system is used in Ru-catalysed aminations, with xantphos as a ligand, known as transfer hydrogenation. [15]

2.2.6 Effect of catalyst precursor on hydroformylation-hydrogenation

Hydroaminomethylation and hydrogenation reactions are commonly catalysed by a cationic rhodium precursor due to the increased hydrogenation activity of these species.[16] The cationic precursor, $[Rh(cod)_2][BF_4]$, and another neutral precursor, $[Rh_2(acac)_2]$ were applied to the screening conditions.

As discussed, a previous study used $[Rh(cod)_2][BF_4]$ to form acetals from alkenes in a polar solution.[17] However, the study also noticed that the HBF_4 formed *in-situ* also enabled acetal formation. Therefore the standard neutral precursor conditions were run with additional HBF_4 to determine if any effect was due to HBF_4 formed *in-situ*.

Figure 2.17 Toluene at 120 °C

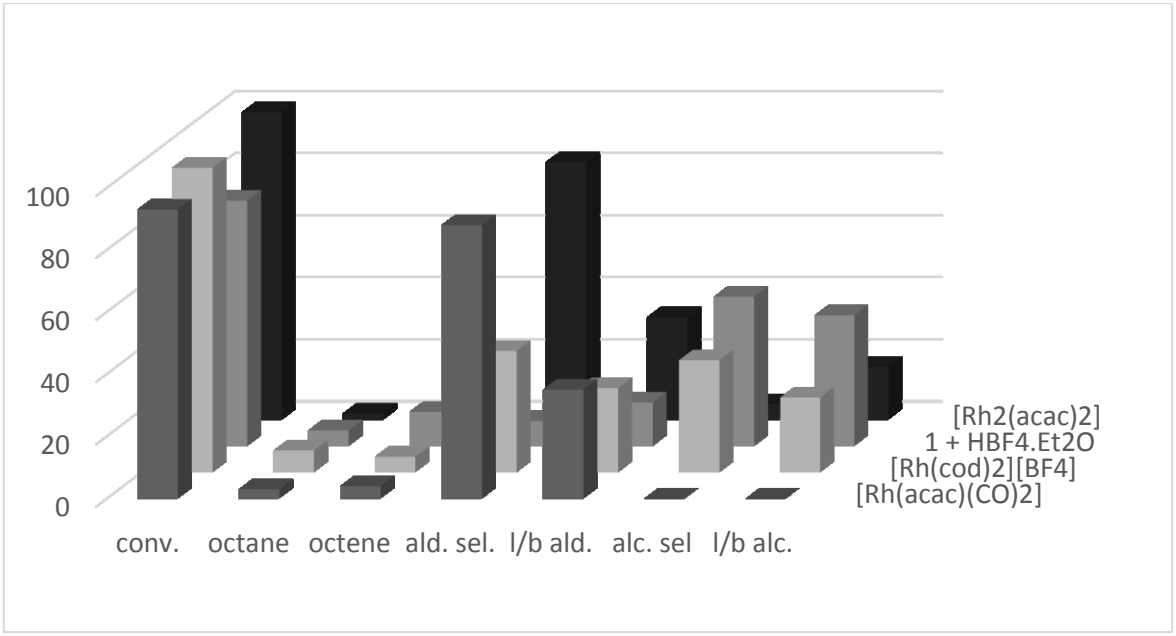

Conditions: : [Rh precursor] (0.1 mol%), xantphos (14.1 mg, 0.3 mol%), Rh/P (1:6), 1-octene (1.28 mL, 8 mmol), n-decane (0.18 mL, 1 mmol), toluene:^{i}PrOH (2 mL, cat. stock), toluene (8 mL), T (120 °C), P (24 bar (cold)), CO:H_2 1:1 (from syn-gas bottle) , 700 rpm, t (6 hours with 1 hour preformation). [HBF_4][Et_2O] (15.8mg, 11 equiv).

In toluene at 120^{o}C the neutral Rh precursors give similar results (table 10, entries 1 and 4) showing high aldehyde selectivity with reasonable l/b ratios. The rhodium dimer induces some alcohol selectivity. The cationic precursor (table 2.10, entry 2) produces alcohols with high l/b ratios but this is coupled with an undesirable increase in the amount of hydrogenated alkene. Excess HBF_4 (table 2.10, entry 3) is detrimental to the reaction resulting in a lower conversion and a higher isomerization activity, but there is a greater increase in alcohol selectivity and l/b ratio than seen for the cationic precursor. Excess HBF_4 does result in a 6% yield of 'higher ends' (not presented in table), unassigned peaks occurring on the chromatograph at a higher retention time than the nonanol peak, which may arise from aldol condensation. There is no such increase in higher ends when [$Rh(cod)_2$][BF_4] is used.

Figure 2.18 Water at 120 °C

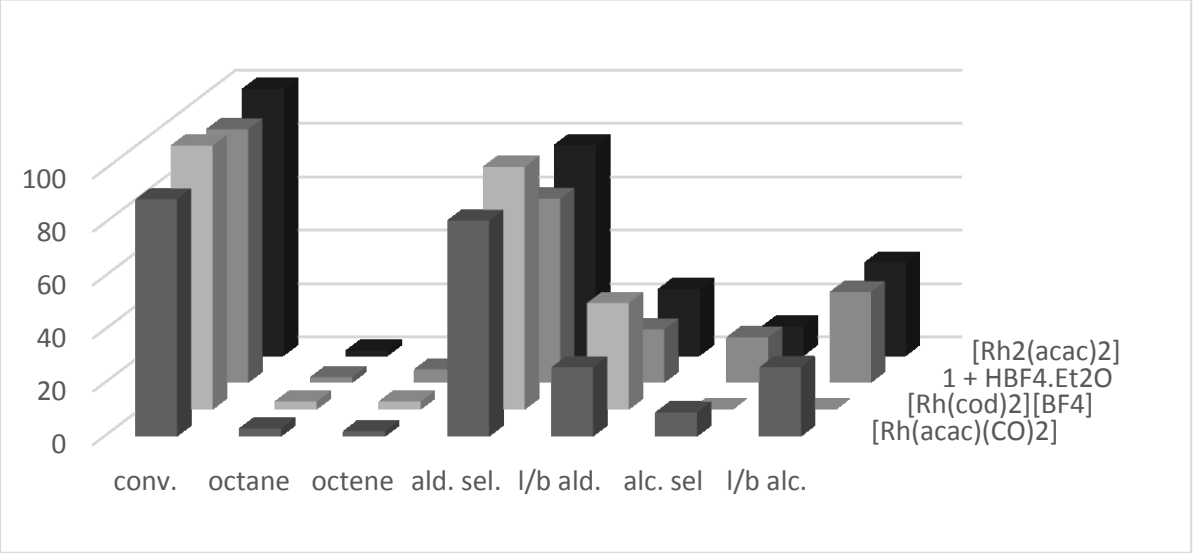

Conditions: : [Rh precursor] (0.1 mol%), xantphos (14.1 mg, 0.3 mol%), Rh/P (1:6), 1-octene (1.28 mL, 8 mmol), n-decane (0.18 mL, 1 mmol), toluene:^{i}PrOH (2 mL, cat. stock), water (8 mL), T (120 °C), P (24 bar (cold)), CO:H_2 1:1 (from syn-gas bottle) , 700 rpm, t (6 hours with 1 hour preformation). [a][HBF_4][Et_2O] (15.8 mg, 11 equiv).

Excess water increases the alcohol selectivity for the two neutral precursors (entries 1 and 4) whilst decreasing the yield of isomerized and hydrogenated octene. In the cationic and excess HBF_4 systems (entries 2 and 3) hydrogenation activity is lower, completely lost in the case of the [$Rh(cod)_2$][BF_4], but the aldehyde selectivity is much higher for [$Rh(cod)_2$][BF_4], therefore the hydroformylation is not impeded. Excess HBF_4 only produces 1% higher ends under these conditions but there is still a slight increase in the isomerization activity of the catalyst. It may

be possible that the excess water removes the HBF_4 from the organic layer which results in a decrease in the hydrogenation activity.

Figure 2.19 Toluene at 160°C

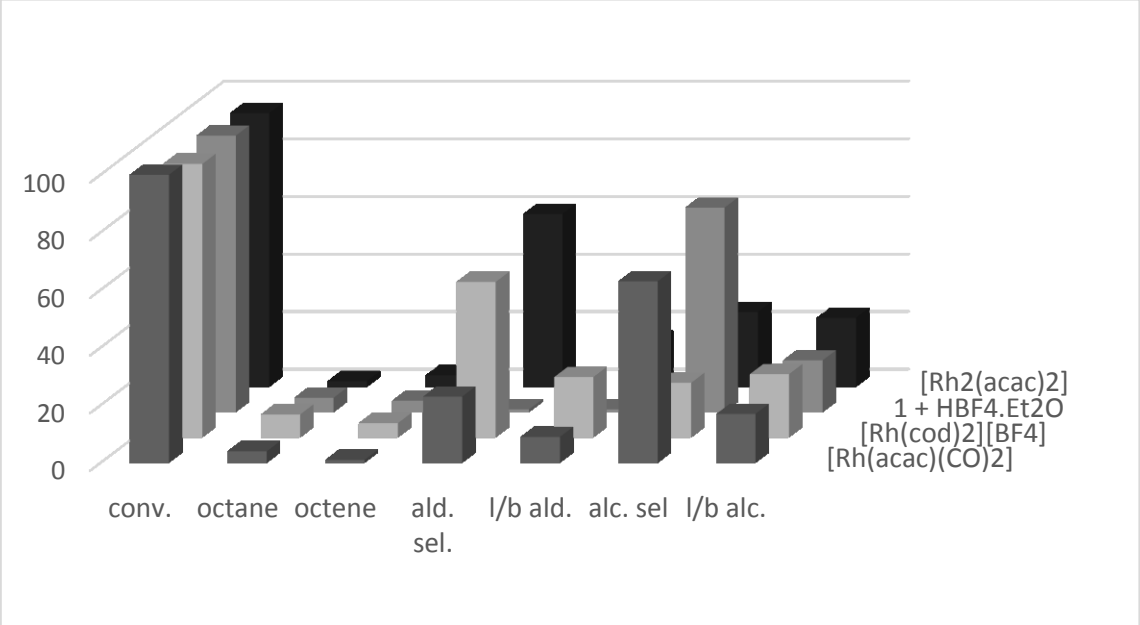

Conditions: : [Rh precursor] (0.1 mol%), xantphos (14.1 mg, 0.3 mol%), Rh/P (1:6), 1-octene (1.28 mL, 8 mmol), n-decane (0.18 mL, 1 mmol), toluene:^{i}PrOH (2 mL, cat. stock), toluene (8 mL), T (160 °C), P (24 bar (cold)), CO:H_2 1:1 (from syn-gas bottle) , 700 rpm, t (6 hours with 1 hour preformation). ^{a}[HBF_4][Et_2O] (15.8mg, 11 equiv).

At 160 °C and in toluene only the cationic precursor does not show an increase in alcohol selectivity (entry 2) but actually has a reduced activity. The highest alcohol selectivity is with [$Rh(acac)(CO)_2$] with extra HBF_4 although this is only 8% more than without it (table 2.13, entries 1 and 3). There was an increased amount of higher ends present as well at 10% (not shown in table). The isomerization products are lower for this system possibly due to an increased rate of hydroformylation. There is a larger difference between the rhodium dimer and the neutral species with the [$Rh(acac)(CO)_2$] giving much more hydrogenation products.

Figure 2.20 Water at 160°C

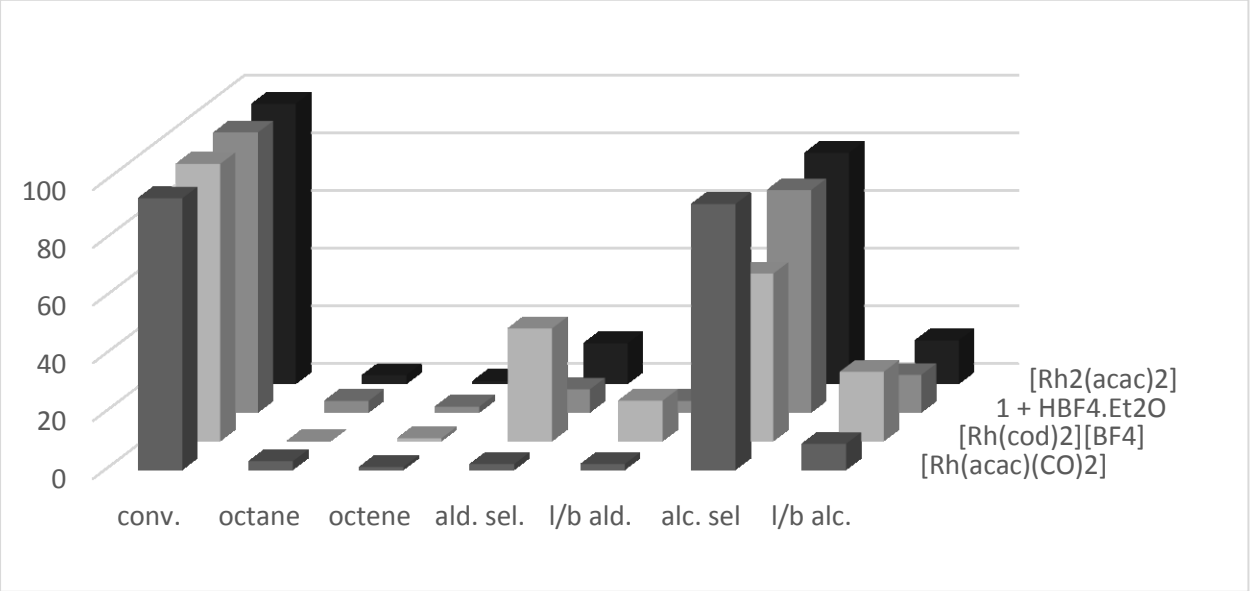

Conditions: : [Rh precursor] (0.1 mol%), xantphos (14.1 mg, 0.3 mol%), Rh/P (1:6), 1-octene (1.28 mL, 8 mmol), n-decane (0.18 mL, 1 mmol), toluene:^{i}PrOH (2 mL, cat. stock), water (8 mL), T (160 °C), P (24 bar (cold)), CO:H_2 1:1 (from syn-gas bottle) , 700 rpm, t (6 hours with 1 hour preformation). [a][HBF_4][Et_2O] (15.8mg, 11 equiv).

Under the standard "on-water" conditions, each precursor achieves the highest alcohol selectivity, with the standard [Rh(acac)$(CO)_2$] outperforming the rest. The cationic precursor has the lowest alcohol selectivity at 58% and there is suppression of the hydrogenation and isomerization of the octene. There is still a substantial amount of higher ends produced in this system, 6%, but this is lower than when the reaction is run in toluene only.

Overall these results show that the cationic precursor is not suitable for these conditions. While it did produce higher alcohol selectivity in toluene at low temperatures it is not reliable in the presence of water. The highest selectivity is still achieved using [Rh(acac)$(CO)_2$].

As mentioned previously cationic complexes are often more active hydrogenation catalysts than their neutral equivalents. Some hydroaminomethylation studies have explored the interconversion between these two systems.[18] There is evidence that water droplets have an intrinsic anionic charge at their surface.[19] This anionic charge may stabilize any cationic species formed from the neutral precursor, which can contribute to the hydrogenation activity. The activity of the neutral complex may be because it is more stable in the presence of water.

2.2.7 Influence of the ligand on the hydroformylation-hydrogenation reaction:

The investigations discussed so far have focused on xantphos. However, other bidentate ligands have been reported for both hydroformylation and hydrogenation catalysis. A selection was applied to the standard screening conditions.

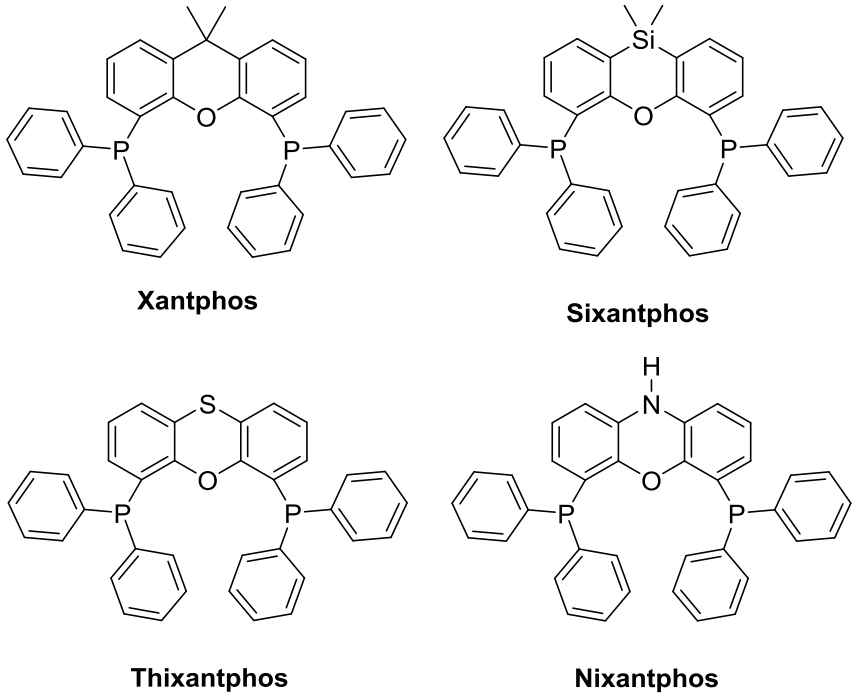

Figure 2.21 Xantphos type ligands

Xantphos and its derivatives are wide bite angle ligands that were developed for hydroformylation by Piet van Leeuwen.[7] As discussed in chapter 1, the unique bite angle (β_n) of these ligands produces a high linear/branched ratio when used in hydroformylation. Four were selected to screen in the reactions (figure 2.18): xantphos (β_n : 111.7°), sixantphos (β_n : 108.7°), thixantphos (β_n : 109.4°), and nixantphos (β_n : 114.2°).

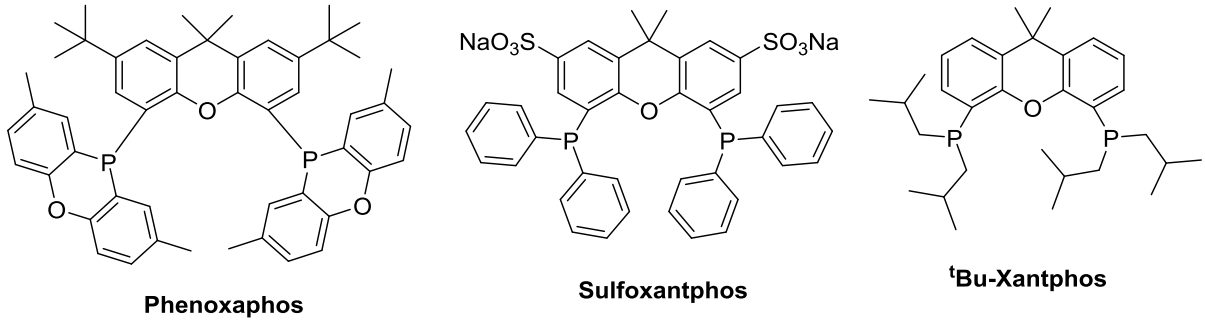

Figure 2.22 Phenoxaphos, tBu-xantphos and Sulfoxantphos

In addition to the standard xantphos ligands, three ligands with the same xanthene back-bone, but with other properties were selected (figure 2.19). Phenoxaphos is a xantphos ligand with phenoxaphosphine appendages and was previously synthesized by van der Veen, and its performance in hydroformylation reported by van Leeuwen.[20] Bite angle is expected to be

120°. It is interesting from a tandem-catalysis perspective because it gives some conversion of internal octenes to positive l/b ratios of aldehydes. If successful in the on-water system it may present a way to carry out the much sought after isomerization-hydroformylation-hydrogenation reaction.[21] It was synthesized according to a previously published procedure that is outlined in the methods section.

Sulfoxantphos is a water soluble variant of xantphos.[22] It has seen use in biphasic hydroformylation of alkenes including 1-hexene, but it gives low conversion at higher chain lengths due to the biphasic nature of the system. However, with propene it is applicable in recyclability studies as the solubility of propene in water is reasonable at higher temperatures and therefore catalysis can take place. This phase dependence on the conversion may give an insight into the phase behavior of the on-water system.

The alkyl chains on ^{t}Bu-xantphos should increase the electron density on the metal and make it behave in a similar way to the trialkyl phosphines Cole-Hamilton reported for the conversion of alkenes into alcohols in protic solvents. [9]

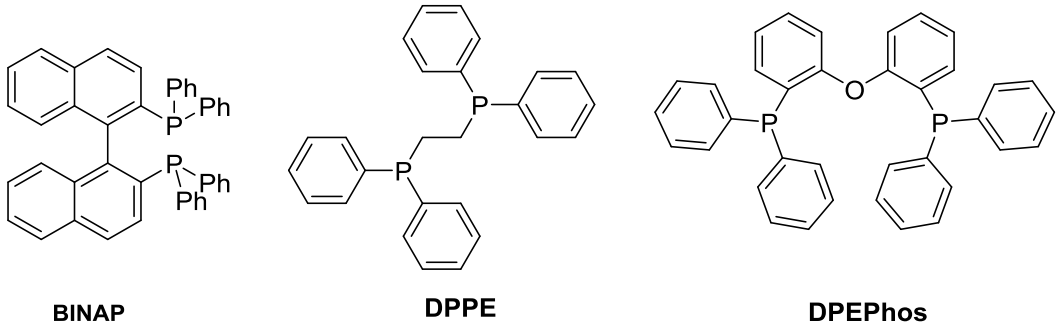

Figure 2.23 Non-xantphos bidentate ligands

Three bidentate ligands without the xanthene backbone were also screened (figure 2.3) for hydroformylation-hydrogenation activity. BINAP (2,2'-bis(diphenylphosphino)-1,1'-binaphthyl) and DPPE (diphenylphosphinoethane) form a 6-membered and a 5-membered ring, respectively, when coordinated to the metal. The complex derived from BINAP and Ru is a well-known hydrogenation catalyst.[23] DPEPhos ((Bis((2-diphenylphosphino)phenylether)) is similar to xantphos but does not have a fused backbone and therefore is far more flexible. This ligand also contains the hemilabile oxygen that can possibly coordinate the rhodium and which has been proposed as a requirement for a hydrogenation mechanism activity on a tethered xantphos catalyst system.[24]

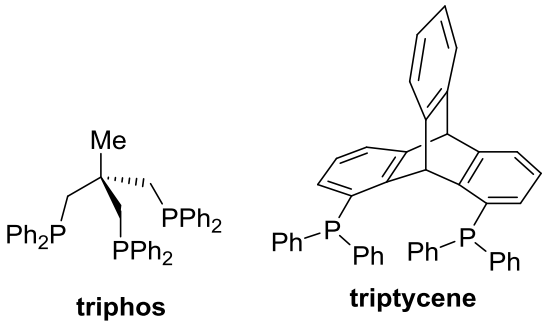

Figure 2.24 Triphos and triptycene

Triphos (figure 2.21) is not bidentate, but has been shown to form a rhodium complex capable of catalyzing hydroformylation and hydrogenation. [25] If the hemilability of the oxygen in xantphos induces the hydrogenation activity then perhaps this species will mimic this. The ligand triptycene was also applied as a test for the influence of this hemilabile oxygen.

In the results below for the reactions run in water and toluene at 120 °C and 160 °C the ligands have been divided into three categories: the standard xantphos-like ligands, sixantphos, thixantphos, xantphos and nixantphos; the xantphos-like ligands with special properties, tBu-xantphos, sulfoxantphos, phenoxaphos, DPEPhos; and finally other multidentate ligands DPPE, triphos, BINAP, triptycene and also a run with no ligand.

Figure 2.25 Xantphos like ligands, toluene 120 °C

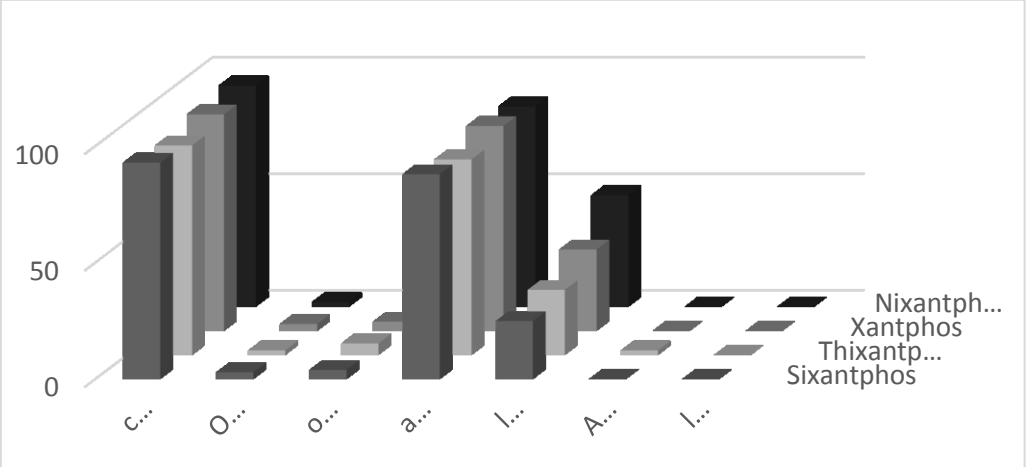

Figure 2.26 Alternative xantphos ligands, toluene 120 °C

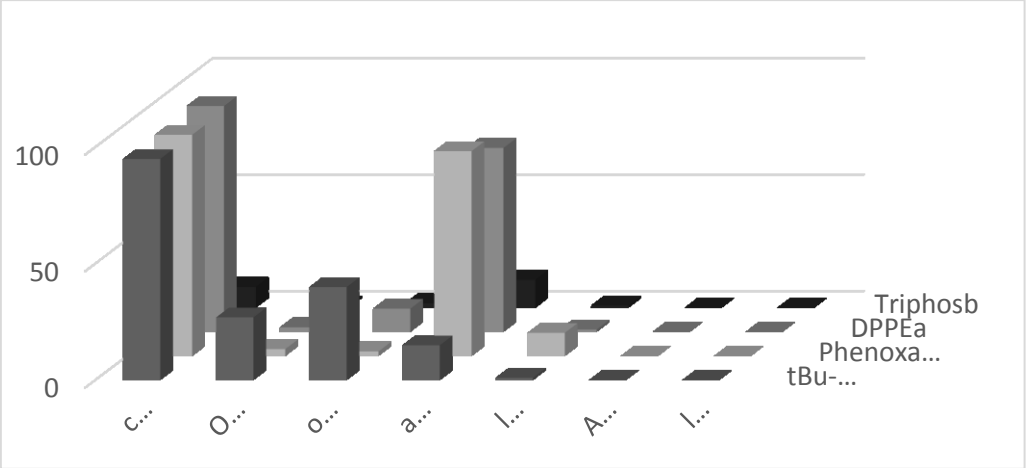

Figure 2.27 Bidentate phosphorus ligands, toluene 120 °C

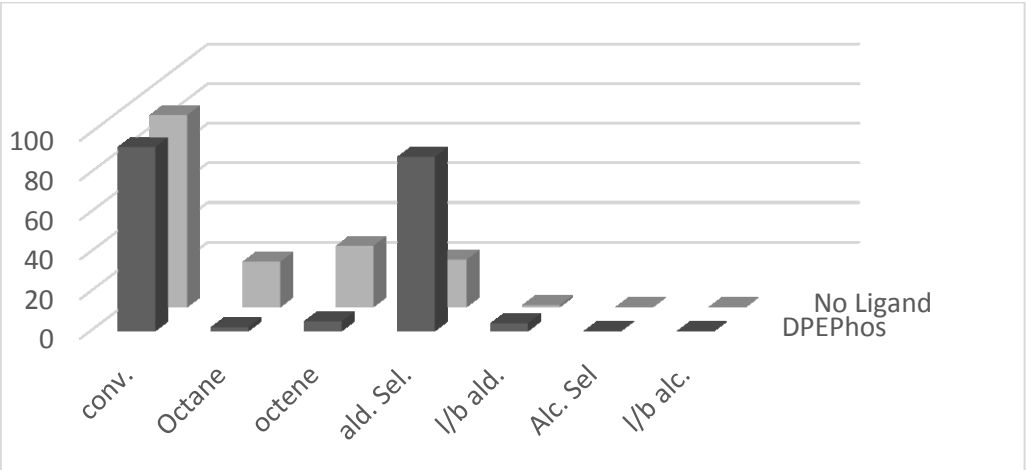

Conditions: [Rh(acac)$(CO)_2$] (2.1 mg, 0.1 mol%), **Ligand (0.3 mol%)**, Rh/P (1:6), 1-octene (1.28 mL, 8 mmol), n-decane (0.18 mL, 1 mmol),), toluene:^{i}PrOH (2 mL, cat. stock), toluene (8 mL), T (120 ^{o}C), P (24 bar (cold)), CO:H_2 1:1 (from syn-gas bottle) , 700 rpm, t (6 hours with 1 hour preformation). [a]Only 1 equivalent was used: Rh/P (1:2) [b]Rh/P (1:9).

The catalysis in toluene at 120 ºC is dominated by hydroformylation, although there is also isopropanol present as this is used in the formation of stock solution and was shown to improve alcohol selectivity in other conditions (see section 2.2.5). Xantphos and similar ligands give good aldehyde selectivities and the highest l/b ratio for the aldehydes (figure 2.22).

In previous studies at 80 °C and 20 bar CO/H_2 the ligands induced l:b ratios of: sixantphos 34, thixantphos 57, xantphos 52 and nixantphos 69. These are placed in order of bite angle within the tables above and below. There is an approximate increase in l/b ratio with bite angle under these conditions. [7]

The other bidentate ligands give comparable aldehyde selectivities, with low hydrogenation and isomerization activity of the alkene, but lower l/b ratios for the aldehyde. Using DPPE and BINAP as ligands show a higher amount of isomerized octene. In early studies it was found that these ligands produce low linear/branched ratios due to the prevalence of the ea coordination isomer (see chapter 1).[26] BINAP, in combination with a cationic rhodium precursor, has been reported to perform hydrogenation, but with the neutral precursor the hydrogenation activity was minimal.[23]

The unmodified rhodium carbonyl species performs hydroformylation but there is also an increased amount of hydrogenated and isomerized alkene which results in a lower selectivity and l/b ratio of the aldehyde. Similar results were obtained when ^{t}Bu-xantphos was used which indicates the ligand has degraded and the catalyst is comprised of the unsupported neutral precursor.

Most catalyst systems show conversion of the olefin with the exceptions of triphos and sulfoxantphos. Sulfoxantphos is a water soluble xantphos-type ligand. The sulfoxy groups that give the ligand its solubility in water also prevent it from being fully soluble in organic solvents. The sulfoxantphos-rhodium complex formed is not present in the same phase as the substrate and therefore does not perform hydroformylation, isomerization or hydrogenation.

Although there are reports of rhodium-triphos complexes mediating hydroformylation under these conditions it does not.[25] If ligand degradation is at fault then the results would be comparable with the unmodified rhodium precursor, however, the level of isomerization and hydrogenation activity detected is well below that of the ligand-free system. It may be that triphos is forming a complex that does not facilitate one of the steps in the hydroformylation cycle.

Figure 2.28 Xantphos like ligands, water 120 °C

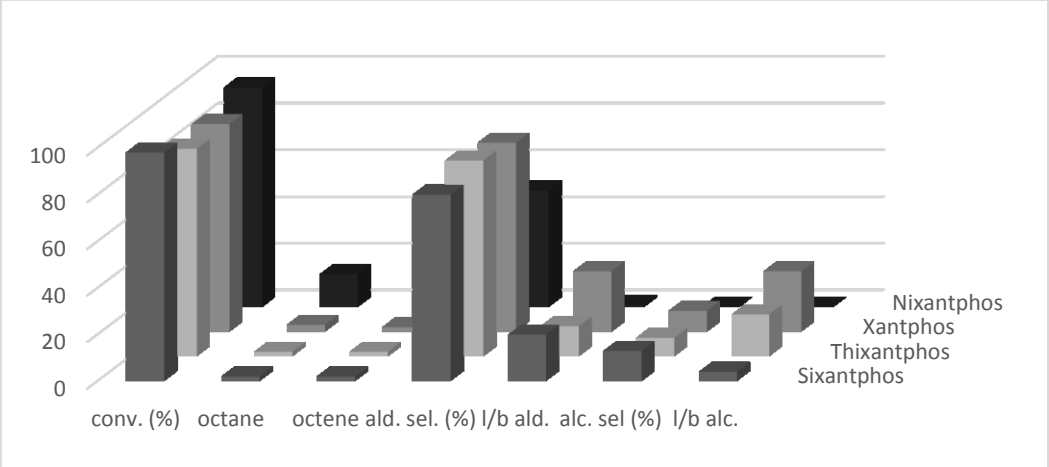

Figure 2.29 Alternative xantphos ligands, water 120 °C

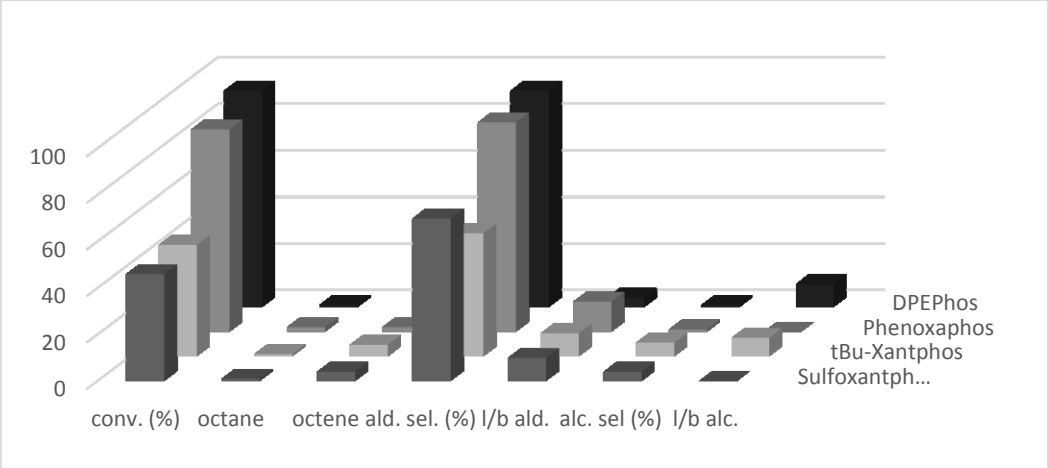

Figure 2.30 Bidentate phosphorus ligands, water 120 °C

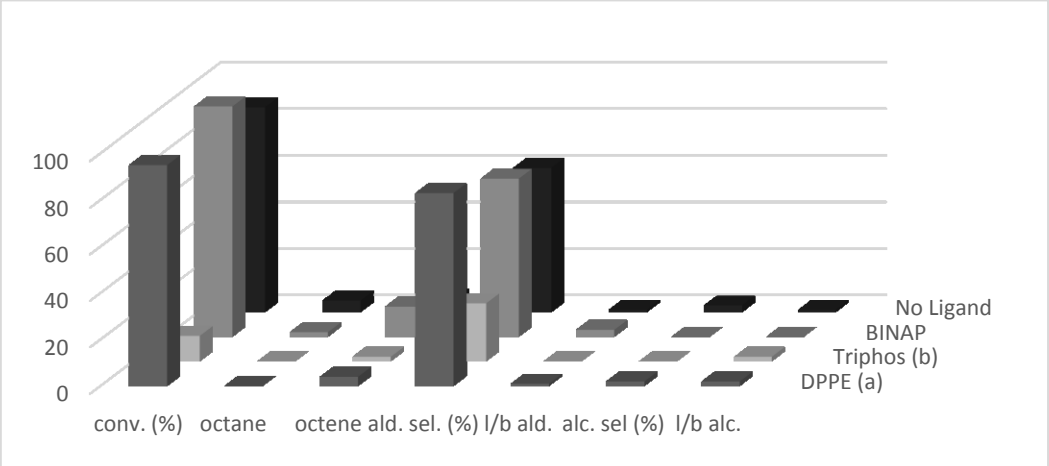

Conditions: [Rh(acac)$(CO)_2$] (2.1 mg, 0.1 mol%), Ligand (0.3 mol%), Rh/P (1:6), 1-octene (1.28 mL, 8 mmol), n-decane (0.18 mL, 1 mmol),), toluene:^{i}PrOH (2 mL, cat. stock), water (8 mL), T (120 ^{o}C), P (24 bar (cold)), CO:H_2 1:1 (from syn-gas bottle) , 700 rpm, t (6 hours with 1 hour preformation). [a]Only 1 equivalent was used: Rh/P (1:2) [b]Rh/P (1:9)

Replacing 8 mL of toluene with 8 mL of water creates a definite biphasic system and alters the performance of the catalyst. In the xantphos-type ligands a small increase in alcohol selectivity is accompanied by a small decrease in aldehyde selectivity. The exception to this trend is nixantphos which when used leads to a lower hydroformylation activity and higher alkene isomerization and hydrogenation activity. Nixantphos also loses its l/b selectivity.

Under these conditions the l/b ratio of the aldehdyes in order of bite angle is: 20, 13, 26, 1, which completely removes the approximate correspondence of l/b ratio with bite angle discussed with relation to the results in table 2.14. There is also no relationship between bite angle and alcohol selectivity.

The effect of the water on the unmodified rhodium carbonyl is to increase the aldehyde selectivity accompanied by a substantial decrease in hydrogenation and isomerization of the octene.

The tBu-xantphos catalyst also sees a suppression of hydrogenation and isomerization of the octene, but the hydroformylation shows an increase in the l/b ratio of the aldehydes which indicates the ligand/metal complex is now active in catalysis, although the conversion is still below 50%.

Sulfoxantphos is another metal/ligand complex that sees an improved performance in the presence of water. With a medium it is soluble in, the catalyst starts to perform hydroformylation, although it is at a lower conversion than those more capable of being soluble in the organic phase.

The conversion remains low when triphos is used as a ligand. BINAP does not show a change in reactivity; retaining a comparatively high isomerization activity from the toluene system, in contrast, DPPE sees a drop in the isomerization activity but the aldehyde activity is still quite high.

Figure 2.31 Xantphos like ligands, toluene 160 °C

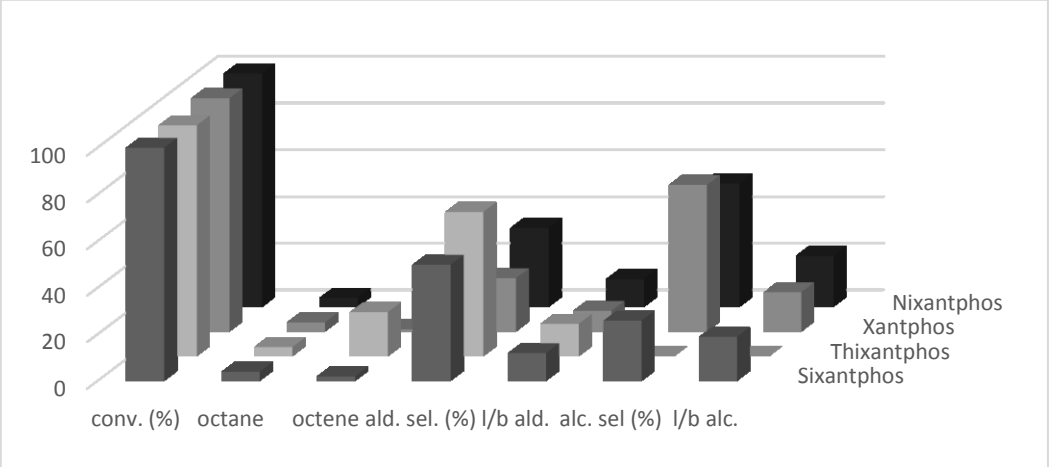

Figure 2.32 Alternative xantphos ligands, toluene 160 °C

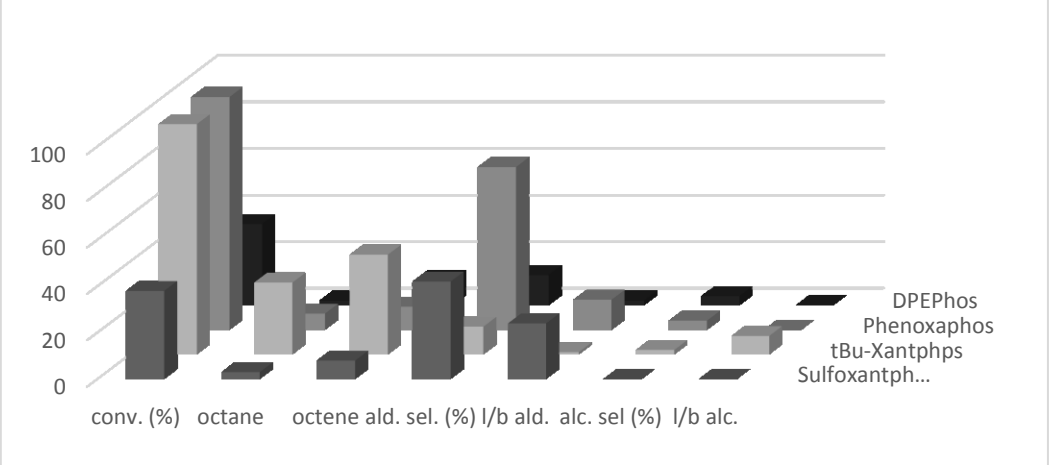

Figure 2.33 Bidentate phosphorus ligands, toluene 160 °C

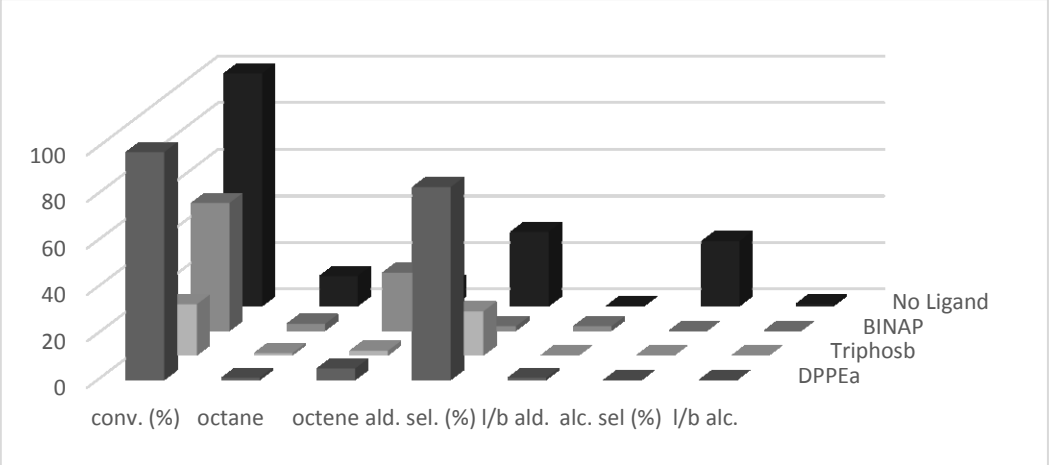

Conditions: [Rh(acac)$(CO)_2$] (2.1 mg, 0.1 mol%), Ligand (0.3 mol%), Rh/P (1:6), 1-octene (1.28 mL, 8 mmol), n-decane (0.18 mL, 1 mmol),), toluene:^{i}PrOH (2 mL, cat. stock), toluene (8 mL), T (160 ^{o}C), P (24 bar (cold)), CO:H_2 1:1 (from syn-gas bottle) , 700 rpm, t (6 hours with 1 hour preformation). ^{a}Only 1 equivalent was used: Rh/P (1:2) ^{b}Rh/P (1:9)

At temperatures of 160 °C the toluene system shows improved conversion in for all catalysts. Xantphos and Nixantphos show high alcohol selectivity with good l/b ratios, although these l/b ratios and the aldehyde l/b ratios are lower than at 120 °C due to the higher rate of isomerization at higher temperatures. Sixantphos is less effective at aldehyde hydrogenation but still effective. As above, there is no correlation between bite angle and any of the results.

Thixantphos demonstrates a higher alkene isomerization activity than the other xantphos derivatives but the amount of hydrogenated alkene is lower and the linear/branched ratio of the aldehyde remains high. A study at 80 °C found that it also demonstrated higher alkene isomerization than the other ligands.[5]

Sulfoxantphos has a much higher conversion than at 120 °C, but lower than in water. No alcohol hydrogenation, high aldehyde l/b ratios, low octene hydrogenation and isomerization all indicate a ligand-modified catalyst at work. The higher temperature may render the charged species more soluble in the organic phase or the rate of the reaction may be faster.

The unreactive triphos catalyst has its best performance, although this is well below the other systems. The apparently low selectivity to conversion is due to the formation of uncharacterized compounds of higher mass.

DPEPhos shows a drop in conversion and a rise in alkene isomerization, but not alkene hydrogenation.

The unmodified rhodium species shows higher conversion, and lower alkene isomerization and hydrogenation products than at 120 °C although this may be due to the accelerated rate of hydroformylation and the consequent alcohol formation. There is no selectivity in these steps as the unmodified catalyst does not show a preference between the linear and the branched product.

Figure 2.34 Xantphos like ligands, water 160 °C

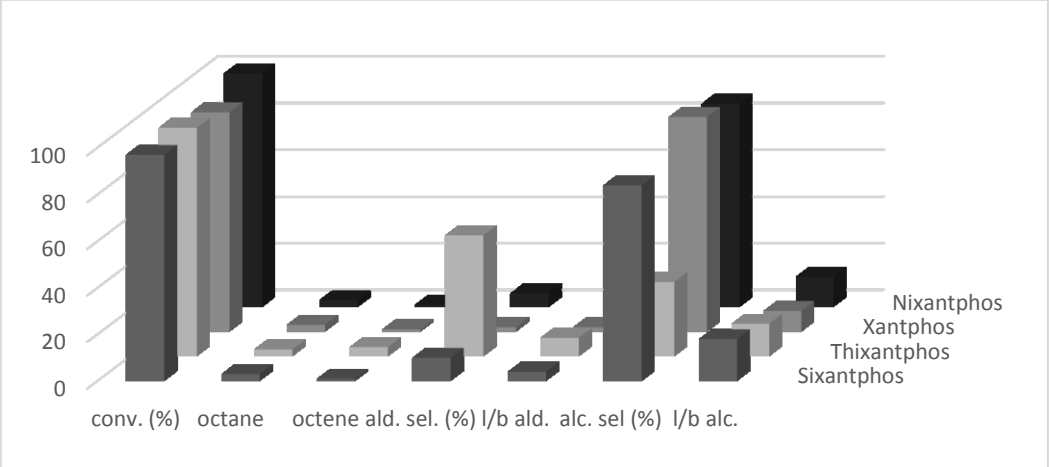

Figure 2.35 Alternative xantphos ligands, water 160 °C

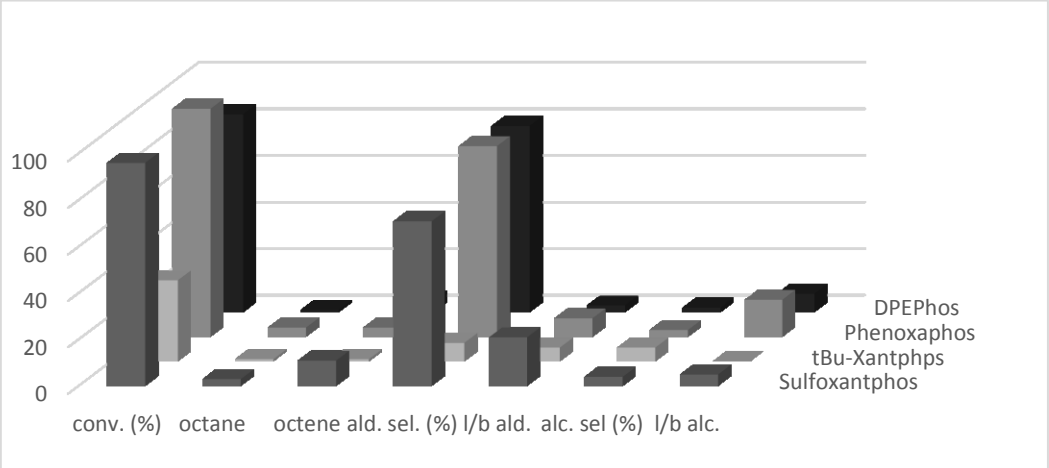

Figure 2.36 Bidentate phosphorus ligands, water 160 °C

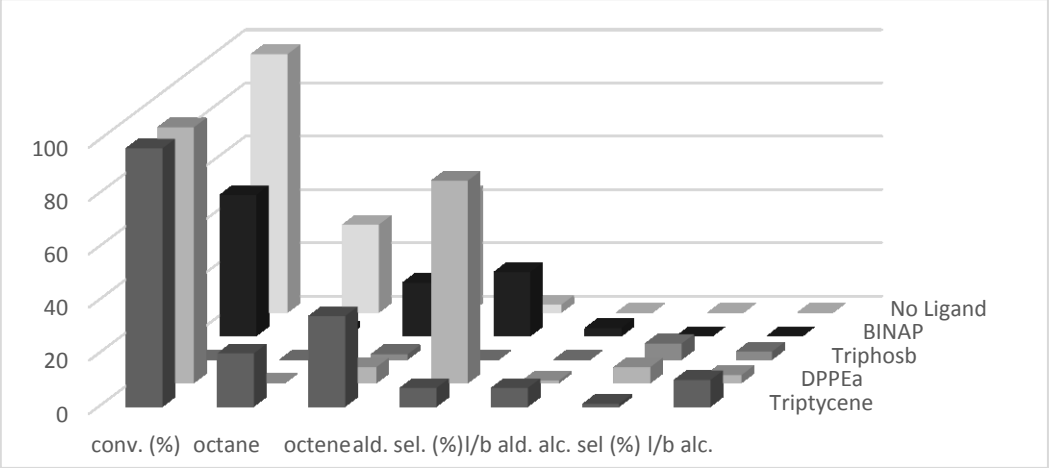

Conditions: [Rh(acac)$(CO)_2$] (2.1 mg, 0.1 mol%), Ligand (0.3 mol%), Rh/P (1:6), 1-octene (1.28 mL, 8 mmol), n-decane (0.18 mL, 1 mmol),), toluene:^{i}PrOH (2 mL, cat. stock), water (8 mL), T (160 ^{o}C), P (24 bar (cold)), CO:H_2 1:1 (from syn-gas bottle) , 700 rpm, t (6 hours with 1 hour preformation). [a]Only 1 equivalent was used: Rh/P (1:2) [b]Rh/P (1:9)

The final screening conditions see the introduction of water and a higher temperature of 160 ^{o}C. Xantphos, Sixantphos and Nixantphos all demonstrate high alcohol selectivity with very low alkene hydrogenation and isomerization activity. The highest l/b ratio of the alcohol is when sixantphos is used but this is due to the lower conversion of the aldehydes. There is no correlation between bite angle and l/b ratio of the aldehydes, l/b ratio of the alcohols and hydrogenation activity.

Use of all other ligands show low alcohol selectivity. This is the most important result thus far: only xantphos and xantphos-like ligands are capable of inducing the on-water hydroformylation/hydrogenation activity. This may be due to the presence of the hemilabile oxygen in the backbone or the unique bite angle.

However, not all xantphos-type ligands do induce the activity: sulfoxantphos, phenoxaphos, and ^{t}Bu-xantphos all give rise to low alcohol selectivities. ^{t}Bu-xantphos has low conversion rates, even lower than the ligand-free system.

The ligand-free system (figure 2.33) has a higher yield of alkene isomerization and hydrogenation products and also a lesser amount of hydroformylation products.

The non-xantphos-like bidentate ligands DPPE, BINAP and DPEPhos each have different outcomes. DPPE shows relatively little influence in the presence of the water but BINAP demonstrates an increase in aldehyde selectivity from 2% to 24%. DPEPhos demonstrated a steep rise in conversion, fall in isomerization and an 80% aldehyde selectivity. The results of DPEPhos are in line with those produced at lower temperature conditions.

Using sulfoxantphos gives the highest conversion at all conditions, but the low alcohol selectivity may indicate that the species capable of performing hydrogenation is not capable of dissolving in the produced aldehydes to achieve hydrogenation. Using triphos gave the lowest conversion of any ligand, almost 0%. The alcohol selectivity could simply arise from residual alcohol within the autoclave from errors as a result of ineffective cleaning method.

Triptycene was also tested under these conditions. Tritptycene is a ligand similar to xantphos, but with an inflexible back-bone that has seen use in hydrocyanation.[27] It is more difficult to find information on its performance in hydroformylation possibly due to the difficulty in its synthesis. The results show it to be ineffective in hydroformylation-hydrogenation, favouring olefin isomerisation and hydrogenation products, possibly due to solubility difficulties in the system resulting in a catalyst more similar to that without a ligand.

2.2.8 Mixed ligand systems

Cole-Hamilton et al. reported a mixed ligand system capable of performing hydroformylation and hydrogenation consisting of a trialkylphosphine and a xantphos ligands.[28] Xantphos promotes hydroformylation with a high l/b ratio and the trialkylphosphine promotes hydrogenation activity. Such cooperativity between ligands is an established route towards tandem catalysis.

It was decided to add triphenylphosphine to the hydroformylation system and study the effect. While the triphenylphosphine may also inhibit catalysis by competitively binding with the H_2. it may increase the l/b ratio of the final product by occupying the vacant site required for β-H elimination. This effect was observed by Unruh and Hughes and discussed in chapter 1.[6] No ^{i}PrOH was added in these runs.

Figure 2.37 [Rh(acac)(CO)$_2$] and xantphos with additional PPh$_3$ in toluene

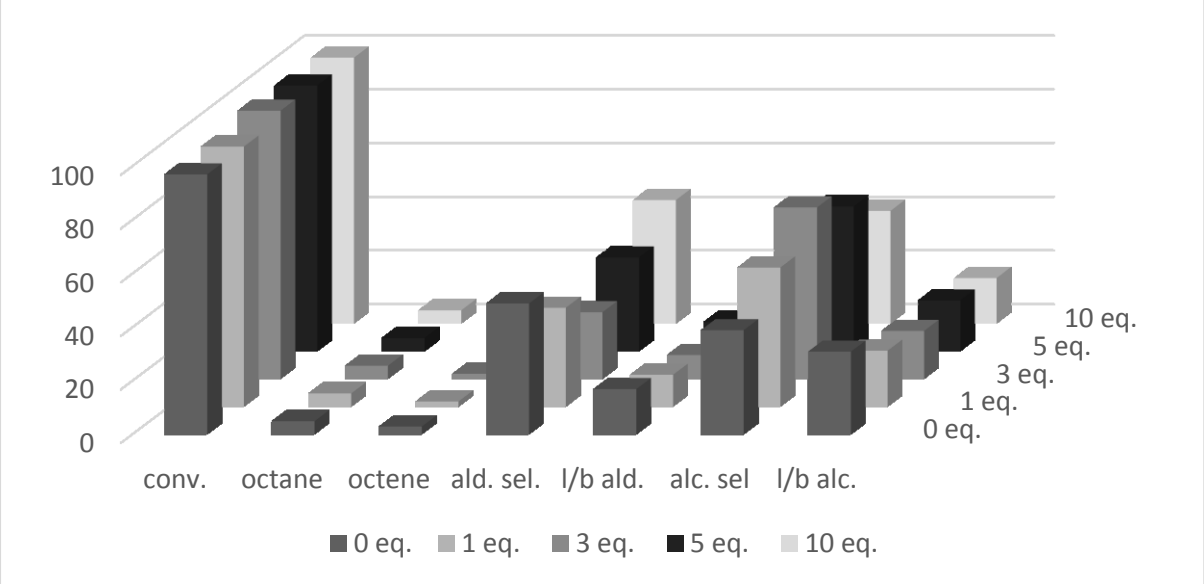

Conditions: [Rh(acac)(CO)$_2$] (2.1 mg, 0.1 mol%), xantphos (14.1 mg, 0.3 mol%), triphenylphosphine (varies), Rh/L (1:6), 1-octene (1.28 mL, 8 mmol), n-decane (0.18 mL, 1 mmol), toluene (8 mL + 2mL cat. stock), T (160 ^{o}C), P (24 bar (cold)), CO:H_2 1:1 (from syn-gas bottle) , 700 rpm, t (6 hours with 1 hour preformation)

The addition of PPh_3 is beneficial to the hydrogenation activity of the system. 3 equivalents is the optimal amount of PPh_3 to add as the alcohol selectivity is highest at 64%. There is a lower l/b ratio as a consequence of the increase in alcohol selectivity. 10 equivalents of PPh_3 starts to inhibit the hydrogenation reactivity.

Table 2.1 [Rh(acac)(CO)$_2$] and xantphos with additional PPh$_3$ in water

Entry	Equiv. PPh_3	conv. (%)	Octane	Octene	ald. sel (%)	l/b ald.	alc. sel (%)	l/b alc.
1[a]	1 eq.	92	3	2	91	58	0	N/A
2[b]	0 eq.	92	3	3	84	30	4	38
	3 eq.	99	3	2	82	23	9	19
3[c]	0 eq.	98	4	2	53	19	38	30
	5 eq.	99	4	2	42	16	50	21
4[d]	0 eq.	92	4	3	5	6	88	12
	10 eq.	96	4	2	27	9	65	12

Conditions: [Rh(acac)(CO)$_2$] (2.1 mg, 0.1 mol%), xantphos (14.1 mg, 0.3 mol%), triphenylphosphine (varies), Rh/L (1:6), 1-octene (1.28 mL, 8 mmol), n-decane (0.18 mL, 1 mmol), toluene (2 mL, cat. stock), water (8 mL), P (24 bar (cold)), CO:H$_2$ 1:1 (from syn-gas bottle) , 700 rpm, t (6 hours with 1 hour preformation), [a] T (80 °C) [b] T(120 °C), [c] T (140 °C), [d] T(160 °C).

The catalytic screening tests in water were run at varying temperatures. However, compared to the standard on-water versions a higher hydrogenation rate is observed for 3 (entry 2) and 5 (entry 3) equivalents with 10 equivalents of PPh_3 inhibiting the hydrogenation activity (entry 4). Although the hydrogenation selectivity is increased the l/b ratio is unchanged, therefore the original hope that addition of the extra ligand would improve l/b ratios was unsupported.

2.2.9 Monodentate ligands: PPh$_3$ and P^{n}Bu$_3$

The earliest examples of ligand-modified rhodium hydrogenation and hydroformylation catalysis used triphenylphosphine as a ligand.[29] Diebolt reported no hydrogenation when PPh_3 was used as a ligand.[4] However the presence of water may still impact the hydroformylation reaction in other ways. Cole-Hamilton showed that when trialkylphosphines are used in protic solvents hydrogenation products were obtained.[30]

As discussed above, hydrogenation and hydroaminomethylation catalysts are often based on a cationic precursors, therefore [Rh(cod)$_2$][BF$_4$] was used to see if this would induce any hydrogenation activity.

Figure 2.38 Monodentate ligands in toluene at 120°C

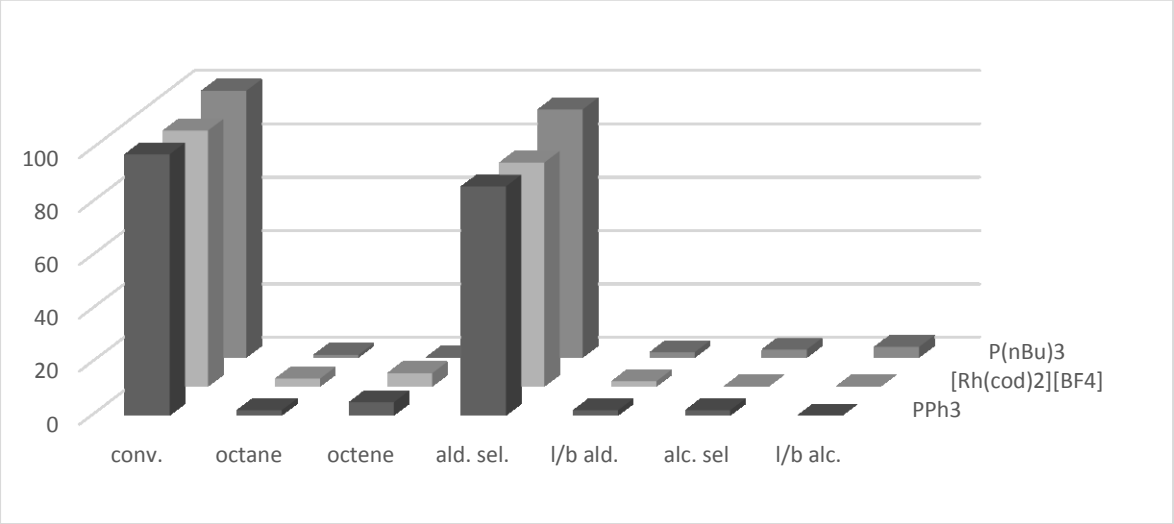

Conditions: : [a] $[Rh(CO)_2(acac)]$ (2.1 mg, 0.1 mol%), PPh_3 (12.8 mg, 0.6 mol%), Rh/P (1:6), 1-octene (1.28 mL, 8 mmol), n-decane (0.18 mL, 1 mmol), toluene (2 mL, cat. stock), toluene (8 mL), T (120 °C), P (24 bar (cold)), $CO:H_2$ 1:1 (from syn-gas bottle) , 700 rpm, t (6 hours with 1 hour preformation). $[HBF_4][Et_2O]$ (15.8mg, 11 equiv). [b] $[Rh(cod)_2][BF_4]$ (3.3 mg, 0.1 mol%).[c] $P(^nBu)_3$ (9.9 mg, 0.6 mol%).

In toluene at 120 ˚C the hydroformylation occurs rapidly with a high aldehyde selectivity, low alkene hydrogenation and isomerization activity in all systems. The l/b ratio is poor, as is expected for monodentate ligands. There is lower isomerization activity when $P(^nBu)_3$ is used (entry 3). Compared to the xantphos and cationic precursor system (table 2.10, entry 2) the cationic precursor displays much lower alcohol selectivity: 0% to 36%.

Figure 2.39 Monodentate ligands in water at 120 °C

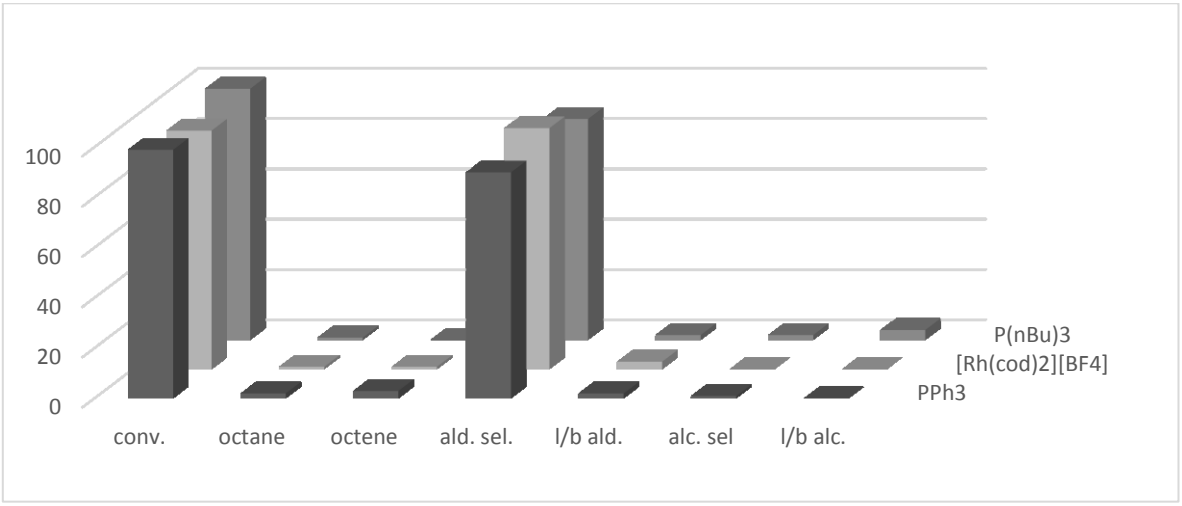

Conditions: : [a] $[Rh(CO)_2(acac)]$ (2.1 mg, 0.1 mol%), PPh_3 (12.8 mg, 0.6 mol%), Rh/P (1:6), 1-octene (1.28 mL, 8 mmol), n-decane (0.18 mL, 1 mmol), toluene (2 mL, cat. stock), water (8 mL), T (120 °C), P (24 bar (cold)), $CO:H_2$ 1:1 (from syn-gas bottle) , 700 rpm, t (6 hours with 1 hour preformation). $[HBF_4][Et_2O]$ (15.8mg, 11 equiv). [b] $[Rh(cod)_2][BF_4]$ (3.3 mg, 0.1 mol%).[c] $P(^nBu)_3$ (9.9 mg, 0.6 mol%).

With water, the hydroformylation occurs rapidly with a high aldehyde selectivity, low alkene hydrogenation and isomerization activities. The l/b ratio is poor, as is expected for mono-dentate ligands. In this on-water system the aldehyde selectivity was improved and the amount of isomerized and hydrogenated by-products was lower.

Figure 2.40 Monodentate ligands in toluene at 160 °C

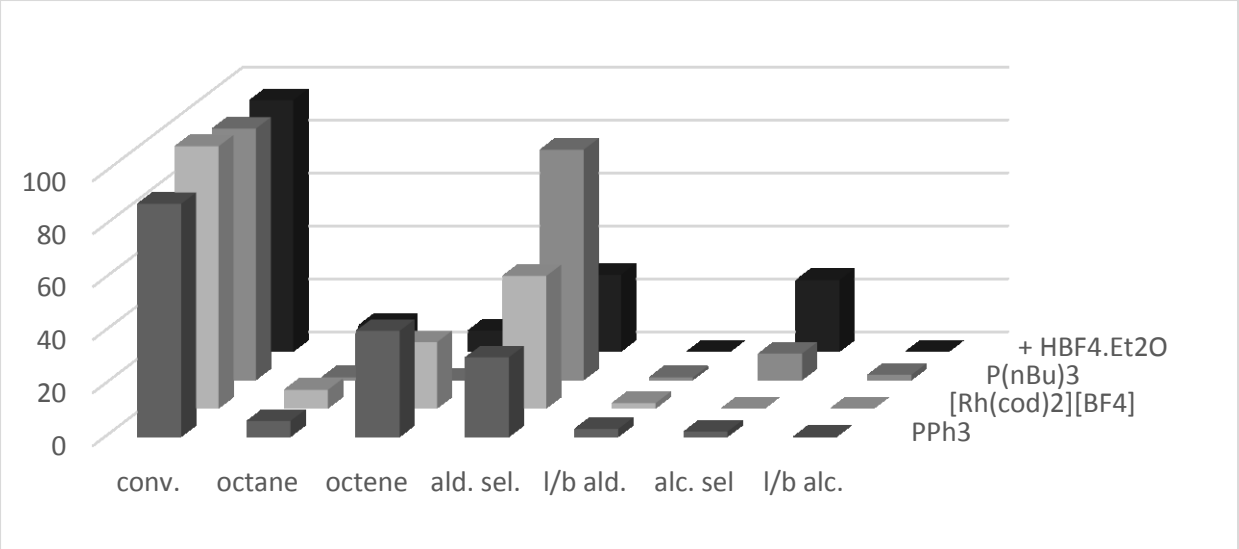

Conditions: : [a] $[Rh(CO)_2(acac)]$ (2.1 mg, 0.1 mol%), PPh_3 (12.8 mg, 0.6 mol%), Rh/P (1:6), 1-octene (1.28 mL, 8 mmol), n-decane (0.18 mL, 1 mmol), toluene (2 mL, cat. stock), toluene (8 mL), T (160 °C), P (24 bar (cold)), $CO:H_2$ 1:1 (from syn-gas bottle) , 700 rpm, t (6 hours with 1 hour preformation). $[HBF_4][Et_2O]$ (15.8mg, 11 equiv). [b] $[Rh(cod)_2][BF_4]$ (3.3 mg, 0.1 mol%). [c] $P(^nBu)_3$ (9.9 mg, 0.6 mol%).[d] $HBF_4.Et_2O$ (1 equiv)

At 160 °C there is a big increase in the amount of isomerized alkene. At these high temperatures the ligand will be more prone to dissociation leaving a vacant site for β-hydride elimination required for the isomerization to take place. There is a possibility that the formation of HBF_4 *in situ* can influence the reaction, as observed for hydroformylation-acetalisation,[17] therefore 1 equivalent of HBF_4 was added. An increase in the alcohol selectivity with a decrease in the isomerization activity is apparent due to an increase in the hydrogenation of the octene. There is a greater effect when $HBF_4.Et_2O$ is present in the mono-dentate system compared to the bidentate system (table 2.12).

$P(^nBu)_3$ does not facilitate isomerization of the alkene. This is a consequence of the change in electron density on the metal, which is higher with this ligand. The main mechanism of alkene isomerization is β-H elimination which requires a vacant coordination site. If the metal is more electron rich then the CO ligands will be more tightly bound as a consequence of stronger π-back donation.

Figure 2.41 Monodentate ligands in water at 160 °C

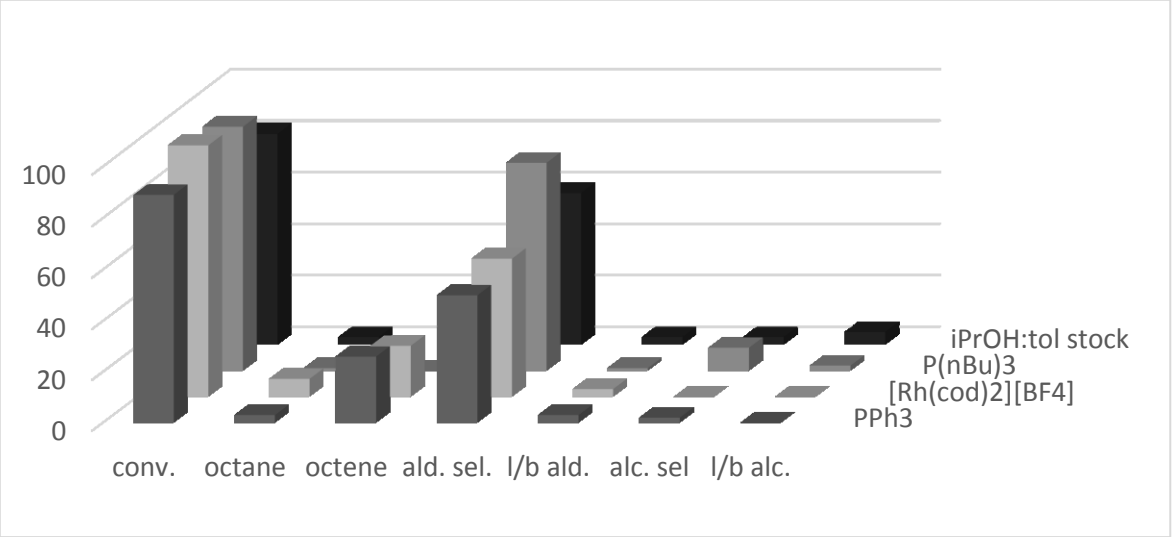

Conditions: : [a] $[Rh(CO)_2(acac)]$ (2.1 mg, 0.1 mol%), PPh_3 (12.8 mg, 0.6 mol%), Rh/P (1:6), 1-octene (1.28 mL, 8 mmol), n-decane (0.18 mL, 1 mmol), toluene (2 mL, cat. stock), water (8 mL), T (160 °C), P (24 bar (cold)), $CO:H_2$ 1:1 (from syn-gas bottle) , 700 rpm, t (6 hours with 1 hour preformation). $[HBF_4][Et_2O]$ (15.8mg, 11 equiv). [b] $[Rh(cod)_2][BF_4]$ (3.3 mg, 0.1 mol%). [c] $P(^nBu)_3$ (9.9 mg, 0.6 mol%). [d] toluene:^{i}PrOH (2 mL cat. stock)

In the established on-water conditions at high temperatures there is very little alcohol selectivity. With $[Rh(acac)(CO)_2]$ and PPh_3 (entry 1) there was drop in isomerization and an increase in aldehyde selectivity, although not to the extent of a xantphos system. Addition of isopropanol (entry 4) to the stock solution further improves the aldehyde selectivity and decreases the isomerization of alkene. There is a slight improvement in the $[Rh(cod)_2][BF_4]$ system (entry 2). In both PPh_3 cases, the lower temperature conditions are superior for hydroformylation. These monodentate systems show no hydrogenation activity under syn-gas conditions.

2.2.10 Influence of the equivalents of water co-solvent

The addition of water to the reaction has been shown to have beneficial effects. However, it is still to be established if there is a relationship between the volume of water added and the effect induced. If the catalytic enhancement is due to phase behaviour then there would expected to be a dependence on the amount of water added; however, if the water is influential at a mechanistic level then the volume of water should not make a difference, provided it is in excess of the catalyst.

Figure 2.42 Amount of water co-solvent added

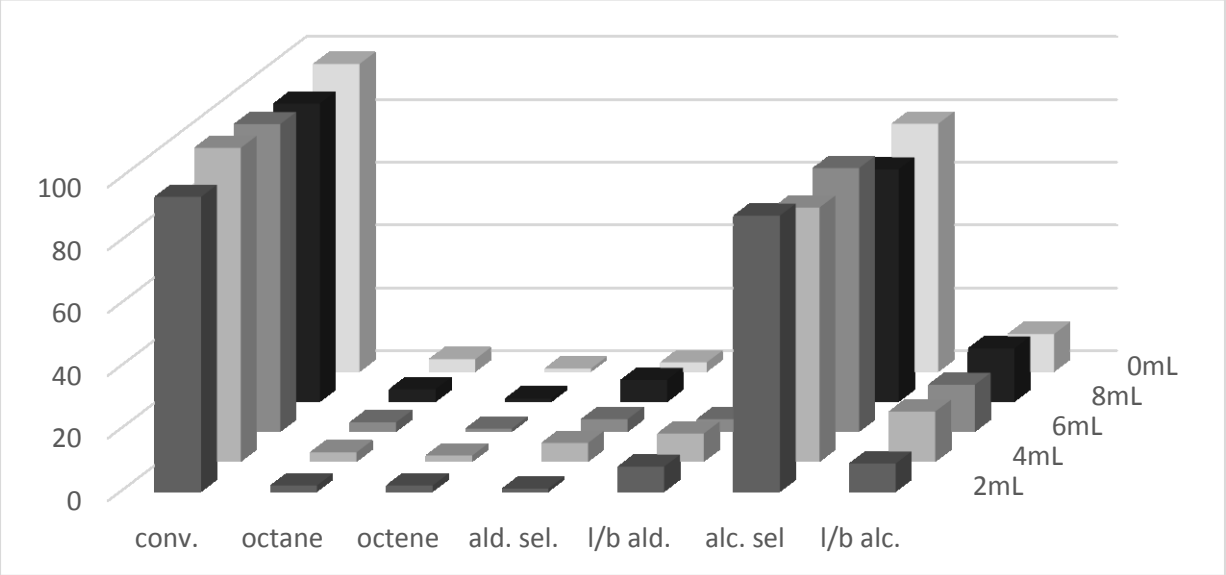

Conditions: [Rh(acac)$(CO)_2$] (2.1 mg, 0.1 mol%), xantphos (14.1 mg, 0.3 mol%), Rh/P (1:6), 1-octene (1.28 mL, 8 mmol), n-decane (0.18 mL, 1 mmol), toluene:iPrOH (2 mL, cat. stock), water (varies), T (160 ^oC), P (24 bar (cold)), CO:H_2 1:1 (from syn-gas bottle) , 700 rpm, t (6 hours with 1 hour preformation)

These screenings show that the effect of the water is not dependent on the amount of water added. The lower conversion for 8mL here is proven to be lower than in other runs (table 2.3). If the hydrogenation activity was a consequence of phase behaviour of the system then the volume of water would be expected to have an effect. However these results show that the amount of water is not important; simply its presence is enough to induce activity.

When the reaction is run within just the toluene:^{i}PrOH catalyst stock solution surprisingly the result is the comparable as when run in water. It is not neat but the solution can be considered very concentrated. There is still the presence of the iPrOH, without which there would be a lower conversion expected, the equivalent to a run in toluene (table 2.8) which showed an alcohol selectivity of 48%. These results indicate the isopropanol and water are active components in hydrogenation.

2.2.11 Summary of the screenings and reaction profiles

A standard hydroformylation catalyst system of [Rh(acac)$(CO)_2$] in toluene performs well at 120 °C generating aldehydes, albeit with a lower l/b ratio than that achieved at lower temperatures. When 8 mL of water is used as the solvent the multiphasic nature of the system improves the rate of hydroformylation and lowers the amount of isomerised and hydrogenated alkene.

At higher temperatures hydrogenation becomes pronounced with 39% alcohol selectivity at 160 °C. Substituting the toluene for water increases this selectivity to 88% with reasonable alcohol l/b ratios. An increase in alcohol selectivity in toluene is also observed when some alcohol is added, isopropanol providing the best result with 63% selectivity to 39% without it. Ultimately running the system in just 2 mL of the toluene:isopropanol solution proved to be just as effective as running it in water. Reaction screenings show that there is rapid hydroformylation activity with a slower rate of hydrogenation.

Screenings that were carried out in the 'on-water' system revealed that to achieve hydrogenation the ligand must be a xantphos type ligand as mono-dentate and other bidentate ligands do not induce hydrogenation. This may be due to the unique bite angle of these ligands, although within the xantphos like ligands there is not the same correlation between bite-angle and alcohol selectivity that is seen for l/b ratio in hydroformylation. Possibly their stability in solution and the hemi-labile oxygen capable of binding to the rhodium could also contribute to their unique performance.

A cooperative ligand effect was observed with 3 equivalents of PPh_3 increasing the amount of hydrogenation from 39% to 64% in toluene at 160 °C. It was also discovered that a gas ratio of 1:1 CO:H_2 is more selective for alcohols than a ratio of 1:2 CO:H_2 as it lowers the amount of alkanes produced. Addition of $HBF_4.Et_2O$ resulted in an increase in hydrogenation activity in toluene at 160 °C (63% vs 71%) but a lower amount in water at 160 °C (92% vs 77%). Many hydrogenation catalysts are based on cationic species but the use of cationic precursors in water at 160 °C resulted in a poorer performance.

2.2.8 High-temperature NMR spectroscopic experiments

The hydroformylation-hydrogenation tandem catalysis reaction is triggered at temperatures higher than 120 °C. In order to determine if this activity is a result of a change in the catalyst at high temperatures, specialist NMR spectroscopic experiments were performed by Dr John Iggo. As discussed in section 1.2.3, NMR spectroscopy has been applied to rhodium catalysts before; ^{1}H and ^{31}P NMR spectra can reveal the presence of a hydride and the binding conformation of the P ligands. However, there are pressure and temperature limits on conventional NMR tubes and spectrometers and the system under investigation lies out-with these.

Iggo has developed a specialist cell capable of running NMR experiments at elevated temperatures and pressures.[31] He has previously worked with van Leeuwen on hydroformylation systems.[32] As the aqueous/organic system was not compatible with the NMR cell, to investigate the hydroformylation-hydrogenation system the precursor and ligand was dissolved in toluene-d^8. Although this system does not produce as much alcohol as the on-water system it can still produce hydrogenation products above 120 °C. The ^{1}H NMR spectra are presented below (figure 2.44).

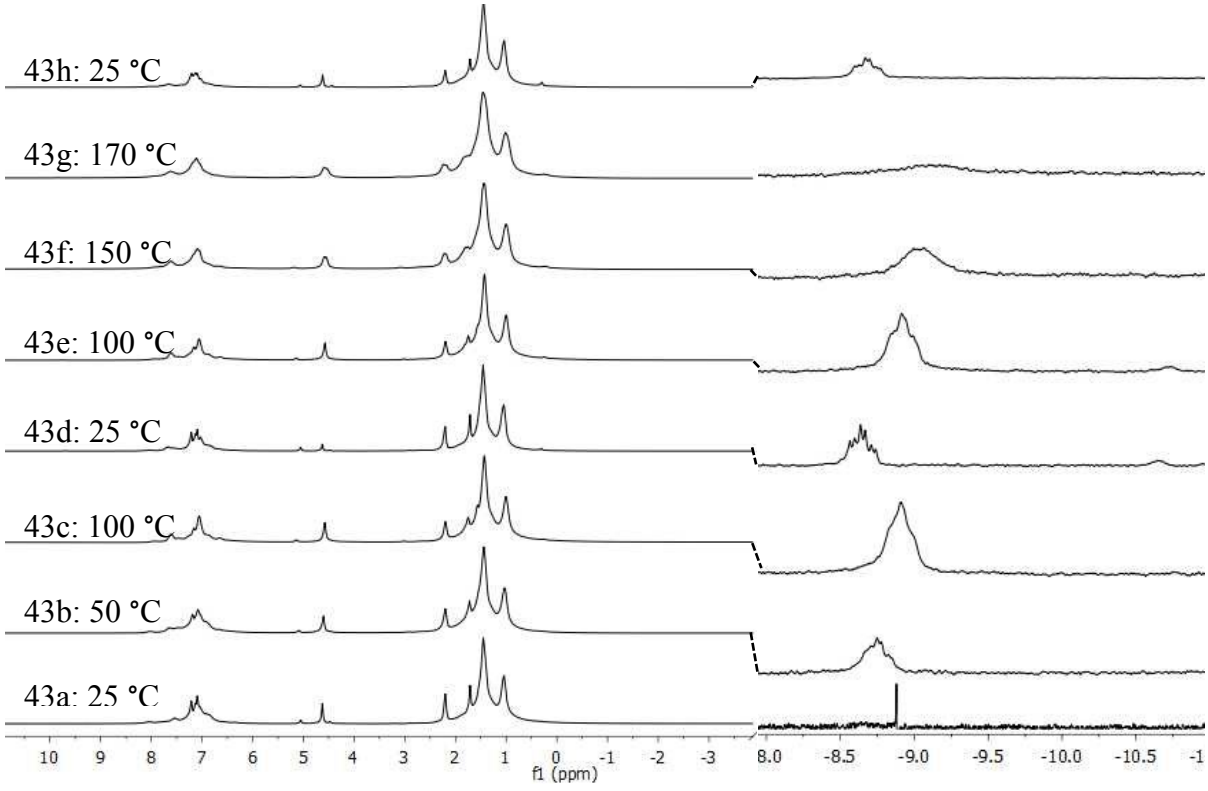

Figure 2.43 ^{1}H NMR Conditions: [Rh(acac)(CO)$_2$] (15 mg, 0.058 mmol) Xantphos (40 mg, 0.070 mmol), Rh/P (1:2.4), toluene-d8 (3 mL). The intensity of the hydride region has been increased for clarity. The variable temperature spectra are recorded at 4.7T (^{1}HNMR = 200 MHz). a) 25 °C, 36 bar CO/H$_2$, total flow rate: L$_n$/h, t:24h b) 50 °C, 36 bar CO/H$_2$, total flow rate:0 L$_n$/h, t:24h c) 100 °C, 36 bar CO/H$_2$, total flow rate: 4 L$_n$/h, t: 24h d) (after overnight) 25 °C, 13 bar CO/H$_2$, , total flow rate: 4 L$_n$/h, t: 48h e) 100 °C, 36 bar CO/H$_2$, total flow rate: 4 L$_n$/h 4, t:48h f) 150 °C, 36 bar CO/H$_2$, total flow rate: 4 L$_n$/h, t:48h g) 170 °C, 36 bar CO/H$_2$, total flow rate: 4 L$_n$/h, t:48h h) 25 °C, 36 bar CO/H$_2$, t:48h

The system consists of [Rh(acac)(CO)$_2$] and xantphos under continuous syn-gas pressure and was heated step-wise. The hydride region shows a pseudo triplet of doublets at approximately δ_H (ppm) = -8.6 (^{1}J(Rh,H) = 14.4 Hz, ^{1}J(P,H) = 6.2 Hz), most clearly defined in spectrum **44d** which is at 25°C and 13 bar, after being heated to 100 °C and 36 bar then cooled under syn-gas overnight. This resonance shifts up-field at higher temperatures, from -8.5 ppm to approximately -9.0 ppm, and is very broad at 170 °C. There is another small hydride resonance observed at δ_H (ppm) = -10.5 ppm (**44d**, **44e**) which could possibly be the apical-equitorial isomer, although the ^{31}P NMR spectrum (figure 2.45) does not support this.

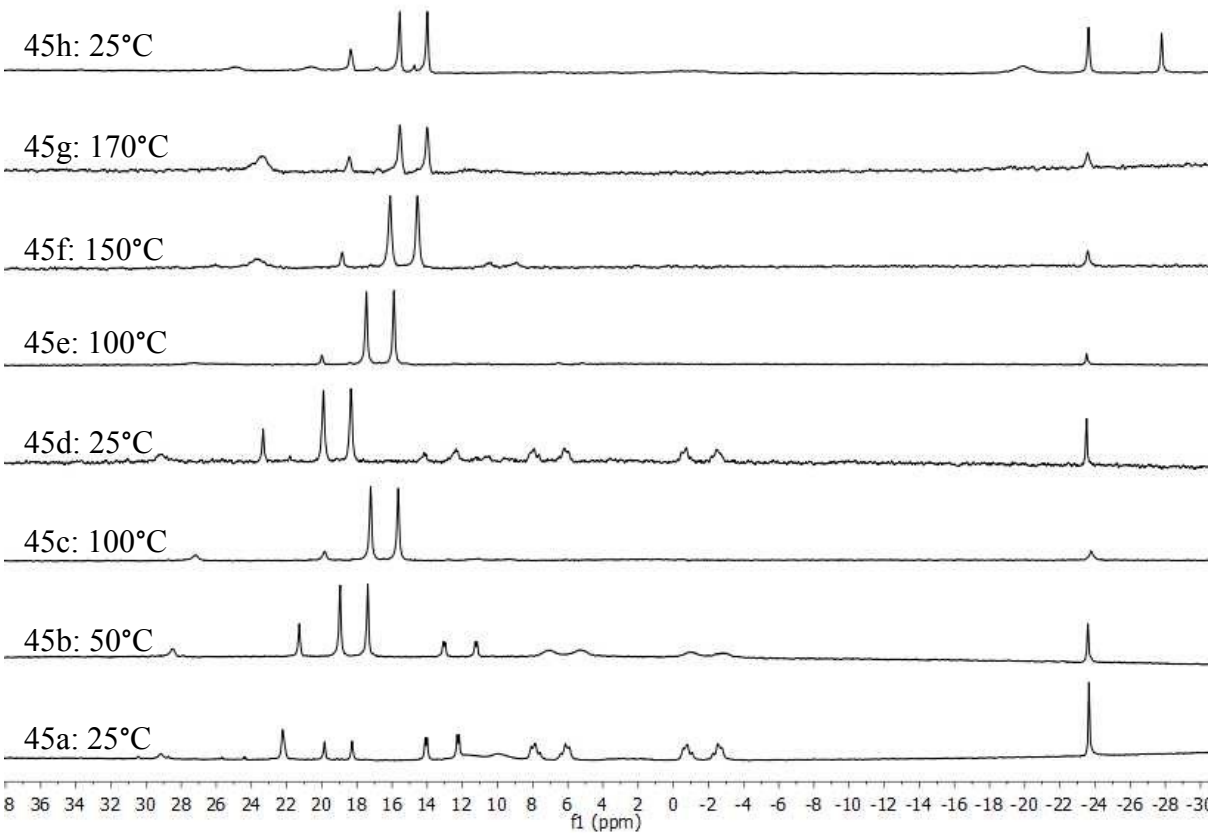

Figure 2.44 ^{31}PNMR spectra. Conditions: [Rh(acac)(CO)$_2$] (15 mg, 0.058 mmol) Xantphos (40 mg, 0.070 mmol), Rh/P (1:2.4), toluene-d8 (3 mL). The variable temperature spectra are recorded at 4.7T (1H = 200 MHz). **a)** 25 °C, 36 bar CO/H$_2$, total flow rate: 0 L$_n$/h, t:24h **b)** 50 °C, 36 bar CO/H$_2$, total flow rate: 0 L$_n$/h, t:24h **c)** 100 °C, 36 bar CO/H$_2$, total flow rate: 4 L$_n$/h, t: 24h **d)** (after overnight) 25 °C, 13 bar CO/H$_2$, total flow rate: 4 L$_n$/h, t: 48h **e)** 100 °C, 36 bar CO/H$_2$, total flow rate: 4 L$_n$/h, t:48h **f)** 150 °C, 36 bar CO/H$_2$, total flow rate: 4 L$_n$/h, t:48h **g)** 170 °C, 36 bar CO/H$_2$, total flow rate: 4 L$_n$/h, t:48h **h)** 25 °C, 36 bar CO/H$_2$, t:48h

In the ^{31}P NMR spectra, the free ligand has a resonance at -22.6 ppm and this was used as a reference for alignment; although this resonance is affected by temperature it facilitates comparison of the other resonances. After immediate addition of syn-gas (**45a**) there is the formation of 4 new complexes (structures shown in figure 3.10): [Rh$_2$(Xantphos)$_1$(CO)$_6$] (**46c**) δ_P (ppm) = 13.02 (dd, ^{1}J(Rh,P) = 147.1 Hz, ^{2}J(Rh,P) = 9.8 Hz), [Rh$_2$(Xantphos)$_2$(CO)$_4$] (**46e**) δ_P (ppm) = 6.9, -1.75 (dm, ^{1}J(Rh,P) = 147.1) , [HRh(Xantphos)(CO)$_2$] (**46b**) δ_P (ppm) = 20.6 (d, ^{1}J(Rh,P) = 127.5 Hz) and possible [Rh(acac)(xantphos)(CO)] (**46a**) species at δ_P (ppm) = 2.2 (very broad) and 10.0.

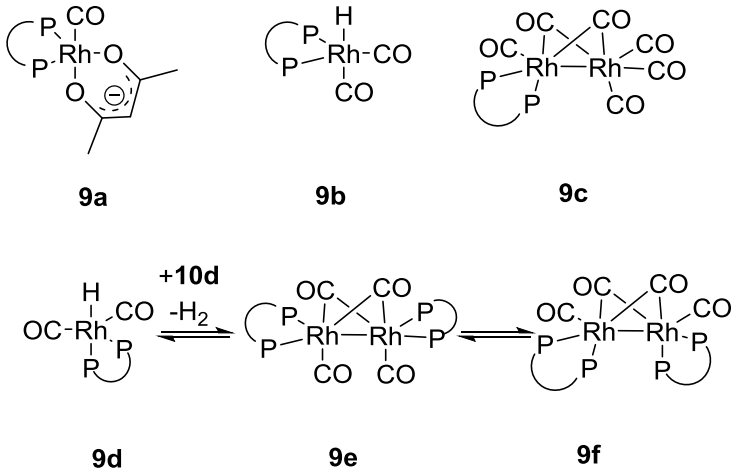

Scheme 2.9 Possible species observable in the high pressure ^{31}P NMR (figure 2.44)

Most of the complexes disappear by 100 °C (**45c)** leaving only species **46b** although they can be seen to re-form at low temperatures again (**45d)**. The main change at higher temperatures is that the spectra shifts to lower frequency: the resonance at δ_P (ppm) = 20.6 (attributed to **46b**) at 25 °C (**45d**) shifts to δ_P (ppm) = 15 at 170 °C (**45g**). However in all the spectra there are two singlets that have to be assigned: at 150 °C (**45f**) δ_P (ppm) = 19 and 23.

One of these peaks can be assigned as the oxidised xantphos ligand, through comparison with Blackmond's report which show an oxidised xantphos at δ_P = 27 ppm under conditions of ^{31}P NMR (202 MHz, 300K, DMAc-d_9).[33] This is most likely the sharper resonance at 19 ppm as this remains steady throughout the experiment.

The other peak is a broad and possibly poorly defined multiplet, but it is not the doublet expected of a phosphorus bound to rhodium, as is the case for species **46b**. After cooling down to room temperature from 170 °C (**45h**) the peak appears to disappear and there is possibly a doublet at 23 ppm, but with a splitting of 352.2 Hz this is unlikely. It could possibly be the oxidised P binding or being influenced by the rhodium. In **45h** there is also another peak present at -29 ppm, which is in the range of the free ligand and not the oxidized ligand. It is unclear what this may be.

In conclusion from these NMR experiments the major species present at high temperature is the ee-xantphos rhodium monohydride **45b,** as observed as the multiplet in the hydride region of the ^1H NMR spectrum and as a defined doublet in the high pressure ^{31}P NMR spectrum. This has been previously reported as the major resting state in the catalytic cycle of hydroformylation.[34]

2.3 Proposed catalytic cycles

2.3.1 Hydrogen activation in the hydroformylation mechanism

In constructing an auto-tandem catalysis hydroformylation-hydrogenation mechanism from the data collected it must be coherent with the standard hydroformylation mechanism. The basic requirement for hydrogenation is the transfer of hydrogen to the aldehyde. There are several possibilities: inner-sphere hydrogenation, outer-sphere hydrogenation, transfer hydrogenation and water-gas shift reaction.

In the hydroformylation catalytic cycle (scheme 2.9 below, fully discussed in section 1.2.7) there is a step in which a Rh-acyl complex activates a molecule of hydrogen before reductive elimination re-generates the active 4-coordinate species.

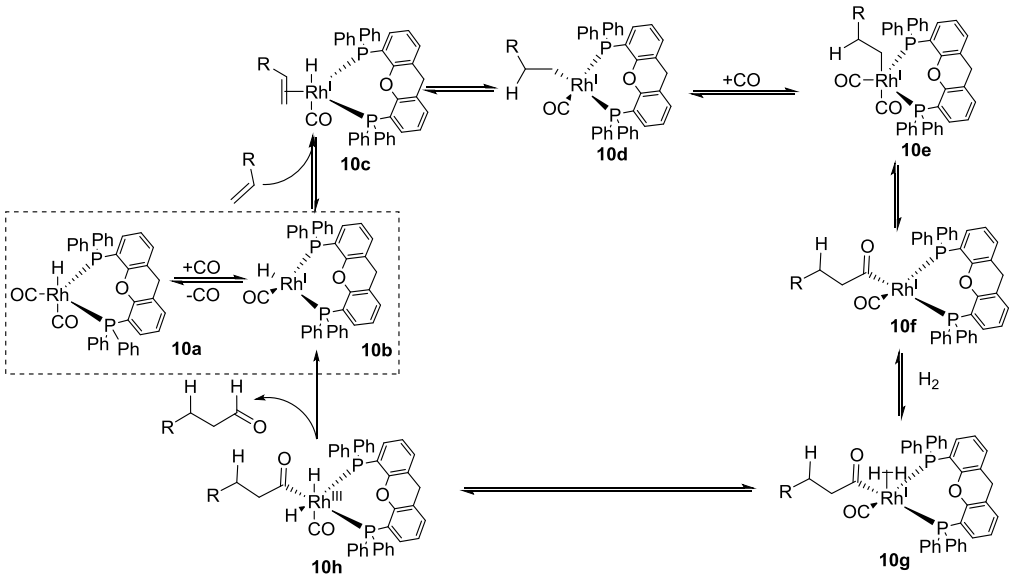

Scheme 2.10 Hydroformylation mechanism

In hydroformylation, the activation of the H_2 occurs after the migratory insertion of the alkyl onto a carbonyl, forming the 4-coordinate acyl species (**10f**). The acyl **10f** coordinates H_2 to form **10g** which then undergoes oxidative addition to form **10h**, an 18 electron Rh^{III} complex. Oxidative addition is favoured by a more electron rich metal centre, CO ligands and phosphites remove electron density so should have a negative influence on this stage. Phosphines increase electron density, therefore the catalysts should have faster rates of hydrogenation, although this is off-set by the rate limiting factor of dissociating a carbonyl (**10a** to **10b**).

2.3.2 Possible hydrogenation of aldehydes mechanism

The difference between aldehyde hydrogenation and alkene hydrogenation is the polarity of the bond. While terminal alkenes can form the linear or branched Rh-alkyl complexes (**10d**) the insertion still forms a Rh-C bond. If an aldehyde is substituted into a hydroformylation-like mechanism then there is a choice between forming a Rh-O bond or a Rh-C bond. The mechanisms in schemes 2.11 and 2.12 show this.

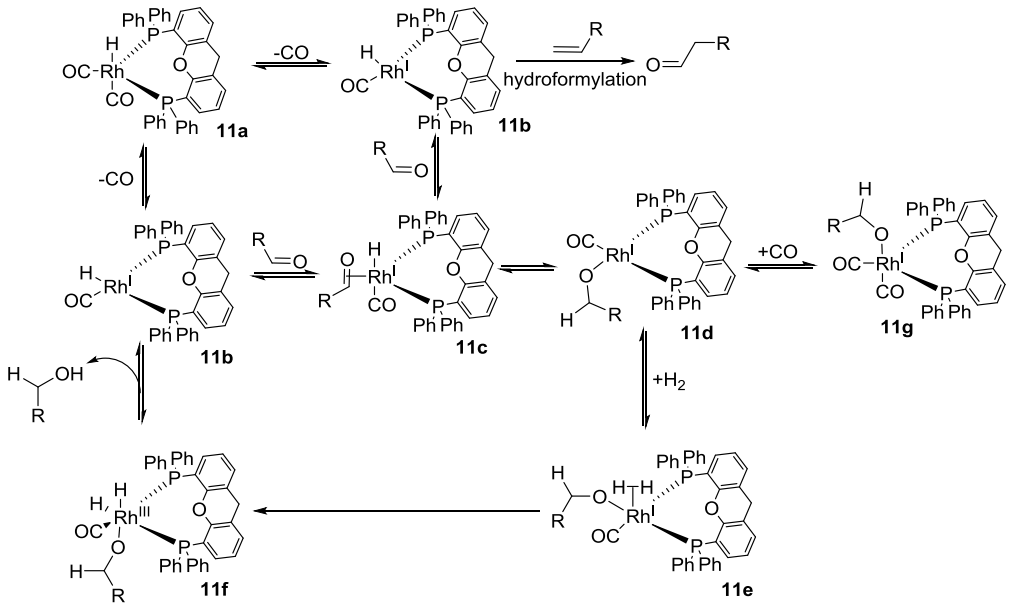

Scheme 2.11 Proposed hydrogenation mechanism with an alkoxide intermediate

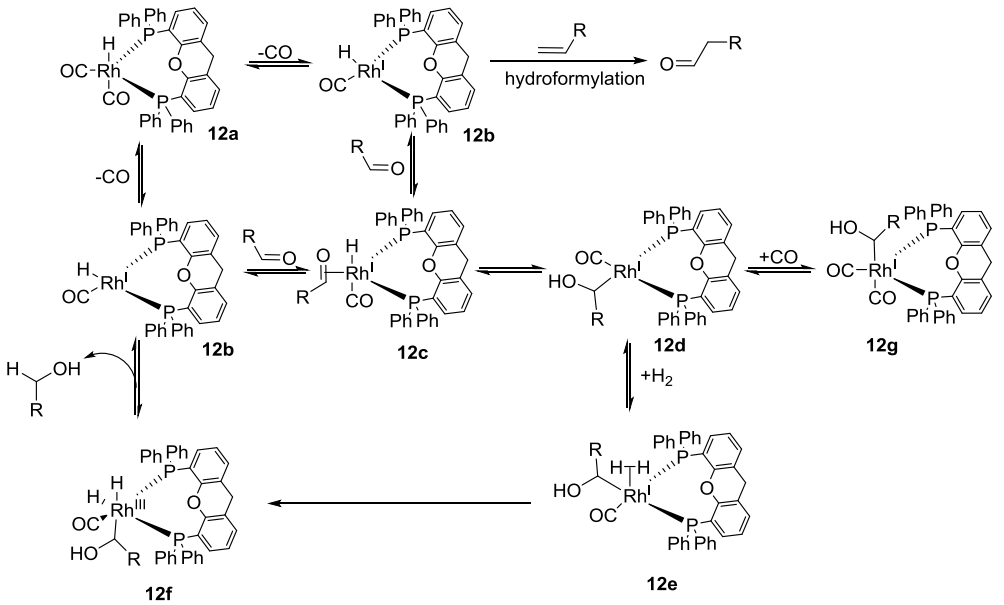

Scheme 2.12 Proposed hydrogenation mechanism with a hydroxyalkyl intermediate

Starting from the resting state of the hydroformylation catalyst (**11a**, **12a**) the first stage is dissociation of a CO ligand to give a 4-coordinate, square-planar intermediate (**11b**, **12b**). To

this the aldehyde or the alkene can coordinate to begin the hydrogenation or hydroformylation cycles, respectively.

The geometry of the complex with the associated aldehyde (**11c**, **12c**) would be a 5 coordinate species with the hydride ligand in an axial position, similar to that proposed for hydroformylation. The aldehyde can insert into the metal-hydride bond either in the carbonyl carbon, with the oxygen binding to the metal, forming an alkoxide ligand (**11d**), or in the oxygen forming a hydroxyalkyl complex (**12d**). The equivalent alkyl complex in the hydroformylation mechanism (scheme 2.9) (**10d**) coordinates another CO before forming an acyl complex (**10f**). However, in the hydrogenation mechanism this would make an inactive 5-coordinate species (**11g**, **12g**). This competition between CO and H_2 might contribute to the slower rate of hydrogenation compared to hydroformylation however if it was significant then plot 3.3.7 would expected to have an increased rate of hydrogenation due to an increased ratio of H_2 to CO.

Following this step, the coordination of a molecule of hydrogen will form **11e** and **12e** and oxidative addition gives the Rh^{III} di-hydride complexes **11f** and **12f**. From the di-hydrides, reductive elimination occurs to regenerate the species **11b** and **12b.** This is a mechanism that closely follows hydroformylation however it does not explain why the isopropanol or water has a positive effect on catalysis or why it is that xantphos like ligands are necessary. There are also reports, discussed in section 3.3.5, that rhodium monohydrides are not active enough for hydrogenation.[35]

2.3.3 Hemi-labile L(P,O,P) Hydrogenation Mechanism

The mechanism of hydroformylation-hydrogenation can be compared to Reek and van Leeuwen's switchable hydroformylation-hydrogenation catalyst, consisting of a nixantphos ligand tethered to a silica-support (scheme 3.13).[24] On silica, $[Rh(P\text{-}P)(CO)]^+$ has been identified and catalyses hydroformylation with an aldehyde l/b ratio of 65. However, a high amount of nonanol was also detected and under hydroformylation conditions a mixture of both $[HRh(P\text{-}P)(CO)_2]$ (**13a**) and $[Rh(P\text{-}P)(CO)]^+$ (**13b**) are present on the surface of the support.

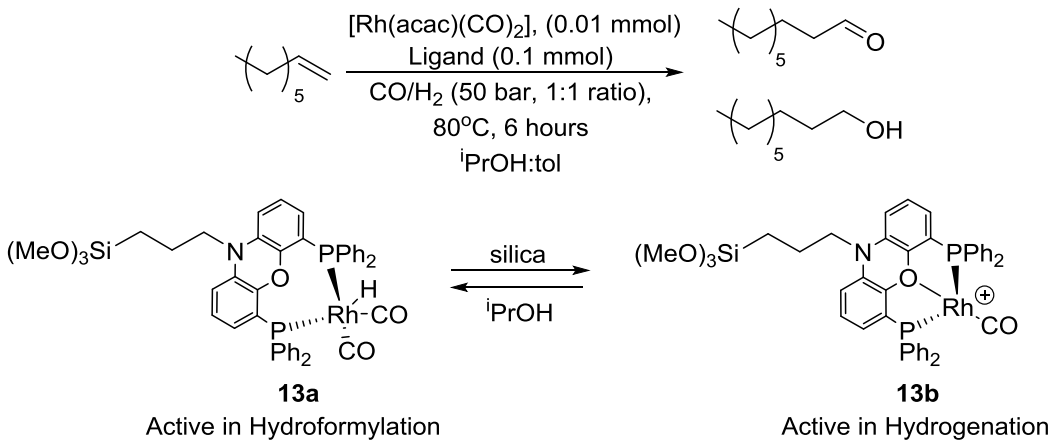

Scheme 2.13 Reek and van Leeuwen's switchable hydroformylation/hydrogenation catalyst[24]

It is proposed that the acidic silica protonates the rhodium then reductive elimination of H_2 gives the cationic species **13b**, responsible for hydrogenation activity. This is supported by IR and NMR spectroscopy. The cationic species **13b** features the xantphos bound in a κ(P,O,P) chelate fashion. If this is a vital feature of the hydrogenation catalyst it may explain why only xantphos type ligands induce hydrogenation activity in the 'on-water' screenings (section 2.2.6). Although, in this immobilised system isopropanol supresses the hydrogenation activity rather than enhancing it. An atmosphere of hydrogen returns the hydrogenation activity. Applying this to scheme 3.11 results in scheme 3.14.

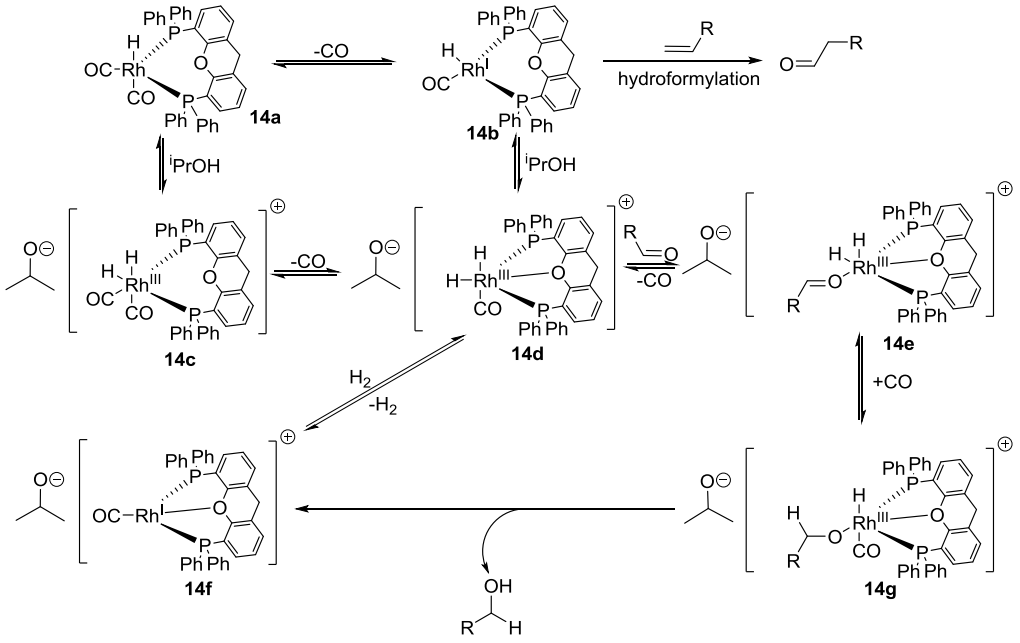

Scheme 2.14 Proposed catalytic cycle for the hemi-labile oxygen xantphos mechanism

In Van Leeuwen's system the addition of isopropanol is proposed to deactivate the acidic silanols on the silica surface. Although it may be possible that within the on-water system

discussed above the small amount of isopropanol or water acts as the silica does in the immobilised system. If so, the temperature dependence may relate to the ease of deprotonation of the isopropanol. There would also be a negative influence from the partial pressure of hydrogen as it would push the equilibrium towards the hydride rather than reductive elimination of hydrogen, this is observed in section 3.3.7 where a lower rate of hydrogenation is observed despite a higher partial pressure of H_2.

The resting state for the hydroformylation catalyst (**14a**) can progress to the active hydroformylation catalyst (**14b**) by loss of a carbonyl. **14b** can coordinate an alkene and perform hydroformylation as outlined in scheme 2.11, or it can be protonated by ^{i}PrOH which then forms **14d** consisting of a cationic 18 electron Rh^{III} dihydride cation with a $^{i}PrO^{-}$ anion. The hemi-labile oxygen of the xantphos is coordinated, as proposed by van Leeuwen and Reek (scheme 2.13), and which has been shown to take part in catalysis in the case of Ru transfer hydrogenation.[36]

14d can also be formed by the reaction of **14a** with isopropanol to form the charged species **14c**, which is also an 18 electron dihydride, but with a CO instead of the hemilabile oxygen. **14c** then dissociates a CO and the hemi-labile oxygen binds to the rhodium. The difference between the pathways from **14a** to **14d** depend on the ability of isopropanol to protonate the Rh, presumably an easier task for the more electron rich and less sterically hindered **14b**. Furthermore **14b** is known to be the start of the hydroformylation cycle therefore is inherently present in solution, although will rapidly react with the alkene to perform hydroformylation which is why the hydroformylation occurs far faster than hydrogenation, which only occurs once a significant amount of the alkene is consumed.

14d can then undergo reductive elimination of H_2 to give the cationic species **14f,** similar to that proposed by van Leeuwen and Reek, but with the isopropyl anion, rather than the silica, acting as a counter-charge. **14f** is a 16 electron species so could coordinate a carbonyl for added stability or it can coordinate and activate hydrogen by oxidative addition, returning to **14d**.

To progress along the cycle a vacant coordination site must be created in **14d** for the aldehyde to bind and form **14e**. This can occur by loss of CO or the xantphos oxygen can dissociate. The strength of the Rh-O vs the Rh-CO bond and the entropic favourability of a CO molecule dissociating and re-associating vs breaking the κ(P,O,P) chelate would need to be considered for the more favourable pathway to be determined. The active role of the xantphos oxygen in

this mechanism is supported by the lack of hydrogenation activity from other bidentate ligands in section 2.2.6.

After migratory insertion of H onto the O or the C (shown above) of the aldehyde a CO or the xantphos O will re-coordinate to maintain the 18 electron species **14g**. From **14g**, reductive elimination of nonanol results in **14f** which, as discussed above, can activate hydrogen and close the cycle.

The coordination of the hemi-labile oxygen to the rhodium centre, resulting in a κ(P,O,P) tridentate ligand has been observed crystallographically, most often in octahedral complexes.[37] Alternatively, in the immobilised system, oxygen of the silica can also perform this function, as they must be close enough to protonate the metal and act as an anionic counter-ions therefore should be capable of binding as well. There are reports of DPEPhos performing catalysis dependent on the coordination of this central oxygen where xantphos does not, but in section 2.2.6 this was not found to be the case.[38]

2.3.4 ^{i}PrOH Assisted Proton Transfer Hydrogenation Mechanism

An alternative role for the isopropanol/water is to act as a hydrogen shuttle. This has been reported by Schrock and Osborn for ketone hydrogenation catalysed by a cationic rhodium catalyst (scheme 3.15).[35] The catalyst consisted of mono-dentate Lewis Basic PMe_2Ph ligands with anionic counter-ions present. Addition of 1% water by volume induced the best increase in the rate of ketone hydrogenation and also inhibited olefin reduction.

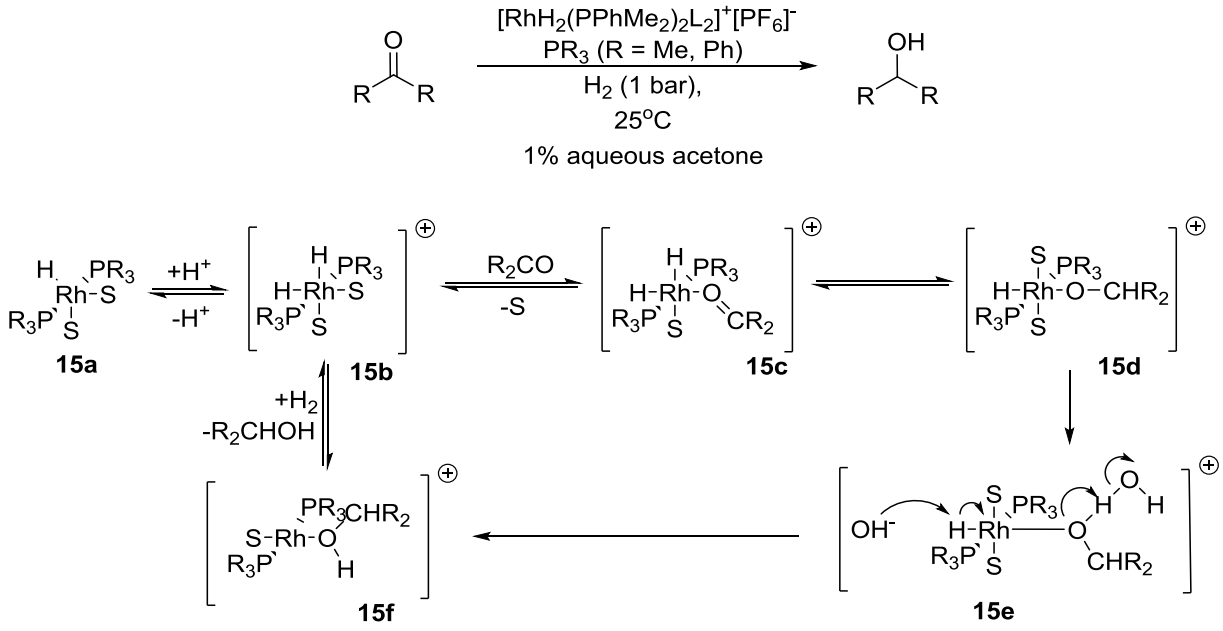

Scheme 2.15 Schrock's water promoted hydrogenation mechanism[35]

The ketone coordinates to the metal (**15c**) and then a 1,3-hydride migration from the cis-site to the carbon on the ketone group occurs (**15d**). To generate the alcohol, water facilitates proton shuttling: deprotonating the metal at the same time as protonating the alkoxy-group (**15e**). The authors report that ethanol also promotes reduction. The water can also deprotonate the cationic species and make a neutral monohydride species, but this was found to be inactive in hydrogenation until HBF_4 is added. NEt_3 also hinders the reaction by deprotonating the active dihydro complex.

The mechanism was investigated further in DFT studies.[39] An inner-sphere and an outer-sphere mechanism of hydrogenation were considered, with the calculations favouring the former. The rate determining step was calculated to be the transfer of the hydride to the ketone. This is followed by reductive elimination assisted by two water molecules. There are also DFT calculations that show H_2O and other H-bond donors assisting in activating H_2 for oxidative addition when it is bound to Ru-catalysed systems.[40]

Applying the concepts of hydrogen shuttling to scheme 2.11 results in a mechanism as presented in scheme 2.16.

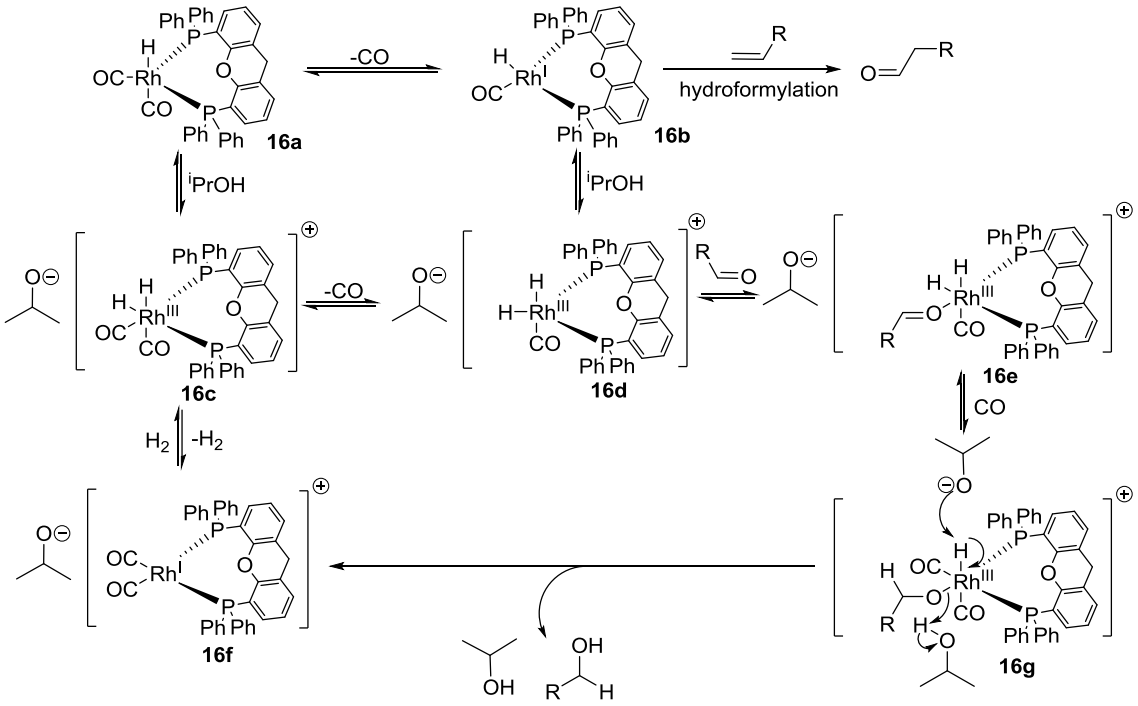

Scheme 2.16 Isopropanol assisted proton transfer mechanism

This is similar to scheme 2.14 but the oxygen of the xantphos does not bind to the rhodium, any vacant sites are occupied by CO as in hydroformylation. Although binding the hemi-labile

oxygen is still a possibility, keeping in line with the xantphos-only hydrogenation described in section 2.2.6.

In **16g** the hydride is proposed to migrate to the C of the aldehyde, although it could possibly migrate to the O (see scheme 3.12). In this mechanism the isopropanol acts as a counter-ion and also promotes the liberation of nonanol in a similar mechanism to that proposed by Schrock and Osborn (**15e**).

Applying information from Schrock's reports to the 'on-water' mechanism some points can be taken: it is energetically favourable to have an inner sphere mechanism and water or alcohols can take an active role in shuttling protons as well as H-bonding to stabilize intermediates. That the hydride preferentially migrates to the carbon would indicate that the mechanism in scheme 3.11 would be preferred.

However these insights must be taken cautiously as there are crucial differences between the systems. Schrock uses monodentate phosphine alkyl ligands that are more electron donating than xantphos, there are counter-ions to stabilize this cationic species and the entire system occurs in pure H_2 rather than syn-gas. The observation that the neutral monohydride is an inactive species in hydrogenation raises doubts about schemes 3.11 and 3.12 as these are based on the neutral monohydride. But, if temperature is able to increase the reactivity of the monohydride it may still explain the hydrogenation activity. Cationic species are not suitable for CO ligands as the lower electron density will not favour the characteristic π^*-back bonding, that is why more Lewis basic ligands are favourable for those catalysts.

2.3.5 Inner-sphere hydrogenation Mechanism

As discussed above, an inner-sphere hydrogenation is more favourable than an outer-sphere mechanism. One of the most established catalysts for alkene hydrogenation is Wilkinson's catalyst (section 1.2.3). This species works by an inner-sphere mechanism (scheme 3.17).

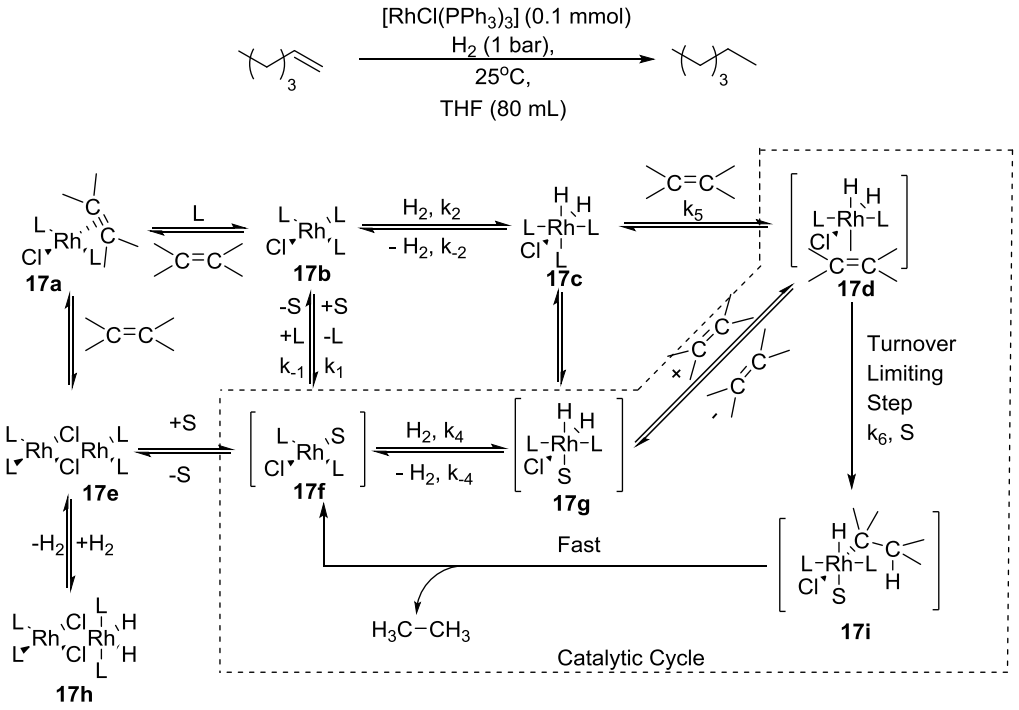

Scheme 2.17 Wilkinson's Catalyst inner-sphere mechanism of hydrogenation[41]

The main catalytically active component is a neutral Rh^{I} complex (**17b**), which consists of phosphine ligands coordinated in a trans fashion and a chloride that does not transfer from the metal, unlike the hydrides of the hydroformylation catalyst. In this case, hydrogen is activated before the olefin is coordinated, the hydrogen-first mechanism. The alternative olefin-first mechanism is favoured by the cationic phosphine-ligated rhodium catalysts Schrock proposes above. Coordinating solvent is necessary to assist the catalyst by keeping binding sites open (**17f**).

Monodentate ligands, the possibility of bridging Cl to form a dimer (**17e**), the presence of a fixed Cl ligand and the lack of CO ligands all mean that there is a very large difference between this system and the proposed pathway for the on-water system. However, some elements of this mechanism can be applied to the mechanism in scheme 3.11 and these are presented below (scheme 3.18).

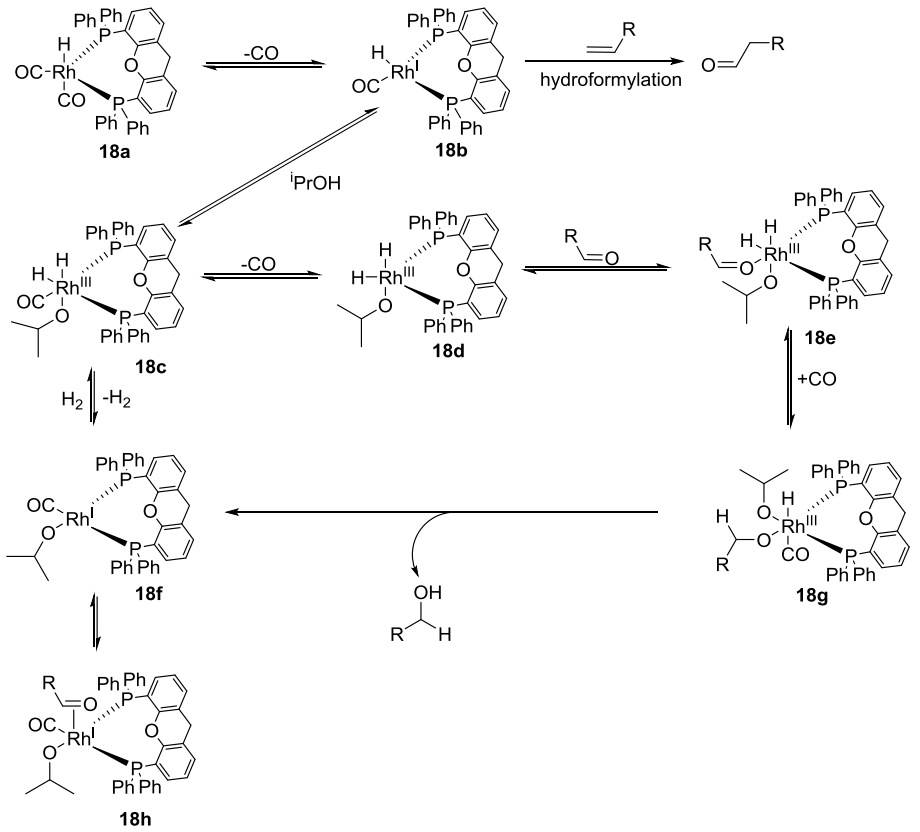

Scheme 2.18 Inner-sphere hydrogenation mechanism with coordinated isopropanol

In this case the isopropanol undergoes oxidative addition to the metal rather than acting as an acid to protonate and act as an anionic counter-charge as shown in schemes 3.14 and 3.16. The species that coordinates the aldehyde is a di-hydride (**18d**) and undergoes a hydride transfer, shown to the carbonyl C (**18g**), followed by reductive elimination to form **18f. 18f** is a Rh^{I} species, but the charge is contributed by the coordinated isopropyl anion. **18f** then activates a molecule of hydrogen to regenerate a Rh^{III} dihydride (**18d**) from which dissociation of a CO ligand is required to before the aldehyde can coordinate.

Central to the mechanisms above is the transition from a Rh^{I} monohydride to a Rh^{III} dihydride and then the formation of a cationic rhodium species. Kalck studied a Rh^{I}-Rh^{III} dinuclear trihydride complex which could fragment and make two active catalysts: a hydroformylation and a hydrogenation catalyst (scheme 2.19).

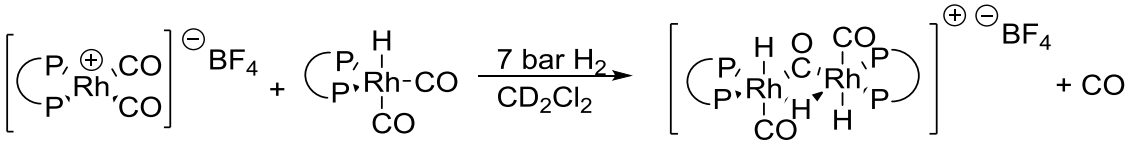

Scheme 2.19 Formation of a Rh dinuclear trihydride

The cationic dicarbonyl is converted into a cationic dihydride, detectable by ^{1}H NMR spectroscopy, which then reacts with the monohydride to make the trihydride. The cationic species needs a counter-ion to be stable but in the 'on-water' system anionic charge in the water, the $acac^-$ from the $[Rh(acac)(CO)_2]$ complex or the ^{i}PrOH can also perform this role.[42] The di-hydride, mono-hydride and tri-hydride were all observable under a pressure of 7 bar 1:1 $CO:H_2$. .

2.3.6 Alternative Hydroformylation-Hydrogenation Mechanisms

The schemes above are all proposed to be compatible with hydroformylation and use hydrogen as a hydrogenation source. Two alternative mechanisms, still based on rhodium, are Cole-Hamilton's alkyl phosphine system and Breit's super-molecular two ligand system.

Cole-Hamilton's auto-tandem rhodium-catalysed hydroformylation-hydrogenation system (scheme 2.20) generates alcohols without forming intermediate aldehydes.[9] Lewis basic trialkylphosphines operate in protic solvents. High conversion is obtained at 100 °C although the presence of excess ligand lowers the yield. The mechanism of this reaction was supported by D-labelling studies and NMR/IR spectroscopy. A transfer of the hydride to the aldehyde can form hydroxylalkyl and alkoxide intermediates but the oxophilicity of rhodium being low, a hydroxyalkyl intermediate (**20g**) was proposed to form, a different proposal to Schrock's ketone hydrogenation catalyst above (**15d**). When PPr^i_3 was used, more Lewis basic than PEt_3, only aldehyde was detected. This was proposed to be due to a direct protonation of the rhodium complex (**20f**) causing reductive elimination of the aldehyde before the alcohol can be formed.

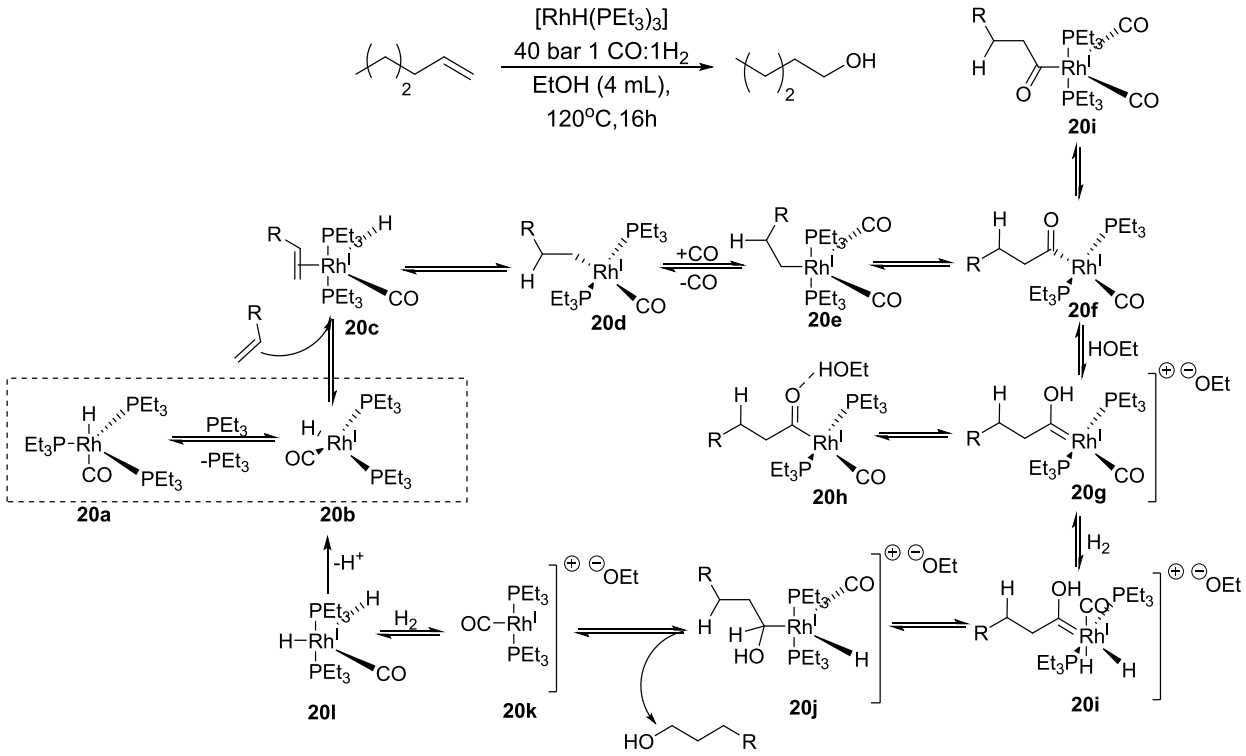

Scheme 2.20 Cole-Hamilton's hydroformylation-hydrogenation mechanism[43]

Later work investigated the cooperative effects between ligands like xantphos and additional PEt_3. The l/b ratios for the alcohols are lower than in the results in this thesis, <5.2, and there is increased isomerisation activity.[28] The electron rich acyl intermediate is proposed to be key in the catalysis to make the alcohol without liberating the aldehyde. Like the on-water system the catalyst preferentially hydrogenates linear aldehydes.

The mechanism in scheme 3.20 shows that alcohol can act as a counter-ion to stabilise a rhodium complex, as has been proposed in schemes 3.14, 3.16, and 3.18. However, PEt_3 as a ligand is much more electron donating than xantphos. CO and xantphos are electron withdrawing ligands and although a pentavalent $[Rh(COMe)(CO)_2(PEt_3)_2]$ (**20i**) is discussed in the report, the authors conclude that a loss of CO is required to provide enough electron density to make the acyl electronegative enough to be protonated (**20f** to **20g**). Therefore the direct protonation of an intermediate in schemes 3.14, 3.16 and 3.18 is highly unlikely.

The alternative to an inner sphere hydrogenation mechanism would be an outer-sphere mechanism like Breit's hydroformylation-hydrogenation mechanism with a rhodium catalyst supported by a guanidinium ligand (**21b**) performing hydrogenation (scheme 3.21).

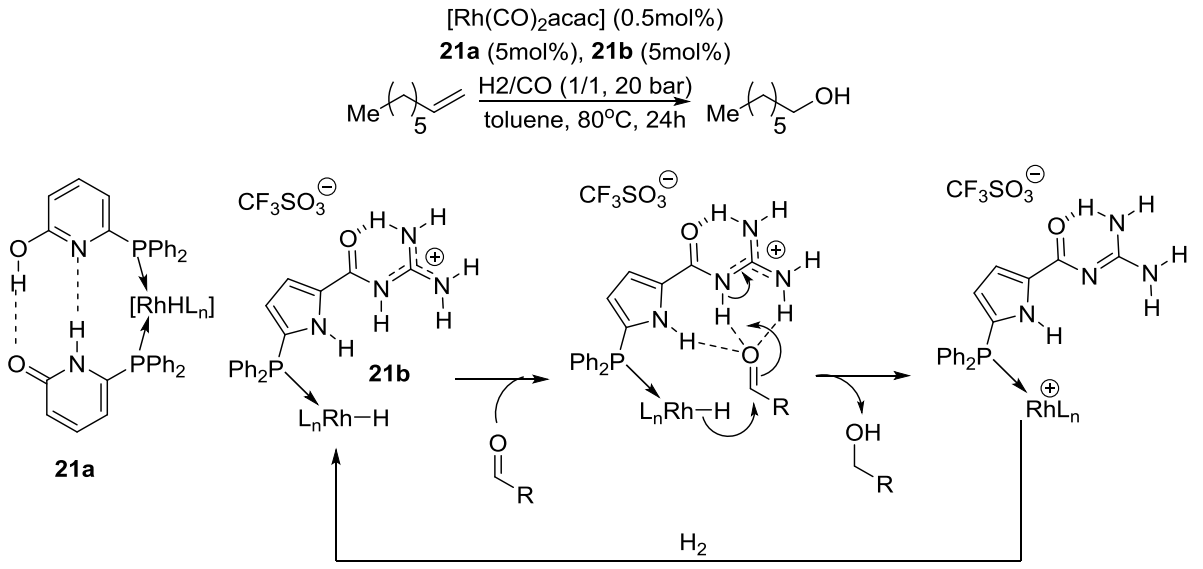

Scheme 2.21 Breit's outer-sphere hydroformylation-hydrogenation auto-tandem catalysis system

The initial hydroformylation is carried out by a complex **21a** which coordinates a bidentate ligand, itself assembled by H-bonding, to give aldehydes with good l/b ratios. In hydroformylation, this catalyst performs slightly better than xantphos due to the electron-withdrawing properties of the pyridone. The authors note that above 110°C the selectivity drops due to the disruption of the H-bonding. [44]

This mechanism is similar to Cole-Hamilton's system that operates using an external proton source acting as a component in hydrogenation. The regeneration of the active hydrogenation catalyst **21b** may occur because of a heterolytic cleavage of H_2 or a proton transfer from Rh activated H_2 to the guanidine ligand. The solvent is CH_2Cl_2 as alcohols interfere with the hydrogen-bonding network and interrupt the mechanism of catalysis. The presence of CF_3SO_3H is required to act as an anion source for the cationic species. The species **21b** is completely selective for aldehyde reduction over ketone reduction.

In the 'on-water' system there has been discussion about the possibility that hydrogen bonding can stabilise intermediates in catalysis. But under the high temperature conditions hydrogen bonding would break down therefore the mechanism is more likely to be one of the inner sphere mechanisms proposed in schemes 2.14, 2.16 and 2.18 than anything resembling schemes 2.20 or 2.21.

2.3.7 Alternative roles for water in hydroformylation-hydrogenaiton mechanism

While the mechanisms proposed above do not need water, in line with the experiments in chapter 2, there could still be an influence from its presence. For example Sharpless reported an increase in reaction rate when reactants for the Diels-Alder reaction were stirred vigorously together with water: an explanation for this is the increase in local substrate concentration as a result of the biphasic nature of the system. [13]

This idea was recently revisited by Beattie and McErlean, who proposed that hydroxide ions are stabilized at the water-organic interface in an emulsion. This lowers the pH and explains why acid-catalysed reactions, such as the Diels-Alder reaction, occur faster in water-organic emulsions. Theoretical studies elaborate on and support, this idea.[45]

In hydrogenation catalysis the negative charge at the water interface, according to the McErlean model, could facilitate stabilization of a cationic species which can catalyse reduction, effectively acting as a counter-ion to stabilize the cationic species without necessarily interacting with the catalyst.[19]

Another explanation could be that at the elevated temperatures the Water-Gas Shift reaction is occurring (scheme 3.15).[46] Both hydroformylation and reduction are observed under the water-gas shift conditions and combining them is termed hydrohydroxymethylation (scheme 2.22).

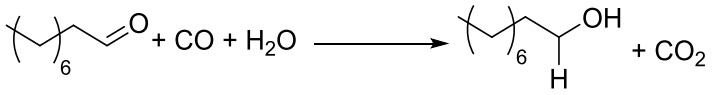

Scheme 2.22 Potential Water-Gas Shift reaction scheme

Laine studied the hydroformylation and hydrohydroxymethylation of 1-pentene using several metal clusters, including $Rh_6(CO)_{16}$. The reaction systems were pressurized 55 bar of CO and are in a 3M KOH solution at 135ºC or 150ºC.[47] Laine observed hydrogenation to occur much faster than hydroformylation, not something that is observed in Vogt's system. Since Kalck's 1985 review, it appears the majority of water-gas shift literature concerns heterogeneous catalysts.[46]

The water-gas shift reaction is unlikely in the hydroformylation-hydrogenation system as it is ligand dependent and there are similar enough hydrogenation systems to support an active hydrogenation pathway.

2.4 Conclusions and Future Work

These results show that the hydrogenation activity is not at the expense of the hydroformylation activity; the hydroformylation activity is incredibly rapid but the hydrogenation of the aldehyde occurs at a slower rate. The hydrogenation of the aldehyde is preferred over hydrogenation of the alkene at a gas ratio of 1:1 $CO:H_2$ (section 2.2.6). It was previously established that elevated temperatures are required for complete hydrogenation activity and the results in chapter 2 add to this. The most important findings are the results in section 2.2.10 that showed that the volume of water is not necessary to induce hydrogenation and can actually be omitted, provided that alcohol is present, with isopropanol giving the best results (section 2.2.4).

Other important details from the screenings are that xantphos-like ligands are necessary for hydrogenation, although not hydroformylation (section 2.2.6). In the absence of isopropanol then 3 equivalents of PPh_3 boosts hydrogenation activity (section 2.2.8). Cationic rhodium precursors induce hydrogenation activity at lower temperature and in toluene but neutral rhodium precursors perform better at higher temperature and in the presence of water (section 2.2.6).

The high pressure NMR results show that the main species in solution at elevated temperatures is the $[RhH(CO)_2(Xantphos)]$ with the ligand coordinated in an ee-mode, as expected from previous hydroformylation studies. This is observed in the consistence of hydroformylation activity (section 2.2) through-out the reaction. Also important to note is that the aldehyde is definitely produced as an intermediate and is converted into alcohol over time.

Reaction profiles for the main auto-tandem hydroformylation-hydrogenation mechanism have been produced. These show that hydroformylation is rapid and hydroformylation activity is not lost during the reaction or is exchanged for hydrogenation activity. Linear aldehydes are hydrogenated preferentially followed by the branched aldehydes, as the decreasing alcohol l/b ratio over time shows. The high pressure NMR spectroscopic results showed that at elevated temperatures the main complex observed is $[HRh(CO)_2(xantphos)]$ (**10b**), which is the same as the resting state in hydroformylation.

Based on **10b** as a resting state the hydrogenation can occur orthogonally to the hydroformylation by a monohydride mechanism (schemes 2.11 and 2.12) or a cationic rhodium di-hydride mechanism (scheme 2.14, 2.16 and 2.18). A high amount of hydrogenation activity can be induced simply by the presence of isopropanol in toluene rather than water lends support to an active role of the isopropanol.

At any point in the catalytic cycle an electron withdrawing CO ligand can be replaced by a more electron donating PPh_3 ligand which would increase the electron density on the metal and assist in activation of the hydrogen. This matches the boost to hydrogenation that extra equivalents of PPh_3 have, as reported in section 2.2.8.

If the key step is a protonation of the rhodium catalyst by isopropanol or water then the presence of a base should inhibit the reaction: by deprotonating the rhodium di-hydride or preventing the isopropanol from protonating the rhodium catalyst to begin with. But that the addition of a base had no effect on the final selectivity (table 2.21) questions the validity of this theory. However, repeating with excess of base and monitoring the effect on the hydrogenation rate would clarify this.

There is ample evidence in the literature for this mechanism: Schrock has shown that rhodium monohydrides are not active in hydrogenation[35] and Kalck reported that there can be a conversion between monohydrides and di-hydrides that exist in the same solution.[42] Schrock also demonstrated water or alcohols can influence hydrogenation through proton shuttling.[39] Cole-Hamilton reported that alcohols can protonate and act as a counter-ions to rhodium complexes[9] and van Leeuwen reported a hydroformylation-hydrogenation system based on a cationic rhodium complex generated from protonation of a monohydride by acidic silica silanols.[24] The immobilised nixantphos is proposed to coordinate in a κ(P,O,P), a binding scheme supported in literature.[36]

However, there are many more techniques and parameters to elucidate the true mechanism. More high-pressure NMR experiments with added isopropanol should reveal if a di-hydride or a cationic species can be created in solution in the presence of the alcohol. Some DFT calculations that could calculate the energy, and thus feasibility, of the catalytic cycle would be useful. Changing the electronic properties of the xantphos ligand and monitoring the rate of hydrogenation would also be interesting; if made more electron donating then it should be easier to protonate the rhodium centre. Diphosphites would be an interesting ligand to look at as they were avoided for their moisture sensitivity but as the reaction does not need to occur in water they could still be used.

2.5 Materials and Methods

All solvents were dried in a solvent purification system and stored over 4Å molecular sieves under argon. Solvents were degassed in a sonicator. Chemicals were purchased from Aldrich or Fisher and used without further purification unless specified. 1-octene and decane were filtered over aluminum oxide to remove peroxides. Syn-gas 1:1 $CO:H_2$ was purchased from BOC. Triptycene was synthesized by group member Eszter Fazekas by a method to be published in her thesis. ^{t}Bu-xantphos and Nixantphos were kindly provided by the group of Prof Arno Behr at Technische Universität Dortmund.

NMR spectra were recorded on a Bruker AVA400 spectrometer for ^{1}H (399.90 MHz); a Bruker AVA500 spectrometer ^{1}H (500.23 MHz), ^{13}C (125.76 MHz), ^{1}H DOSY, ^{1}H COSY, ^{1}H-^{13}C HSQC or a Bruker PRO500 spectrometer ^{1}H (500.23 MHz), ^{13}C (125.76 MHz), ^{31}P (202.50 MHz), ^{119}Sn (186.45 MHz).

2.5.1 Synthesis of phenoxaphos

The procedure was taken from the thesis of Dr Maria Segarra-Maset.[48]

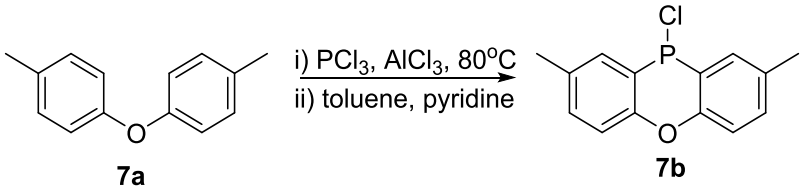

Scheme 2.23: Synthesis of phenoxaphos

PCl_3 (12.5 mL, 0.14 moles), $AlCl_3$ (4.9g, 0.037 moles), and p-tolylether (4.9g, 0.025 moles) (**7a**) were heated under reflux overnight. Excess PCl_3 was distilled off and a solution of pyridine (6mL) in toluene (50mL) was added dropwise. The crude yellow solution was filtered through Celite before removing the toluene under vacuum. Yield: 3.2g (49%). ^{1}H NMR (500.23MHz, $CDCl_3$, 300K) δ_H (ppm): 2.43 (s, 6H, *aromatic CH₃*), δ_H 7.25 (d, 2H, *aromatic CH*), δ_H 7.38 (dd, 2H, *aromatic CH*), δ_H 7.62 (dd, 2H, *aromatic CH*). ^{31}P NMR (202MHz): δ_P 37.18

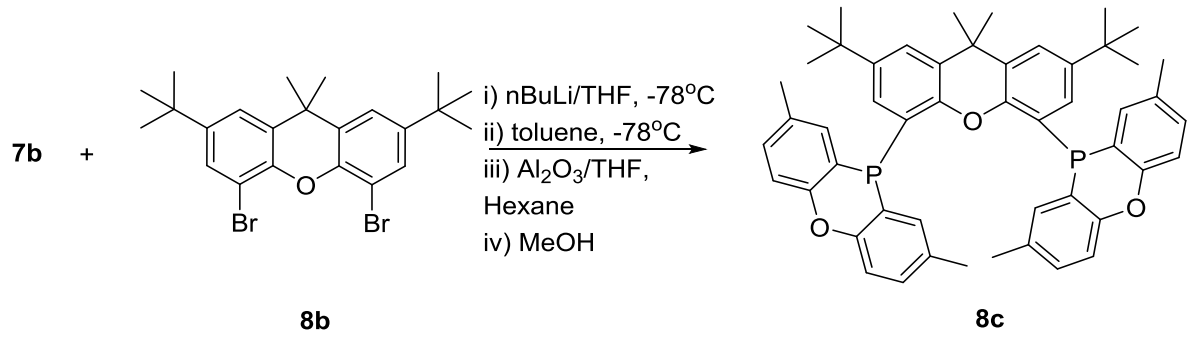

Scheme 2.24 Synthesis of phenoxaphos

4,5-dibromo-2,7-ditertbutyl-9,9-dimethylxanthene (**8b**) (2.87g, 6.00 mmol) was placed in THF (100mL) in a dry ice/acetone bath. A solution of ^{n}BuLi/hexanes (2.5 M, 9.9 mL) was added dropwise. After stirring for 4 hours 2,7-dimethyl-10-chlorophenoxaphosphine (**7b**) (1.99g, 7.6 mmol) in toluene (20mL) was added. After stirring overnight the THF was removed under vacuum, the crude solid dissolved in toluene and filtered over neutral aluminum oxide. The solvent was removed and the product obtained as a pure white powder by recrystallization in toluene/^{i}PrOH. The purity was determined by NMR and matched previously reported synthesis. Yield: 1.113g (28%). ^{1}H NMR (500MHz, $CDCl_3$, 300K) δ_H (ppm): 1.12 (s, 18H, *$C(CH_3)_3$ xanthene*), δ 1.58 (s, 6H, *CH_3 xanthene*), δ 2.39 (s, 12H, *CH_3 phosphino groups*), δ 6.75 (m, 2H, *aromatic CH xanthene*), δ_H 7.15 (d, 4H, *aromatic CH phosphino*), δ 7.22 (dd, 4H, *aromatic CH phosphino*), δ 7.28 (d, 2H, *aromatic CH xanthene*), δ 8.08 (d, 4H, *aromatic CH phosphino*). ^{31}PNMR (202MHz, $CDCl_3$, 300K) δ_P (ppm): -70.74

2.5.2 Catalysis Procedure

Before the screenings were performed the established experimental procedure was improved. Previously, the dry reagents were weighed into an autoclave and the substrate and solvent were then added directly under argon before pressurization and heating. It is difficult to consistently weigh such small quantities and so a stock solution of rhodium precursor and ligand in toluene or toluene/alcohol was made up and partitioned between the autoclaves. This also minimized the possibility of the catalyst being exposed to air. To allow catalyst formation autoclaves with addition funnel attachments were used and the substrates added after one hour at the pressure desired and temperature.

After 6 hours the autoclaves are placed in water baths to cool down before venting. A portion of the organic layer was removed and dissolved in DCM before analyzing the products using a Shimadzu GC-2010 FID, equipped with a AOC-20i auto injector. Agilent J&W Ultra 2 column, 25 m, 0.2 mm inner diameter, 0.33 μm film thickness. Injection mode: split ratio: 10.0,

temperature: 280°C, carrier gas: He, pressure: 105.5 kPa, total flow: 11.3 mL/min, column flow: 0.66 mL/min, linear velocity: 24.3 cm/s, split ratio: 50, detector temperature: 305°C. Program: 50°C, hold 7 mins, increase by 20°C/min to 280°C, hold 3 minutes. Response factors were calculated with respect to the decane internal standard.

2.5.3 Calculations for GC-FID analysis

2.5.3.1 Response Factors

Response factors were calculated by plotting the Area/1000000 against mass (g) and using the gradients of the lines of best fit to calculate response factors with respect to the decane internal standard. The area/1000000 was used because the limitations in excel resulted in imprecise initial area/mass gradients on the order of 9E+08 with no significant figures. Response factors are given in table 30.

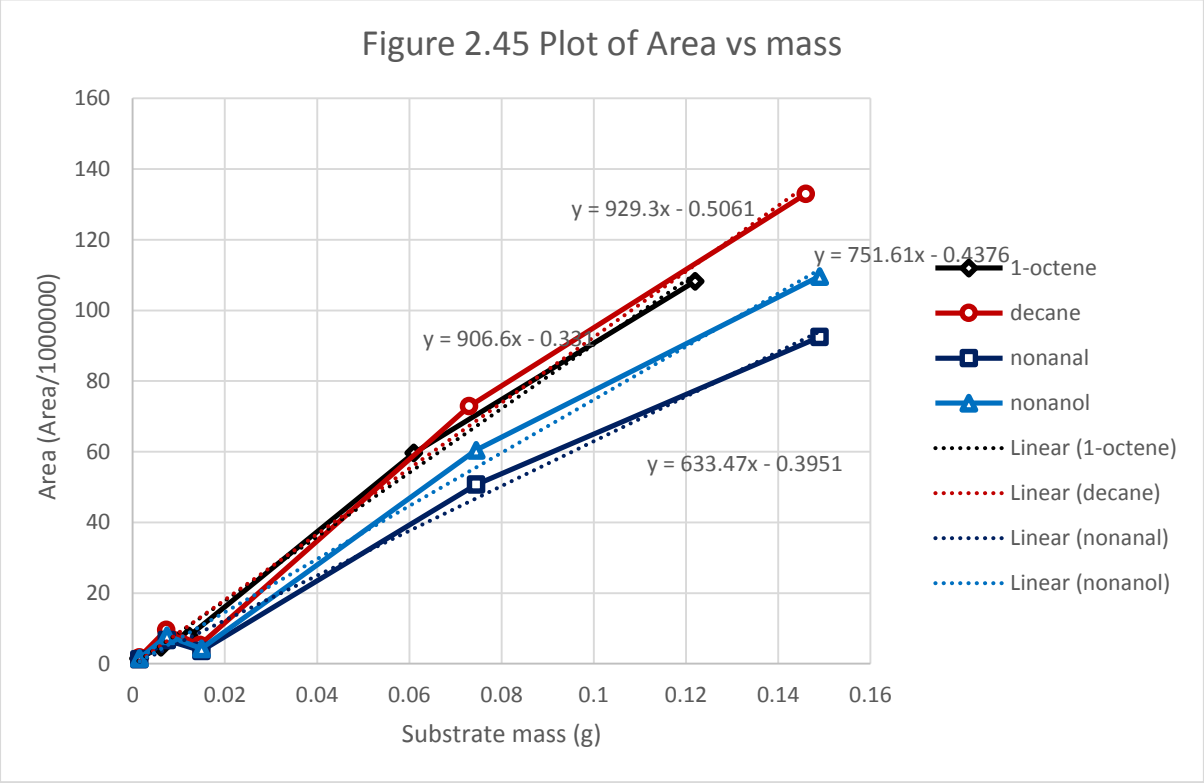

Table 2.2 Calculation of Response Factors

Substrate	Area/mass	Area/mass (Substrate) / Area/mass (Standard)	Response Factor (Rf)
Octene	906.6	0.9756	1.0250
Decane	929.3	1	1
Nonanal	633.47	0.6817	1.4670
Nonanol	751.6	0.8088	1.2364

2.5.3.2 Molecular Weights (g/mmol)

mol.wt (1-octene) = 0.11224 g/mmol

mol.wt (octane) = 0.11423 g/mmol

mol.wt (decane) = 0.14229 g/mmol

mol.wt (nonanal) = 0.14224 g/mmol

mol.wt (nonanol) = 0.14426 g/mmol

2.5.3.3 Conversion

mass(1-octene) = $(A_{octene}*mass_{decane})/(A_{decane}*Rf_{octene})$

mmol(1-octene) = mass(1-octene)/mol.wt(1-octene)

conversion(1-octene) = 100 – ((mmol(octene)/mmol (octene)*100)%

2.5.3.4 Yields (product)

mass(product) = $(A_{product}*mass_{decane})/(A_{decane}*Rf_{product})$

mmol(product) = mass(product)/mol.wt(product)

yield(product) = ((mmol(product)/mmol (octene)*100)%

2.5.3.5 Selectivity

Selectivity (product) = Yield (product)/(Total Yields + (100 - Conversion))*100%

For the reaction profiles the materials and method, response factors and calculations of yield and conversion are the same as those outlined in section 2.5.2.

Initial attempts to replicate Diebolt's reaction profiles were unsuccessful because the reproducibility between runs was poor. Sampling was performed by extracting an aliquot of the reaction mixture through a capillary then extracting, in the case of the aqueous system, or diluting, in the case of toluene, the organic phase in dichloromethane. The poor reproducibility was proposed to be a consequence of the phase behaviour of the aqueous/organic system resulting in a variable amount of organic phase present in each sample. However, revisiting the sampling after improving the method (see chapter 2) resulted in definite reproducibility between the runs and the plots above were produced.

The high pressure NMR measurements were performed on a Bruker AMX2-200WB spectrometer using home-built high-pressure NMR probes or in a sapphire tube in a commercial 10 mm probe. CO, and nitrogen were purchased from BOC. Alkenes and NMR solvents were purchased from Aldrich and dried over activated molecular sieves and degassed before use.

2.6 References

[1] L. A. van der Veen, P. C. J. Kamer, P. W. N. M. van Leeuwen, *Angew. Chem. Int. Ed.* **1999**, *38*, 336-338.

[2] L. Diab, T. Šmejkal, J. Geier, B. Breit, *Angew. Chem. Int. Ed.* **2009**, *48*, 8022-8026.

[3] B. Hamers, E. Kosciusko-Morizet, C. Müller, D. Vogt, *ChemCatChem* **2009**, *1*, 103-106.

[4] O. Diebolt, C. Muller, D. Vogt, *Catalysis Science & Technology* **2012**, *2*, 773-777.

[5] M. Kranenburg, Y. E. M. van der Burgt, P. C. J. Kamer, P. W. N. M. van Leeuwen, K. Goubitz, J. Fraanje, *Organometallics* **1995**, *14*, 3081-3089.

[6] O. R. Hughes, J. D. Unruh, *J. Mol. Catal.* **1981**, *12*, 71-83.

[7] L. A. van der Veen, P. H. Keeven, G. C. Schoemaker, J. N. H. Reek, P. C. J. Kamer, P. W. N. M. van Leeuwen, M. Lutz, A. L. Spek, *Organometallics* **2000**, *19*, 872-883.

[8] P. W. N. Van Leeuwen, *Rhodium Catalyzed Hydroformylation, Vol. 22*, Kluwer Academic Publishers, 3300 AA Dordrecht, The Netherlands, **2000**.

[9] J. K. MacDougall, M. C. Simpson, M. J. Green, D. J. Cole-Hamilton, *J. Chem. Soc., Dalton Trans.* **1996**, 1161-1172.

[10] C. P. Casey, L. M. Petrovich, *J. Am. Chem. Soc.* **1995**, *117*, 6007-6014.

[11] J. R. Briggs, J. Klosin, G. T. Whiteker, *Org. Lett.* **2005**, *7*, 4795-4798.

[12] B. Hamers, P. S. Bäuerlein, C. Müller, D. Vogt, *Adv. Synth. Catal.* **2008**, *350*, 332-342.

[13] S. Narayan, J. Muldoon, M. G. Finn, V. V. Fokin, H. C. Kolb, K. B. Sharpless, *Angew. Chem. Int. Ed.* **2005**, *44*, 3275-3279.

[14] J. A. Osborn, F. H. Jardine, J. F. Young, G. Wilkinson, *Journal of the Chemical Society A: Inorganic, Physical, Theoretical* **1966**, 1711-1732.

[15] D. Pingen, C. Müller, D. Vogt, *Angew. Chem. Int. Ed.* **2010**, *49*, 8130-8133.

[16] R. R. Schrock, J. A. Osborn, *J. Am. Chem. Soc.* **1976**, *98*, 2134-2143.

[17] O. Diebolt, C. Cruzeuil, C. Müller, D. Vogt, *Adv. Synth. Catal.* **2012**, *354*, 670-677.

[18] D. Crozet, A. Gual, D. McKay, C. Dinoi, C. Godard, M. Urrutigoïty, J.-C. Daran, L. Maron, C. Claver, P. Kalck, *Chemistry – A European Journal* **2012**, *18*, 7128-7140.

[19] J. K. Beattie, in *Colloid Stability*, Wiley-VCH Verlag GmbH & Co. KGaA, **2010**, pp. 153-164.

[20] E. Zuidema, P. E. Goudriaan, B. H. G. Swennenhuis, P. C. J. Kamer, P. W. N. M. van Leeuwen, M. Lutz, A. L. Spek, *Organometallics* **2010**, *29*, 1210-1221.

[21] Y. Yuki, K. Takahashi, Y. Tanaka, K. Nozaki, *J. Am. Chem. Soc.* **2013**, *135*, 17393-17400.

[22] M. Schreuder Goedheijt, P. C. J. Kamer, P. W. N. M. van Leeuwen, *J. Mol. Catal. A: Chem.* **1998**, *134*, 243-249.

[23] R. Noyori, H. Takaya, *Acc. Chem. Res.* **1990**, *23*, 345-350.

[24] A. J. Sandee, J. N. H. Reek, P. C. J. Kamer, P. W. N. M. van Leeuwen, *J. Am. Chem. Soc.* **2001**, *123*, 8468-8476.

[25] C. Bianchini, A. Meli, M. Peruzzini, F. Vizza, P. Frediani, J. A. Ramirez, *Organometallics* **1990**, *9*, 226-240.

[26] A. R. Sanger, *J. Mol. Catal.* **1978**, *3*, 221-226.

[27] L. Bini, C. Muller, D. Vogt, *Chem. Commun.* **2010**, *46*, 8325-8334.

[28] I. I. F. Boogaerts, D. F. S. White, D. J. Cole-Hamilton, *Chem. Commun.* **2010**, *46*, 2194-2196.

[29] D. Evans, J. A. Osborn, G. Wilkinson, *Journal of the Chemical Society A: Inorganic, Physical, Theoretical* **1968**, 3133-3142.

[30] J. K. Macdougall, M. C. Simpson, D. J. Cole-Hamilton, *Polyhedron* **1993**, *12*, 2877-2881.

[31] A. Torres, N. Molina Perez, G. Overend, N. Hodge, B. T. Heaton, J. A. Iggo, J. Satherley, R. Whyman, G. R. Eastham, D. Gobby, *ACS Catalysis* **2012**, *2*, 2281-2289.

[32] S. C. van der Slot, P. C. J. Kamer, P. W. N. M. van Leeuwen, J. A. Iggo, B. T. Heaton, *Organometallics* **2001**, *20*, 430-441.

[33] Y. Ji, R. E. Plata, C. S. Regens, M. Hay, M. Schmidt, T. Razler, Y. Qiu, P. Geng, Y. Hsiao, T. Rosner, M. D. Eastgate, D. G. Blackmond, *J. Am. Chem. Soc.* **2015**, *137*, 13272-13281.

[34] J. M. Brown, A. G. Kent, *Journal of the Chemical Society, Perkin Transactions 2* **1987**, 1597-1607.

[35] R. R. Schrock, J. A. Osborn, *Journal of the Chemical Society D: Chemical Communications* **1970**, 567-568.

[36] D. Pingen, M. Lutz, D. Vogt, *Organometallics* **2014**, *33*, 1623-1629.

[37] M. R. M. Nelson, Victoria University of Wellington **2015**.

[38] G. L. Moxham, H. E. Randell-Sly, S. K. Brayshaw, R. L. Woodward, A. S. Weller, M. C. Willis, *Angew. Chem. Int. Ed.* **2006**, *45*, 7618-7622.

[39] V. Polo, R. R. Schrock, L. A. Oro, *Chem. Commun.* **2016**, *52*, 13881-13884.

[40] G. Kovács, A. Rossin, L. Gonsalvi, A. Lledós, M. Peruzzini, *Organometallics* **2010**, *29*, 5121-5131.

[41] J. F. Hartwig, *Organotransition Metal Chemistry*, University Science Books, United States of America, **2010**.

[42] D. Crozet, D. McKay, C. Bijani, A. Gual, C. Godard, C. Claver, L. Maron, M. Urrutigoity, P. Kalck, *Dalton Transactions* **2012**, *41*, 3369-3373.

[43] P. Cheliatsidou, D. F. S. White, D. J. Cole-Hamilton, *Dalton Transactions* **2004**, 3425-3427.

[44] B. Breit, W. Seiche, *J. Am. Chem. Soc.* **2003**, *125*, 6608-6609.

[45] A. Gray-Weale, J. K. Beattie, *PCCP* **2009**, *11*, 10994-11005.

[46] P. Escaffre, A. Thorez, P. Kalck, *J. Mol. Catal.* **1985**, *33*, 87-118.

[47] R. M. Laine, *J. Am. Chem. Soc.* **1978**, *100*, 6451-6454.

[48] M. D. Segarra Maset, ICIQ - Universitat Rovira i Virgili (Tarragona), **2010**.

Chapter 3: Molecular Weight Enlarged Catalysis

3.1 Introduction

In chapter 1 the importance of increasing the efficiency of industrial processes was discussed. Chapters 2 and 3 were dedicated to rhodium catalysed auto-tandem hydroformylation-hydrogenation catalysis as a means of increasing efficiency. Chapter 4 will discuss an alternative approach to increasing efficiency: molecular weight enlargement of homogeneous catalysts for use with membrane filtration. This will increase the efficiency of an industrial process by improving the recyclability of the catalyst and enabling easier purification of the final products. As a target reaction the carbonation of epoxides to cyclic carbonates was studied.

3.1.1 Production of Carbonates

Cyclic carbonates are industrially relevant compounds as they have a diverse range of applications such as: polar aprotic solvents, electrolytes for Li-ion batteries and intermediates in fine chemical manufacturing. They also see use as constituents for oils and paints and raw materials in the synthesis of polycarbonates and polyurethanes.[1]

The first patents for the manufacture of carbonates appeared in the 1950s, using an ammonium halide catalyst. However, the catalyst suffered from low stability, recyclability, air sensitivity, and required high pressures and temperatures to be effective.[2] Phosgene can be used in the synthesis of carbonates, however as this is a chemical warfare agent, discovering a more benign synthetic pathway is desirable.

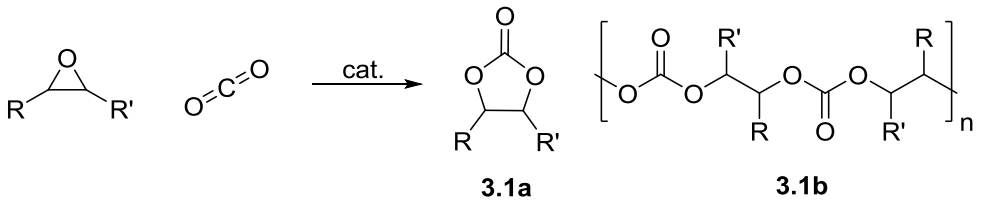

Figure 3.1 Cyclic carbonate (3.1a) and polycarbonate (3.1b)

One method for the production of carbonates is the catalysed coupling of epoxides with carbon dioxide (CO_2) (figure 4.1). CO_2 is especially desirable as a reagent because it is abundant, non-toxic and excess emissions are contributing towards man-made climate change.[3] The proposed mechanism for coupling of CO_2 and epoxides involves a nucleophile (Nu) to activate the epoxide at either carbon, both mechanisms are presented below (schemes 3.1 and 3.2), although the less sterically crowded carbon is favoured (scheme 3.2).[4] The negative charge on the O is often stabilised by a Lewis acid, such as a metal or a positively charged organic moiety. The

negative charge then attacks the electropositive carbon of CO_2 or the CO_2 inserts into the M-O bond. The anionic oxygen centre then attacks the C with the original nucleophile in an intermolecular S_N1 reaction which removes the nucleophile and liberates the carbonate.

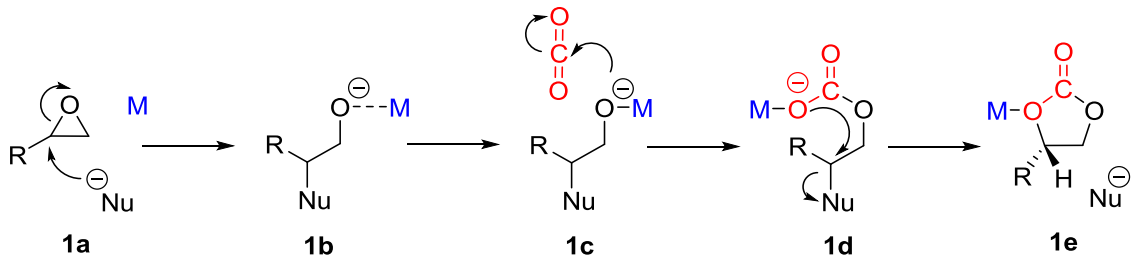

Scheme 3.1 Attack at most sterically hindered epoxide C

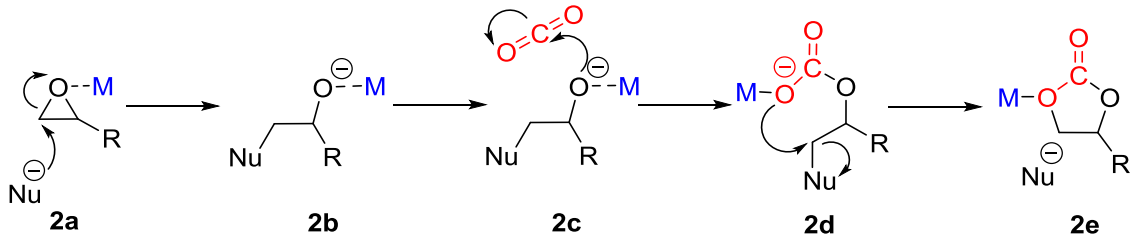

Scheme 3.2 Attack at least sterically hindered epoxide C

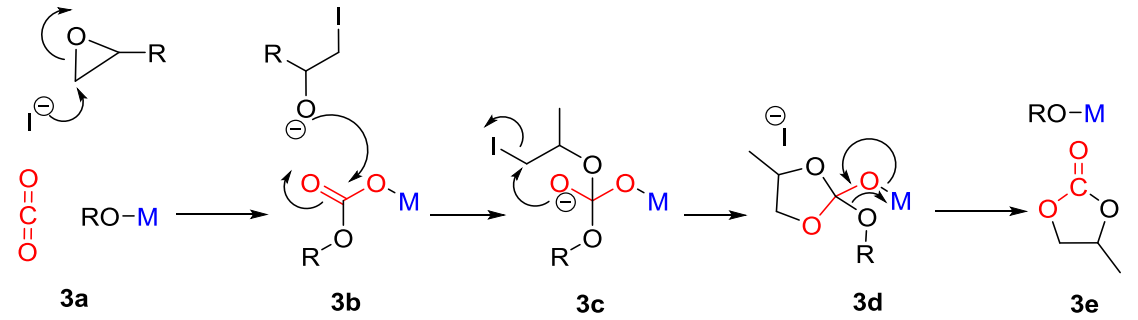

Scheme 3.3 Mechanism with insertion into the M-OR bond

Another mechanism for the formation of cyclic carbonates sees the CO_2 insert into a M-OR bond (scheme 4.3) to activate the CO_2 in tandem to the activation of epoxide.[5] It is possible for the negative charge on the O of the CO_2 to attack another epoxide, rather than the C-Nu, which leads to the co-polymerisation of epoxides and CO_2 to form polycarbonates (figure 3.1). This is often the case when a metal ion or complex is present to stabilise the anion.[6] In recent years, cooperative bimetallic systems that can also pre-arrange a second epoxide to facilitate chain growth have been reported.[7]

The current state of the art for epoxide and CO_2 couplings to form cyclic carbonates uses Salen ligands with a co-catalyst, typically a Lewis base (figure 3.2).[8] The Salen scaffold can

encompass a variety of metals, commonly Co^{III}, Cr^{III}, Al^{III}, and can be tethered to a solid support, such as alumina or silica for increased recyclability and ease of separation.[9]

3.1.2 Tin catalysis

Sn^{IV} halide salts have been shown to be active as Lewis acid catalysts for epoxide-sulfide reactions.[10] There are examples of Sn^{II} and Sn^{IV} salen catalysts (figure 3.2) for carboxylation of epoxides. Salen ligands allow control of the oxidation state, the geometry at the metal centre and can be modified to change the electronic and steric properties of the central metal. Sn^{IV} salen complexes have axial ligands present on the metal that dissociate prior to the epoxide binding. Sn^{IV} is more Lewis acidic than Sn^{II} and as a result exhibits a better catalyst turn over frequency (TOF): Sn^{II} is 187 h^{-1} and Sn^{IV} is 524 h^{-1} for the catalytic carboxylation of propylene oxide. 4-Dimethylaminopyridine (DMAP) is often used as a co-catalyst. [11]

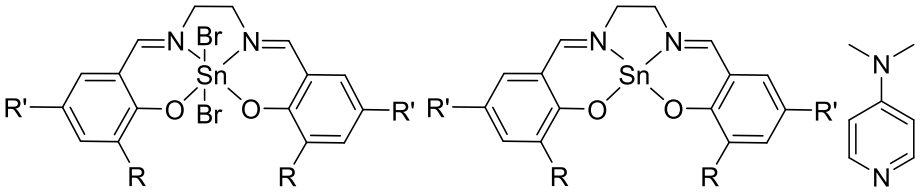

Figure 3.2 Sn^{IV} and Sn^{II} salen catalysts and DMAP co-catalyst [11]

The Lewis acidity of the tin can be further improved by the presence of electron withdrawing groups (EWG) in the salen aromatic rings: R' = OMe (an electron donating group) results in a TOF of 301 h^{-1} and Br results in a TOF of 524 h^{-1} for Sn^{IV}. Typical reaction conditions for these catalysts are 8 bar of CO_2, 0.032 mol% catalyst loading, at 120 °C for 4 hours. Dialkyltin(IV) species are known to be active in CO_2 activation, including the formation of dimethyl carbonate (DMC) from methanol and CO_2. The mechanism of this has been studied by Ballivet-Tkatchenko (scheme 4.4).[5]

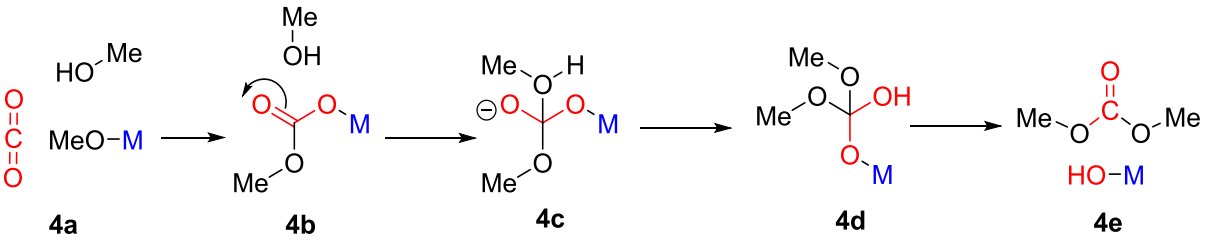

Scheme 3.4 Formation of DMC

While such tin catalysts are active and air stable, making a tethered salen complex is challenging; the synthesis of salen ligands is complex and can be expensive and characterising immobilised species is more difficult than characterising the analogous homogeneous species.

An alternative Sn^{IV} catalyst combines an easy to prepare molecular weight enlarged tin-POSS ((polyoligomericsilsesquioxane) complex with a nanofiltration membrane reactor.[12]

4.1.3 Molecular Weight-Enlarged Catalysis

Molecular weight enlargement is a process by which a catalyst can be made more bulky through the addition of an inert moiety that prevents the catalyst from passing through a membrane, but does not interfere in reactivity. The reactants and products are free to diffuse in and out of the membrane. Vankelecom published an extensive review on solvent-resistant nanofiltration in 2008.[13] A definition of nanofiltration is that the membrane must be impermeable to any molecules over 2 nm in size. The driving force for filtration in these systems is a pressure gradient.

Several options are available for molecular weight enlargement of homogeneous catalysts, presented in table 3.1. In utilising each one there are considerations of ease of synthesis, the capacity for retention within a membrane and the cost.

Table 3.1 Overview of Molecular Weight Enlargement techniques

Entry	Support	Synthesis	Retention	Cost
1	Polymer[14]	Facile	Poor	Very Cheap
2	Dendrimer[15]	Difficult	Good	Expensive
3	Dendron[16]	Reasonable	Good	Reasonable
4	Hyperbranched Polymer[17]	Easy	Reasonable	Cheap
5	Dendronized Polymer[18]	Hard	Very Good	Reasonable
6	POSS[19]	Easy	Very Good	Cheap

Polymers are long chains of monomers that can have functionalities that can bind catalysts but their commonly linear structure can render them susceptible to fitting through the pores of the membrane, thus they often show poor membrane retention. Dendrimers and dendrons are large branching organic molecules that contain a functional unit capable of engaging in chemistry and are more rigid than polymers, therefore are retained better.[20] They can be mixed with polymers to give dendronized polymers or the concepts of dendrimers can be applied to polymers to make hyper-branched polymers which show improved retention over the linear analogues.

POSS (figure 3.3) is an easy to synthesise silica cage that features organic moieties that enable solubility in organic solvents, but it is large and rigid enough not to fit through membrane pores.[19] Cole-Hamilton combined POSS with functionalised dendrimers in the hydroformylation of 1-octene.[21] The POSS molecule has a volume of 1.5 nm.[22]

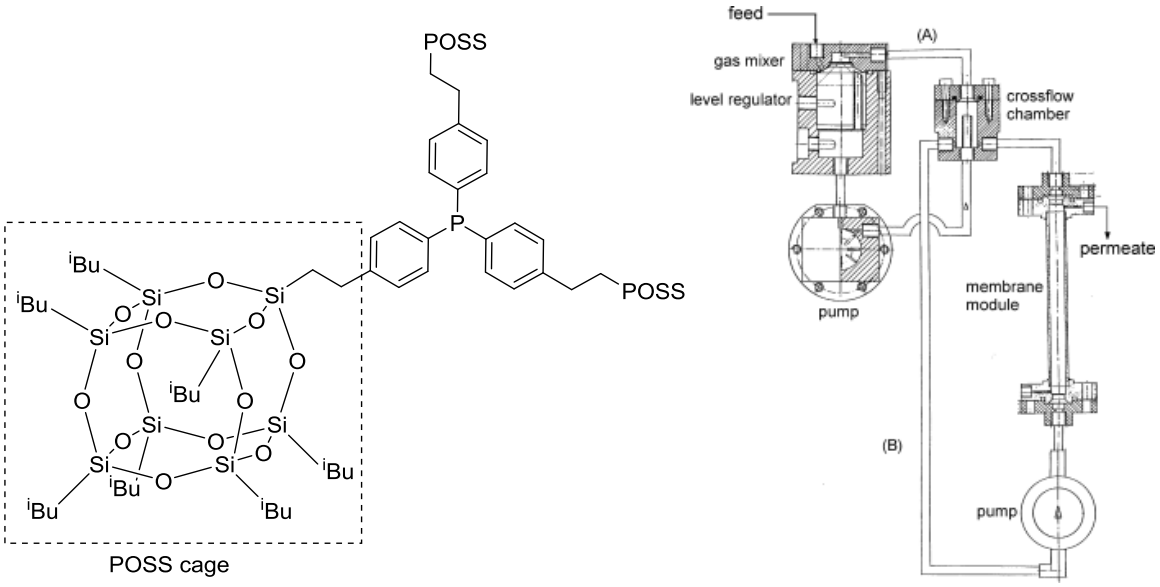

Figure 3.3 Triphenylphosphine modified POSS and membrane reactor set-up[23]

The support is matched with different membrane options: typically ceramic or polymeric. Polymeric membranes are synthesised from polymeric building blocks, such as aromatic fused porphyrins, and feature excellent control of pore size and retention, but can dissolve in organic solvents and show poor resistance against high pressures and temperatures.[24] Ceramic membranes are made of inorganic materials, typically oxides such as TiO_2 or ZrO_2, and are capable of withstanding higher temperatures and pressures and are more resistant to organic solvents; however it is more difficult to get a standardised pore size.[25] Both membrane types are commercially available.

Tethering carbonate catalysts to solid supports has also been reported: Sakai tethered a phosphonium bromide to a silica/alumina support (scheme 3.5) and discovered that the support had an effect on the catalysis, with silica performing best.[26] This was reasoned to be as a result of the hydrogen bonding of the silica OH groups stabilising the anionic intermediate (as the M in scheme 3.2).[27] The nature of the alkyl groups on the phosphonium salt did not affect catalysis.

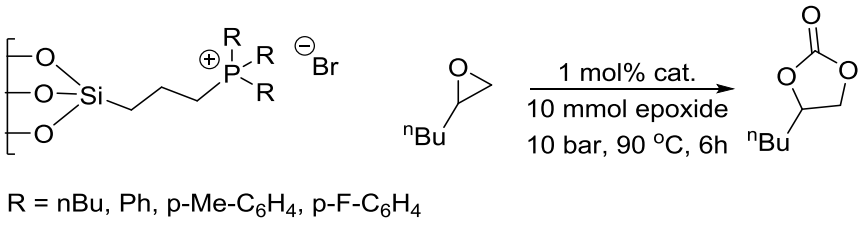

Scheme 3.5 Sakai's tethered phosphonium halide catalyst

Kleij has also reported trihydroxybenzene and triazolium iodide moieties immobilised on a polystyrene particle.[28] While conversions are initially as high as 84% they drop to 48% over four sequential runs. TON are very low at only 21 or 1.16 (h^{-1}) TOF. Conversion can be improved again by periodically regenerating the catalyst through the addition of MeI. Zhang and co-workers made a polymer supported ionic liquid capable of catalysing the cycloaddition of CO_2 and the epoxides (scheme 3.6).[14]

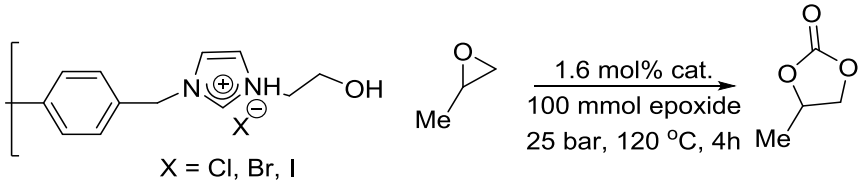

Scheme 3.6 Zhang's polymer supported ionic liquid catalyst

Recently Rioux reported a flow system for the production of cyclic organic carbonates (scheme 3.7).[29] The system consists of a sequential Re/H_2O_2 catalysed epoxidation of olefins, done in an aqueous phase, and Al and TBAI (tetrabutylammonium iodide) co-catalysed carboxylation, performed in an organic phase.

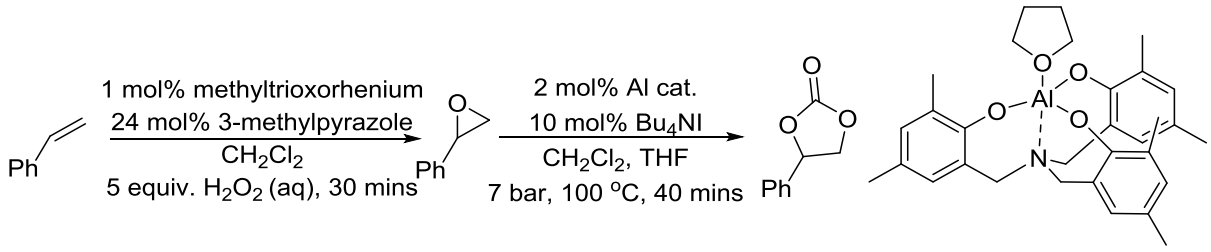

Scheme 3.7 Rioux's cascade epoxidation and carboxylation flow set-up

This system is not a continuous flow system as although the two phases are introduced into the reactor at the same time, a PTFE membrane separates the organic epoxide product phase from the aqueous Re catalyst phase before CO_2 is introduced and the carboxylation takes place in a separate chamber.

With production of cyclic carbonates under investigation in the Vogt group the ease of synthesis of POSS and its promising retention behaviour, was combined with the high pressure capacity of TiO_2 ceramic membranes. Previous work within the Vogt group has successfully coupled a triphenylphosphine ligand to the POSS for 1-octene hydroformylation and carried out a continuous flow experiment with a TiO_2 membrane reactor (figure 3.3).[23]

The work presented in this chapter builds upon preliminary studies by Andreas Skowron† and the MChem project of Sami Gesslbaur‡ and seeks to synthesise and characterise the POSS tethered catalysts, broaden the substrate scope of the reaction, and test the compatibility with a simple membrane set-up.

3.2 Results and Discussion

3.2.1 Synthesis of POSS catalysts

There are two types of MWE catalysts to synthesise: the Sn^{IV} species (scheme 3.8), which acts as the M in schemes 1-4, and a phosphonium iodide (scheme 3.9), which acts as the Nu in schemes 1-4.

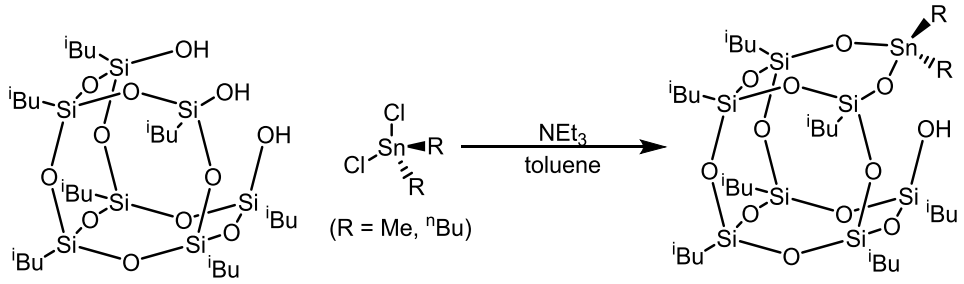

Scheme 3.8 General scheme for synthesis of Sn-POSS complex

In the tin catalyst the geometry is tetrahedral and the tethering to the POSS cage occurs by condensation of two moles of HCl to form Sn-O bonds. The residual OH may allow an exchange of the SnR_2 species between the Si-O functionalities and may also play a part in catalysis, as reported by Sakai in silica immobilised carbonate catalysts.[26]

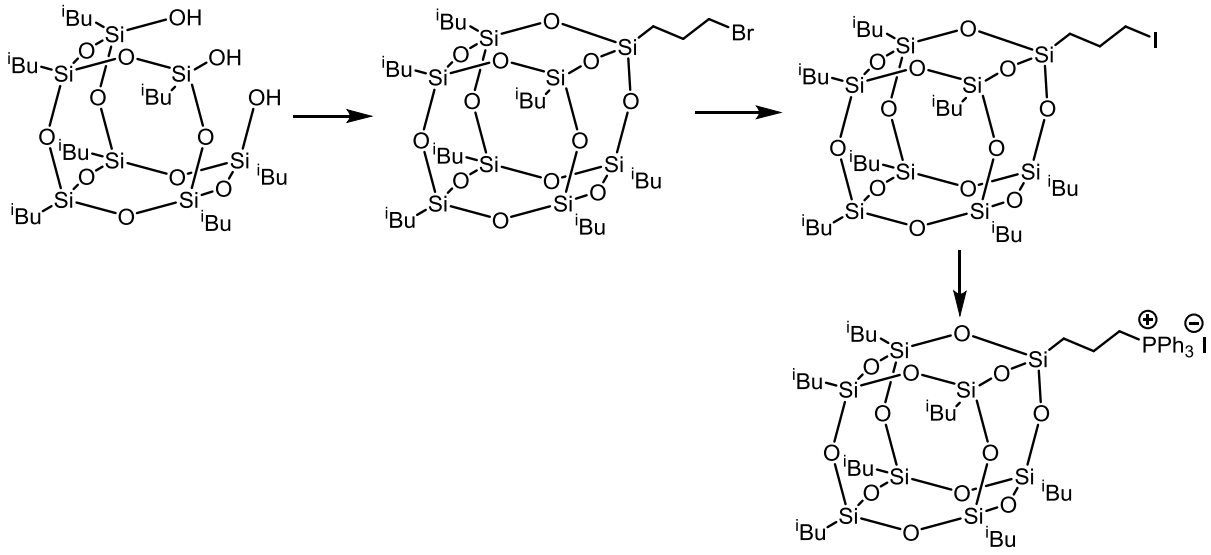

Scheme 3.9 General scheme for synthesis of [I][PPh_3]-$(CH_2)_3$-POSS

3.2.1 $^{i}Bu_7$-POSS NMR spectroscopic analysis

The ^{i}Bu-POSS starting material was provided by Hybrid Catalysis and was recrystallized in hot acetone prior to use. It can be easily prepared by incomplete condensation of $RSi(Cl)_3$ groups.[30]

In the $^{i}Bu_7$-POSS molecule the proton and carbon atoms present are on the hydroxyl and isobutyl groups bound to the silicon. An S_3 axis of rotation is present in the molecule, running between the hydroxyl groups in the uncapped corner and through the isobutyl-silicon on the opposite side of the molecule. This results in three different isobutyl environments: those attached to the three silicons with hydroxyl groups, the three corner silicons and the final corner silicon opposite to the uncapped corner. This is reflected in the ^{1}H NMR spectrum (figure 3.4).

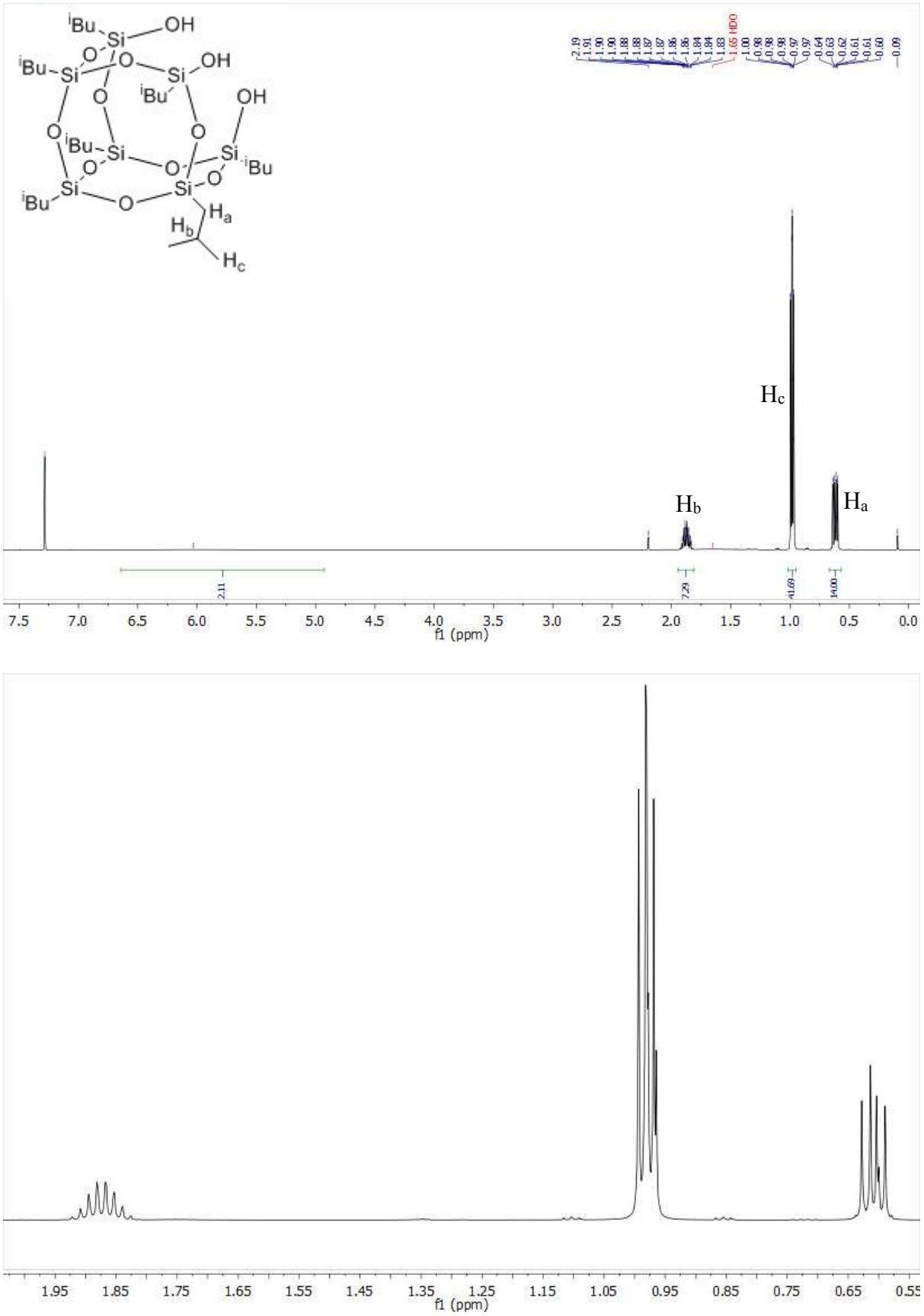

Figure 3.4 ^{1}H NMR ($CDCl_3$, 500.23 MHz, 25 °C) spectrum of $^{i}Bu_7$-POSS and enlarged isobutyl region

There is an extremely broad peak at 6.0 ppm with an integral of 3H corresponding to the 3 OH groups.

Although the symmetry of the molecule places the isobutyl groups into different space categories, outlined above, the signals of the isobutyl CH_3 (H_c), CH_2 (H_a) and CH (H_b) groups overlap so that the overall integrals correspond to a total of 42H, 14H and 7H respectively. The expected splitting pattern of the CH isobutyl group would be a nonet, as a consequence of coupling to 8H, with an expected intensity of 1:8:28:56:70:56:28:8:1 however in the ^{1}H NMR spectra (figure 3.4) a 10 line multiplet with a splitting pattern of 1:9:36:84:126:126:84:36:9:1 is observed. This is a consequence of the overlap of two different but almost equally sized nonets and the peaks are slightly misshapen as a result of the overlap being not quite perfect.

The CH_3 peak, H_c, is three doublets overlapping, as identified by a 2D HSQC experiment (figure 3.5), each with a J(H,H) of 7Hz: 0.970 and 0.984, 0.975 and 0.987, 0.988 and 1.000. As a result of the overlap the peak resembles a triplet. The intensity of one of the doublets is approximately a third of the other two due to this being the lone CH on the capped corner of the POSS cage.

In the CH_2 peak the three doublets are between: 0.593 and 0.607, 0.603 and 0.618, 0.616 and 0.630. As in the CH_3 peak there is one peak that is 1/3 the size of the other two. The CH_2 peak is more up-field than standard, this is due to the proximity of the electropositive silicon atom.

The ^{1}HNMR spectra show three different proton environments for the three different isobutyl environments. Similarly, the ^{13}CNMR spectrum also shows three different C resonances: 25.78, 25.72 and 25.62 designating CH_3; 23.94, 23.90 and 23.88 designate CH; and 23.29, 22.87 and 22.50 designating CH_2 as evidenced in the HSQC spectrum (figure 3.5). The peak at 2.2 is residual acetone from the recrystallization of the ^{i}Bu$_7$-POSS.

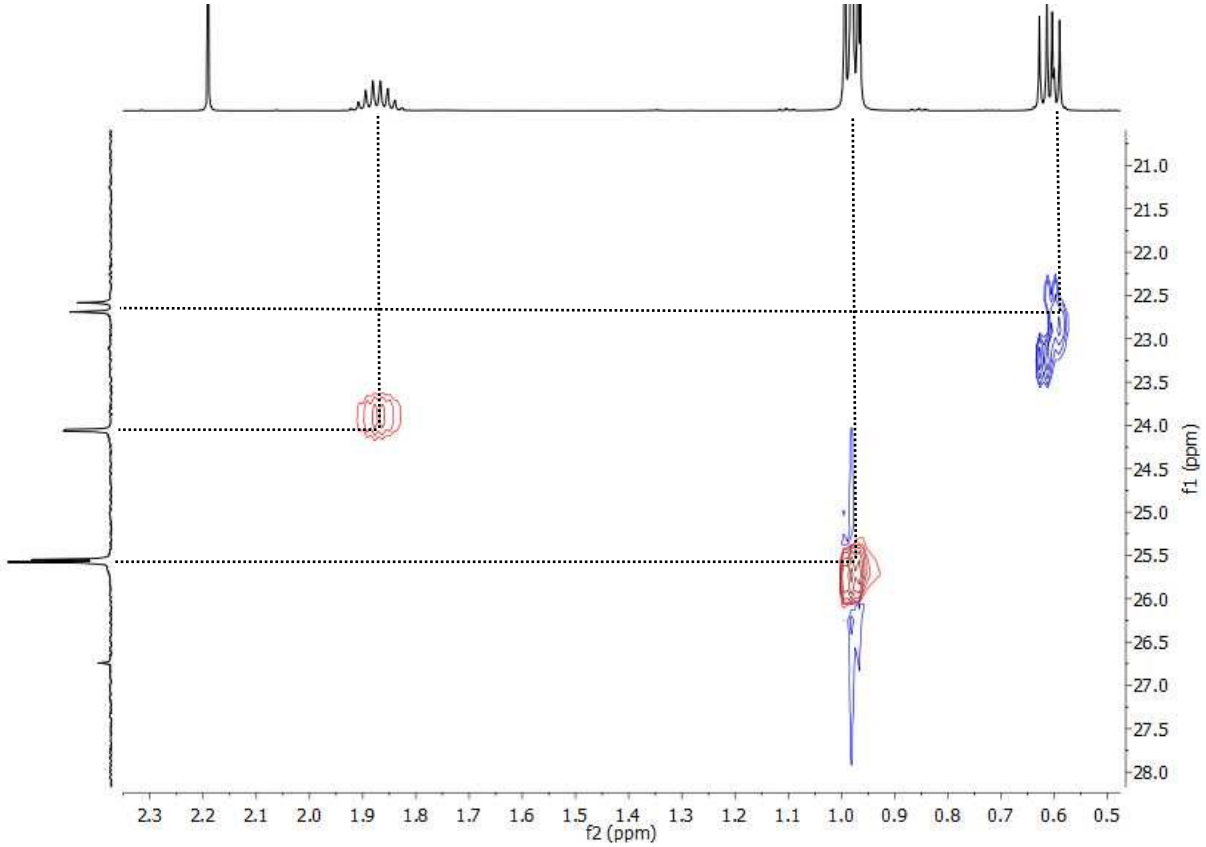

Figure 3.5 HSQC of (^{i}Bu)$_7$-POSS ($CDCl_3$, 500.23 MHz, 25 °C) spectrum of ^{i}Bu$_7$-POSS

Providing further characterisation of the starting POSS-material the mass was determine by MALDI-TOF (figure 3.6) and prominent peaks of m/z: 791 (M), 813 m/z ($M+Na^+-H^+$) were identified. Full methodology is presented in the materials and methods section.

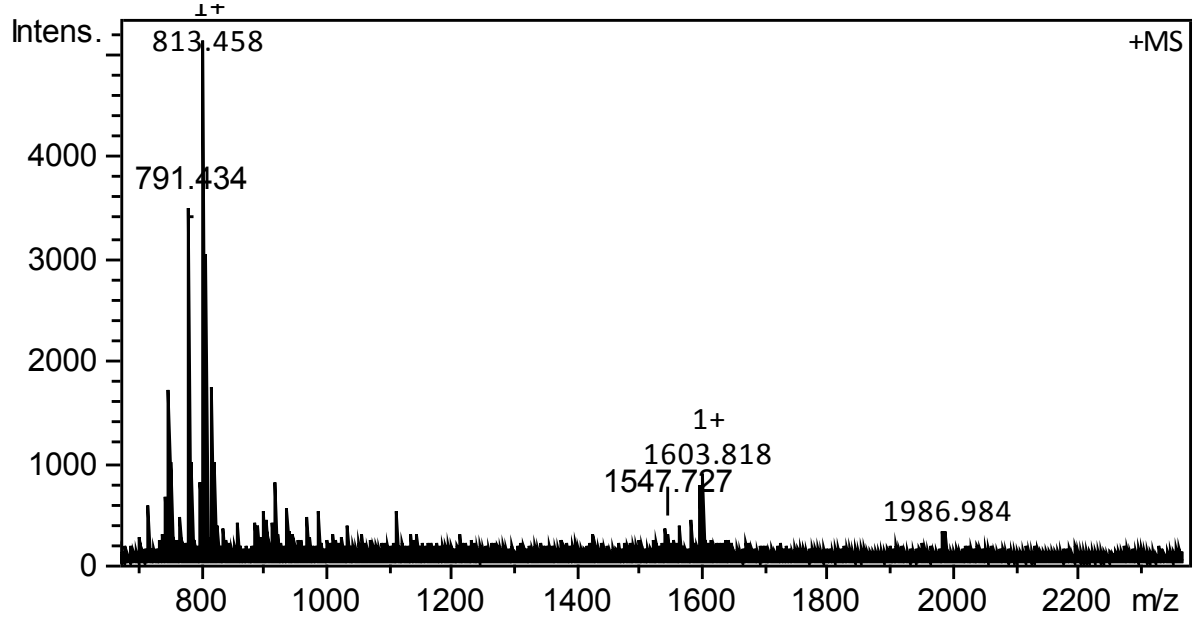

Figure 3.6 MALDI-TOF spectra of ^{i}Bu$_7$-POSS molecule

3.2.2 $SnMe_2$-(^{i}Bu)$_7$-POSS synthesis and spectroscopic analysis

The synthesis of the SnR_2-POSS species is quite straightforward. Solid SnR_2Cl_2 is mixed with the (^{i}Bu)$_7$-POSS in a 1:1 ratio and NEt_3 neutralises the HCl formed from the formation of Sn-O bonds. The final white crystalline product is obtained by filtering off the salts over alumina using hexane as solvent. The yield is 79%. The species is readily soluble in several organic solvents such as $CDCl_3$, C_6D_6 and toluene.

Incorporating the dimethyltin catalyst into the POSS changes the symmetry in the molecule. There is now a mirror plane between the Sn and the opposite Si. This is reflected in the ^{1}H NMR spectra (figure 3.7) as the CH_3 and CH_2 peaks are more complicated. However the J(H,H) is still retained at 7 Hz.

The geometry of the tin is tetrahedral shown by ^{1}H NMR spectroscopy. The methyl on the tin sit in a mirror plane thus their peaks are distinct. If the tin was square planar they would be equivalent and the position of the peaks would be as a result of potential splitting due to the NMR-active spin 1/2 ^{119}Sn nuclei. However as the natural abundance of the NMR active Sn nuclei is small: ^{115}Sn (0.34%), ^{117}Sn (7.68%), ^{119}Sn (8.59%), giving a total of 16.6%, [31] there are small satellite peaks either side of the two methyl peaks but the peaks themselves are distinct methyl groups.

The isobutyl group signals have changed compared to those in figure 3.4. The integrals of the overall total CH_3, CH_2 and CH are the same as before, 42, 14 and 7 respectively, when normalised to methyl peaks of the $SnMe_2$ group so there is not a mixture of starting and final material. Otherwise the ratios would be different.

The peaks themselves have become more complex multiplets. The CH_2 peak is the most straightforward to assign with 5 possible environments as observed by the 5 possible doublets: 0.79 (2H, **c**), 0.80 (2H, **b**), 0.83(4H, **d**), 0.86(4H, **a**) and 0.92(2H, **e**) (assigned in figure 3.7). This implies that there is now 5 different environments in the POSS cage and the symmetry is dictated by the Cs point group. The CH peak is a large 11 signal multiplet with asymmetric intensity and a smaller nonet up-field and the CH_3 peak is a complex overlapping of multiple doublets.

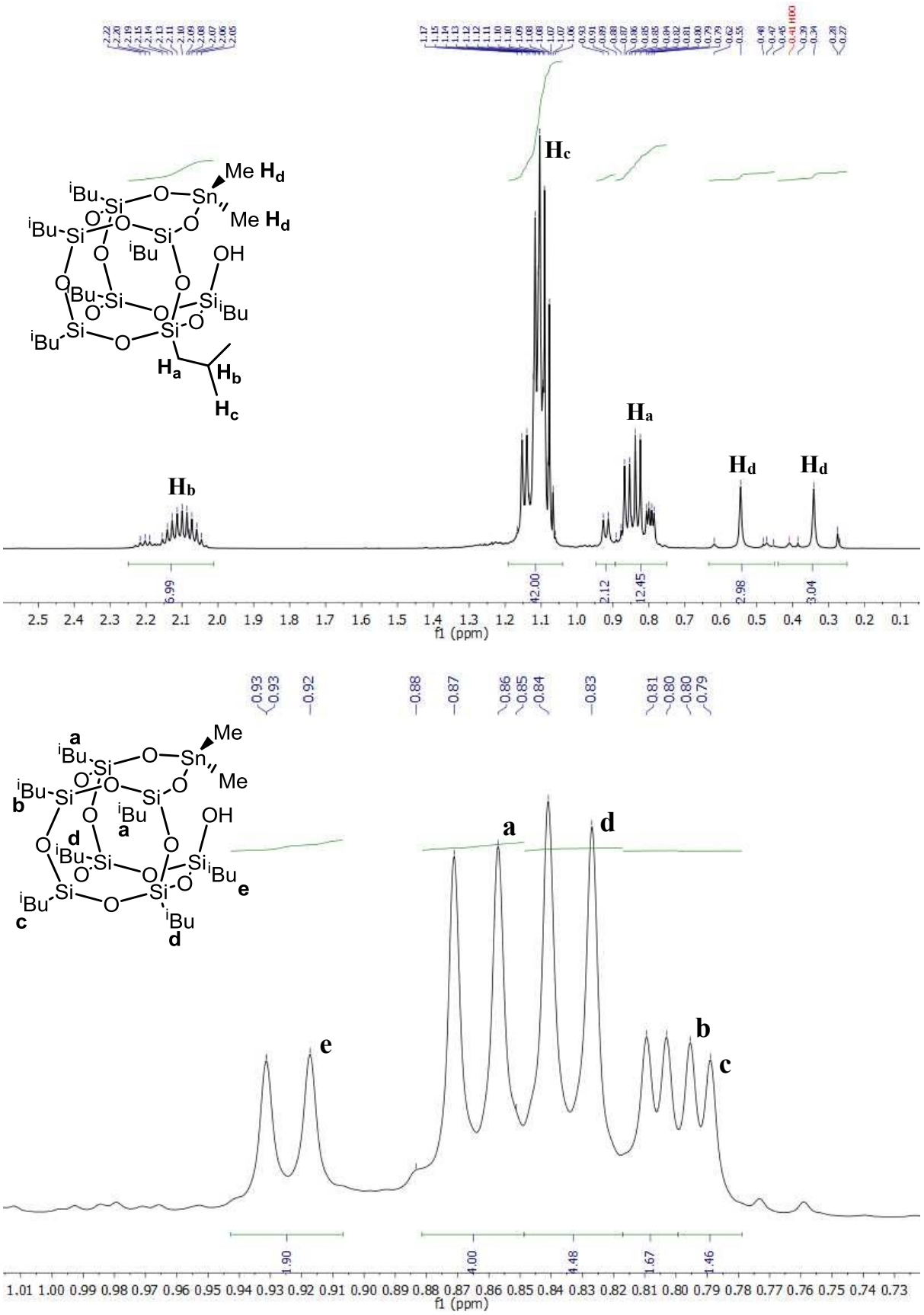

Figure 3.7 ^{1}H NMR spectrum of $SnMe_2$-POSS (C_6D_6, 500.23 MHz, 25 °C) and assignment of the CH_2 isobutyl splitting pattern

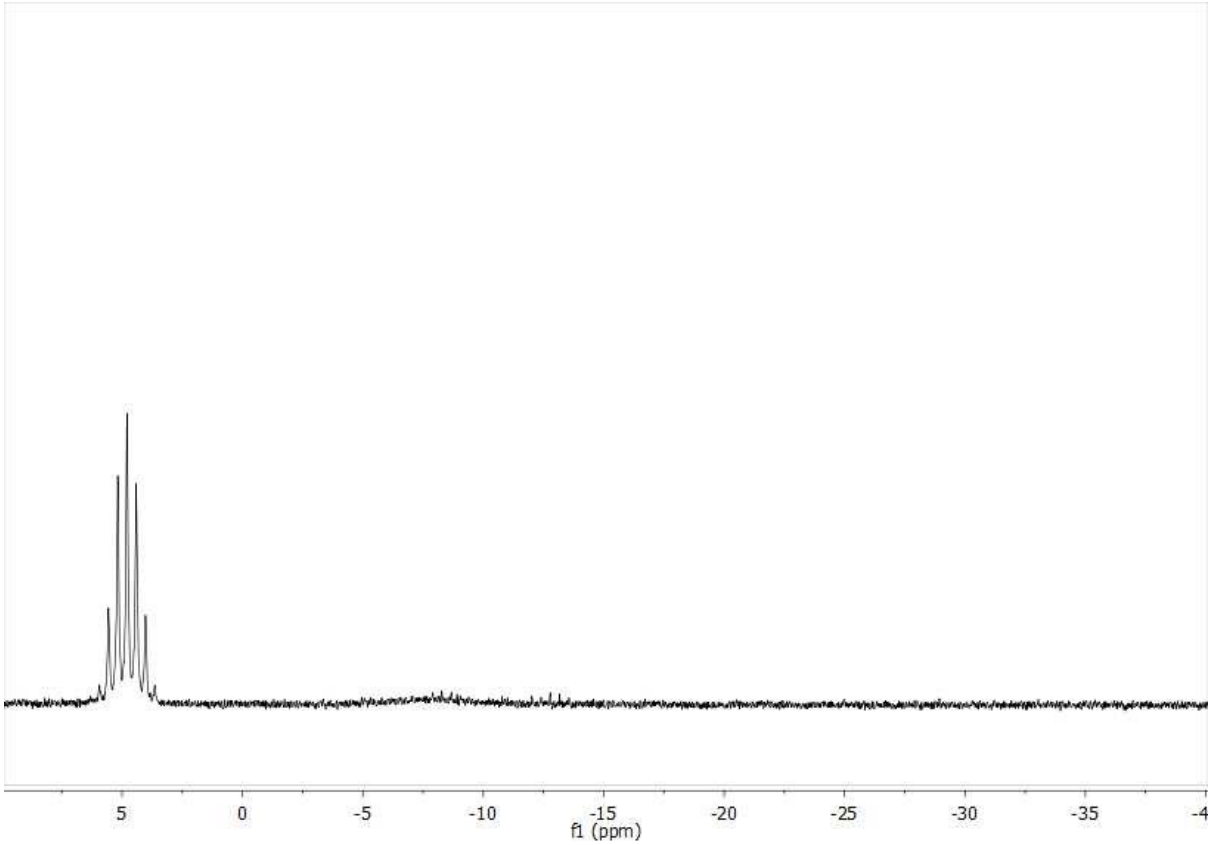

Figure 3.8 Proton coupled ^{119}Sn NMR spectrum of $SnMe_2$-POSS (C_6D_6, 186.45 MHz, 25 °C)

The ^{119}Sn NMR spectrum (figure 3.8) shows a distinct heptet at 4.8 ppm from the coupling to the 6 protons on the 2 Me groups. There is just this peak which shows no residual starting material or dimeric Sn coupling. It also counters the possibility that elimination of Me can occur from the POSS species and Sn catalyst with a single Me and 3 O bonds can be formed, this would show a quartet.

The HSQC (figure 3.9) of the complex shows the C assignments of the $^{i}Bu_7$-POSS above remain relatively unchanged with the butyl CH_3 between 25-27 ppm, the butyl CH peaks coming at 24 ppm and the butyl CH_2 peaks mostly at 22-23 ppm, however some are also overlapping the CH peaks. The CH_3 groups on the tin show a small signal between 0-1 ppm, however in the DEPT-135 (figure 3.10) these are more clearly two peaks.

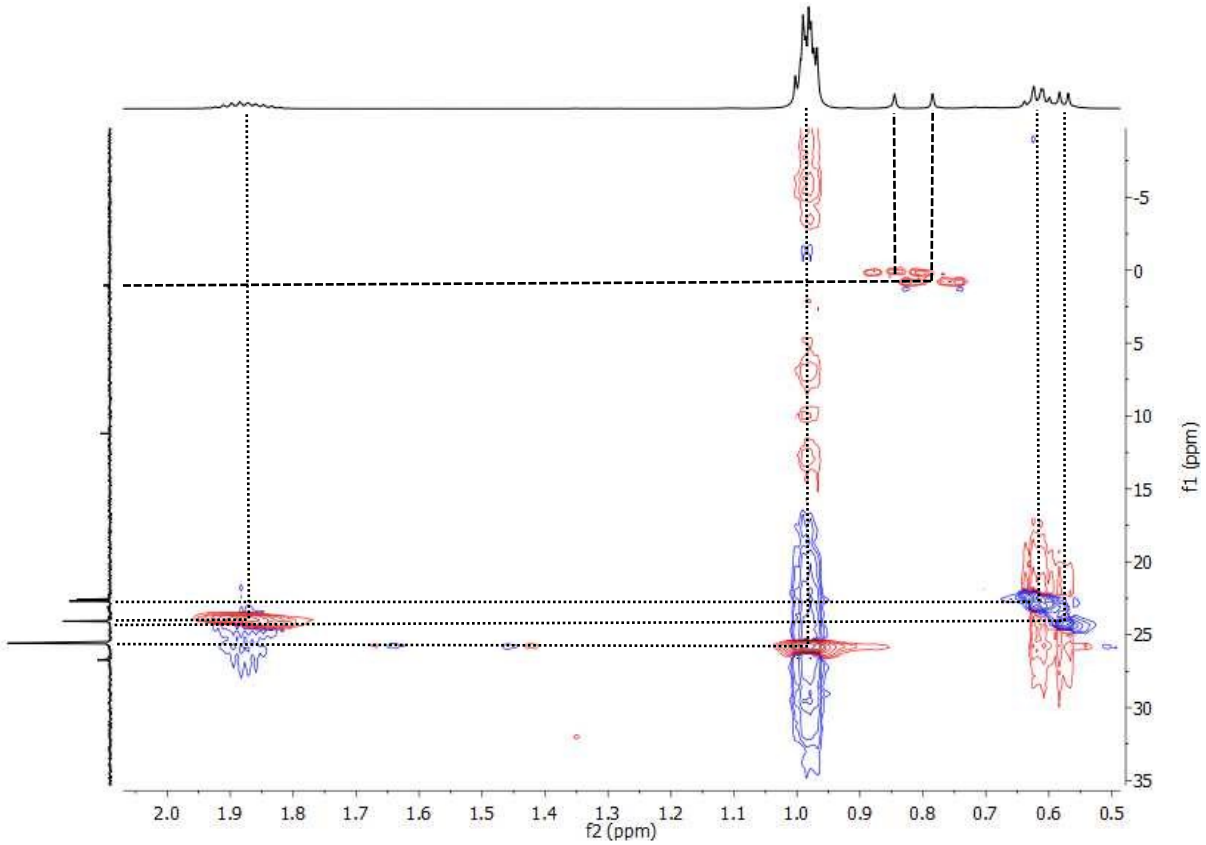

Figure 3.9 HSQC spectrum of $SnMe_2$-POSS (C_6D_6, 500.23 MHz, 25 °C)

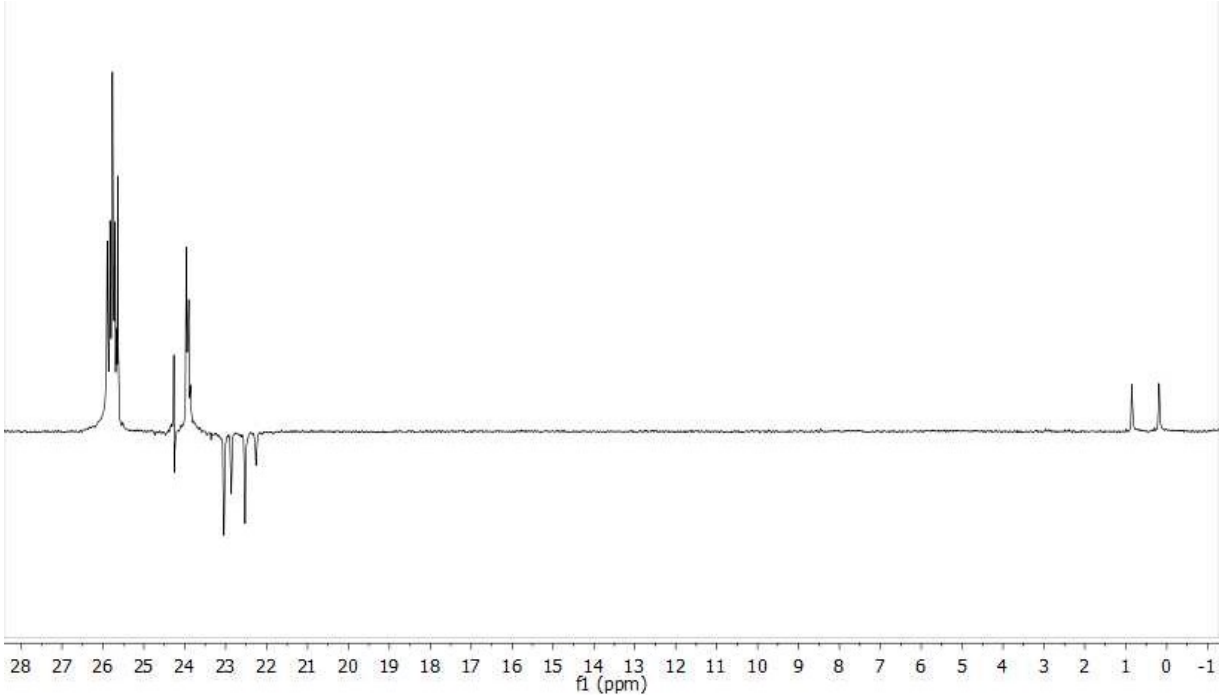

Figure 3.10 ^{13}C NMR DEPT-135 spectrum of the $SnMe_2$-$(iBu)_7$POSS cage showing the two Sn-Me_2 C between 0-1 ppm (C_6D_6,125.76 MHz, 25 °C)

There is the possibility that the $SnMe_2$ catalyst dissociates from the POSS cage in solution to perform catalysis as a discrete metal catalyst before returning to the POSS as a resting state,

this is known as a 'boomerang catalyst' and such a mechanism has been observed for polymer supported ruthenium catalyst for olefin metathesis.[32] This would be problematic from the perspective of membrane catalysis because leaching would be inevitable. To check this possibility a DOSY experiment was performed (figure 3.11). DOSY (diffusion ordered spectroscopy) organises different NMR signals by their diffusion coefficient through solution. In this experiment a definitive single species for the $SnMe_2$ and the POSS was observed.

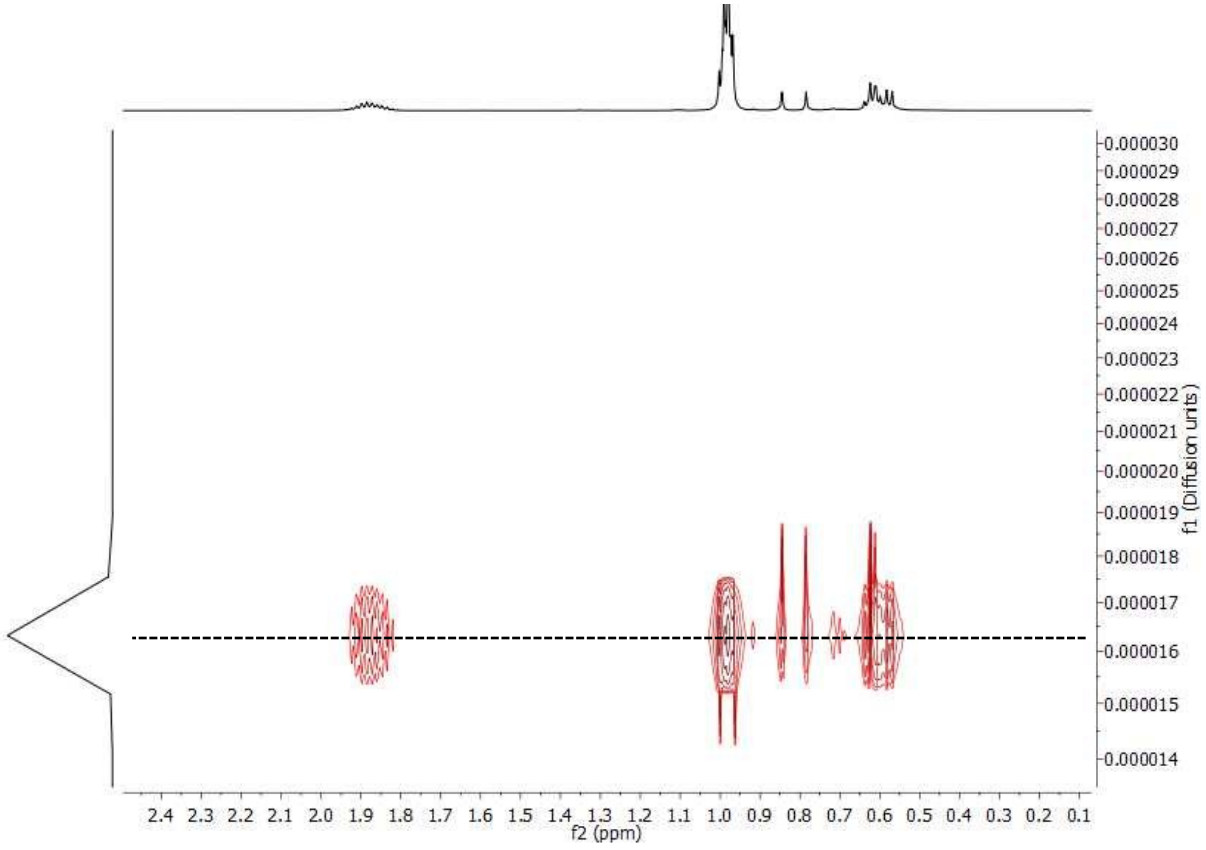

Figure 3.11 DOSY NMR spectrum of $SnMe_2$-POSS (30 mg in 0.7 mL $CDCl_3$, 500.23 MHz, 25 °C)

Although the DOSY spectrum shows a single species, with all the assigned ^1H NMR peaks in phase, the MALDI-TOF analysis (figure 3.12) shows a peak at 813 m/z which corresponds to the POSS cage without the Sn species.

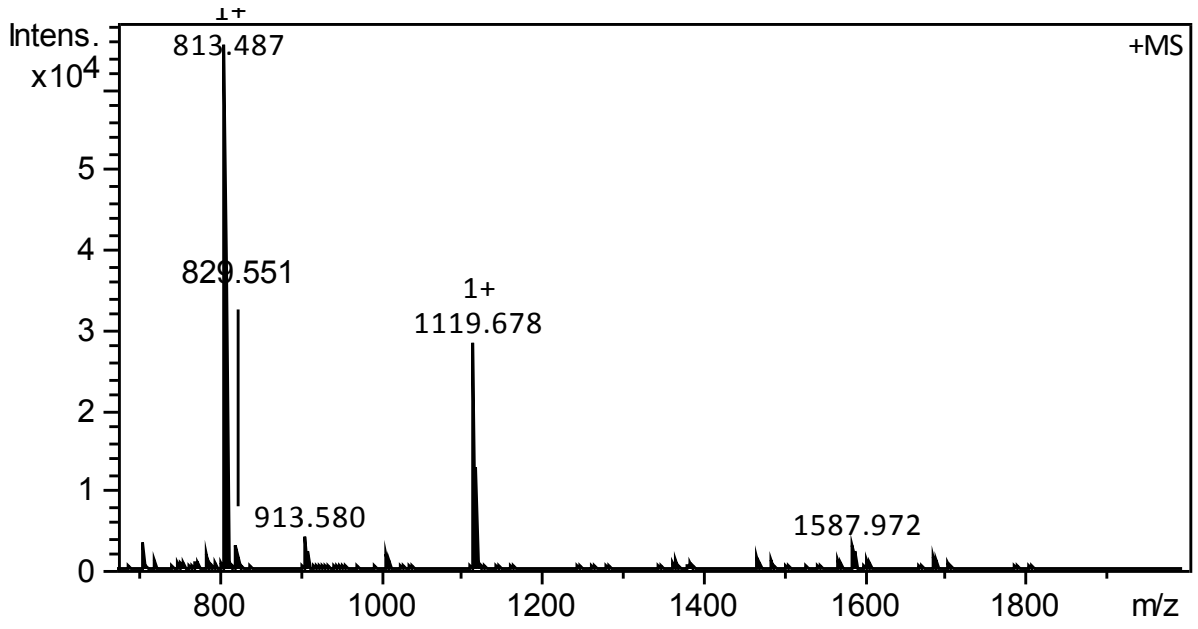

Figure 3.12 MALDI-TOF spectra of $SnMe_2$-POSS molecule

There is no peak corresponding to the molecular weight of the catalyst detected. The initial ionisation of the nature of MALDI-TOF may have cleaved the tin complex from the POSS cage.

3.2.3 Spectroscopic analysis of Sn(^{n}Bu)$_2$-(^{i}Bu)$_7$-POSS catalyst

The synthesis of Sn(^{n}Bu)$_2$-(^{i}Bu)$_7$-POSS follows the same method as the Sn(Me)$_2$-(^{i}Bu)$_7$-POSS outlined above using a 1:1 ratio of Sn(^{n}Bu)$_2$Cl$_2$ and trisilanol POSS. Purification by passing a hexane solution of the crude material over a plug of alumina resulted in a white solid in 81% yield of Sn(^{n}Bu)$_2$-(^{i}Bu)$_7$-POSS.

As in the $SnMe_2$ system, incorporating the tetrahedral dibutyltin catalyst into the POSS changes the symmetry of the catalyst resulting a Cs point group. The signals of the n-butyl groups overlap some peaks of the POSS butyl groups but 2D COSY enables assignment of the two spin systems.

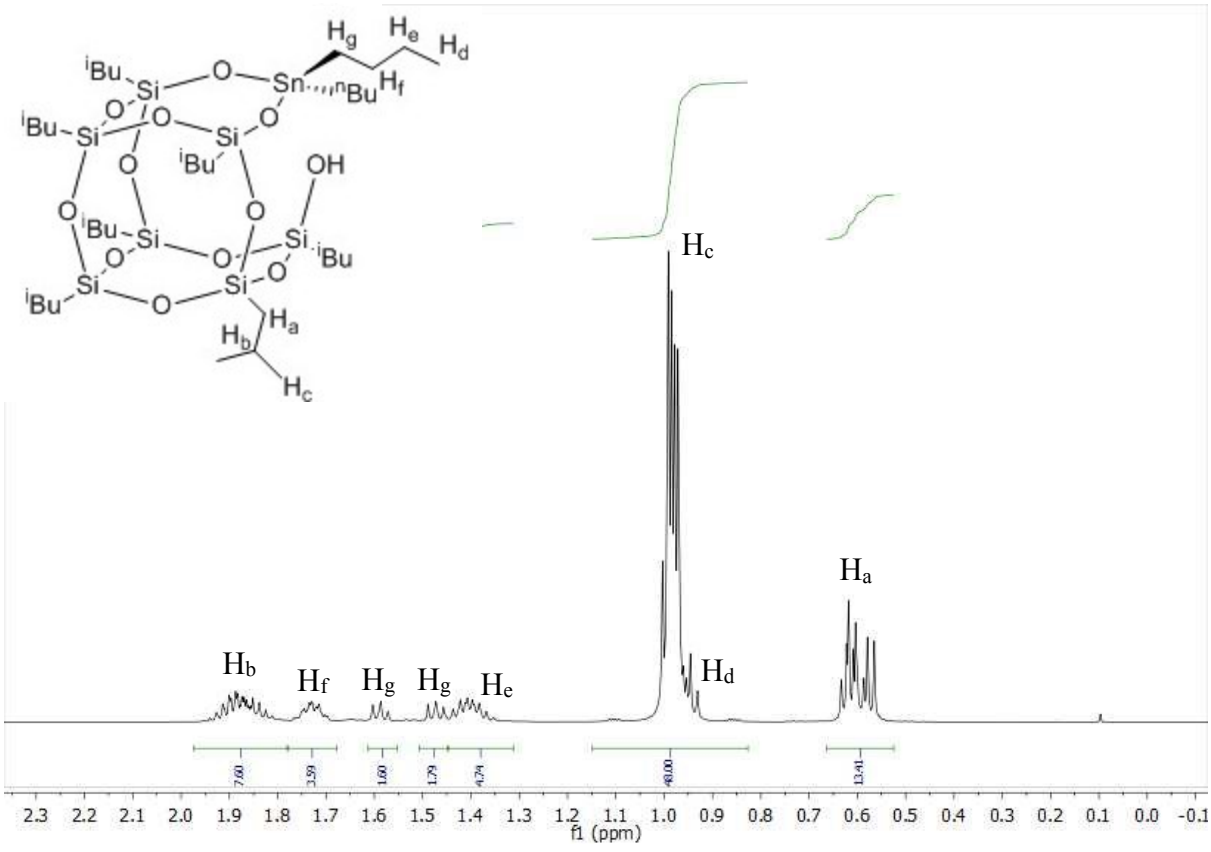

Figure 3.13 ^{1}H NMR spectrum of $SnBu_2$-POSS ($CDCl_3$, 500.23 MHz, 25 °C)

The POSS peaks can be assigned as 0.60, 0.99 and 1.88. The methyl group of the n-butyl groups overlap the methyl groups of the isobutyl therefore the total integral of that region is a 48H. As with the $SnMe_2$ analogue; the tetrahedral geometry of the tin renders the n-butyl groups non-equivalent therefore each CH_2 peak is a pair of super-imposed multiplets rather than a multiplet of doublets. Moving towards the Sn: CH_2 coupled to methyl is an overlapped sextet at 1.40 J1(H,H) of 7.5 Hz, the next CH_2 is a superimposed multiplet based on a quintet at 1.73 J(H,H) of 7.5Hz. The closest CH_2 to the Sn occurs as a two separate triplets at 1.47 and 1.58 each with an integral of 2H and a J(H,H) of 8 Hz. This assignment is confirmed by COSY (figure 3.14) and HSQC (figure 3.15) experiments.

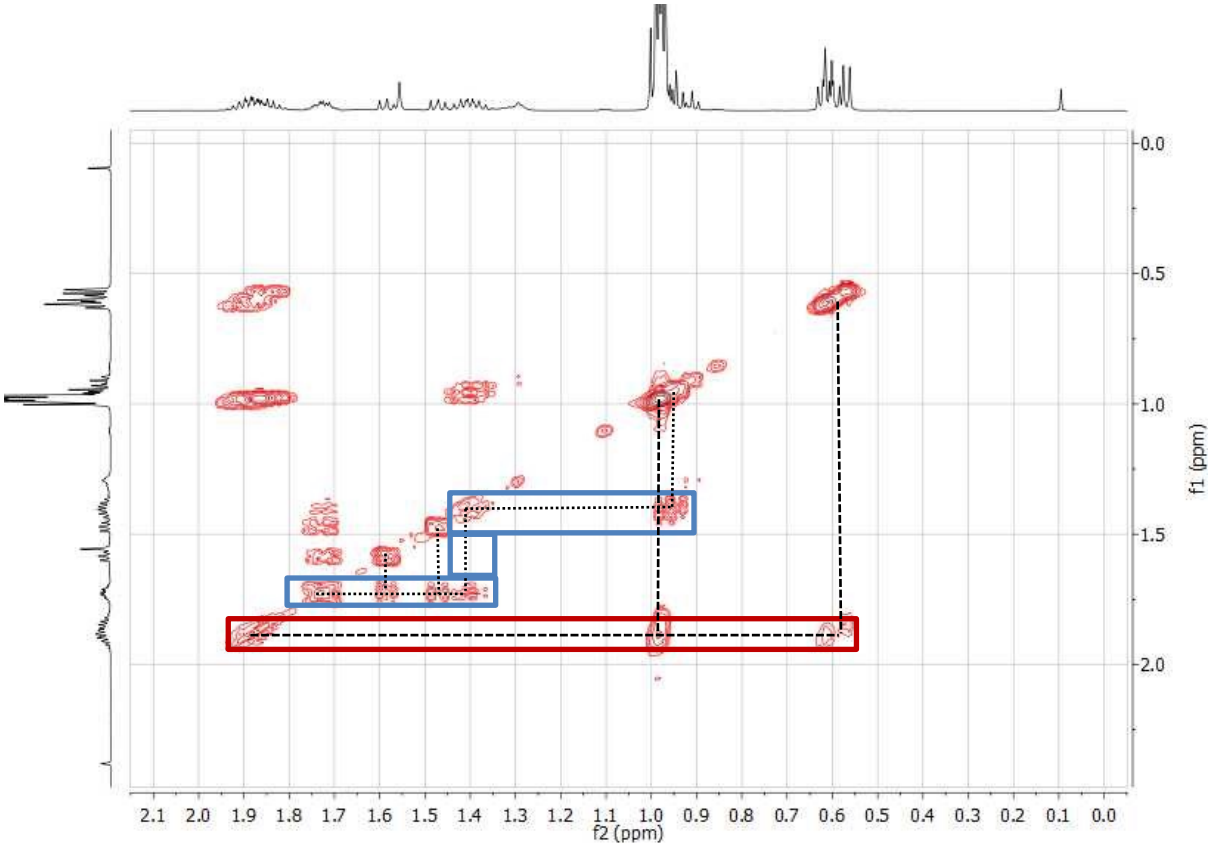

Figure 3.14 COSY-NMR (CDCl3, 500.23 MHz, 25 °C) spectrum of $SnBu_2$-POSS. Spin systems are marked in blue for the alkyl chains and red for the POSS cage.

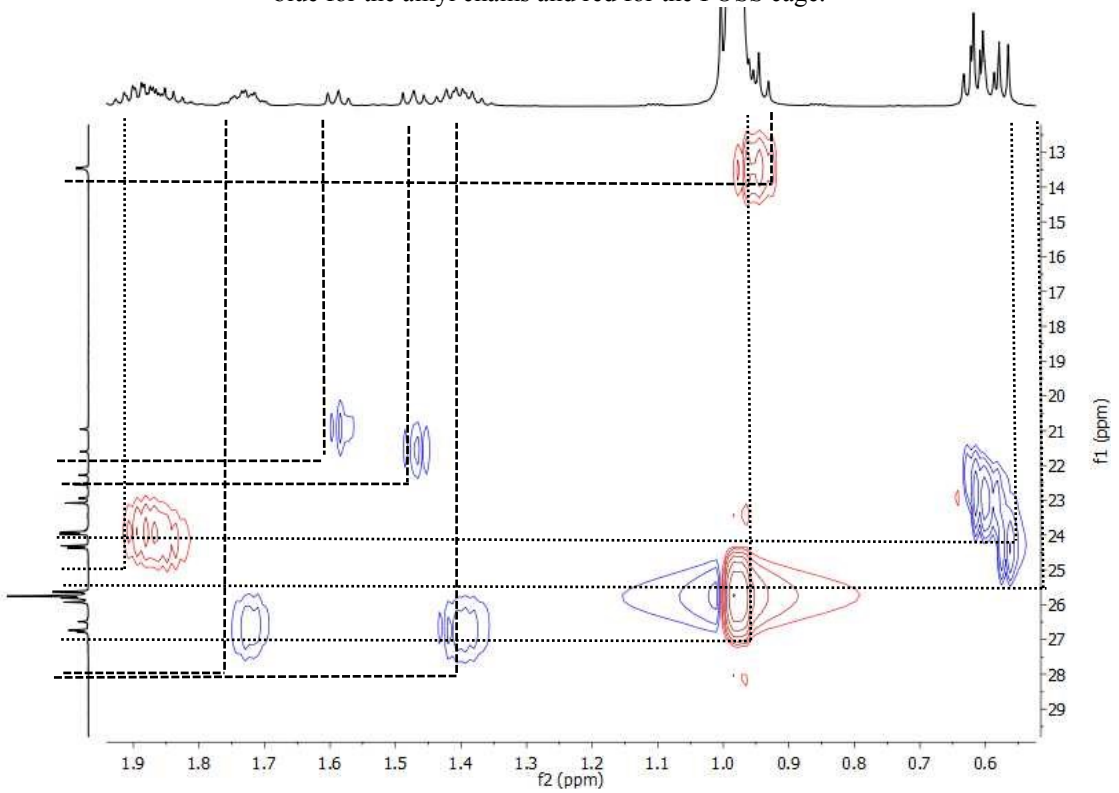

Figure 3.15 HSQC-NMR spectrum (CDCl3, 500.23 MHz, 25 °C) of $SnBu_2$ –POSS with DEPT processing showing the CH_2 groups as blue

The HSQC spectrum also has some DEPT processing so the CH and CH_3 groups appear in red and the CH_2 groups appear in blue. The ^{i}Bu CH_2 groups of the POSS appear at 22.2, 22.5, 22.9, 23.06 and 24.4 ppm either side of the ^{i}Bu CH groups at 23.94 ppm. The CH_2 groups of the alkyl chain appear at 21.0, 21.6, 26.5 and 26.7 ppm. The CH_3 groups at the end of the alkyl chain appear at 13.5 ppm while the CH_3 groups on the iBu are at 25.7 ppm. A 1D ^{13}CNMR with DEPT-135 processing is shown in figure 3.16.

In general there is a minimal shift in the signals of the POSS molecule with the SnR_2 attached showing

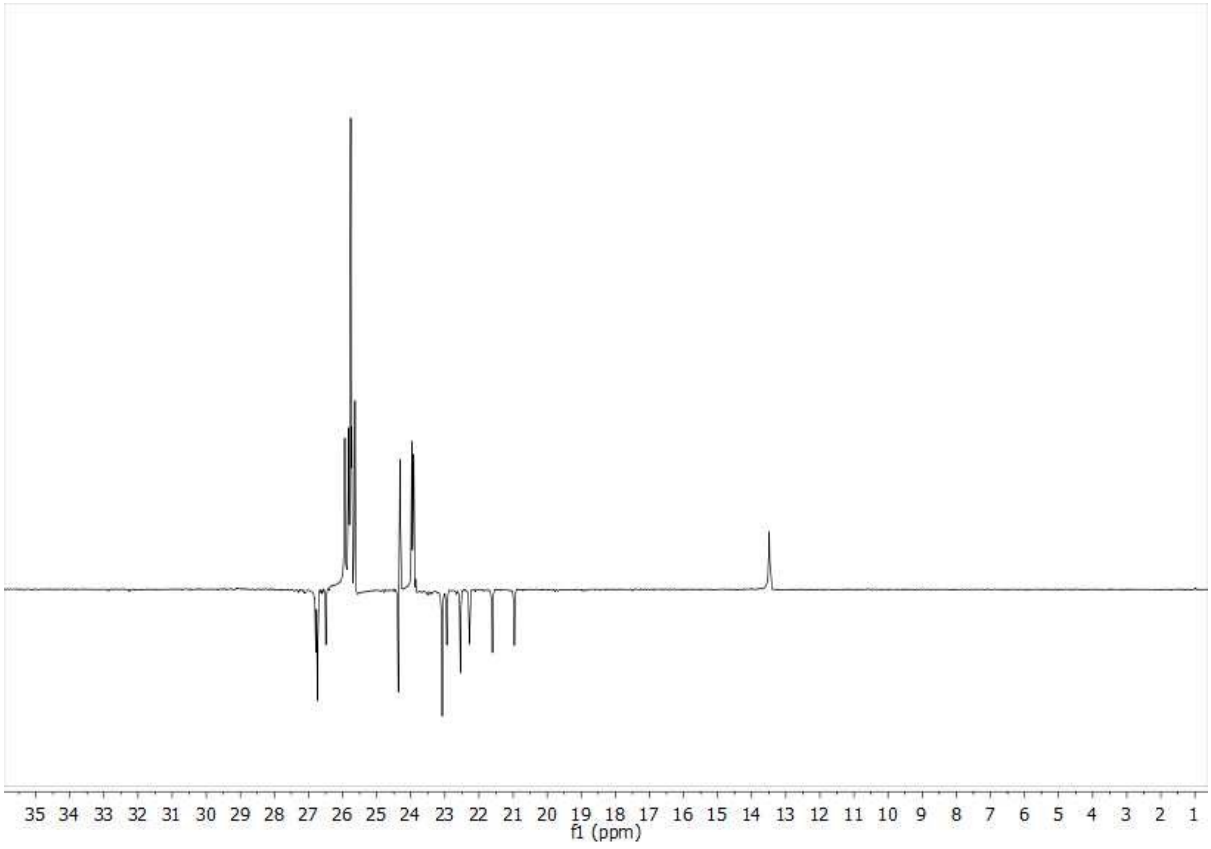

Figure 3.16 $SnBu_2$-POSS ^{13}C NMR spectrum with DEPT-135 processing (C_6D_6, 125.76 MHz, 25 °C)

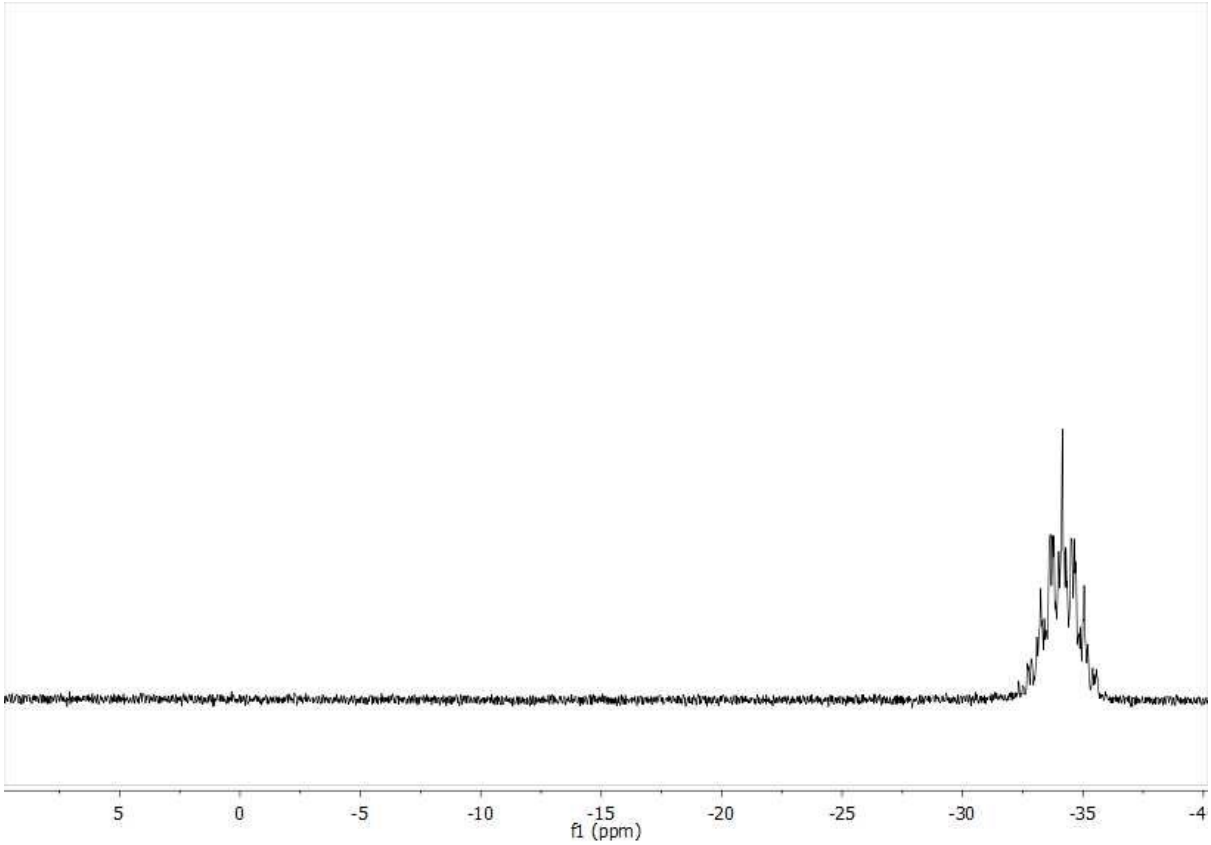

Figure 3.17 ^{119}Sn NMR spectrum of $SnBu_2$-POSS (C_6D_6, 186.45 MHz, 25 °C)

The ^{119}Sn NMR spectrum (figure 3.17) shows a distinct multiplet that resembles a pentet split further by the ^{2}J couplings. The peak has also appears to a lower frequency than that for the $SnMe_2$-POSS complex: from 5 ppm to -34 ppm. The presence of a nearby C-C σ-bond on the ^{n}Bu group provides electron density to shield the Sn nucleus.

As in the $SnMe_2$-POSS case MALDI-TOF (figure 3.18) analysis does not show a peak at the expected m/z and instead shows a peak corresponding to the POSS cage at 813 ($M+Na^+-H^+$).

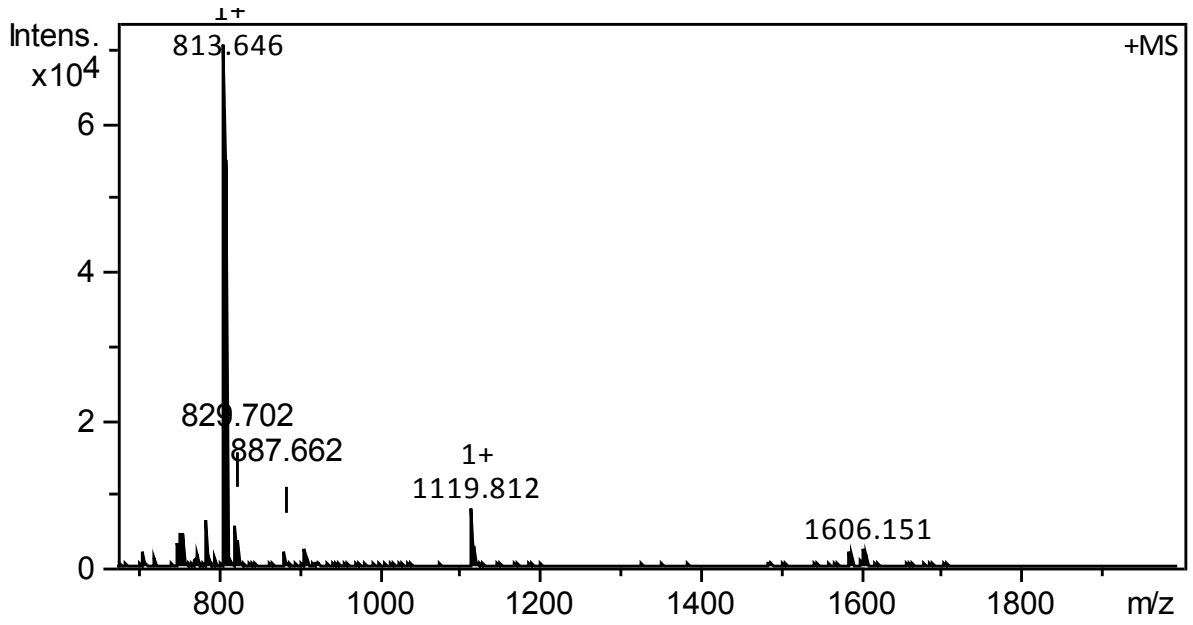

Figure 3.18. MALDI-TOF spectrum of $SnBu_2$-POSS

3.2.4 Synthesis of $Br(CH_2)_3$-(^{i}Bu)$_7$POSS

The three step synthesis of the phosphonium iodide begins with addition of an alkyl bromide to the trisilanol POSS cage. This is done by adding 1 equivalent of (3-bromopropyl)trichlorosilane to the trisilanol POSS cage in the presence of excess trimethylamine to quench the HCl produced from the formation of Si-O bonds. Purification gave an orange solid in 89% yield.

The addition of the alkyl-bromide chain adds the three signals of the butyl chain to the (^{i}Bu)$_7$-POSS ^{1}H NMR spectrum (figure 3.19) each with an integral of 2H, thus corresponding to the alkyl halide moiety. These are at 3.06, 1.95 and 0.80 ppm. The peak at 0.8 ppm overlaps the CH_2 signal of the butyl groups so the total integral of the region is 16H. The splitting indicates that the peak at 3.06 ppm is the triplet nearest the bromide, shifted downfield due to the electronegative bromide atom. The peak at 1.96 ppm is a multiplet resembling a pentet placing it in the centre of the chain (H_e). The peak overlapping 0.80 ppm is the CH_2 closest to the silicon (H_f), being less electronegative than C the Si provides shielding and so it is downfield compared to the rest of the signals. The COSY also confirms this pattern (figure 3.20). The butyl CH_2 groups resemble a triplet but this is due to overlapping doublets, the ^{1}J(H,H) is 7 Hz. The ^{1}J(H,H) is also 7 Hz for the CH_3 doublet.

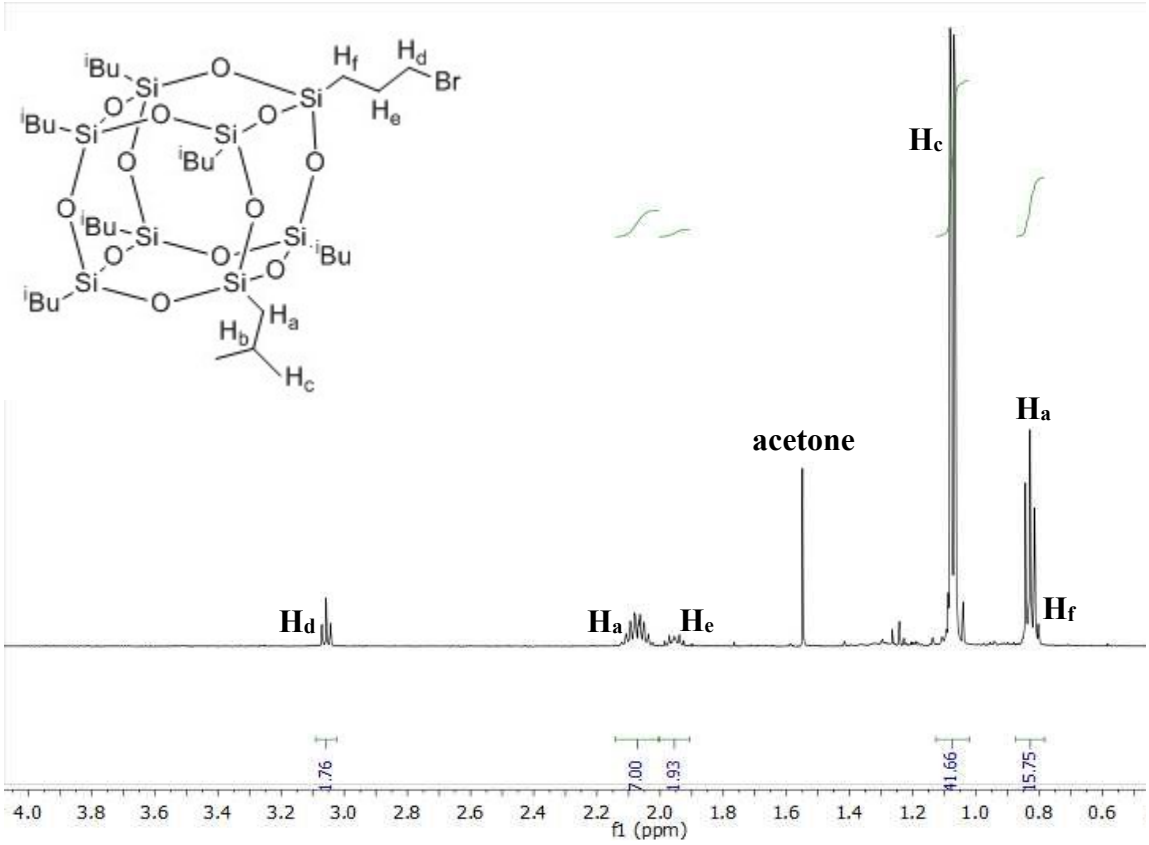

Figure 3.19 ^{1}H NMR spectrum of CH_2Br-$(CH_2)_2$-($^{i}Bu_7$)POSS ($CDCl_3$, 500.23 MHz, 25 °C)

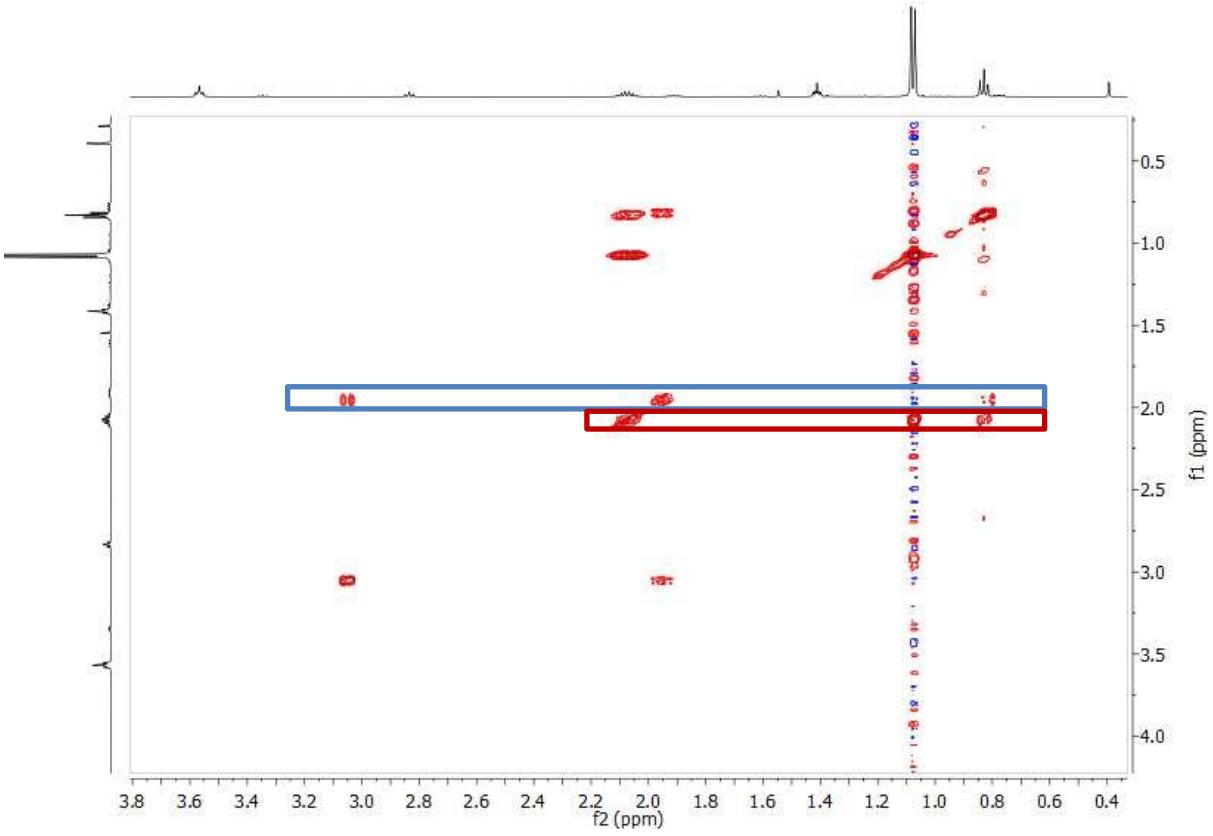

Figure 3.20 COSY-NMR spectrum ($CDCl_3$, 500.23 MHz, 25 °C) of Br-$(CH_2)_3$-($^{i}Bu_7$)POSS Spin systems are marked in blue for the alkyl chain and red for the POSS cage. There is some dislocation in the horizontal trace.

The MALDI-TOF spectrum (figure 3.21) of the species showed a peak at m/z 961 (M^++Na^+) and 978 (M^++K^+) which corresponds to the molecular weight with an additional sodium cation and a potassium cation respectively.

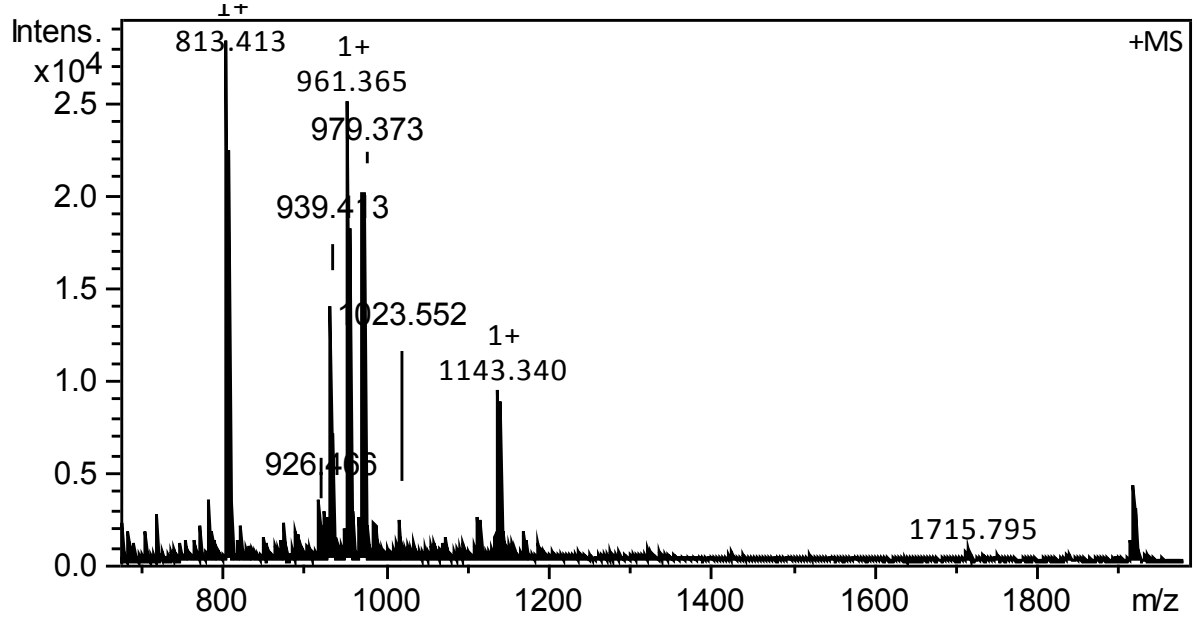

Figure 3.21 MALDI-TOF spectrum for Br-$(CH_2)_3$-(^{i}Bu$_7$)POSS

3.2.5 Synthesis of I$(CH_2)_3$-(^{i}Bu)$_7$POSS

To convert the alkyl bromide into the alkyl iodide a Finkelstein reaction was performed. The product from the previous stage was dissolved in THF with 1 equivalent of NaI. After refluxing overnight the salts were removed by a water/CH_2Cl_2 wash. A white solid was collected in 82% yield.

The main difference in the ^{1}H NMR spectrum between the I-alkyl-POSS and the Br-alkyl-POSS is that I is less electronegative than Br and so the CH_2 peak at 3.06 is shifted to 2.83 and the peak at 0.80 shifts to 0.77, the triplet splitting pattern is now observable as it no longer overlaps the CH_2 of the POSS cage. The CH_2 peaks of the POSS cage still resemble a triplet. The COSY spectrum confirms this assignment (figure 3.23).

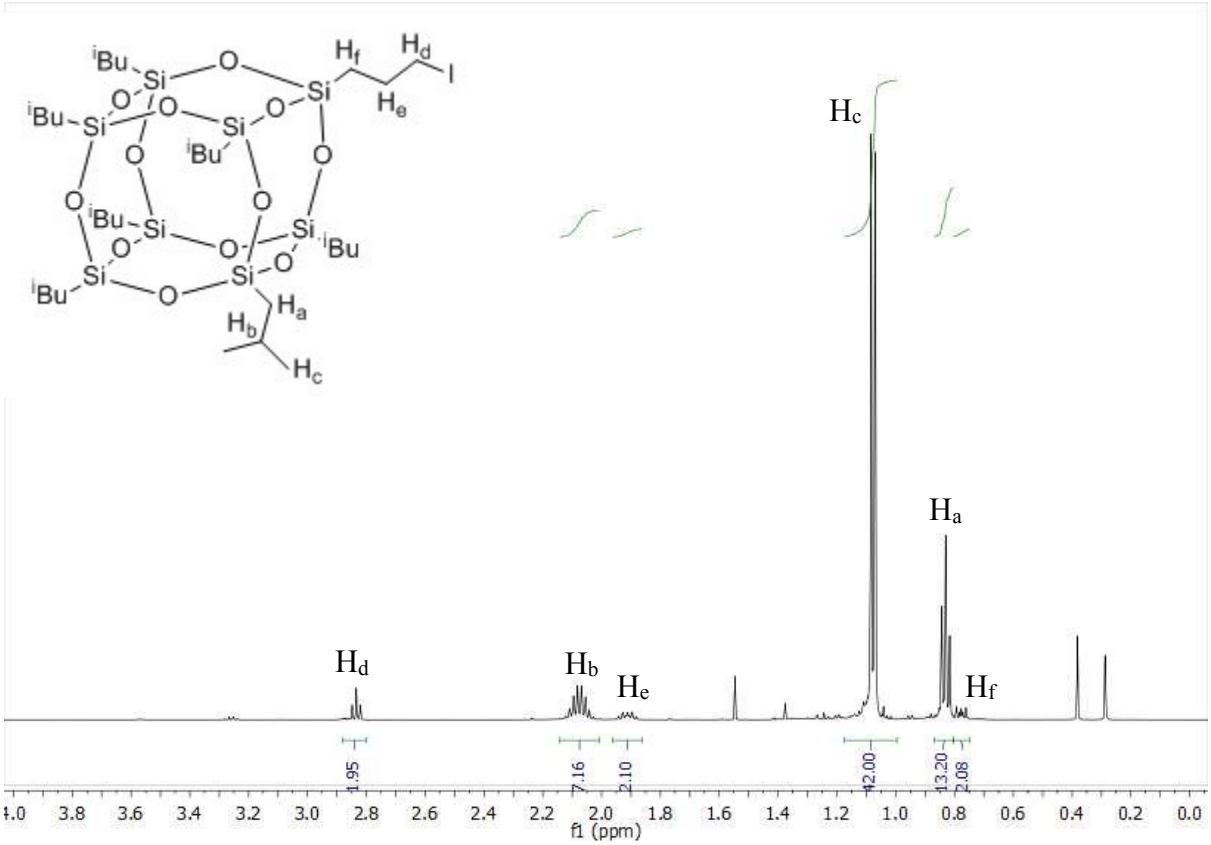

Figure 3.22 ^{1}H NMR spectrum ($CDCl_3$, 500.23 MHz, 25 °C) of I-$(CH_2)_3$-($^{i}Bu_7$)POSS

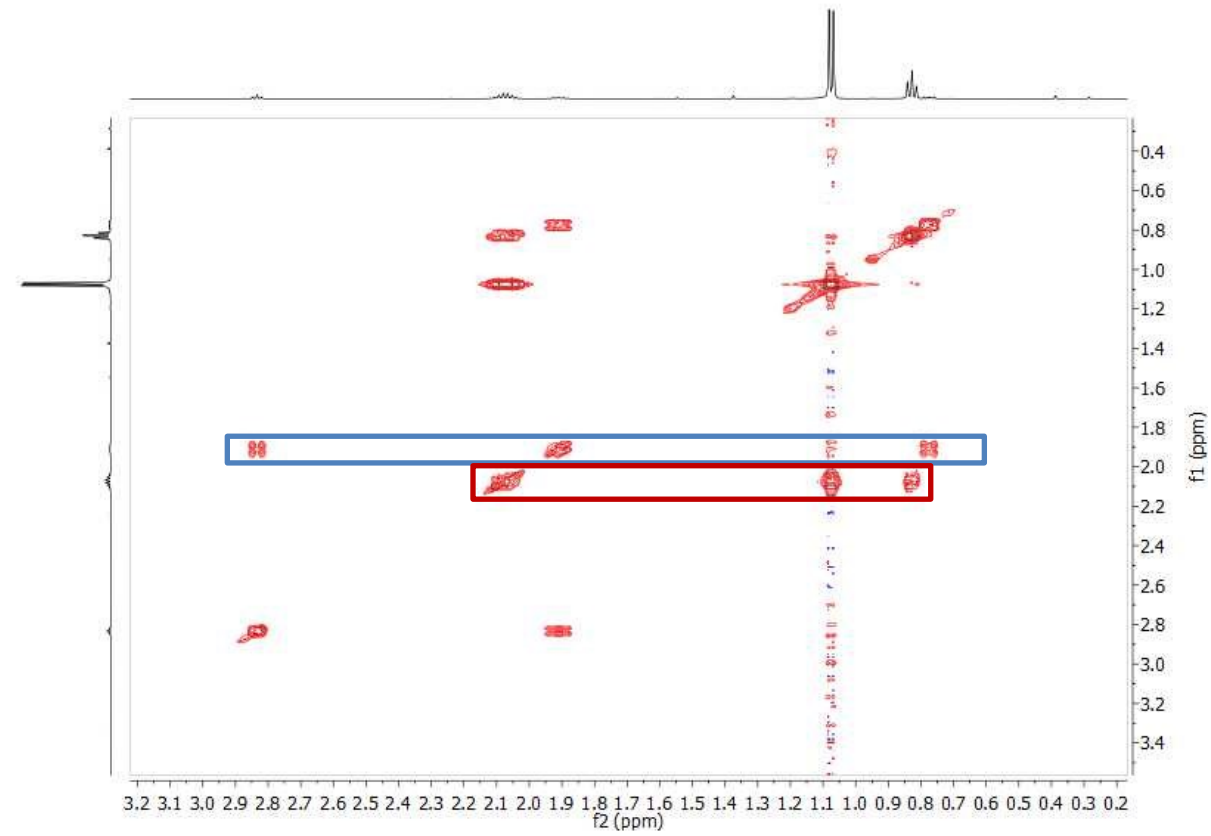

Figure 3.23 COSY-NMR spectrum ($CDCl_3$, 500.23 MHz, 25 °C) of I-$(CH_2)_3$-($^{i}Bu_7$)POSS. Spin systems are marked in blue for the alkyl chain and red for the POSS cage.

The MALDI-TOF spectrum (figure 3.24) also has a larger mass as a consequence of changing from Br to I with the peak 985.4 (M^+), 1007.4 (M^++Na^+) and 1025.4 (M^++K^+).

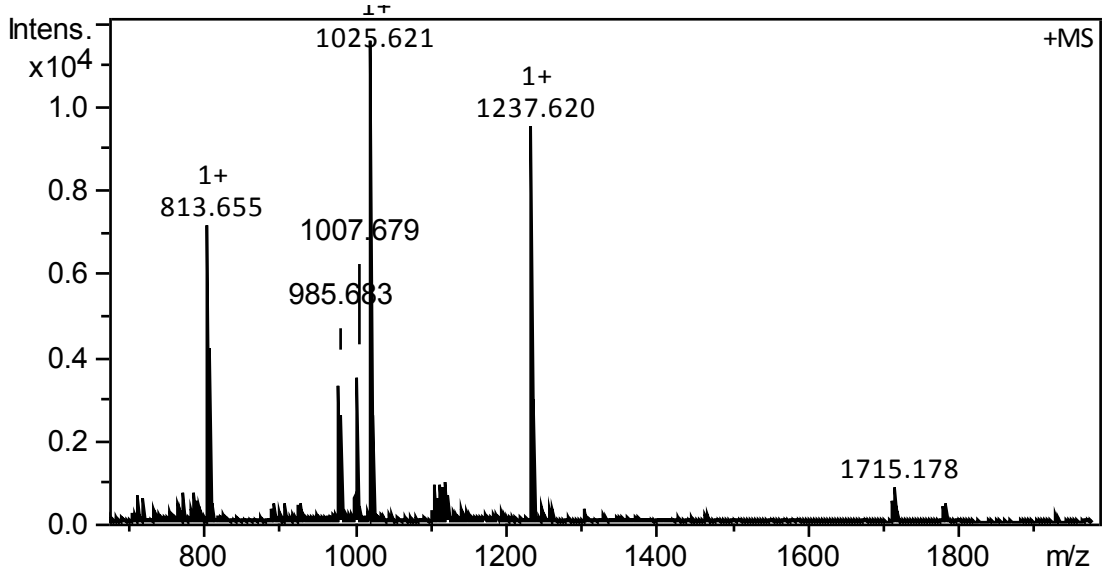

Figure 3.24 MALDI-TOF spectrum of I-$(CH_2)_3$-(^{i}Bu$_7$)POSS

3.2.6 Synthesis of [PPh_3][I]-$(CH_2)_3$-(^{i}Bu$_7$)POSS

The final step in the synthesis of the co-catalyst was to create the phosphonium iodide species. This was done by heating the iodo-alkyl species at reflux with PPh_3 in 1,2-dimethoxyethane. Addition of hexane caused a fine white solid to crash out in 71% yield.

In the ^{1}HNMR spectrum (figure 3.25) of [PPh_3][I]-$(CH_2)_3$-(^{i}Bu)$_7$POSS the introduction of the PPh_3 is observed with signals in the aromatic region with a total integral of 15 they correspond to one set of the *meta*-CH_2 with a shift at 7.73 ppm and a splitting of triplet of doublets (^{1}J = 7.8 Hz, ^{2}J = 3.4 Hz) and an integral of 6. The *para*-CH and *ortho*-CH_2 protons overlap at 7.84 ppm in a complex multiplet with a total integral of 9. The shifts of the alkyl chain change so that the closest signal to the iodide shifts from 2.83 to 3.82 ppm, the central CH_2 shifts from 1.92 to approximately 1.8 ppm, now overlapping the 7 CH of the isobutyl groups to give a total integral of 9H, the CH_2 nearest the silica is now no longer overlapping the CH_2 of the butyl but is seen near the CH_3 of the isobutyl groups shifting from 0.77 to 1.06. The symmetry of the entire molecule changes and now the isobutyl peaks of the POSS molecule split into two peaks: with total integrals equal to the original 7, 42 and 14.

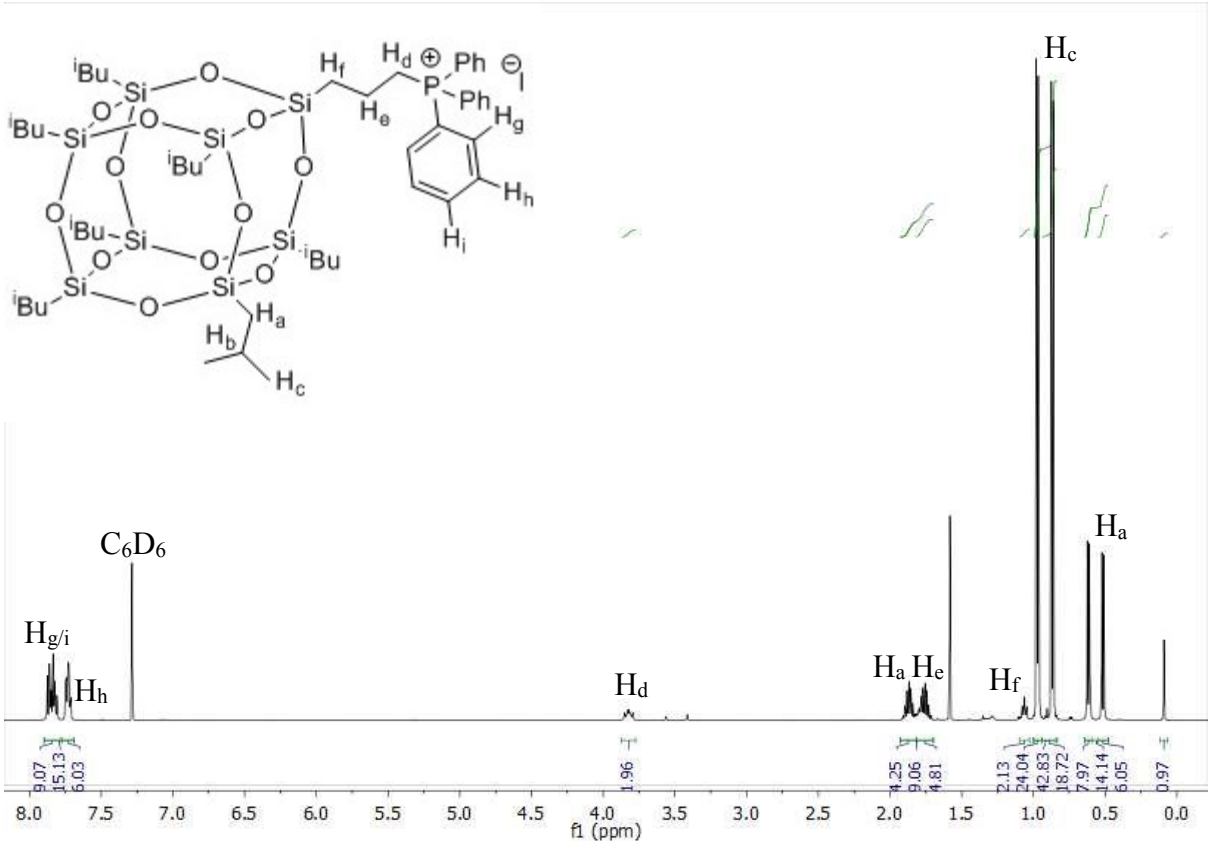

Figure 3.25 ^{1}H NMR spectrum ($CDCl_3$, 500.23 MHz, 25 °C) of [I][$PPh_3CH_2(CH_2)_2$]-($^{i}Bu_7$)POSS

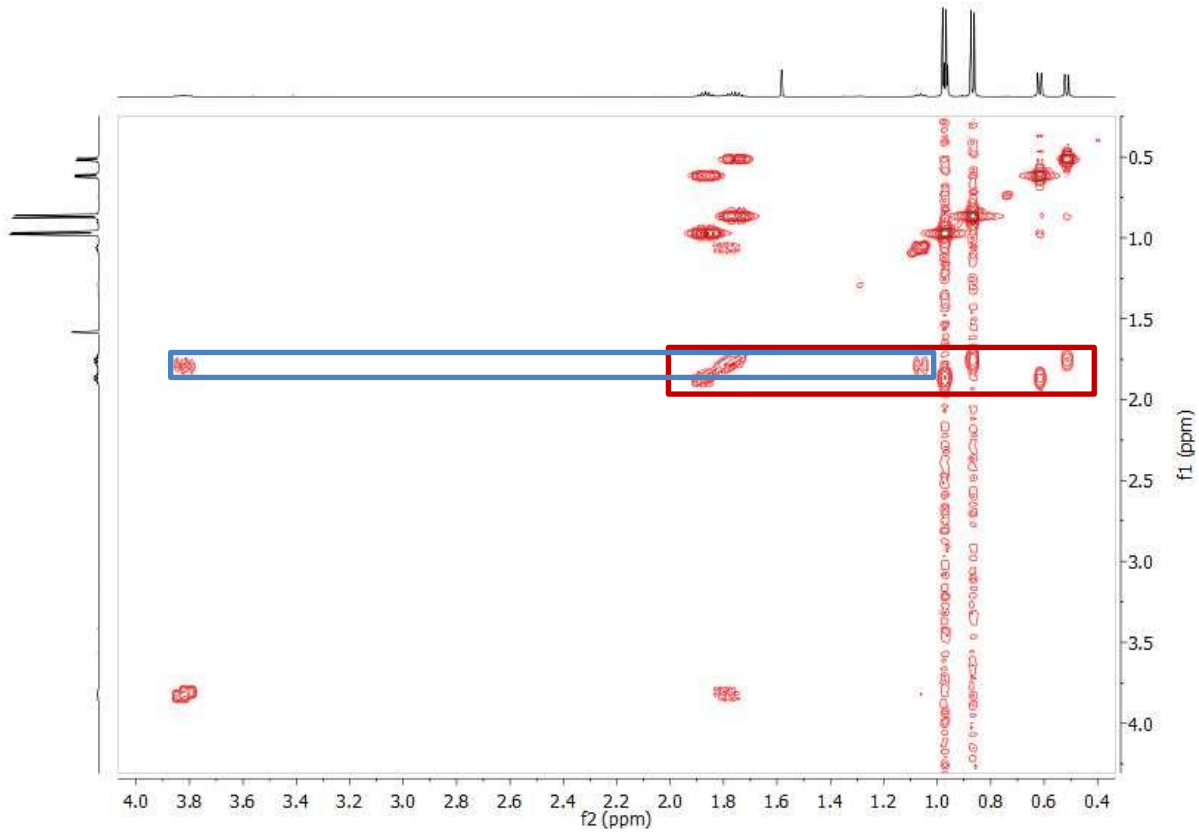

Figure 3.26 COSY-NMR spectrum ($CDCl_3$, 500.23 MHz, 25 °C) of [I][PPh_3-$(CH_2)_3$-($^{i}Bu_7$)POSS. Spin systems are marked in blue for the alkyl chain and red for the POSS cage.

Although the peaks are now spilt the spin systems are still the same: as evidenced in the COSY (figure 3.26).

The proton coupled ^{31}PNMR spectrum shows a single peak at 23.5ppm (figure 3.27). The shift of free triphenylphosphine is -6.00 ppm.[33] The high oxidation state of the P: +5 compared to +3 produces a de-shielded P and so the peak shifts downfield.

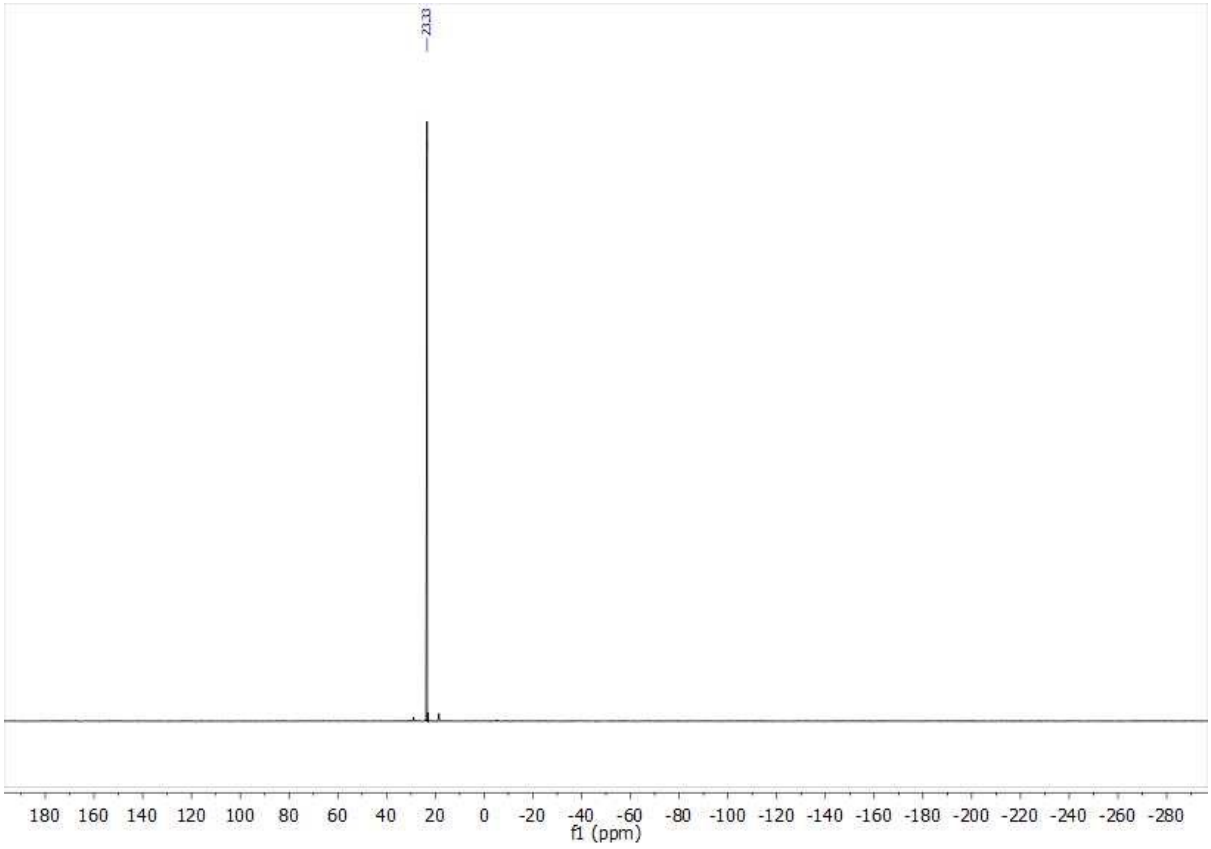

Figure 3.27 $^{31}P\{^{1}H\}$ NMR spectrum ($CDCl_3$, 500.23 MHz, 25 °C) of [I][PPh_3]-$(CH_2)_3$-($^{i}Bu_7$)POSS

The MALDI-TOF spectrum (figure 3.28) shows a peak at 1248 (M) and 1271 ($M+Na^+$).

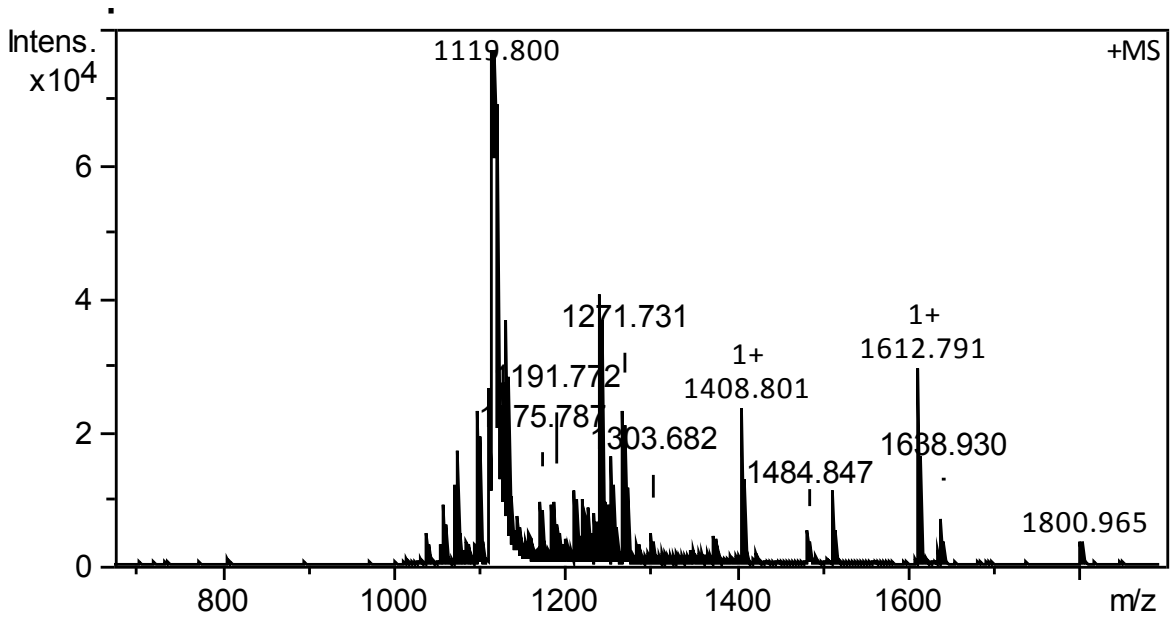

Figure 3.28 MALDI-TOF spectrum of the [I][PPh_3]-$(CH_2)_3$-(^{i}Bu$_7$)POSS

3.2.5 Epoxide/CO_2 coupling catalysis

Following the successful synthesis and characterisation of the POSS molecules the next stage was to optimise catalysis for the reaction of epoxides and CO_2 (scheme 3.5).

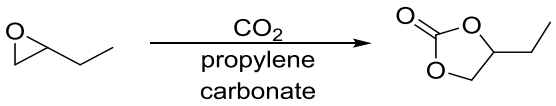

Scheme 3.5 Carbonation of epoxy butane

The catalysis screenings were carried out in neat 1,2-epoxybutane (7 mL) with a catalyst loading of 0.04 mol% and a co-catalyst loading of 0.18 mol%. These are lower catalyst loadings than those used in the immobilised catalysts discussed above which are between 1-2 mol%. As a benchmark $ZnCl_2$ and TBAI were initially used to ensure the experimental methodology was good. The results are presented in table 3.2.

Table 3.2 Parameter Screening

Entry	Cat.	I^- source	Temperature (°C)	Pressure (bar)	Conversion (%)	TON
1	$ZnCl_2$	TBAI	110	30	< 99	1000
2	$ZnCl_2$	TBAI	110	50	< 99	1000
3	$SnMe_2$-POSS	$[PPh_3I]$-POSS	110	50	< 99	1000
4	$SnMe_2$-POSS	$[PPh_3I]$-POSS	80	50	93	936
5	$SnMe_2$-POSS	$[PPh_3I]$-POSS	80	30	92	926
6	$SnMe_2$-POSS	$[PPh_3I]$-POSS	80	10	82	825
7	$SnMe_2$-POSS	$[PPh_3I]$-POSS	80	5	82	825
9	$SnBu_2$-POSS	$[PPh_3I]$-POSS	80	30	93	939

Conditions: Cat. (0.04 mol%), $[PPh_3I$-POSS] (0.18 mol%), 1,2-epxoybutane (80 mmol, 1000 equiv), propylene carbonate (8 mmol), P CO_2 (varies), T (varies), 700 rpm, t 6 h. TON: mol.substrate consumed/mol.catalyst

Conversions were calculated by ^1H NMR spectrum (figure 3.29). The integral of the propylene carbonate peak was set at 4.9 ppm (H_m) was set as 1 and the integral of the epoxide peak at 2.89 ppm (H_c) was compared to the integral of the product carbonate peak at 4.65 ppm (H_f).

Despite the relatively low loadings, the catalysts performed just as well as the immobilised species discussed above. This demonstrates that the homogeneous nature of the catalyst and co-catalyst, capable of dissolving in solution, have much greater activity than the equivalent heterogenized immobilised species. Lower CO_2 pressure did result in lower conversions however this may be due to a lower rate of reaction and simply running the experiment for a longer time could bring these conversions higher.

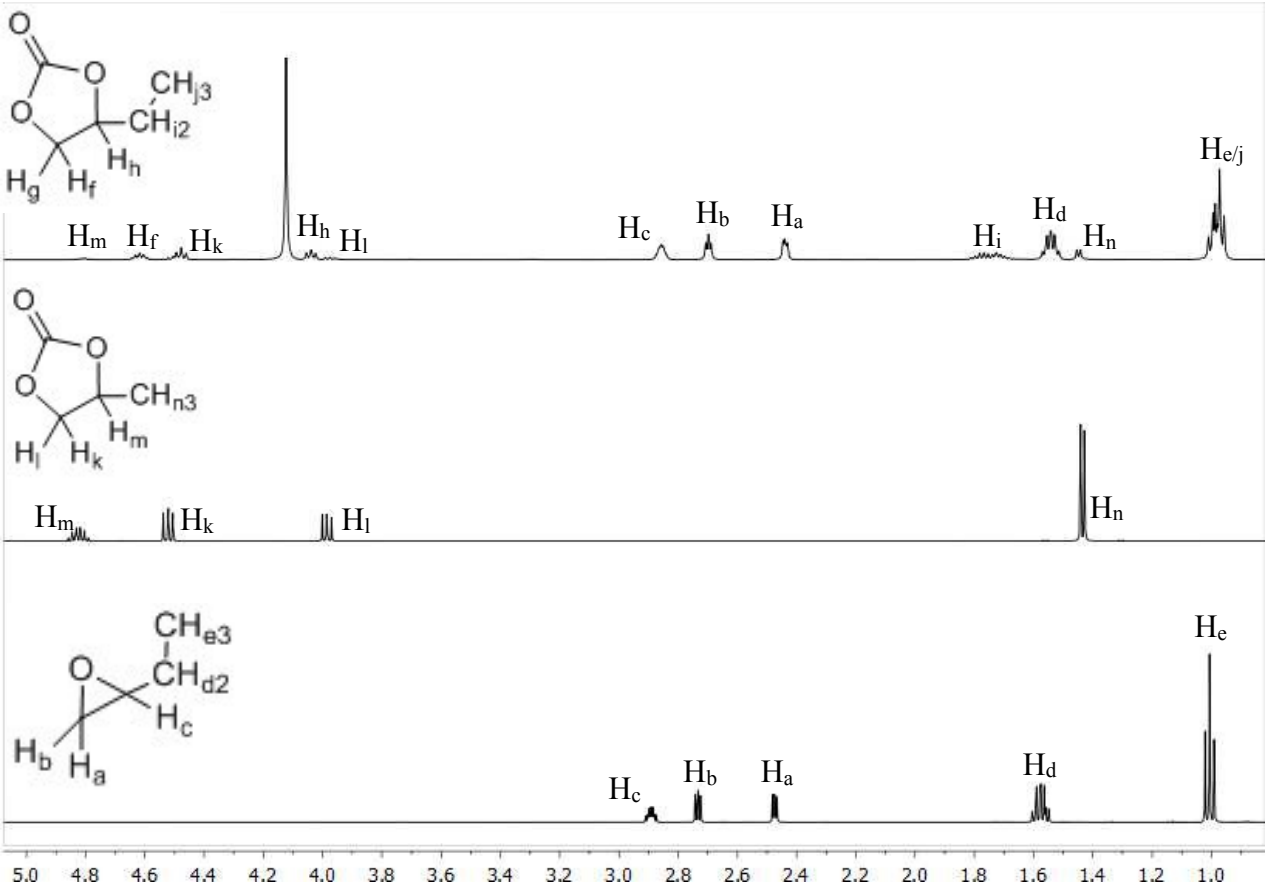

Figure 3.29 ^{1}H NMR spectrum ($CDCl_3$, 500.23 MHz, 25 °C): example NMR of the 1,2-epoxybutane catalysis with 1,2-epoxybutane (bottom), propylene carbonate (middle) spectra for comparison. Conversion was calculated using the ^{1}H NMR integrals for the epoxide (H_c) and product carbonate (H_f) with propylene carbonate (H_m) set at 1 to act as an internal standard.

Initial screenings focussed on lowering the temperature and pressure which the reaction was run at; as the more benign the conditions, the more compatible with the membrane it would be. The conditions were improved to a minimum of 5 bar and 80°C giving 82% conversion after 6 hours.

Following the screening of the catalyst conditions, the epoxide scope was expanded (table 3). 1,2-epoxyhexane (entry 2) has a longer aliphatic chain than 1,2-epoxybutane but would be expected to react similarly. The other epoxides have different electronic properties: epicholorohydrin (entry 3) has a less electron rich epoxide due to the electron withdrawing chloride. The opposite is the case for 1,2-epoxy-3-phenoxypropane (entry 4), which has an electron donating phenyl group. However, the aromatic ring may change the solubility and result in an increased steric bulk. Cyclohexene oxide (entry 5) is an internal epoxide that can be less reactive.

Table 3.3 Substrate Screening

Entry	Starting Material	Product	Sub-Entry	Catalyst	Conversion (%)	TON
1	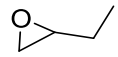	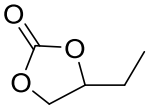	a	$Sn(Me)_2$-POSS	94	946
			b	$Sn(^nBu)_2$-POSS	93	939
2	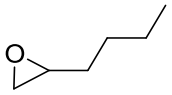	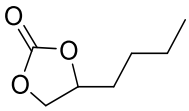	a	$Sn(Me)_2$-POSS	96	966
			b	$Sn(^nBu)_2$-POSS	100	1000
3	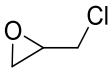	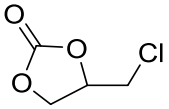	a	$Sn(Me)_2$-POSS	89	895
			b	$Sn(^nBu)_2$-POSS	78	789
4	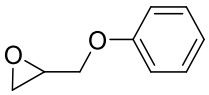	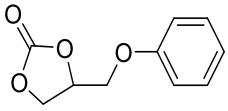	a	$Sn(Me)_2$-POSS	92	921
			b	$Sn(^nBu)_2$-POSS	91	916
5	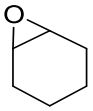	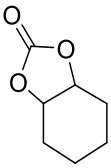	a	$Sn(Me)_2$-POSS	8	85
			b	$Sn(^nBu)_2$-POSS	7	68
6	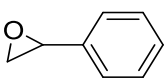	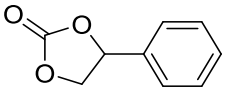	a	$Sn(Me)_2$-POSS	88	885
			b	$Sn(^nBu)_2$-POSS	81	814

Conditions: [$Sn(R)_2$-POSS] (0.04 mol%), [PPh_3I-POSS] (0.18 mol%), Epoxide (80 mmol), Propylene Carbonate (std) (8 mmol), P CO_2 (30 bar), T (80 °C), 700 rpm, t 6 h

1,2-epoxybutane (entry 1), 1,2-epoxyhexane (entry 2), epichlorohydrin (entry 3), 1,2-epoxy-3-phenoxypropane (entry 4) and 1,2-epoxystyrene (entry 6) were all converted with reasonable yields.

Overall the $SnMe_2$ species performed better than the $SnBu_2$ species for the coupling of the epoxides with CO_2, with conversions of: 1,2-epoxybutane (entry 1) 94% vs 93%, epichlorohydrin (entry 3) 89% vs 78%, and 1,2-epoxystyrene (entry 6) 88% vs 81%. This trend is possibly a consequence of a combination of sterics and electronics: the butyl groups are larger so will have a greater steric clash with the reactants than the methyl groups and show a slightly increased shielding on the Sn^{IV} nucleus, as observed in the lower frequency chemical shifts of the $SnBu_2$-POSS compared to $SnMe_2$-POSS in the Sn-NMR (figures 7 and 15), therefore the Lewis acidity of the $SnBu_2$-POSS catalyst will be possibly weaker and therefore so will its performance in catalysis.

The exception to $SnMe_2$-POSS performing better than $Sn(^nBu)_2$-POSS is 1,2-epoxyhexane (entry 2), which may be as a result of the similarity of the long chain alkyl groups on the catalyst and the substrate. The lower yield of 1,2-epoxy-3-phenoxypropane can be a consequence of the formation of product that is solid under the reaction conditions, melting point is 100°C, thus preventing the catalyst from converting the entire amount of substrate. The catalyst struggled to react cyclohexene oxide (entry 5), but internal functional groups are less reactive due to steric hindrance and electronic stability.

The lower yield of epichlorohydrin (entry 3) may be a result of the electronic influence on the mechanism. The lower yield: 89% vs 94%, for $SnMe_2$ catalaysed carbonylation of 1,2-epoxybutane, implies that the electronics are detrimental to the mechanism. Also important to note is the large gap in performance of $SnMe_2$-POSS vs $Sn(^nBu)_2$-POSS, with conversions of 89% and 78%, respectively. This implies that the electronics must also affect the coordination of the Lewis acid. By applying charge distribution to scheme's 1 and 2 (scheme 3.6) the influence of the electronics can be discussed.

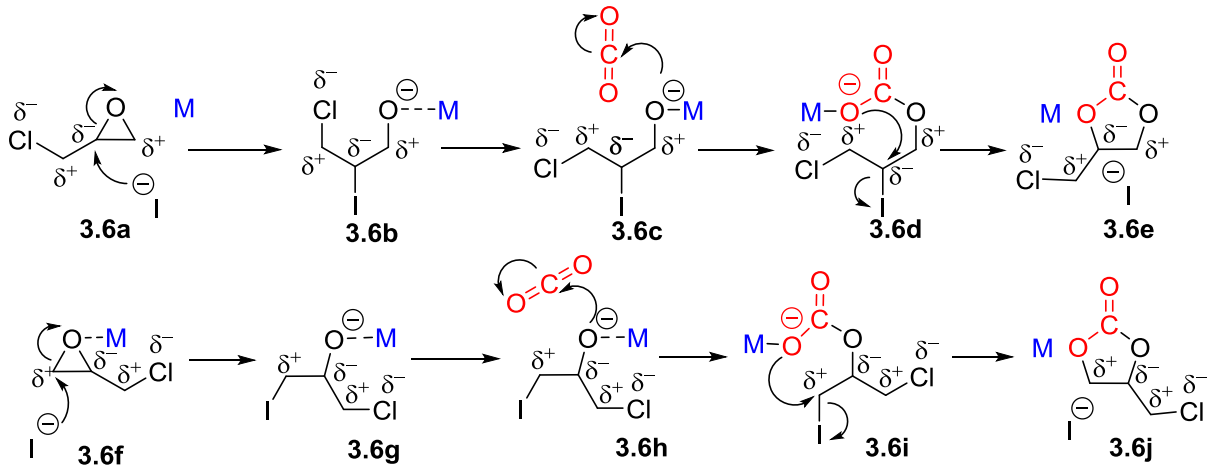

Scheme 3.6 Charge distribution in the carboxylation mechanism showing the attack of the nucleophile to the least hindered C (bottom) and most hindered C (top)

If the nucleophile attacks the most hindered carbon (**3.6a**) the charge distribution is unfavourable, the electrophile being more electronegative due to the influence of the chlorine. Consequently when the I leaves at the end of the mechanism (**3.6d**) it is through attack of the negative charge at a more electronegative carbon; this is unfavourable thus reactivity would be expected to be poorer. However in this situation the intermediate could also be stabilised: with the oxygen anion next to a δ^+ charge on the adjacent carbon (**3.6c**).

The opposite charge distribution is the case in the mechanism of the attack in the least hindered C (**3.6f**), which would be more favourable as the C is more electropositive. Although now in the intermediate the anionic charge on the oxygen is adjacent to a δ^- C (**3.6g**) and this is an unfavourable charge distribution. However the Sn^{IV} catalyst can accept some of the negative charge to counter-act this effect. This may be the origin of the better performance of the $SnMe_2$-POSS vs $Sn(^nBu)_2$-POSS in epichlorohydrin (entry 3.3) as $SnMe_2$-POSS is a better Lewis acid.

The lower reactivity observed for epichlorohydrin in the $SnMe_2$-POSS catalysed epoxide/CO_2 coupling was also reported in Sakai's silica immobilised catalysts with a yield of 85% after 20 hours, compared to 99% yield of 1,2-epoxybutane after 6 hours in equivalent conditions.[26]

When the $SnMe_2$-POSS and $SnBu_2$-POSS catalysts are compared to the Sn^{IV} salen species reported by Nygen they show comparable activity for the carboxylation of propylene oxide with the TON varying between a minimum of 116 to a maximum of 2096 but averaging at 681.[11] The conditions of those catalysts are 8 bar of CO_2, 0.032 mol% catalyst loading, 1/5

cat/co-catalyst, and a temperature of 120 °C for 4 hours. CH_2Cl_2 is used as a solvent where-as the Sn-POSS catalysts occurred in neat solution.

3.2.6 Membrane Retention Studies

In order to test the compatibility of the system in a continuous flow reactor a 'cat in a cup' experiment was set-up (figure 3.24). The set-up of a continuous flow membrane reactor has a loop of solvent with the catalyst and substrate dissolved in it which allows the reaction to occur. There is a point where this solution passes through a membrane module that allows the product, and any unreacted substrate, to pass to a collection vessel while the enlarged catalyst is retained in the reaction loop by the membrane to continue to perform catalysis.

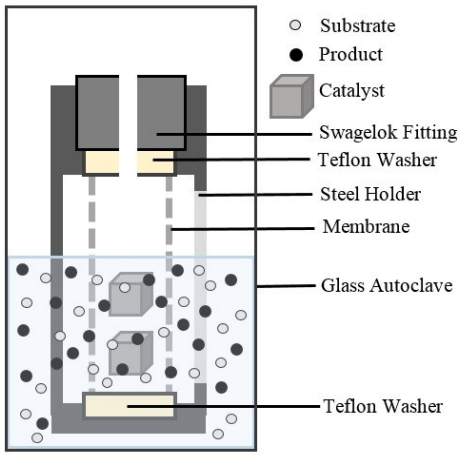

Figure 3.30 Diagram of the 'Cat in a cup' set-up showing the Teflon washers compressing the ceramic membrane containing the catalyst. The substrates and product that can flow in and out of the membrane [23]

The key step to investigate in this set-up was the retention of the enlarged catalyst by the membrane. This was done by placing the catalyst and co-catalyst within a ceramic TiO_2 membrane (figure 3.30), itself clamped in a membrane holder, which was then placed within a reaction vessel filled with 1,2-epoxybutane and was able to be pressurised with a static headspace of CO_2. The 1,2-epoxybutane and CO_2 could permeate through the membrane and react. The carbonate could then diffuse out of the membrane while the catalyst is retained. The $SnMe_2$-POSS and $[I][PPh_3]$-$(CH_2)_3$-POSS catalyst and co-catalyst itself was a white powder that is soluble in solution.

Immersing in an oil bath permits heating and sampling was possible by the addition of a specially designed capillary sample unit. The capillary descended into the solution outside the membrane to detect any conversion and any leaching. To avoid the chance of a gas pressure

gradient building up on one side of the membrane the Swagelok fitting at the top was not tightened but as this was above the solvent level no catalyst could leach through that pathway.

The membrane holder was a stainless steel frame with a threaded fitting at the top so a Swagelok fitting could be added to seal the top and compress the 0.9 nm TiO_2 membrane between two Teflon washers, this should prevent leaching between a rough cut ceramic membrane and the steel holder. The ceramic 0.9 nm TiO_2 is available as a long individual piece that can be cut to the appropriate length. This set up should allow the product, substrate and CO_2 to flow in and out, but the catalyst and co-catalyst should remain within the membrane chamber.

1,2-Epoxybutane (70 cm^3) and CO_2 (5 bar) was used with $Sn(Me)_2$-POSS (0.147g, 0.16 mmol) and $[PPh_3][I]$-POSS (0.745g, 0.60 mmol). A glass autoclave with a pressure limit of 5 bar was used. Heating was performed by submerging the autoclave within an oil bath at 50°C. There was no stirring or agitation of any kind. Leaching was monitored by sampling the solution through a capillary and analysis by UV/Vis and NMR. The CO_2 pressure was re-filled to 5 bar periodically. Conversion was monitored by periodic sampling by a capillary and analysed by GC/FID and NMR spectroscopy.

It was discovered that conversion increased slowly, but overall fairly steadily (figure 3.31).

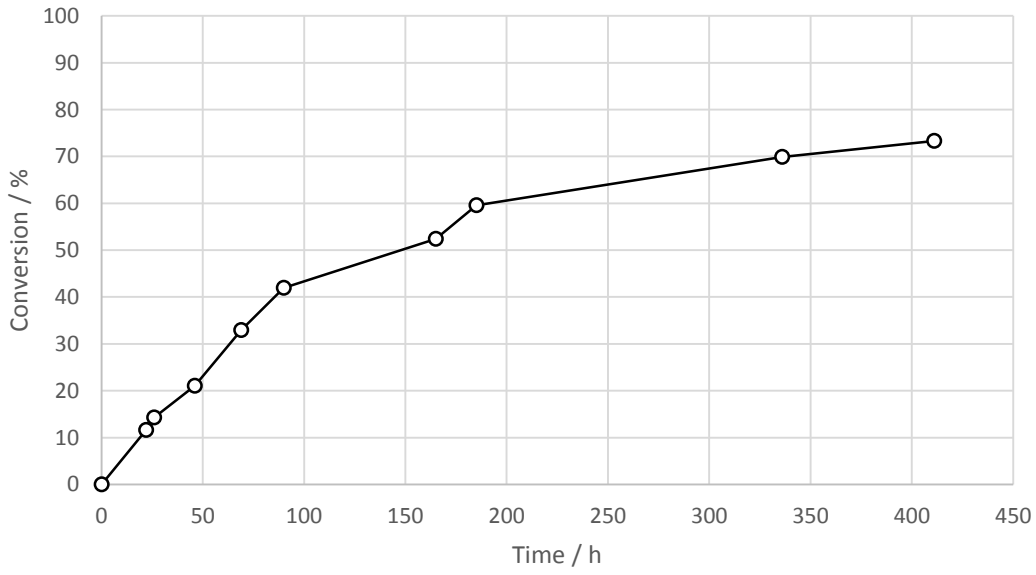

Figure 3.31 Conversion of 1,2-epoxybutane with time using $Sn(Me)_2$-POSS/$[PPh_3][I]$-POSS inside a 0.9 nm TiO_2 membrane. Reaction conditions: 1,2-epoxybutane / $[PPh_3][I]$-POSS / $Sn(Me)_2$-POSS = 5365/4/1, pCO_2 = 5 bar, T = 50 °C, 411 h. $Sn(Me)_2$-POSS (0.15 mmol, 0.03 mol%), $[PPh_3][I]$-POSS (0.6 mmol, 0.12 mol%)

The conversion was calculated by using the same NMR integrals as in the screening. The conversion increases linearly until 90 hours then there is a period with a lower rate (between 90 and 165 hours), then the rate between the two measurements increases again. This is due to an increase in the pressure which can increase the rate of the reaction. However following this the conversion flattens off as the reactor was left to continue without further addition of CO_2. In an actual reactor set-up the pressure would be constant and should withstand higher pressures, resulting in better rates of conversion. However the higher pressure may also have an impact on the leaching of the catalyst.

A factor to consider is the amount of CO_2 dissolved in solution and the rate at which this occurs. In previous CO_2 catalysis run in toluene it was the rate of CO_2 dissolution that has been shown to be rate limiting.[34] Because the pressure was not held constant it is hard to draw useful kinetic information from this reaction. Using a mass flow controller to maintain a constant pressure and monitor the gas uptake would provide the necessary data for kinetic data.

To determine the effectiveness of the set-up the concentration of $[PPh_3][I]$-POSS leaching was monitored. This was calculated by UV/Vis-spectroscopy of samples taken with a capillary suspended in solution on the outside of the membrane. This was compared to a concentration curve made by known amounts of the catalyst (see materials and methods below) (table 3.4).

Table 3.4 Leaching of [I][PPh_3]-(CH_2)$_3$-POSS based on UV/Vis measurements

Entry	Time (hours)	Absorbance (at 268 nm)	Concentration (C_{UV} = A/εl) mg/mL	Leaching ((C_{UV}/C_{max})* $mass_{final}/mass_{sample}$*100) %
1	0	0.133	0.36	10.9
2	22	1.376	3.75	73.8
3	46	0.679	1.85	108.2
4	69	1.616	4.41	121.2
5	336	0.876	2.39	105.1
6	446 (inside membrane)	3.001	6.93	95.6

7	446 (outside membrane)	3.111	7.18	100

The final readings (entries 6 and 7) were taken when the autoclave was depressurised and opened. As these readings were approximately the same this was taken as the maximum amount of leaching. The values of leaching for the previous time points were determined from this value. The volume of the POSS molecule is approximately 1.4 nm and the cut off value for the TiO_2 membrane was 0.9nm so it should be retained fairly reasonably.

Unfortunately there was a distinct amount of leaching observed with complete leaching observed within 46 hours. The results in table 4 have a large error associated with them due to the lack of stirring, a highly localised concentration of catalyst and variable sample weight. It was assumed that the same amount of leaching would apply to the tin catalyst as the POSS moieties are the same: the nature of the POSS molecule dictating retention rather than the catalysts themselves. The leaching may be due to a problem with the loading method as care must be taken to avoid cracking the membrane due to over-tightening therefore the seal might not be sufficient. Furthermore the cut membrane has a rough edge that can leave gaps larger than the expected 0.9 nm pore-size.

In the actual membrane reactor the continuous flow set-up would significantly dilute the catalyst in the membrane chamber so there would be less concentration gradient forcing the catalyst through the membrane therefore the level of leaching would be lower.

3.3 Conclusion and Future Work

Three POSS-enlarged catalysts were synthesised and characterised. These catalysts were applied in the coupling of CO_2 and epoxides. The substrate scope was expanded to different epoxides. While a compatibility experiment with the membrane reactor showed leaching, this might be due to the methodology rather than the catalyst/membrane compatibility. The catalyst did not show any signs of loss of activity over a very long period of time, demonstrating the excellent stability of the tin-POSS catalysts.

The ultimate goal of this research is to make a catalyst that is compatible with a continuous flow system therefore until the catalyst has been used in such a system it will not be proven workable. The POSS moiety is very versatile and it would be interesting to combine the POSS/membrane system with state of the art salen ligands. Also of interest would be the successful growth and analysis of crystals of the synthesised catalysts.

It would also be good to use the sample-units on the autoclave to get kinetic information about the influence of pressure, substrate loading, temperature, and solvents. The reactions were performed in neat epoxide. Finding a suitable organic solvent would be good for compatibility with the membrane.

3.4 Materials and Methods

All solvents were dried in a solvent purification system and stored over 4Å molecular sieves under argon. Solvents were degassed in a sonicator. Chemicals were purchased from Aldrich or Fisher and used without further purification unless specified. Trisilanol POSS was purchased from Hybrid Catalysis B.V, The Netherlands. CO_2 (CP Grade, 14 kg, 50 bar) was purchased from BOC.

The 0.9nm TiO_2 membrane was purchased from Inopor. Industriestraße 1, 98669 Vielsdorf, Germany.

NMR spectra were recorded on a Bruker AVA400 spectrometer for ^1H (399.90 MHz); a Bruker AVA500 spectrometer ^1H (500.23 MHz), ^{13}C (125.76 MHz), ^1H DOSY, ^1H COSY, ^1H-^{13}C HSQC spectra or a Bruker PRO500 spectrometer ^1H (500.23 MHz), ^{13}C (125.76 MHz), ^{31}P (202.50 MHz) and ^{119}Sn (186.45 MHz).

The UV/Vis spectrometer used was a Shimadzu UV-2700.

3.4.1 Synthesis of POSS catalysts

(^{i}Bu)$_7$-POSS

The starting (^{i}Bu)$_7$-POSS material was recrystallized in hot acetone.

NMR: ^1H NMR (500.23 MHz, $CDCl_3$, 300K) δ_H (ppm): 1.88 (m, 7H, CH, *POSS isobutyl*), 0.98 ppm (m, 42H, CH_3, *POSS isobutyl*), 0.61 (m, 14H, CH_2, *POSS isobutyl*). ^{13}C NMR (125.76 MHz, $CDCl_3$, 300K) δ_C (ppm): 22.5 (CH_2, *POSS isobutyl*), 22.6 (CH_2, *POSS isobutyl*), 22.9 (CH_2, *POSS isobutyl*), 23.2 (CH_2, *POSS isobutyl*), 23.9-24.0 (CH, *POSS isobutyl*), 25.7-25.8 (CH_3, *POSS isobutyl*). MALDI m/z: 791 (M), 813 m/z ($M+Na^+-H^+$)

SnMe$_2$-(iBu)$_7$POSS

$SnMe_2Cl_2$ (5g, 0.023 mol) and ^{i}Bu$_7$-POSS (18g, 0.023 mol) were dissolved in toluene (250 mL). NEt_3 (12.7mL, 0.09 mol) in toluene (50mL) was added dropwise and the mixture stirred overnight. The toluene was filtered over alumina and the solvent removed. Hexane (100mL) was added, the solution filtered again and then the solvent evaporated off. The white crystalline solid was recovered. (16.70g, 0.018 mol, 79% yield).

NMR: ^{1}H NMR (500MHz, $CDCl_3$, 300K) δ_H (ppm): 0.34 (3H, s, CH_3, *$SnMe_2$*), 0.47 (3H, s, CH_3, *$SnMe_2$*), 0.84 (m, 14H, CH_2, *POSS isobutyl*), 1.12 (m, 42H, CH_3, *POSS isobutyl*), 2.12 (od, 7H CH, *POSS isobutyl*). ^{13}C NMR (125.76 MHz, $CDCl_3$, 300K) δ_C (ppm): 0.13 (CH_3, *methyl*), 0.82 (CH_3, *methyl*), 22.25 (CH_2, *POSS isobutyl*), 22.49 (CH_2, *POSS isobutyl*), 22.85 (CH_2, *POSS isobutyl*), 23.05 (CH_2, *POSS isobutyl*), 23.90 (CH, *POSS isobutyl*), 24.23 (CH_2, *POSS isobutyl*), 25.48-25.9 (CH_3, *POSS isobutyl*). ^{119}Sn NMR (186.45 MHz,$CDCl_3$,300K) δ_{Sn} (ppm): 4.8 (hept, *$SnMe_2$*)

$SnBu_2$-(iBu)$_7$POSS

$SnBu_2Cl_2$ (5g, 0.016 mol) and $^{i}Bu_7$-POSS (13g, 0.016 mol) were dissolved in toluene (250 mL). NEt_3 (12.7mL, 0.09 mol) in toluene (50mL) was added dropwise and the mixture stirred overnight. The toluene was filtered over alumina and the solvent removed. Hexane (100mL) was added, the solution filtered again and then the solvent evaporated off. The white crystalline solid was recovered. (9.86g, 0.010 mol, 81% yield).

NMR: ^{1}H NMR (500.23 MHz, C_6D_6, 300K) δ_H (ppm): 0.61 (m, 14H, CH_2, *POSS isobutyl*), 0.99 (m, 42H, CH_3, *POSS isobutyl*), 0.98 (m, 6H, CH_3, *n-butyl*), 1.41 (m, 4H, CH_2, *n-butyl*), 1.47 (t, 2H, CH_2, *n-butyl*), 1.58 (t, 2H, CH_2, *n-butyl*), 1.73 (m, 4H, CH_2, *n-butyl*) 1.88 (m, 7H, CH, *POSS isobutyl*). ^{13}C NMR (125.76 MHz, $CDCl_3$, 300K) δ_C (ppm): 13.45 (CH_3, n-butyl), 20.96 (CH_2, *propyl*), 21.60 (CH_2, *propyl*), 22.28 (CH_2, *POSS isobutyl*), 22.54 (CH_2, *POSS isobutyl*), 22.94 (CH_2, *POSS isobutyl*), 23.07 (CH_2, *POSS isobutyl*), 23.86-23.97 (CH, *POSS isobutyl*), 24.31 (CH, *POSS isobutyl*), 24.37 (CH_2, n-*butyl*), 25.62-25.95 (CH_3, *POSS isobutyl*), 26.49 (CH_2, n-*butyl*), 26.71 (CH_2, n-*butyl*). ^{119}Sn NMR (186.45 MHz,$CDCl_3$,300K) δ_{Sn} (ppm): -34 (m, *Sn(^{n}Bu)$_2$*)

Br(CH$_2$)$_3$-(^{i}Bu)$_7$POSS

Trisilanol-heptaisobutyl-POSS (10.6g, 0.013 mol) was placed in a schlenk flask and dried under vacuum for 1 hour. DCM (50mL) was added to dissolve the POSS and the flask cooled in an ice-bath. A DCM (50mL) solution of (3-bromopropyl)trichlorosilane (3.44g, 0.013 mol) and triethylamine (9.4 mL, 0.067 mol) in was added dropwise. The reaction was left stirring overnight under Ar. The DCM was removed then the solids dissolved in hexane:ethyl acetate and then the salts filtered over a short column. The product was purified on a column to give an orange solid (11.15g, 0.012 mmol, 89% yield).

^{1}H NMR (500.23 MHz, C_6D_6, 300K) δ_H (ppm): 3.06 (t, 2 H, *CH_2 propyl*), 2.06 (m, 7 H, *CH isobutyl*), 1.95 (m, 2 H, *CH_2, propyl*), 1.07 (t, 42 H, *CH_3 isobutyl*), 0.85 (m, 14 H, *CH_2 isobutyl*),

0.80 (m, 2 H, *CH_2 propyl*). ^{13}C NMR (125.76 MHz, $CDCl_3$, 300K) δ_C (ppm): 11.3 (CH_2, *propyl*), 22.4 (CH_2, *POSS isobutyl*), 22.5 (CH_2, *POSS isobutyl*), 23.8 (CH, *POSS isobutyl*), 25.7 (CH_3, *POSS isobutyl*), 26.7 (CH_2, *propyl*), 36.3 (CH_2, *propyl*). MALDI m/z: 961 ($M+Na^+$), 978 ($M + K^+$)

$I(CH_2)_3$-(^{i}Bu)$_7$POSS

$Br(CH_2)_3$-(^{i}Bu)$_7$POSS (13.2g, 0.017 mol) and NaI (21.1g, 0.14 mol) were dissolved in THF (100 ml). The mixture was heated at reflux for 48 hours under Ar then passed through a silica plug once cool. The THF was removed on a rotary evaporator to give a yellow solid. The solid was dissolved in DCM and washed with water. The DCM it was dried over $MgSO_4$ and the DCM evaporated to yield a white solid (13.4g, 0.014 mol, 82%).

^{1}H NMR (500.23 MHz, C_6D_6, 300K) δ_H (ppm): 2.83 (t, 2 H, *CH_2 propyl*), 2.08 (m, 7 H, *CH isobutyl*), 1.92 (m, 2 H, *CH_2 propyl*), 1.08 (t, 42 H, *CH_3 isobutyl*), 0.83 (m, 14 H, *CH_2 isobutyl*), 0.77 (m, 2 H, *CH_2 propyl*). ^{13}C NMR (125.76 MHz, $CDCl_3$, 300K) δ_C (ppm): 10.2 (CH_2, *propyl*), 13.9 (CH_2, *propyl*), 22.5 (CH_2, *POSS isobutyl*), 23.8 (CH, *POSS isobutyl*), 25.7 (CH_3, *POSS isobutyl*), 27.6 (CH_2, *propyl*). MALDI m/z: 985.4 (M), 1007.4 ($M+Na^+$), 1025.4 ($M + K^+$)

[PPh_3][I]-(^{i}Bu)$_7$POSS

$I(CH_2)_3$-(^{i}Bu)$_7$POSS (13g, 13.19 mmol) and PPh_3 were placed under argon. 1,2-dimethoxyethane (40 mL) was added and the solution heated at reflux for 48 hours. The white precipitate was crashed out by addition of dry hexane (100mL), the flask cooled in an ice bath and then the precipitated solid collected on a Bruckner funnel (11.64g, 0.0093mol, 71%).

^{1}H NMR (500.23 MHz, C_6D_6, 300K) δ_H (ppm): 7.84 (m, 9 H, *CH phenyl*), 7.73 (td, 6 H, *CH phenyl*), 3.82 (m, 2 H, *CH_2 propyl*), 1.91 – 1.72 (m, 9 H, *CH isobutyl and CH_2 propyl*), 1.06 (t, 2 H, *CH_2 propyl*), 0.98 – 0.86 (m b, 42 H, *CH_3 isobutyl*), 0.63 – 0.51 (m b, 14 H, *CH_2 isobutyl*). ^{13}C NMR (125.76 MHz, $CDCl_3$, 300K) δ_C (ppm): 13.3-13.4 (CH_2, *propyl*), 16.7 (CH_2, *propyl*), 22.4 (CH_2, *POSS isobutyl*), 23.8 (CH, *POSS isobutyl*), 25.0 (CH_2, *propyl*), 25.4 (CH_2, *propyl*), 25.6-25.7 (CH_3, *POSS isobutyl*), 117.7-118.4 (C, *phenyl*), 130.6 (CH, *phenyl*), 133.6 (CH, *phenyl*), 135.2 (CH, *phenyl*). ^{31}P NMR (202 MHz, C_6D_6, 300K) δ_P (ppm): 23.5 (*[PPh_3][I]*). MALDI m/z: 1245 (M), 1274.9 ($M+Na^+$)

3.4.2 Catalysis

Although stored under argon, the catalyst species were weighed on the bench and transferred into an autoclave, fitted with a magnetic stirrer bar, which was then placed under argon again.

The dry epoxide and carbonate standard were added and then the autoclave pressurised with CO_2. Any excess epoxide was quenched with H_2SO_4. The pressure was held constant for 5 minutes to enable the gas to dissolve in the epoxide. The autoclave was placed in a heating jacket on a magnetic stirring plate for 6 hours. The autoclave was cooled in a water bath, vented and then the mixture removed and analysed by GC-FID and NMR spectroscopy.

3.4.3 NMR of substrates:

All epoxides were dried over CaH_2 and distilled. They were stored in the freezer under argon.

1,2-epoxybutane (C_4H_8O): ^{1}H NMR (500.23 MHz, C_6D_6, 300K) δ_H (ppm): 1.01 (3H,t), 1.56 (2H,m), 2.47 (1H, m), 2.73 (1H, dd), 2.90 (1H, m). ^{13}C NMR (125.76 MHz, $CDCl_3$, 300K) δ_C (ppm): 9.6, 25.4, 46.7, 53.3

Cyclohexene oxide ($C_6H_{10}O$): ^{1}H NMR (500.23 MHz, C_6D_6, 300K) δ_H (ppm): 1.25 (2H, m), 1.43 (2H, m), 1.83 (2H, m), 1.96 (2H, m), 3.13 (2H, q).

Propylene carbonate ($C_4H_8O_3$): ^{1}H NMR (500.23 MHz, C_6D_6, 300K) δ_H (ppm): 1.44 (3H, d), 3.99 (1H, dd), 4.52 (1H, dd), 4.82 (1H, m).

1,2-epoxy-3-phenoxypropane ($C_9H_{10}O_2$): ^{1}H NMR (500.23 MHz, C_6D_6, 300K) δ_H (ppm): 2.79 (1H, dd), 2.93 (1H, dd), 3.38 (1H, m), 4.00 (1H, dd), 4.23 (1H, dd), 6.95 (2H, d), 7.00 (1H, t), 7.3 (2H, m). ^{13}C NMR (125.76 MHz, $CDCl_3$, 300K) δ_C (ppm): 44.8, 50.2, 68.7, 114.7, 121.2, 129.5, 158.5

Epichlorohydrin (C_3H_5ClO): ^{1}H NMR (500.23 MHz, C_6D_6, 300K) δ_H (ppm): 2.69 (1H, dd), 2.89 (1H, t), 3.23 (1H, m), 3.58 (2H, m)

Epoxyhexane ($C_6H_{12}O$): ^{1}H NMR (500.23 MHz, C_6D_6, 300K) δ_H (ppm): 0.93 (3H, t), 1.40 (2H, m), 1.46 (2H, t), 1.54 (2H, td), 2.48 (1H, dd), 2.76 (1H, dd), 2.92 (1H, m)

Styrene oxide (C_8H_8O): ^{1}H NMR (500.23 MHz, C_6D_6, 300K) δ_H (ppm): 2.83 (1H, dd), 3.18 (1H, dd), 3.90 (1H, m), 7.31-7.41 (5H, m)

3.4.4 MALDI method

The method for running the MALDI reactions was adapted from Bowers.[35] 40 μL dihydroxybenzoic acid (100 mg/mL in THF), 60 μL POSS compound (1 mg/mL in THF), 20 μL NaI (saturated in THF). Red phosphorus was used as a calibrant.

3.4.5 Calibration of membrane experiments

The leaching of the co-catalyst was assessed by monitoring by UV/Vis-spectrometry as there is a distinct double peak in the UV-Vis (figure 26) for the PPh_3I-alkyl-POSS compared to the free PPh_3 species.

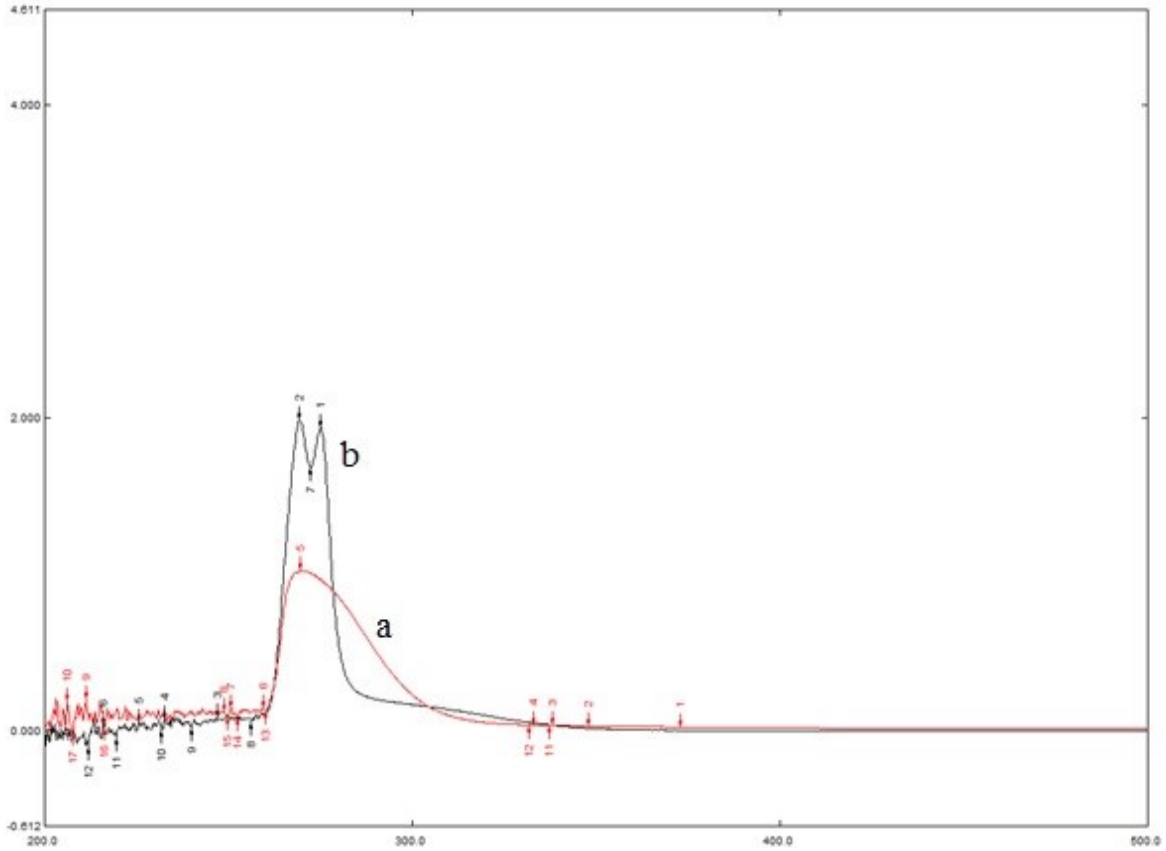

Figure 4.32 UV/Vis reading of a) free PPh_3 and b) $[PPh_3][I]$-POSS in DCM

To calculate the concentration of leached $[I][PPh_3P]$-POSS the molecular extinction coefficient was first calculated.

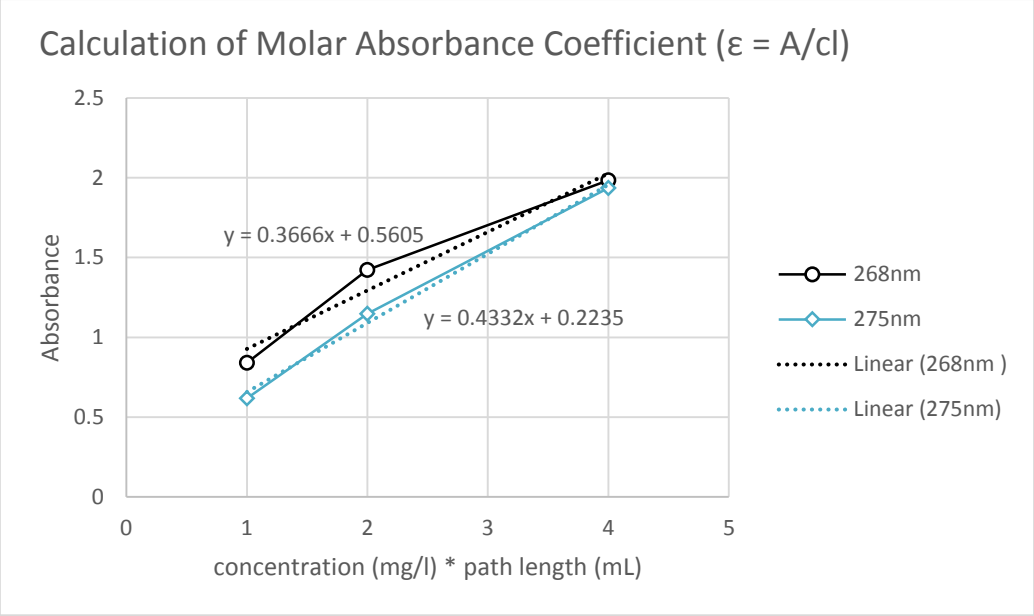

Figure 4.33 Calculation of Molar Absorption Coefficient of PPh_3

ε (268nm) = A/cl = 0.37

Concentration of [PPh_3][I]-POSS (C_{max})

Total volume of 1,2-epoxybutane (0.80 mol, 58.0g, 70 mL) and propylene carbonate (0.09 mol, 9.6 g, 8 mL) = 78 mL

Total mass of reagents = 68.56 g

Mass of [PPh_3][I]-POSS = (0.0006 moles, 0.75 g)

Max Concentration mg/mL = (0.75g*1000 mg/g)/78 mL = 9.60 mg/mL

It was necessary in the final leaching % to take into account the different mass of samples. Using the final measured value inside and outside the membrane as the C_{max} and the $mass_{max}$ the final % was calculated as ((C_{sample}/C_{max})*$mass_{final}/mass_{sample}$*100%).

3.5 References

† Andreas Skowron was a previous PhD student under the supervision of Prof. Dieter Vogt while based at Eindhoven University of Technology. Andreas first synthesised the POSS catalysts and co-catalysts and carried out preliminary tests on 1,2-epoxybutane. This work was to contribute to a publication building upon that work.

‡ Mr. Sami Gesslbauer was a final year MChem student at Edinburgh who worked on this project under the supervision of Lewis Fenton and Prof. Dieter Vogt during the 2016/2017 term. Sami synthesised the POSS molecules, performed their characterisation as well as running the

epoxide catalysis. This work was part of his final year thesis. As of 2017 he will be studying for a PhD in the group of Dr. Charles Romain at Imperial College London.

[1] T. Sakakura, K. Kohno, *Chem. Commun.* **2009**, 1312-1330.

[2] W. J. Peppel, *Industrial & Engineering Chemistry* **1958**, *50*, 767-770.

[3] A. W. Kleij, *Catalysis Science & Technology* **2014**, *4*, 1481-1481.

[4] D. J. Darensbourg, *Chem. Rev.* **2007**, *107*, 2388-2410.

[5] D. Ballivet-Tkatchenko, H. Chermette, L. Plasseraud, O. Walter, *Dalton Transactions* **2006**, 5167-5175.

[6] G. Trott, P. K. Saini, C. K. Williams, *Philosophical Transactions of the Royal Society A: Mathematical, Physical and Engineering Sciences* **2016**, *374*.

[7] J. A. Garden, A. J. P. White, C. K. Williams, *Dalton Transactions* **2017**, *46*, 2532-2541.

[8] A. Decortes, A. M. Castilla, A. W. Kleij, *Angew. Chem. Int. Ed.* **2010**, *49*, 9822-9837.

[9] M. Alvaro, C. Baleizao, D. Das, E. Carbonell, H. García, *J. Catal.* **2004**, *228*, 254-258.

[10] T. Hashiyama, *Medicinal Research Reviews* **2000**, *20*, 485-501.

[11] H. Jing, S. K. Edulji, J. M. Gibbs, C. L. Stern, H. Zhou, S. T. Nguyen, *Inorg. Chem.* **2004**, *43*, 4315-4327.

[12] D. Vogt, A. K. Skowron, C. J. H. Hendriksen, G. Gerritsen, H. C. L. Abbenhuis, *Manuscript in preperation* **To Be Published**.

[13] P. Vandezande, L. E. M. Gevers, I. F. J. Vankelecom, *Chem. Soc. Rev.* **2008**, *37*, 365-405.

[14] J. Sun, W. Cheng, W. Fan, Y. Wang, Z. Meng, S. Zhang, *Catal. Today* **2009**, *148*, 361-367.

[15] E. de Jesús, J. C. Flores, *Industrial & Engineering Chemistry Research* **2008**, *47*, 7968-7981.

[16] A. V. Gaikwad, V. Boffa, J. E. ten Elshof, G. Rothenberg, *Angew. Chem. Int. Ed.* **2008**, *47*, 5407-5410.

[17] R. van de Coevering, R. J. M. Klein Gebbink, G. van Koten, *Prog. Polym. Sci.* **2005**, *30*, 474-490.

[18] B. M. J. M. Suijkerbuijk, L. Shu, R. J. M. Klein Gebbink, A. D. Schlüter, G. van Koten, *Organometallics* **2003**, *22*, 4175-4177.

[19] S. H. Phillips, T. S. Haddad, S. J. Tomczak, *Curr. Opin. Solid State Mater. Sci.* **2004**, *8*, 21-29.

[20] D. Astruc, E. Boisselier, C. Ornelas, *Chem. Rev.* **2010**, *110*, 1857-1959.

[21] L. c. Ropartz, R. E. Morris, D. F. Foster, D. J. Cole-Hamilton, *J. Mol. Catal. A: Chem.* **2002**, *182*, 99-105.

[22] I. Blanco, L. Abate, F. A. Bottino, P. Bottino, *J. Therm. Anal. Calorim.* **2012**, *108*, 807-815.

[23] M. Janssen, J. Wilting, C. Müller, D. Vogt, *Angew. Chem. Int. Ed.* **2010**, *49*, 7738-7741.

[24] N. B. McKeown, P. M. Budd, *Chem. Soc. Rev.* **2006**, *35*, 675-683.

[25] R. W. Baker, in *Membrane Technology and Applications*, John Wiley & Sons, Ltd, **2004**, pp. 89-160.

[26] T. Sakai, Y. Tsutsumi, T. Ema, *Green Chemistry* **2008**, *10*, 337-341.

[27] T. Takahashi, T. Watahiki, S. Kitazume, H. Yasuda, T. Sakakura, *Chem. Commun.* **2006**, 1664-1666.

[28] C. J. Whiteoak, A. H. Henseler, C. Ayats, A. W. Kleij, M. A. Pericas, *Green Chemistry* **2014**, *16*, 1552-1559.

[29] A. A. Sathe, A. M. K. Nambiar, R. M. Rioux, *Catalysis Science & Technology* **2017**, *7*, 84-89.

[30] R. Duchateau, *Chem. Rev.* **2002**, *102*, 3525-3542.

[31] R. K. Harris, D. M. Granty, *Encyclopedia of Nuclear Magnetic Resonance, Vol. 5*, John Wiley & Sons, Chichester, UK, **1996**.

[32] M. Ahmed, A. G. M. Barrett, D. C. Braddock, S. M. Cramp, P. A. Procopiou, *Tetrahedron Lett.* **1999**, *40*, 8657-8662.

[33] J. Schraml, M. Čapka, V. Blechta, *Magn. Reson. Chem.* **1992**, *30*, 544-547.

[34] N. J. Brown, J. E. Harris, X. Yin, I. Silverwood, A. J. P. White, S. G. Kazarian, K. Hellgardt, M. S. P. Shaffer, C. K. Williams, *Organometallics* **2014**, *33*, 1112-1119.

[35] S. E. Anderson, C. Mitchell, T. S. Haddad, A. Vij, J. J. Schwab, M. T. Bowers, *Chem. Mater.* **2006**, *18*, 1490-1497.